CHAIR OF METALLURGY
MONTANUNIVERSITAET LEOBEN

Classification of iron ores regarding their reduction behavior in fluidized bed technologies

Dissertation

by

Michael Skorianz, MSc

handed in at the Montanuniversitaet Leoben/Chair of Metallurgy for attaining the degree of a Doctor of Metallurgical and Mining Sciences.

under the direction of

Univ.-Prof. Dipl.-Ing. Dr. techn. Johannes L. Schenk
(Chair of Metallurgy, Montanuniversitaet Leoben)

peer-revieved by

Univ.-Prof. (em) Dr.-Ing. Dipl.-Wirtsch.-Ing. Heinrich W. Gudenau
(Department of Ferrous Metallurgy, RWTH Aachen)

MONTAN UNIVERSITÄT

Chair of Metallurgy
Montanuniversitaet Leoben
Franz-Josef-Straße 18 – 8700 Leoben, Austria

"Personalities are not shaped by pretty speeches,
but by their own work and achievement"

Einstein

Preface

Foremost, I would like to express my sincere gratitude to my advisor Univ.Prof.Dr Johannes Schenk for the great support during the research work, his good teaching and friendship. I also wish to thank my co-advisor em.Univ.Prof.Dr. Heinrich Wilhelm Gudenau for his scientific support and the pleasant hours spent together.

I would like to extend special thanks to Ass.Prof.Dr. Heinrich Mali for the philosophic and scientific conversations and for his good company.

The financial and technical background for this research project was provided by the industrial partners Siemens VAI Metals Technologies GmbH and voestalpine Stahl GmbH. Here I would like to thank all involved people for the excellent collaboration during the whole project, especially Dr. Jan Friedemann Plaul, Dr. Weiss Bernd, Harald Fischer, Dr. Hado Heckmann, Thomas Bürgler, Kurt Schiefer, Erfried Gangl and Markus Kolberger.

For their kind assistance and cooperation, I wish to thank my graduate and undergraduate students who contributed the scientific work within the research project.

Further more I am grateful to all my colleagues and friends for the good collaboration, the interesting conversations and their camaraderie.

Lastly and most importantly, I wish to thank my family.

Affidavit

I declare in lieu of oath, that I wrote this thesis and performed the associated research myself, using only literature cited in this volume.

Michael Skorianz

30th October 2012

Abstract

The objectives at the forefront of this research are process optimization of fluidized-bed based technologies for iron- and steelmaking and the characterization of the process behavior of different globally traded iron ore brands. Direct reduction or smelting reduction technologies as an alternative to the traditional blast furnace process have been developed in recent years which can use iron ore fines directly without prior benefication processes. The reduction behavior of different iron ore fines were investigated by means of reduction tests and morphological characterization of the iron oxide phases in the iron ore. Tests were performed in a lab scale fluidized bed reactor and petrographical characteristics were investigated for the raw ore and reduced samples during and after the tests. The influence of process mode, residence time, pre-reduction temperature and gas composition for a sequenced fluidized bed reactor system on the reduction behavior of hematite ore was studied. Furthermore, the reduction behavior of different iron ore brands and their morphological evolution during the process could be characterized.

Kurzfassung

Die Ziele dieser Arbeit sind die Prozessoptimierung von auf Wirbelschichtverfahren basierenden Technologien für die Eisen- und Stahlerzeugung und die Bewertung des Prozessverhaltens von weltweit gehandelten Eisenerzen. Direktreduktions- oder Schmelzreduktionsverfahren wurden in den letzten Jahren als Alternative zum traditionellen Hochofenprozess entwickelt. Diese ermöglichen einen direkten Einsatz von Feineisenerzen ohne vorgeschaltete Aufbereitungsprozesse. Das Reduktionsverhalten von verschiedenen Feineisenerzen wurde mittels Reduktionstests untersucht und die Eisenoxid-Phasen wurden morphologisch bestimmt. Die Tests wurden an einem Wirbelschichtreaktor im Labormaßstab durchgeführt und die petrographischen Eigenschaften der Erze wurden im rohen und im reduzierten Zustand während und nach den Tests ermittelt. Die Einflüsse von Prozessführung, Verweilzeit, Vorreduktionstemperatur und Gaszusammensetzung für ein sequentielles Wirbelschicht-Reaktorsystem wurde mittels Hämatit-Erz erprobt. Weiters konnte das Reduktionsverhalten verschiedener weltweit gehandelter Eisenerze und deren morphologische Entwicklung während des Prozesses charakterisiert werden.

Index

Nomenclature

Acronymes

B.E.T	Brunauer-Emmet-Teller
BF	Blast Furnace
BOF	Basic Oxygen Furnace
CDRI	Cold Direct Reduced Iron
DIN	Deutsches Institut für Normung
DR	Direct Reduction
DRI	Direct Reduced Iron
EAF	Electric Arc Furnace
FB	Fluidized Bed
FIOR	Fluosolid Iron Ore Reduction
GOD	Gas Oxidation Degree
GUD	Gas Utilization Degree
H	Hematite
HBI	Hot Briquetted Iron
HCI	Hot Compacted Iron
HDRI	Hot Direct Reduced Iron
HM	Hot Metal
ISO	International Organization for Standardization
L	Limonite
LOI	Loss On Ignition
M	Magnetite
MD	Metallization Degree
MPH	Micro Platy Hematite
Mr	Martite
NG	Natural Gas
OD	Oxidation Degree (also GOD)
PCI	Pulverized Coal Injection

R1	Reactor 1
R2	Reactor 2
R3	Reactor 3
R4	Reactor 4
RD	Reduction Degree
RO	Raw Ore
SGR	Specific Gas Rate
SMD	Sauter Mean Diameter
SR	Smelting Reduction
TGA	Thermogravimetric Analysis
XRF	X-Ray Fluorescence

Symbols

$\dot{V}$	Flow rate
$\Delta G°$	Free enthalpy of formation
ΔH	Enthalpy of reaction
Δp	Pressure drop
ΔQ	Mass fraction
a	Activity
A	Hygroscopic moisture content
Ar	Archimedes number
C	B.E.T.-constant
c_d	Drag coefficient
c_w	Drag coefficient
D	Diameter
d_{eff}	Effective particle diameter
d_{max}	Maximum particle diameter
d_{min}	Minimum particle diameter
d_o	Upper particle diameter
d_p	Particle diameter
d_{SMD}	Sauter mean diameter
d_u	Lower particle diameter
E_L	Enthalpy of the monolayer
F	Dilution factor
$F_{\Delta p}$	Force by pressure drop
F_A	Bouyancy force
F_G	Gravitational force
Fr	Froude number
F_W	Drag force
g	Gravitational acceleration
H	Height of bed

K	Equilibrium constant
k	Inclination
Lj	Ljascenko number
ln	Logarithmus naturalis
log	Logarithmus
M	Ljascenko number
m	Mass
M	Molar mass
Me_xO_y	Metal oxide
n	Amount of substance
η	Dynamic viscosity
n	Load factor
O_{sp}	Specific surface area
p	Pressure
p_0	Pressure above the monolayer
P_{O2}	Partial pressure of oxygen
Q_3	Cumulative mass fraction
R	Gas constant
R	Reducing agent
$RD_{(CA)}$	Reduction degree, calculated from chemical analysis
$RD_{(calc.)}$	Recuction degree, calculated from mass balance
Re	Reynolds number
T	Temperature
t	Time
V	Volume
V_a	Adsorbed volume
v_{Eq}	Consumpted volume
V_m	Volume of a monolayer
w	Mass fraction
w	Velocity
w_{mf}	Minimum fluidization velocity
w_T	Terminal velocity
w_t	Terminal velocity
x	Mass fraction of a class
X	Molar Ratio
y	Non-stoichiometry of wuestite and magnetite
δ	Non-stoichiometry of hematite
ε	Porosity
ε	Voids fraction
v	Cinetic viscosity
$ρ_f$	Fluid density
$ρ_g$	Gas density

ρ_s	Solid density
φ_s	Shape factor
Ω	Ljascenko number

Chemical elements, ions and molecules

Al_2O_3	Aluminium oxide
Ar	Argon
C	Carbon
C_6H_6	Benzene
CaO	Calcium oxide
CH_4	Methane
CO	Carbon monoxide
CO_2	Carbon dioxide
Fe	Iron
Fe^{2+}	Iron(II)-ion
Fe_2O_3	Hematite, Iron(III)-oxide
$Fe_2O_3*3H_2O$	Limonite
$Fe_2O_3*H_2O$	Goethite
$Fe_2O_3*n.H_2O$	Hydrohematite
Fe^{3+}	Iron(III)-ion
Fe_3C	Cementite
Fe_3O_4	Magnetite, Iron(II,III)-oxide
$FeCO_3$	Siderite
Fe_{met}	Metallic iron content
FeO	Wuestite, Iron(II)-oxide
$FeO*TiO_2$	Ilmenite
FeOOH	Limonite
FeS_2	Pyrite
Fe_{tot}	Total iron content
H_2	Hydrogen
H_2O	Water vapor
He	Helium
K	Potassium
K_2O	Potassium oxide
$KMnO_4$	Potassium permanganate
Mg	Magnesium
MgO	Magnesium oxide
Mn	Manganese
Mn^{2+}	Manganese(II)-ion
MnO_4^-	Permanganate-ion
N_2	Dinitrogen

O	Oxygen
P	Phosphor
SiO_2	Silicium oxide
Sn^{2+}	Tin(II)-ion
Ti	Titanium
TiO_2	Titanium oxide

Remark:

In some diagrams and tables, a comma is used as decimal point, because the German version of the spreadsheet program was used for creating the diagrams and tables.

1 Introduction

Due to environmental and economic constraints, alternative ironmaking processes to traditional blast furnace technology have been developed in recent decades. These are direct reduction and smelting reduction technologies, some using iron ore fines directly without prior agglomeration processes. One possible procedure for the reduction of iron ore fines is fluidized bed technology. A general overview of the actual applications of fluidized bed based technologies in direct- and smelting reduction processes are given by Schenk [1].

The target for an optimized reduction process is to use as little energy and resources as possible without downgrading the process efficiency or product quality. The reduction progress from iron ore to metallic iron in the fluidized bed reduction processes is limited, because it is controlled by thermodynamic and morphologic constraints. Several applications of fluidized bed based technologies for iron- and steelmaking have been developed [1]. Some of them run with four sequenced fluidized bed reactors to ensure controlled process operation with stepwise reduction of iron ore from hematite over magnetite and wuestite to metallic iron.

The research project deals with the process optimization of fluidized-bed based technologies for iron- and steelmaking and the determination of reducibility as well as the mineralogical and petrographical characterization of different globally traded iron ore brands. In order to investigate these issues, a novel lab scale fluidized bed reactor was installed in the laboratories of the Department of Metallurgy at the Montanuniversitaet Leoben. With this new fluidized bed facility, all relevant process parameters were able to be measured continuously during the experiments.

Regarding the influence of reduction sequences on reducibility of iron ore fines, a 3-stage reduction operation was compared to a 4-stage reduction procedure, taking into account the influence of the start temperature in the pre-reduction sequence. The influence of residence time, start temperature and gas composition on the reduction behavior was studied by means of a 3-stage reduction operation.

In order to investigate and compare the reduction behavior of different globally traded iron ore brands, a standardized test methodology has been developed. Additionally, a sampling system for the fluidized bed reactor has been installed to extract samples during the reduction process. The chemical, morphological and structural evolution of the material during reduction in the magnetite, wuestite and iron stability field could be characterized. Due

to recurring deviations in chemical analysis of the reduced iron ore samples, an anonymous interlaboratory test with selected laboratories was carried out. The results render statements and predictions in terms of accuracy and analysis error of Fe_{tot}, Fe_{met}, Fe^{2+} and Fe^{3+}.

Combined with the gathered process data, the reduction progress could be defined and compared with chemical analyses, morphology and mass balances. Furthermore, compared to prior research work, the facility enables tests closer to real industrial operation conditions. The tests executed with this new facility as well as the developed methodologies provided clear evidence for a better prediction of reducibility of iron ores in the fluidized bed process.

Objectives in detail

This thesis was established at the Chair of Metallurgy, Montanuniversitaet Leoben, under the supervision of Prof. Johannes L. Schenk. Based on the necessity of process enhancement of fluidized bed based direct reduction and smelting reduction technologies, a novel fluidized bed reactor installation was to be put into operation. For this facility, a methodology for the test execution and a method for the evaluation of the test results were to be developed.

In order to characterize different fine iron ore brands regarding their process behavior and their morphological properties during the reduction process, a methodology was to be defined. For these purposes, a sampling system was to be engineered to extract specimens during the process.

After commissioning of the test facility and the definition of the different methodologies, a sequenced 3-stage reduction operation was to be compared to a 4-stage reduction mode. Furthermore, the influence of prereduction temperature, residence time and gas composition on the reduction behavior was to be investigated.

In order to characterize different globally traded iron ore brands, a standardized test series with different iron ores was to be executed to determine the chemical, morphological and structural evolution of the materials during reduction process. Due to recurring deviations in chemical analysis of the reduced iron ore samples, an interlaboratory test with selected laboratories was to be carried out to estimate the analysis error.

2 Direct Reduction and Smelting Reduction – an overviev

Besides the blast furnace process for iron ore reduction, a series of so called direct reduction and smelting reduction technologies have been developed since the 1960's [2]. Some of them are already implemented on an industrial scale and some are still at pilot level.

In Figure 1, the possible procedural ways to make iron and steel are pointed out by means of a carbon-oxygen-phase diagram. The classification of these technologies in terms of energy- and reduction agent supply is shown in Figure 2.

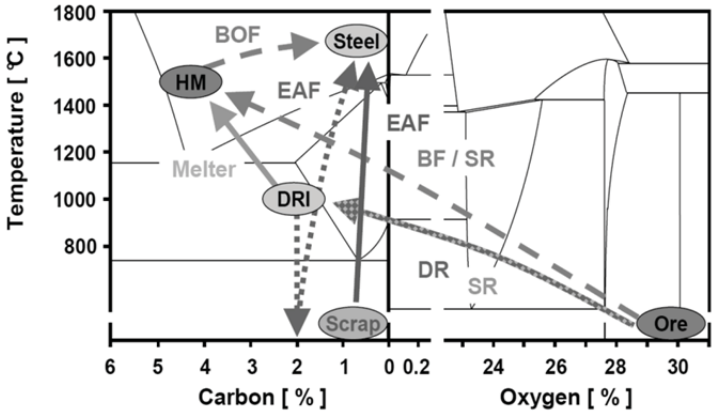

Figure 1: Alternative ways to produce steel [3]

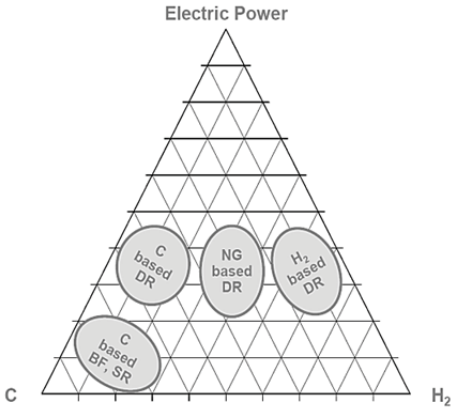

Figure 2: Supply with energy and reduction agents [3]

At the beginning of its development, the direct reduction technologies were considered as alternative techniques to the blast furnace process. Nowadays they are additional techniques especially in terms of scrap supplementation in iron and steelmaking [4].

2.1 Direct Reduction technologies

Direct Reduction is the reduction of iron ores to metallic iron, avoiding the molten phase. The iron ore is reduced in its solid state in a furnace by means of solid, liquid or gaseous reducing agents [4]. The product is direct reduced iron (DRI) with metallization degrees usually between 85 to 94 %. DRI is sometimes briquetted in hot condition to hot briquetted iron (HBI), in order to ease shipping and storage. DRI and HBI are mainly used in electric arc furnaces as a substitute for scrap [5]. HDRI (hot DRI) is charged directly from the reduction aggregate into the subsequent steelmaking facility in hot conditions. The reduction takes part at temperatures usually between 750 °C and 1100 °C in presence of a reducing gas containing H2 and/or CO [5]. The reducing gas can be produced by reforming of natural gas or by means of coal gasification. As iron ore input material, lump ore, pellets or fine ore can be used. This material should be of good quality (high iron content, low content of phosphorous and sulfur, low gangue content). Depending on the input material and its grain size distribution, various processes can be applied (cf. Figure 3).

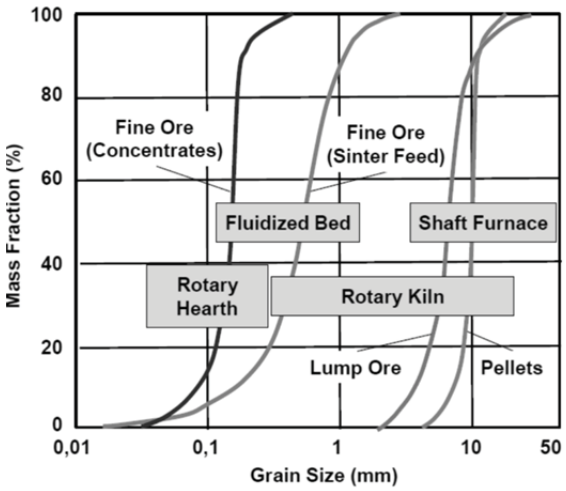

Figure 3: Iron ore properties for direct reduction processes [4,5]

In Figure 4, the classification of the direct reduction processes regarding technological principle, material input and energy source is shown. Actually just some of them are in operation. The most important characteristics for the application of direct reduction technologies are [4]:

- Production of premium quality and cost effective products containing iron, which can compete with scrap and contain a low level of impurities like copper, zinc or tin.
- Less environmental pollution due to avoiding CO_2-emissions produced by coke oven plants, sinter plants or pellet plants.
- Usage of regionally available coal or natural gas instead of coke.
- No production of by-products, which decrease technical and economical flexibility.
- Small production units, which enables companies to produce flexibly according the situation on the market.
- Less complex burden preparation (blast furnace – fluidized bed technologies).

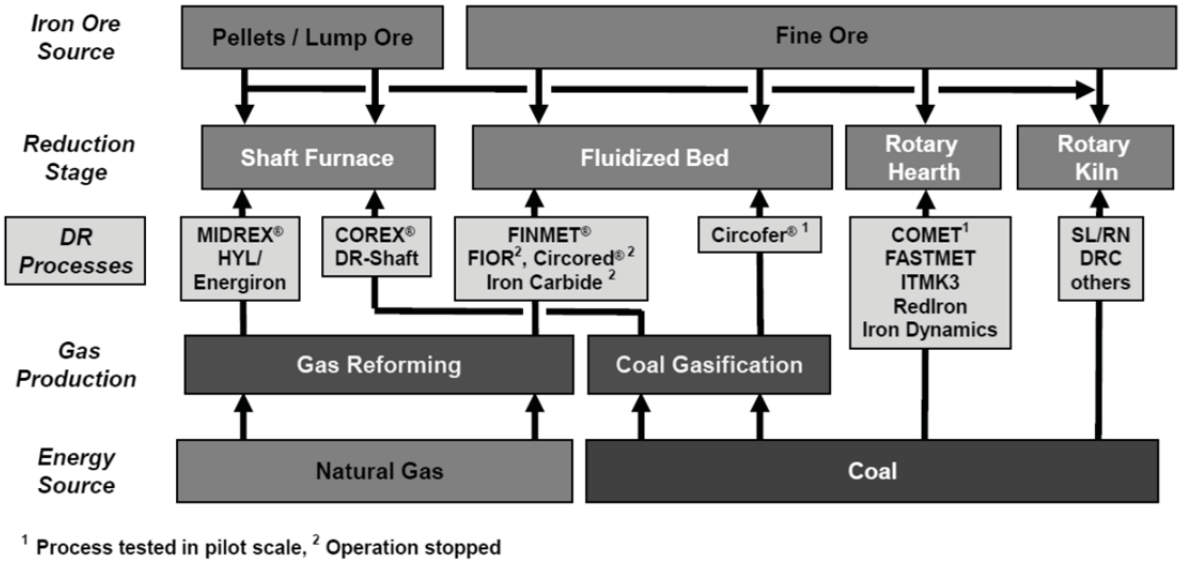

Figure 4: Classification of direct reduction processes [5]

For developing countries:

- Lower energy- and personell costs and, hence, the production of a cheap iron containing product for the export market.
- Less imported scrap.

For industrialised countries:

- Covering the required amount of high quality scrap.
- Direct reduced iron as a input material for premium quality steel grades.

As seen in Figure 5, the annual production of direct reduced iron in 2011 was over 73 million tons with cold direct reduced iron (CDRI) as the largest portion (ca. 60 million tons).

Year	Total	Year	Total	Year	CDRI	HBI	HDRI	Total
1970	0.79	'87	13.52	'03	38.98	8.64	1.83	49.45
'71	0.95	'88	14.09	'04	43.54	8.63	2.43	54.60
'72	1.39	'89	15.63	'05	45.44	8.95	2.60	56.99
'73	1.90	'90	17.68	'06	48.50	8.60	2.69	59.79
'74	2.72	'91	19.32	'07	55.89	8.34	2.99	67.22
'75	2.81	'92	20.51	'08	56.60	8.19	4.24	68.03
'76	3.02	'93	23.65	'09	52.65	6.93	4.86	64.44
'77	3.52	'94	27.37	'10	56.69	7.21	6.47	70.37
'78	5.00	'95	30.67	'11	59.50	7.60	6.22(e)	73.32
'79	6.64	'96	33.30					
'80	7.14	'97	36.19					
'81	7.92	'98	36.96					
'82	7.28	'99	38.60					
'83	7.90	'00	43.78					
'84	9.34	'01	40.32					
'85	11.17	'02	45.08					
'86	12.53							

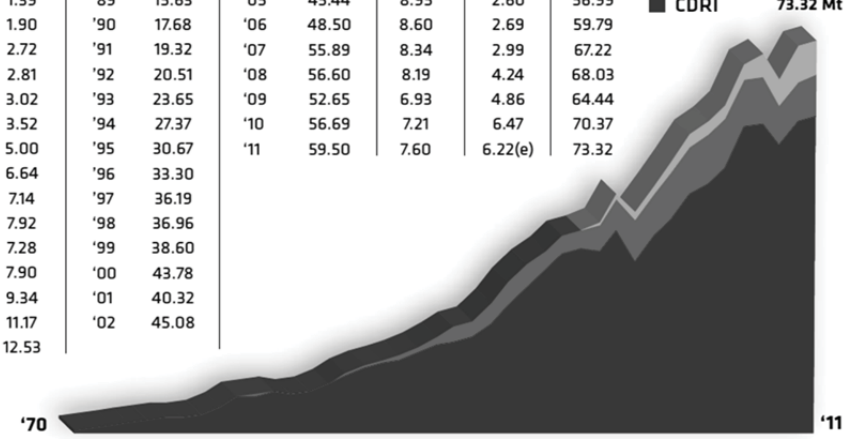

Figure 5: World DRI production by year (in million tons) [6]

2.2 Smelting Reduction technologies

What all smelting reduction processes have in commen is that they produce hot metal by direct use (gasification) of coal, which serves as energy source and reducing agent. In comparison to the blast furnace route, no cokemaking facility is necessary. Many such facilities are designed to process iron ore without prior agglomeration, i.e. sintering or pelletizing [5]. Usually, the process consists of two stages. In the first stage, the iron ore is pre-reduced to DRI and in the second stage the final reduction and the smelting to hot metal is performed. So, the pre-reduction-stage of a smelting reduction process is an integrated direct reduction process.

In all ironmaking processes except for electrical smelting processes, the required heat for the metallurgical reactions is produced by gasification of coal with oxygen or hot blast. The gasified coal generates the reducing gas for the pre-reduction of the iron ore, containing CO and H_2 [5]. In Figure 6, the classifictation of the smelting reduction processes is shown.

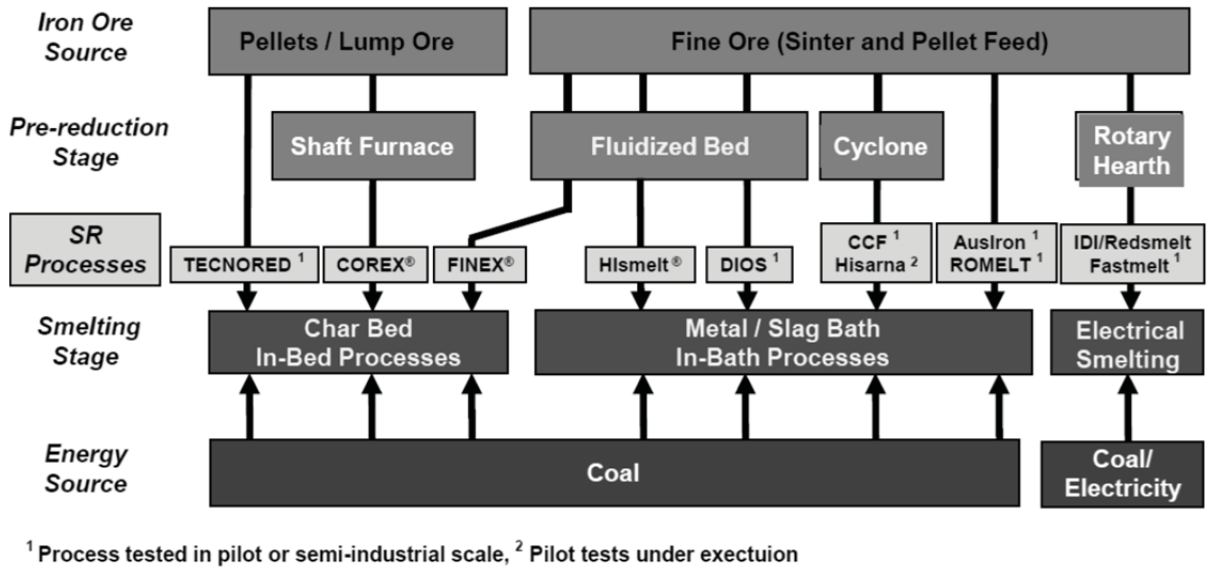

Figure 6: Classification of smelting reduction processes [5]

The smelting reduction stage can be designed as an “In-Bed”-reactor (COREX®, FINEX®, also blast furnace) or as an “In Bath”-reactor (i.e. HISmelt®, Hisarna, ROMELT) (cf. Figure 7). The “In-Bed”-reactor operates with a low oxygen activity due to excess C in the bed. The FeO-content in the slag is low and the hot metal is saturated with C (4 - 5 %). Additionally, the Si, Mn and P content in the hot metal is high. In the “In-Bed”-reactor, the oxygen activity is high due to post combustion. The slag has an increased amount of FeO and the hot metal is not saturated with C (2 - 3 %). No Si, Mn and P is dissolved in the hot metal, but the S-content is high [5].

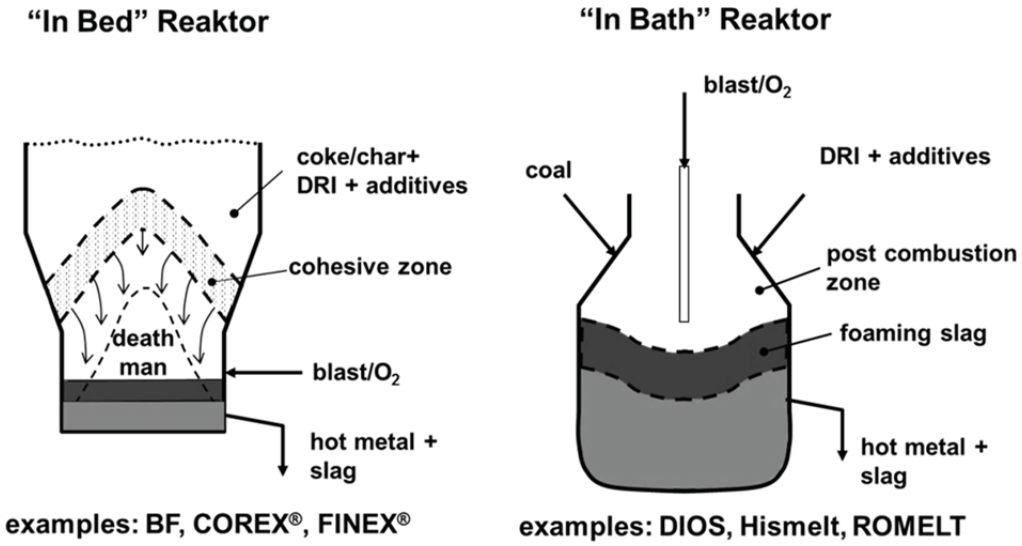

Figure 7: Technological principles of the smelting reduction stage [5]

Currently, seven COREX®-plants for the reduction of lumpy burden with a maximum capacity of 1.5 million tons/year and two FINEX®-plants for fine ore reduction with the same maximum capacity are in operation. A new FINEX®-plant with a capacity of 2.0 million tons is under construction. The only HIsmelt-plant with a capacity of 0.8 million tons/year is in idle status [5]. In Figure 8, the the COREX®- and FINEX®-route is compared to the traditional blast furnace route. In contrast to the blast furnace, the COREX®- and FINEX®-plants have a pre-reduction stage for the reduction of the lumpy burden and fine ore, respectively. The lumpy burden in the COREX®-plant is pre-reduced by means of a shaft furnace. The fine ore in the FINEX®-plant is pre-reduced by means of a sequenced fluidized bed cascade. After pre-reduction, the direct reduced iron is then charged into the so called melter gasifier together with coal and oxygen.

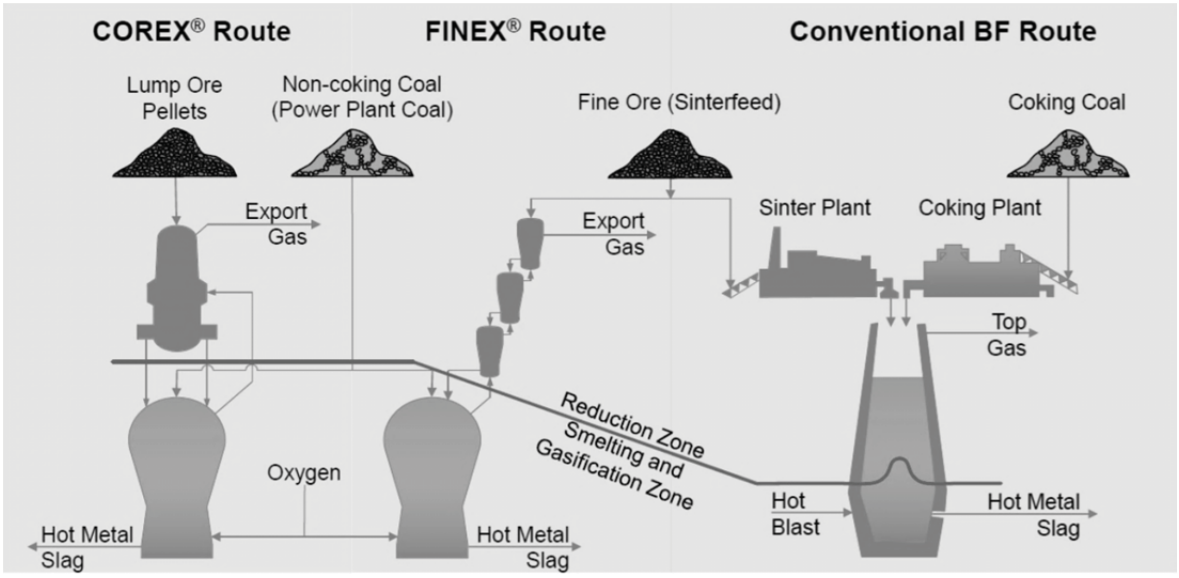

Figure 8: COREX®/FINEX® - Blast furnace comparison [7]

Here, the coal gasification, the final reduction and the smelting of the input material takes place. The product is hot metal, as discussed before. The export gas can be used for energy production [5,7-10].

2.2.1 The FINEX®-technology: Hot metal production from fine ore

The first commercial FINEX®-plant for the production of hot metal from fine ore was set into operation in 2007 in South Korea at POSCO Steel. As mentioned before, the FINEX®-process is designed in two stages (cf. Figure 9). The first stage consists of four sequenced fluidized bed reactors for the direct reduction of sinter feed and the second stage serves as a melter gasifier for the supply of the reduction gas by means of coal gasification, as well as for the final reduction and the smelting of the direct reduced iron to hot metal. Additionally, a gas recycling system is installed.

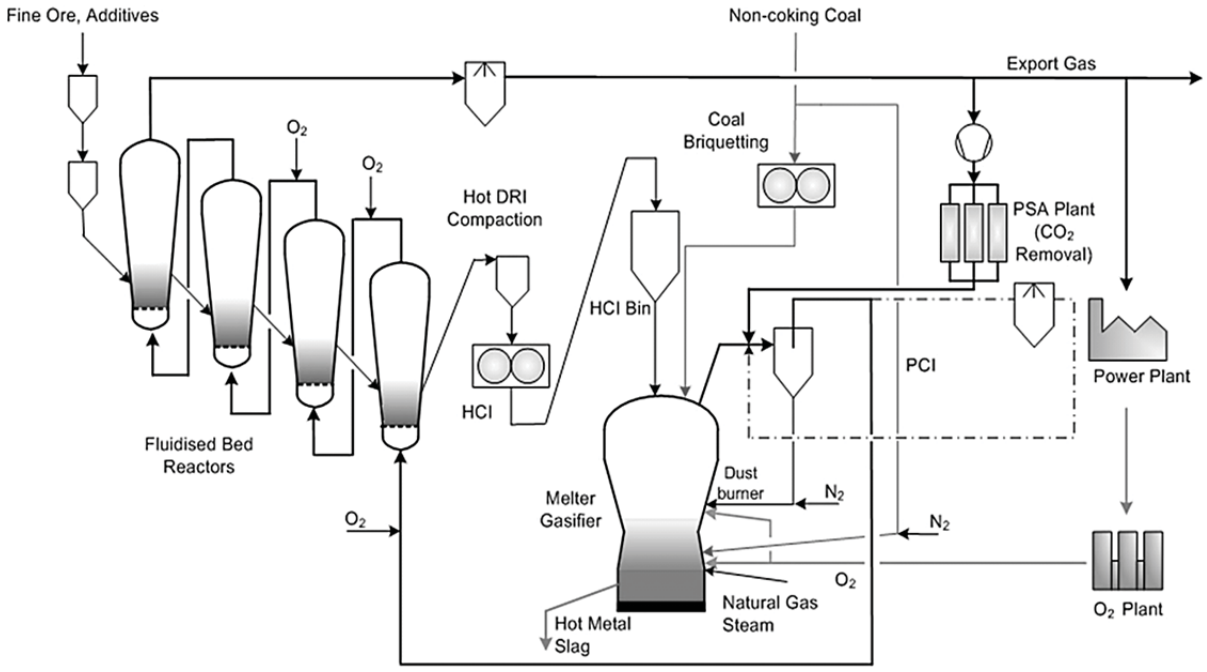

Figure 9: FINEX® - process [5]

Fine ore with grain sizes up to 8 mm is charged into the sequenced fluidized bed reactors by means of a hopper system and flows countercurrently against the reduction gas, which is produced in the melter gasifier. The gas at the inlet of the lowest reactor consists of about 60 % CO and 15 - 20 % H_2. The other components are CO_2, H_2O, CH_4 and N_2. Together with the iron ore, limestone and dolomite are charged as additives. The iron ore is then reduced stepwise to direct reduced iron, which is compacted to hot compacted iron (HCI). The HCI is conveyed in hot condition to a charging bin above the melter gasifier and is charged into its dome with coal. Coal is also injected in pulverized condition as PCI (Pulverized Coal Injection) via the oxygen tuyeres. The required energy for the metallurgical procedure is generated by the gasification of the coal and the PCI with technically pure oxygen. After being cleaned by a dust collector, the reducing gas is conducted to the fluidized bed reactors

for the indirect reduction of the fine ore. The excess reducing gas is cleaned by a wet scrubber after leaving the last reactor. A portion of the gas is compressed and cleaned from CO_2 to be recycled again into the process as reducing gas. The other portion serves as export gas for energy production. The produced hot metal, as well as the slag, is of the same quality as from the blast furnace [5,7-10].

3 Fundamentals of iron ore reduction

The reduction of iron ore is defined as the oxygen removal of an iron oxide to its subordinated oxidation state by a more oxygen-affine reducing agent.

Reduction is defined as the absorbtion of electrons and, respectievely, the deminuition of the oxidation state [4]. In the metallurgical usage, reduction is indicated as the removal of oxygen from oxide (as well as other oxygen containing compound) and its conversion to an element or to the subordinated oxidation state [11]. Therefore a more oxygen affine reducing agent is necessary:

$$Me_xO_y + R \leftrightharpoons Me_xO_{y-1} + RO \tag{3-1}$$

Based on the oxygen potential, it is possible to predict the direction of the chemical reaction. Hence, reduction can only take place, when the oxygen potential of the metal oxide (Me_xO_y) is higher than the oxygen potential of the reducing agent (R). The higher the potential difference, the higher is the driving force for the reaction [4].

3.1 Iron ores and their oxides

Iron makes up about 4.7 % of the Earth's crust and is contained in almost all rocks. Iron ores in general are rocks or minerals, from which iron can be produced commercially with an iron content of about 25 – 70 % or – generally speaking – a mineral which will yield metallic iron when heated in the presence of a reductant. Iron ore consists of different minerals containing iron and gangue [11].

The definition of iron ore types is stated in international ISO standards of the technical committee TC102 – Iron ores and direct reduced iron. Natural iron ores are ores as extracted from mines and are not subjected to any processes of beneficiation other than sizing, whereas processed ores are treated by chemical or physical processes to make them more suitable for iron- and steel production. These iron ores can be divided into different size fractions [12,13]:

- Lump ore: consists of coarse particles with a specified lower size limit between 6.3 mm and 10 mm.
- Fine ore: consists of small particles with a specified upper size limit between 6.3 mm and 10 mm.
- Concentrate: processed ores with a raised percentage of iron content typically between 0.1 mm to 1 mm.
- Pelletfeed: very fine ore fractions in a size range smaller than 0.1 mm.

The most common iron containing minerals are hematite, magnetite and limonite ores, but other ores with less economic importance are also present (cf. Table 1) [11].

Table 1: Mineralogical characteristics of iron ores [11,14,15]

Type	Ore mineral	Chemical formula	Colour	Streak colour	Density [g/cm³]	max.Fe-content [wt.-%]
Oxide	Hematite	Fe_2O_3	steel grey or iron black	red	5.26	70.0
Oxide	Martite	Fe_3O_4 and Fe_2O_3	black or dark red	dark red	5.10 – 5.20	-
Oxide	Magnetite	Fe_3O_4	iron black	black	5.17	72.4
Hydroxide	Limonite	$Fe_2O_3 * 3H_2O$	brown, yellowish brown, yellow	yellowish brown	3.60 – 4.00	59.8
Hydroxide	Goethite	$Fe_2O_3 * H_2O$	brownish black	brownish yellow	4.00 – 4.40	62.9
Hydroxide	Hydrohematite	$Fe_2O_3 * nH_2O$ (n≈0.1)	rich red	red	4.20 – 4.60	69.0
Carbonite	Siderite	$FeCO_3$	pale yellow or brownish black or brownish red	white	3.90	48.3
-	Ilmenite	$FeO * TiO_2$	iron black	black or brownish red	4.50 – 5.00	36.8
Sulphide	Pyrite	FeS_2	bronze yellow to pale brazz yellow	greenish or brownish black	4.80 – 5.10	46.7

Regarding the chemical structure, there are three solid oxides of iron: hematite (Fe_2O_3), magnetite (Fe_3O_4) and wuestite (FeO) [11,16-22]:

Hematite (Fe_2O_3) is the most important iron oxide containing 70 % Fe. Virtually all Fe in Fe_2O_3 is trivalent Fe^{3+} and it is essentially stoichiometric ($Fe_2^{3+}O_3^{2-}$). Hematite ores have a low content of harmful impurities.

Color: Metallic gray to red
Crystal habit: Tabular to thick crystals
Crystal system: Trigonal – hexagonal scalenohedral
Cleavage: None
Fracture: Uneven to sub-conchoidal
Mohs scale hardness: 5.5 – 6.5
Density: 4.9 – 5.3

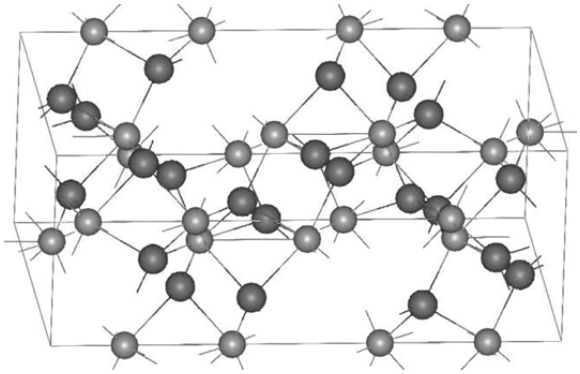

Figure 10: Characteristics and structure of hematite (a-Fe_2O_3), dark grey atoms are oxygen, light grey are iron [23]

Magnetite (Fe_3O_4) is a compound of FeO and Fe_2O_3 (31 % pure FeO) with a total content of 72.4 % Fe, which contains divalent and trivalent iron ($Fe^{2+}Fe_2^{3+}O_4^{2-}$). The ore is rarely pure and often associated with Ti, Mg, Al, Ni, Cr, V or Mn as a spinel crystal structure. Magnetite is characterized by a relatively lower reducibility compared to hematite. It is nearly stoichiometric below 1000°C and has magnetic properties below 570°C.

Color :Black, gray with brownish tint inreflected light
Crystal habit: Octahedral, fine granular tomassive
Crystal system: Isometric Hexoctahedral
Cleavage: Indistinct, parting on {III}, very good
Fracture: Uneven
Mohs scale hardness: 5.5
Density: 5.17– 5.18

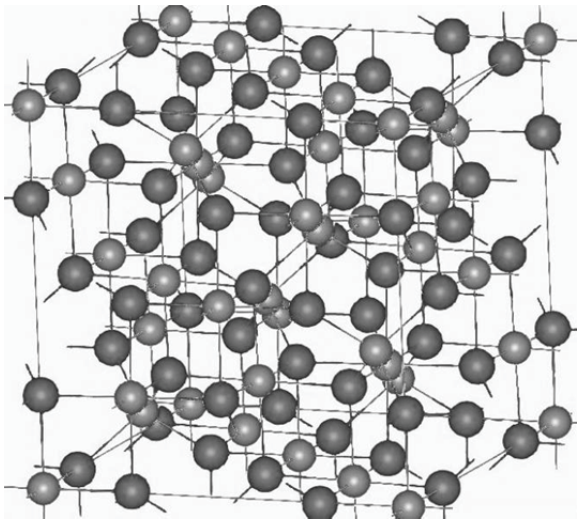

Figure 11: Characteristics and structure of magnetite (Fe_3O_4), light grey atoms are oxygen, dark grey are iron [24]

Wuestite (FeO) is the lowest oxide and is important as an intermediate product during reduction. It is unstable below 570°C, where it decomposes to Fe and Fe_3O_4 (Figure 13). Wuestite exists as a single phase over a range of compositions and is a so called defect mixed crystal with changing amounts of Fe^{2+} and Fe^{3+}-ions, as well as Fe^{2+} vacancies. The wuestite is described by the stoichiometrical formula FeO and is often written as such in thermodynamic discussions, but the chemical denotation of wuestite is $Fe_{1-y}O$, whereas y denominates the iron deficit or the vacancy concentration. The higher the iron deficit (hence, the richer the oxygen content) of the wuestite, the more Fe^{3+}-ions are inclosed in the crystal lattice. With increasing temperature and increasing oxygen partial pressure, the vacancy concentration increases (extension of the wuestite field in the Fe-O phase diagram, cf. Figure

13). The highest Fe content is reached at the equilibrium with metallic iron with an average composition of about $Fe_{0,95}O$.

Color: Greyish white to yellow or brown; colourless in thin section
Crystal habit :Pyramidic,
Crystal system: Cubic
Cleavage: {001} perfect
Fracture: Subconchoidal to rough
Mohs scale hardness: 5 - 5.5
Density: 5.7 g/cm³

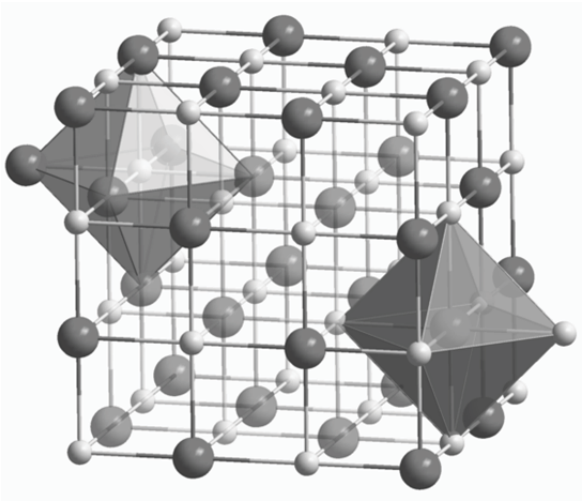

Figure 12: Characteristics and structure of wuestite (FeO):
big atoms are oxygen, small are iron [25]

3.2 Thermodynamics

The Fe-O system (shown in Figure 13) belongs to those phase equilibriums, in which the gaseous phase (in fact the p_{O2}-pressure) plays an important role. The areas of the defect mixed crystals essential for the reduction are magnetite and wuestite [17]. Below 570°C, the so called wuestite temperature, the wuestite is not stable and decomposes to metallic iron and magnetite. From the thermodynamic perspective, the reducibility of oxides or oxide mixtures is defined by their oxygen partial pressures (cf. Figure 13). It can be seen, that the oxygen partial pressure, which is the driving force for the reaction.

$$Me + O_2 \leftrightharpoons MeO_2 \tag{3-2}$$

$$K_p = \frac{a_{MeO_2}}{a_{Me} \cdot p_{O_2}} \tag{3-3}$$

increases with ascending temperature and oxygen content. Every oxide has its own oxygen partial pressure, which is dependent on the temperature and the pressure of the system [17]. The shift of the reaction (3-2) from right to left (i.e. the reduction of MeO_2) can be achieved under the following conditions [11]:

- Shift of the equilibrium by removing of one component at constant value of K_p
- Influencing the equilibrium constants by changing the pressure or temperature of the system

However, this is not possible with iron oxides by physical interventions only, since on the one hand the decomposition temperatures of the oxides at atmospheric pressure are so high, that a technical application would be uneconomical (the decomposition temperature for Fe_2O_3 is 1455 °C at atmospheric pressure). On the other hand, evacuation would only be possible at high vacuum, because of the very low oxygen pressure in the oxides [11,17].

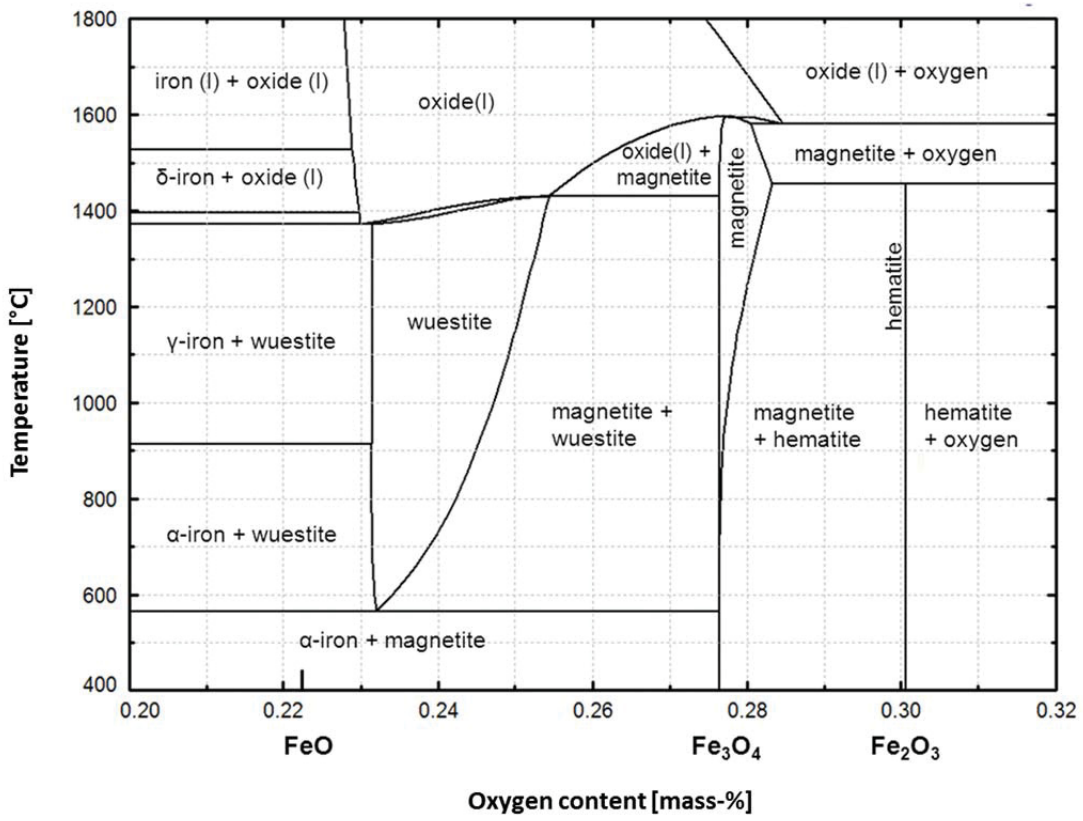

Figure 13: Fe-O phase diagram

In reality, the reduction of the metal oxide can be achieved by adding a solid or gaseous agent (a so called reductant) into the system, which bonds with the oxygen by its own oxidation and is then separated from the system. The reduction is only possible, when the oxygen potential of the reductant is lower than the oxygen potential of the oxide to be reduced. In other words, reduction reactions include two steps: the decomposition of the metal oxide (reduction) and the reaction of the reductant with the released oxygen (oxidation), which can be summarized by a total reaction (cf. equation (3-1)) [4,11,17].

3.2.1 The oxygen potential

As mentioned above, different oxygen partial pressures of gas atmosphere and oxides are responsible for reduction and oxidation. At the chemical equilibrium, the oxygen partial pressures are equal [26]:

$$p_{O_2\,(oxide)} = p_{O_2\,(gas)} \tag{3-4}$$

At different partial pressures, the characteristics of chemical reactions can be calculated by thermodynamic equilibrium conditions. Regrouping the equilibrium constant of equation (3-3) to:

$$p_{O_2} = \frac{1}{K_p} \cdot \frac{a_{MeO_2}}{a_{Me}} \tag{3-5}$$

and including the fact, that oxides or metals contained in the system in pure state have an activity value of one [11], the oxygen partial pressure can be written as

$$p_{O_2} = \frac{1}{K_p} \tag{3-6}$$

Combining this ratio with the standard free energy (Gibbs energy or oxygen potential) [16]:

$$\Delta G° = -R \cdot T \cdot lnK_p \tag{3-7}$$

the relationship can be expressed as [11,16]:

$$\Delta G° = -R \cdot T \cdot ln\frac{1}{p_{O_2}} = +R \cdot T \cdot lnp_{O_2} \tag{3-8}$$

This Gibbs energy (or oxygen potential) characterizes the chemical affinity of an element to oxygen and is valid for every system of an element X and its oxide XO_2 [17]. If ΔG^0 is negative, the reaction can probably occur under proper conditions, whereas a positive value negates the reaction under given conditions and the reverse reaction may take place. So, by means of the oxygen potential, the direction of a reaction can be predicted [11]:

a) If the oxygen potential of the oxide is higher than the one of the reductant, the oxide is reduced.
b) If the oxygen potentials of oxide and reductant are equal, the reaction is in state of equilibrium.
c) If the oxygen potential of the oxide is lower than the one of the reductant, the reduction is not possible.

In other words, a precondition for the proceed of the reduction reaction (here on the basis of equation (3-1) is:

$$p_{O_2\,(RO)} < p_{O_2\,(Me_xO_y)} \quad or \quad \Delta G°_{(RO)} < \Delta G°_{(Me_xO_y)} \tag{3-9}$$

Richardson and Jeffes summarized the oxygen potentials of different oxide systems for solid and liquid phases in the so called Richardson-Jeffes-Diagram (also known as Richardson-Ellingham-Diagram). This diagram is used to illustrate stability areas of metal oxides in dependence on the oxygen potential and the temperature.

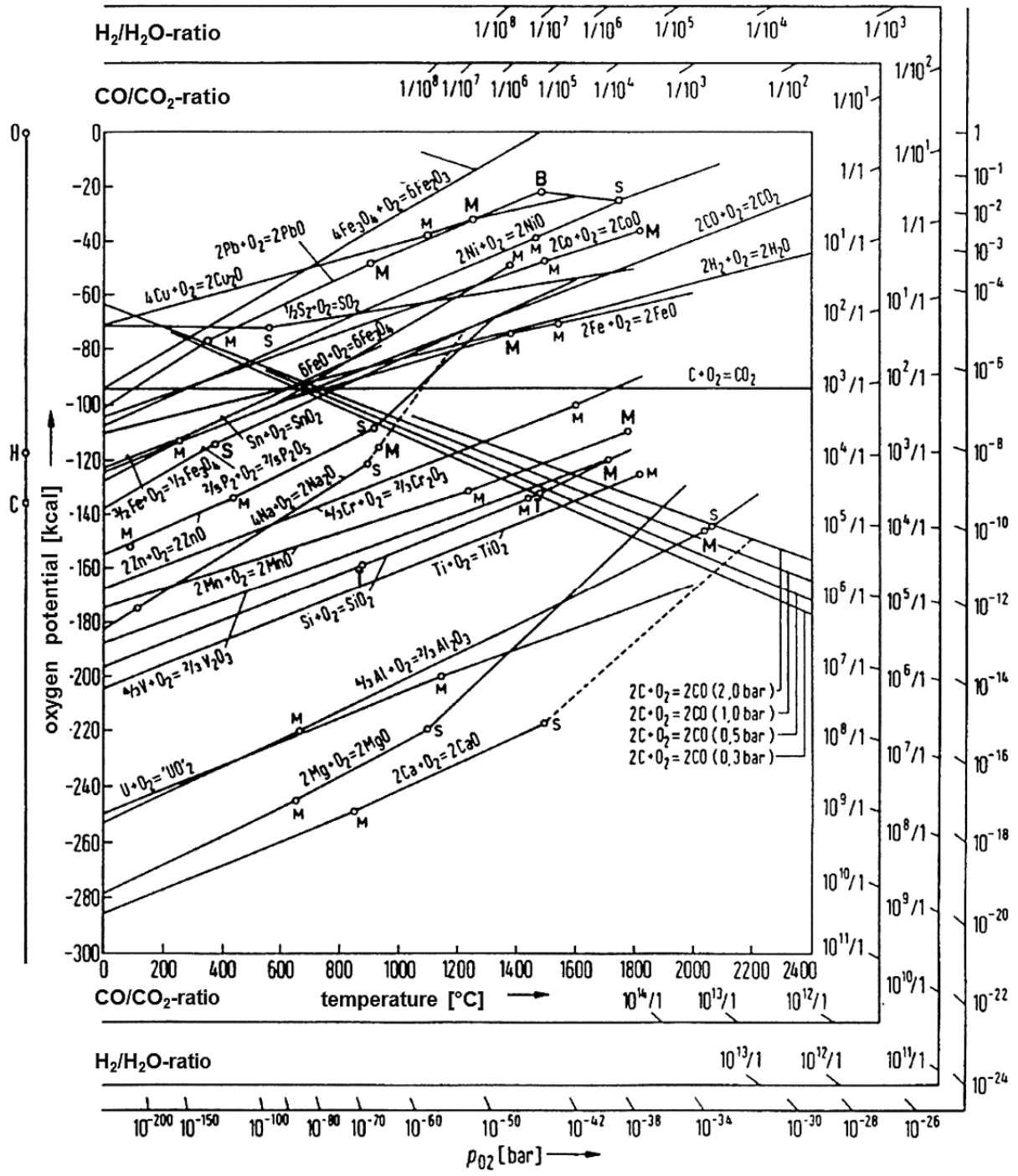

Figure 14: Richardson-Jeffes-Diagram, according to [11]

As seen in Figure 14, the stability of the different oxides increases with decreasing oxygen potential. Almost every potential line shows the same inclination, because of the very similar Entropy-values. The oxygen potential increases with increasing temperature, except carbon. Carbon is able to reduce most of the oxides under blast furnace conditions. Carbon monoxide, as well as hydrogen are also important reductants. Their oxygen potential rises with increasing temperature [11,17].

3.2.2 The indirect reduction of iron oxides

The French Meallurgist Jaques Assenfratz suggested a classification of iron ore reduction based on the type of reducing agent in 1812. The reduction by carbon with formation of CO as final product is called “direct reduction” (contact of ore with charcoal), whereas the reduction by reducing gases (carbon monoxide and hydrogen with formation of CO_2 and H_2O as final procucts) is called “indirect reduction”. The sum of direct and indirect reduction in a reduction process is 100 % [11,27]. For reduction processes in a fluidized bed, the reducing reactions caused by the reaction of the iron oxide phases with the gases CO and H_2 is important [4]. Oxygen is thereby removed progressively from the iron oxides Fe_2O_3 (hematite), Fe_3O_4 (magnetite) and $Fe_{1-y}O$ (wuestite), in order to achieve finely metallic iron [11]:

at T > 570°C: $$Fe_2O_3 \rightarrow Fe_3O_4 \rightarrow FeO \rightarrow Fe \quad (3\text{-}10)$$

at T < 570°C: $$Fe_2O_3 \rightarrow Fe_3O_4 \rightarrow Fe \quad (3\text{-}11)$$

The following simplified chemical equations describe the development of the so called “indirect reduction” (reduction with CO and H_2). Hematite (Fe_2O_3) is reduced to magnetite (Fe_3O_4) as follows [1,11,28]:

$$(3-\delta)\,Fe_2O_3 + (1-3\delta)\,CO \leftrightharpoons 2\,Fe_{3-\delta}O_4 + (1-3\delta)\,CO_2 \quad \Delta H = +52.85\ kJ/mol \quad (3\text{-}12)$$

$$(3-\delta)\,Fe_2O_3 + (1-3\delta)\,H_2 \leftrightharpoons 2\,Fe_{3-\delta}O_4 + (1-3\delta)\,H_2O \quad \Delta H = -11.59\ kJ/mol \quad (3\text{-}13)$$

At temperatures above 570°C the magnetite (Fe_3O_4) is reduced to wuestite ($Fe_{1-y}O$), whereas y has a value of about 0.05 to 0.12:

$$(1-y)\,Fe_3O_4 + (1-4y)\,CO \leftrightharpoons 3\,Fe_{1-y}O + (1-4y)\,CO_2 \quad \Delta H = +36.46\ kJ/mol \quad (3\text{-}14)$$

$$(1-y)\,Fe_3O_4 + (1-4y)\,H_2 \leftrightharpoons 3\,Fe_{1-y}O + (1-4y)\,H_2O \quad \Delta H = +77.59\ kJ/mol \quad (3\text{-}15)$$

The reaction from wuestite to metallic iron is:

$$Fe_{1-y}O + CO \leftrightharpoons (1-y)Fe + CO_2 \quad \Delta H = -17.13\ kJ/mol \quad (3\text{-}16)$$

$$Fe_{1-y}O + H_2 \leftrightharpoons (1-y)Fe + H_2O \quad \Delta H = +24.00\ kJ/mol \quad (3\text{-}17)$$

Below 570°C wuestite is not stable and magnetite is directly reduced to metallic iron.

$$Fe_3O_4 + 4\,CO \leftrightharpoons 3\,Fe + 4\,CO_2 \quad \Delta H = -14.92\ kJ/mol \quad (3\text{-}18)$$

$$Fe_3O_4 + 4\,H_2 \leftrightharpoons 3\,Fe + 4\,H_2O \quad \Delta H = +149.57\ kJ/mol \quad (3\text{-}19)$$

Here also a degradation of wuestite takes place: $4\ FeO \rightarrow Fe_3O_4 + Fe$

The reduction of hematite is irreversible, whereas the reduction steps from magnetite to wuestite and further to metallic iron are reversible and temperature dependent. Compared to hematite, the oxygen potentials of these oxides are lower [11]. From a thermodynamic point of view the gas reduction process is independent from the gas pressure, because the gas

volume does not change. The chemical equilibriums of equations (3-12) to (3-19) as well as their temperature dependency can be described graphically by means of the “Baur-Glaessner-Diagram” (cf. Figure 16).

3.2.3 Equilibrium Diagrams for carbon monoxide and hydrogen atmospheres in the system Fe-C-O_2-H_2

The system Fe-C-O_2-H_2

In Figure 15 the system Fe-C-O_2-H_2 with the chemical equilibria of the iron oxide phases is pictured. Depending on the gas composition and temperature, different regions of the individual solid iron oxide and iron phases (Fe_2O_3, Fe_3O_4, FeO, Fe) can be distinguished. In the system Fe-C-O_2 and Fe-H_2-O_2 the Baur-Glaessner-diagrams are shown for CO/CO_2 and H_2/H_2O as reducing gases respectively.

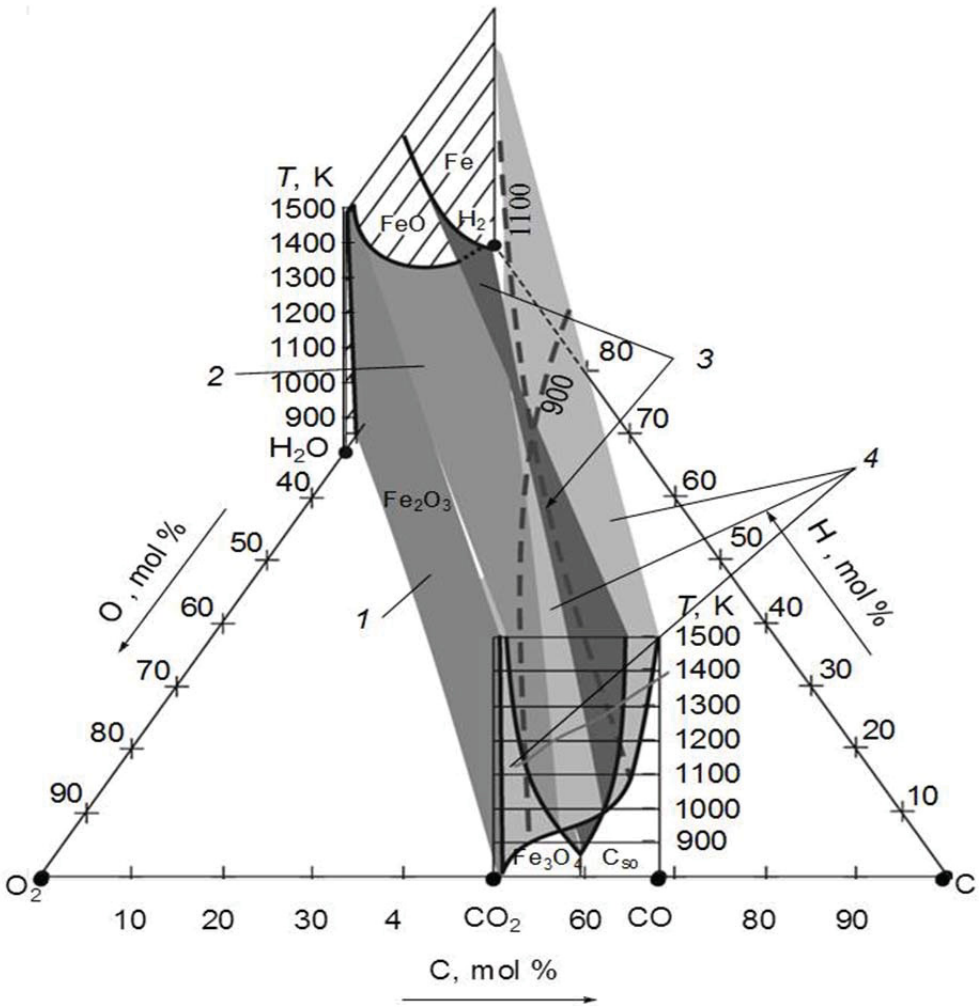

Figure 15 : Diagram of phase–chemical equilibria in the Fe–C–O_2–H_2 system. Three phase equilibrium surfaces: (*1*) Fe_2O_3–Fe_3O_4–gas; (*2*) Fe_3O_4–FeO–gas; (*3*) FeO–Fe–gas; (*4*) Fe–Cso–gas; (- - - -) isotherms of carbon deposition surface [29]

Baur-Glaessner-Diagram

The Baur-Glaessner-Diagram can be deduced from the Richardson-Jeffes-Diagram and describes the system Fe-O-C (cf. Figure 16). This diagram shows the regions of stability of the iron oxide phases dependent on the temperature and the reducing gas composition (cf. Figure 15). It can be employed for gas mixtures of CO/CO_2 and H_2/H_2O respectively (cf. Figure 17). For every reduction reaction, the equilibrium composition in presence of CO/CO_2 and H_2/H_2O can be read off as a function of the temperature [30].

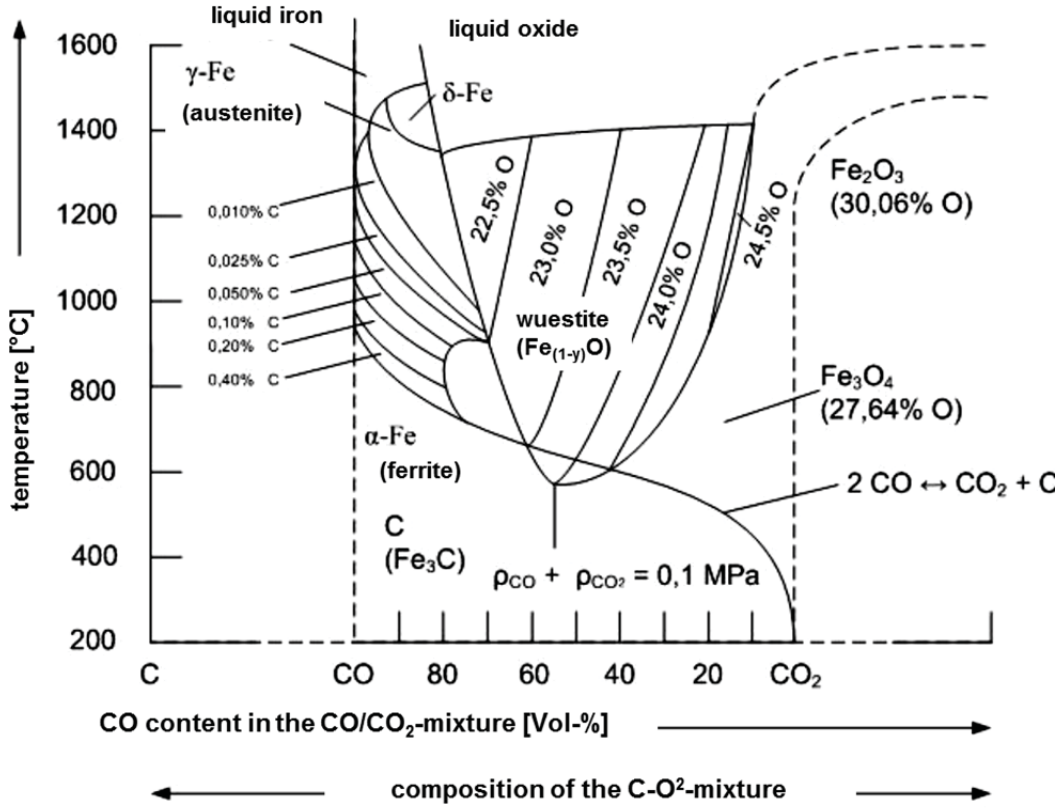

Figure 16: Baur-Glaessner-Diagram for CO/CO_2 atmospheres according to [152]

The solid line refers to pure CO as a reduction gas and the dashed line refers to H_2 as a reduction gas respectively. An important chemical equilibrium is the Boudouard curve with the chemical reaction

$$2CO \leftrightharpoons C + CO_2 \qquad \Delta H = +172.45\ kJ/mol \tag{3-20}$$

representing the CO/CO_2 ratio in the gas mixture. This pressure-dependent equilibrium divides the Baur-Glaessner diagram into two regions. At gas conditions and temperatures above this curve, the reduction is supported due to CO-formation if carbon is present, below the curve CO decomposes to CO_2 and carbon. The Boudouard reaction is pressure dependent because of the different mole ratio of CO and CO_2. Corresponding to LeChatelier's principle, an increase of pressure removes the equilibrium to CO_2 and, hence, the curve to higher temperatures.

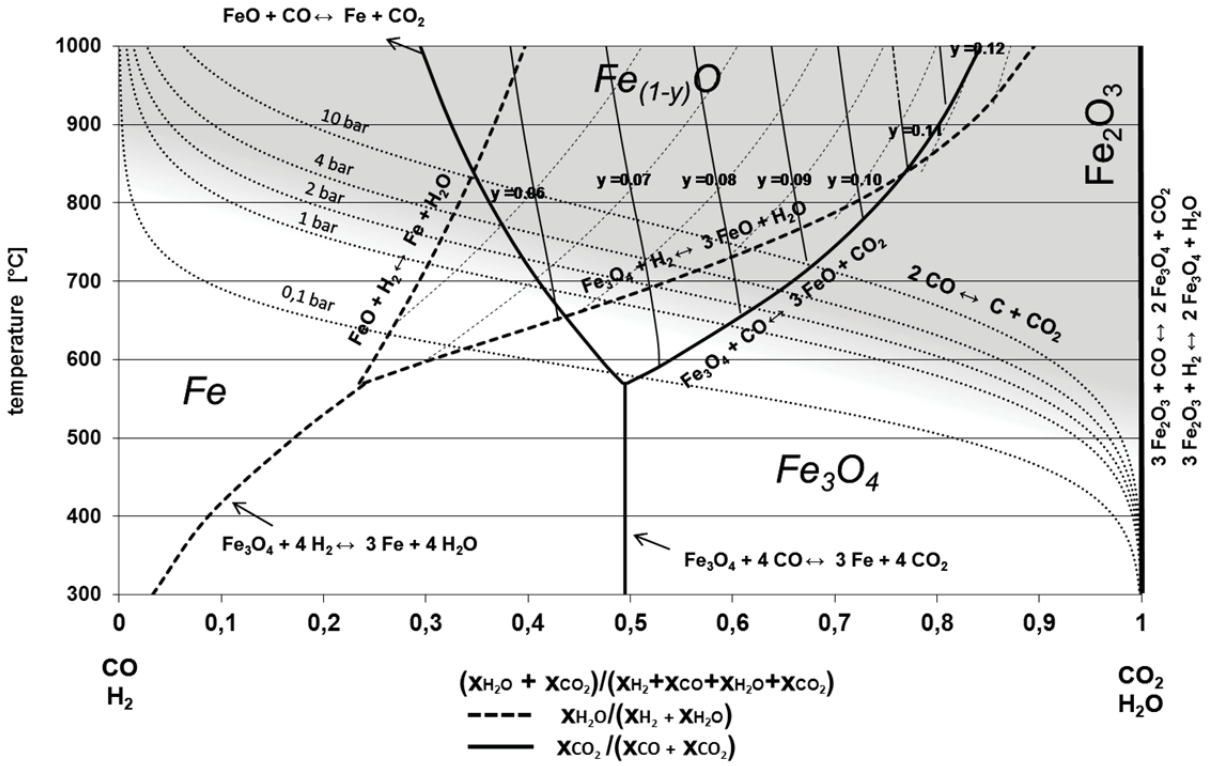

Figure 17: Baur-Glaessner for gas mixtures of H_2/H_2O and CO/CO_2

The equilibrium lines of equations (3-12) and (3-13) coincide with the vertical line at GOD = 1 (Figure 17), because small amounts of CO and/or H_2 in the gas mixture lead to the reduction of hematite to magnetite. The minimum temperature for indirect reduction to iron is defined with the intersection point of the Boudouard-curve with the Fe/FeO equilibrium curve at about 700°C under atmospheric conditions. The endothermic reactions of H_2/H_2O gas mixtures are more efficient with increasing temperature. Comparing the equilibrium lines of the iron oxides with CO/CO_2 and H_2/H_2O gas mixtures, it can be figured out which of the reducing gases is the most efficient at a certain temperature. At 811 °C, CO and H_2 have the same reduction potential [4].

The reducing gas composition can be described by the so called GOD (Gas Oxidation Degree), as well as the GUD (Gas Utilization Degree) and can be calculated as follows [30]:

$$GOD = \left(\frac{x_{H_2O} + x_{CO_2}}{x_{H_2} + x_{H_2O} + x_{CO} + x_{CO_2}}\right) \quad (3\text{-}21)$$

$$GUD = \left(\frac{x_{H_2} + x_{CO}}{x_{H_2} + x_{H_2O} + x_{CO} + x_{CO_2}}\right) \quad (3\text{-}22)$$

With x_i, molar ratio of the gas component i

These numbers are ratios describing the chemical conversion (gas utilization) and represent the reduction force of the gas mixture. The reduction force is increasing, when GOD decreases or GUD increases. The gas utilization is important for the efficiency of a reduction process, where a high value is aspired.

For illustration, a three-dimensional Baur-Glaessner-Diagram with changing $CO/CO_2/H_2/H_2O$ gas compositions is shown in Figure 18. Beginning with the equilibrium diagram of CO/CO_2, the H_2/H_2O equilibrium diagram appears stepwise as a consequence of the decreasing partial pressures p_{CO} and p_{CO2}.

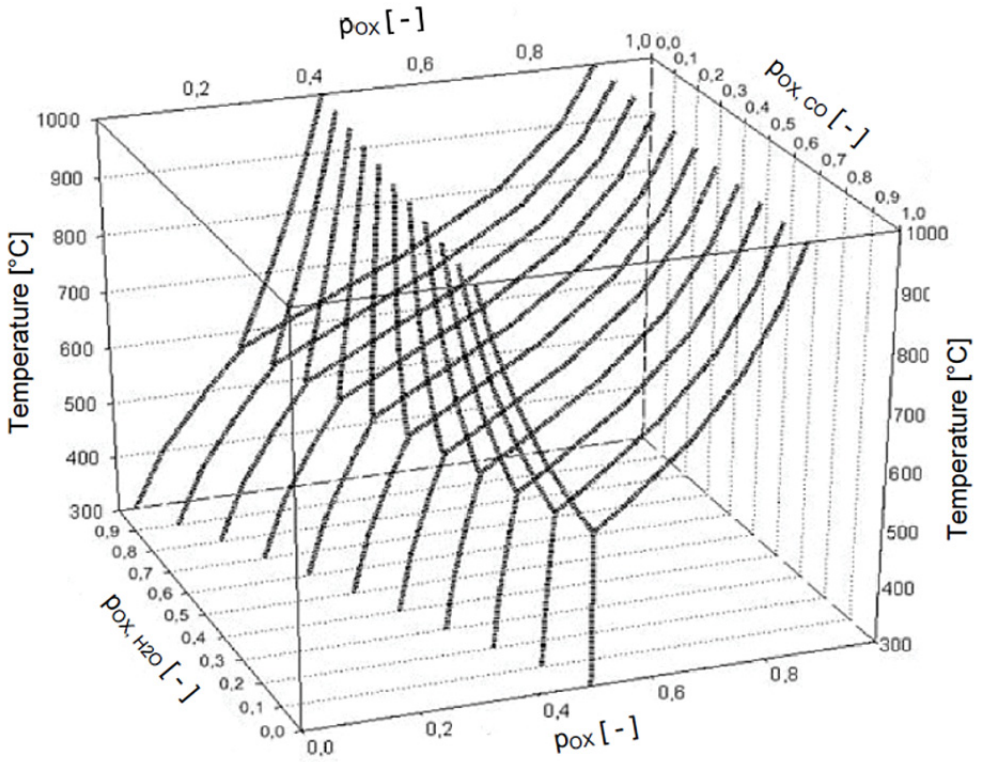

Figure 18: Equilibrium diagram for gas mixtures of H_2, H_2O, CO and CO_2 [28,31]

Rist-Diagram

Another characteristic diagram is the Rist-diagram, a phase diagram for the analysis of mass balances of reduction processes considering the thermodynamical equilibrium of the iron oxide reduction [30] and goes back on a series of papers published by Prof. André Rist et al. in the 1960s [11,32-36]. This diagram represents a stability diagram for iron and iron oxide phases in dependence on the gas mixture CO/CO_2 at a defined temperature, hence, the system Fe-O-C.

The x-axis shows the molar ratio O/C. At ratios up to one, direct reduction occurs. If the ratio is one, the carbon is completely converted to CO (GOD = 0 %). When the ratio is two, the carbon is converted completely into CO_2 (GOD = 100 %) [30].

The y-axis shows the molar ratio O/Fe, representing the oxygen/iron ratio of the different iron oxide reduction steps. Hematite is represented with the ratio O/Fe = 1.5, magnetite with O/Fe = 1.33 and wuestite with O/Fe = 1.05. The oxygen/iron ratio of the wuestite is higher than one, because of the iron deficit in the chrystal lattice of the wuestite.

The relationship shows the exchange of oxygen atoms and carbon during reduction (or the exchange of oxygen between iron oxides and the reduction agent [30]) and is called the

“operating line”. The slope of this line C/Fe is the so called “reducing agent rate” [11]. In Figure 19 the Rist-diagram for the system Fe-O-C and its relationship to the Baur-Glaessner-diagram is shown.

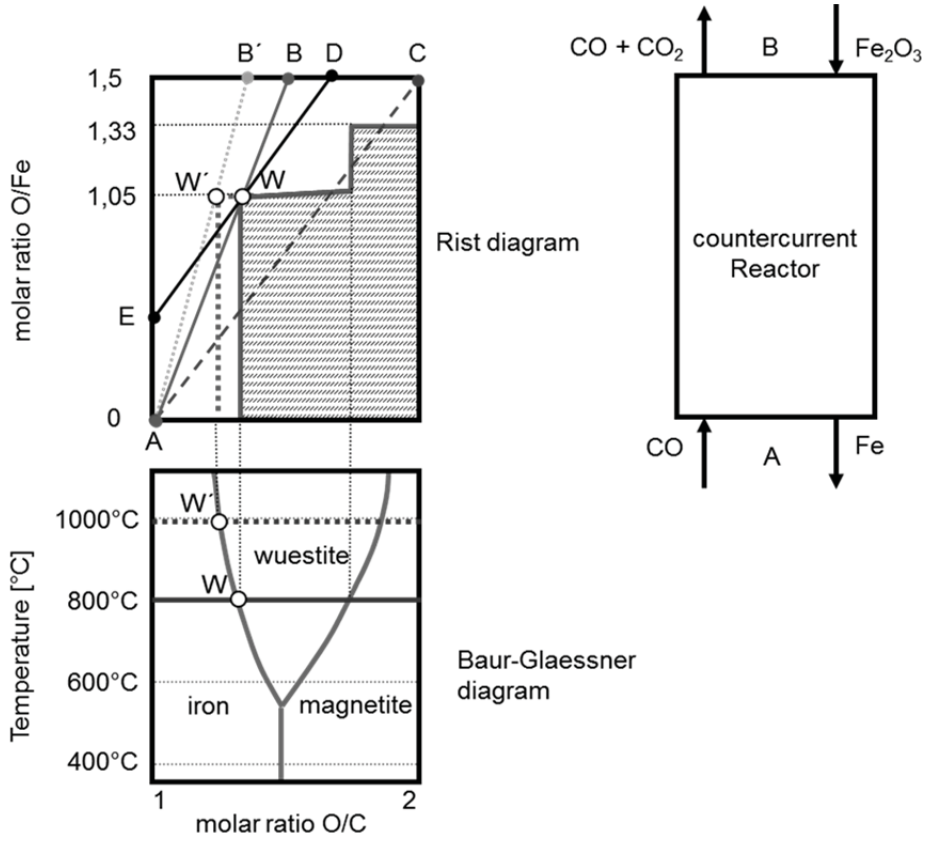

Figure 19: Rist-diagram and its relationship to the Baur-Glaessner-diagram, according to [30]

Line AB represents the operating line of an ideal reduction process, which reduces hematite with pure CO at 800°C completely to iron in a countercurrent flow reactor by means of indirect reduction. Point A relates to the gas mixture of the reduction agent and the composition of the final product (pure iron), whereas point B is representing the gas mixture at the discharge and the iron oxide at the charging point [30].

The so called “W-point” is projects the coexistence line of Fe and FeO (wuestite) at a certain temperature [11]. By shifting the W-point right and/or downward, the slope of the operating line and, hence, the reducing agent rate decreases. If the countercurrent process was processed at 1000 °C, the W-point would move to the left to W’ (operating line AB’). Under these conditions, the slope of the operating line and, hence, the reducing agent rate increases. The O/C-ratio at the discharge decreases at the same time [11,30].

The W-point limits the countercurrent process by means of thermodynamical constraints. An operating line on the right of W is thermodynamically impossible. For example, the operating line AC would require the lowest amount of reducing agents (due to stoichiometrical constraints), but the required gas mixtures for the countercurrent process are thermodynamically impossible. In some regions, wuestite had to be reduced to iron by a gas mixture with an excessive CO_2 content. The same is valid for the reduction of magnetite to wuestite. In regard to the minimum reduction agent use, the theoretically achievable operation line is ED at 800 °C. Under these conditions, hematite would just be reduced to an

amount of about 50 % to metallic iron and wuestite [30]. In this conjunction, operating lines of real processes need to keep a distance to the W-point, because the thermodynamical equilibrium cannot be reached.

For reduction processes containing also H_2 as reduction agent, a modified Rist-diagram representing the system Fe-C-O-H can be used [8,11] (i.e. for processing of coal or hydrogen containing gas). In this case (cf. Figure 20), the x-axis represents the molar ratio $(O+H_2)/(C+H_2)$. Tue to theoretical reasons, the y-axis is representing the molar ratio $(O+H_2)/Fe$, which is – due to the low H_2 content in iron ores – negligible [8,11].

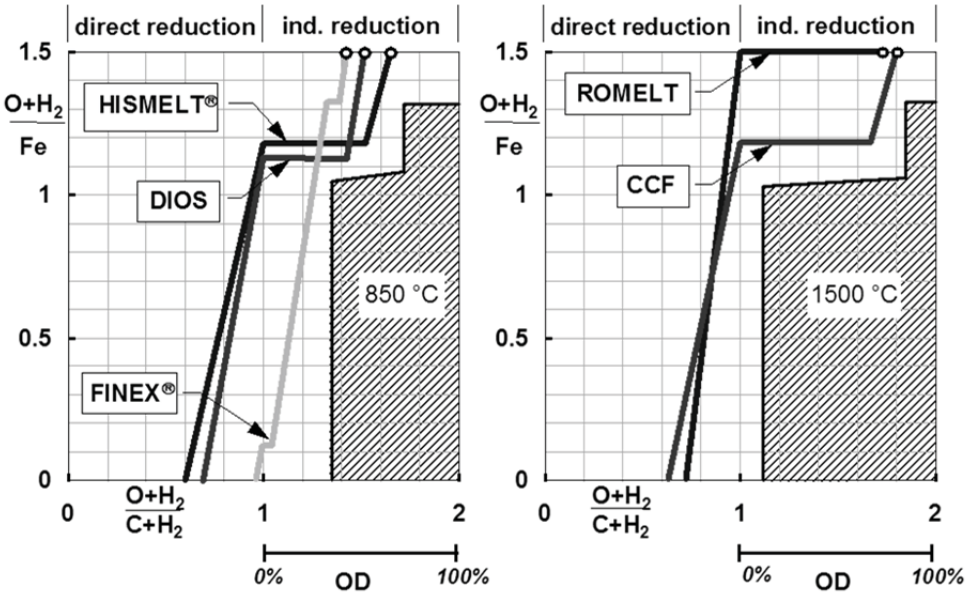

Figure 20: Modified Rist-diagram for the F-C-O-H system with examples, according to [10]

3.2.4 Reduction Degree and Metallization Degree

Based on the chemical analyses of the reduced samples the following formulas are used for the determination of the reduction degree (RD) and the metallization degree (MD). For the calculation of reduction and metallization degree, O (oxygen content), Fe_{tot} (total iron content) and Fe_{met} (metallic iron content) have to be converted into molar fractions [30].

$$RD = \left(1 - \frac{X}{1.5}\right) \cdot 100 \qquad with \quad X = \frac{O}{Fe_{tot}} \qquad (in\ \%) \tag{3-23}$$

$$MD = \frac{Fe_{met}}{Fe_{tot}} \cdot 100 \qquad (in\ \%) \tag{3-24}$$

Hence, the reduction degrees of the pure iron oxide phases are as follows:

Fe_2O_3	RD = 0 %
Fe_3O_4	RD = 11.1 %
FeO	RD = 33.3 %
Fe	RD = 100 %

The coherence between RD and MD is shown in Figure 21. Up to a RD < 33.3 % the oxygen is reduced from the iron oxide lattice and no metallization occurs. Theoretically the whole iron exists as FeO. With further reduction of oxygen and the increase of RD > 33.3 % metallic iron is built. This metallization degree can also be calculated as follows [30]:

$$MD = \frac{RD - 33.3\%}{66.6\,\%} \cdot 100 \qquad \textit{(RD in \%)} \tag{3-25}$$

This equation shows the theoretically ideal coherence between RD and MD and is just valid when the reduction step of every iron oxide phase has completely finished, before the reduction of the next oxide phase starts. In reality, thermodynamic, kinetic and morphologic issues are influencing the reduction progress of the iron oxide phases. So, a reduced iron ore sample with a reduction degree of about 33 % can exist on the one hand as pure FeO (MD = 0 %), on the other hand as a mixture of Fe_2O_3, Fe_3O_4, FeO and metallic iron (MD > 0 %) [30].

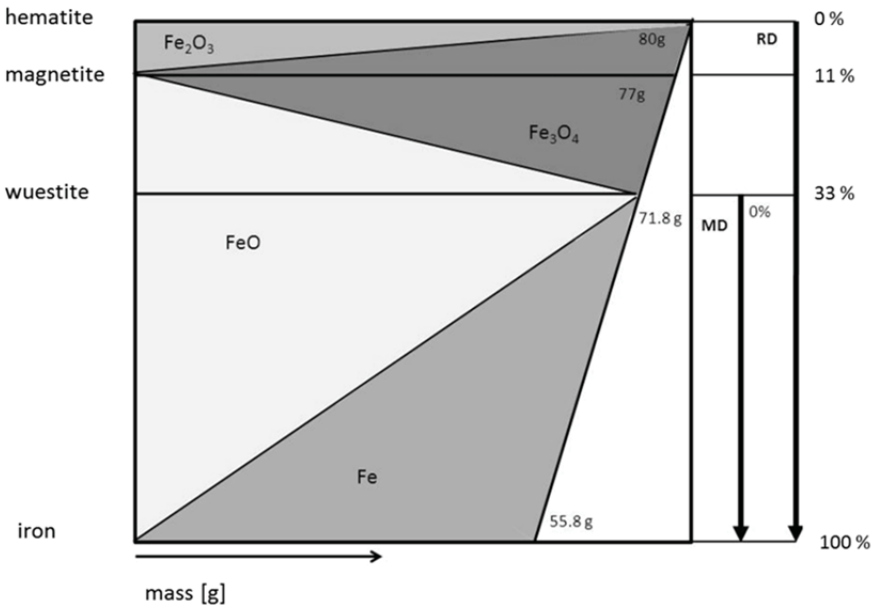

Figure 21: Correlation between RD and MD [37]

3.3 Reduction Kinetics

The reduction kinetics of iron ores deals with the rate at which iron ores or iron oxides are transformed to metallic iron by removal of oxygen [16,17].

The final equilibrium condition of a reaction can be described using thermodynamic information, but thermodynamics cannot predict the rate of reaching the equilibrium state [16]. To understand these kinetics of iron ore reduction, the complex transformation mechanisms from iron ore and its oxides to metallic iron by gaseous reductants have to be considered [16,30].

The crystal lattice of the iron oxides determines the level of difficulty with which oxygen can be removed from the iron ore by the reducing gases. This ore-property is often referred to as the reducibility, which generally depends on particle size, shape, porosity, crystal structure

particle- and pore size distribution and gangue content [16]. Due to these widely ranging properties of solid raw materials, a high number on influential parameters are a result [28].

3.3.1 Heterogeneous solid-state reduction of iron ores

Regarding kinetics, chemical reactions can be either homogeneous (single phase, no phase-transformation) or heterogeneous (two or more phases, with phase transformation) in solid or liquid state [11,17]. The reduction of iron oxides in solid state represents heterogeneous reactions with solid phases and gas phases, which are separated by an interface [16].

The reactants, existing in different phases, have to be transported to a common reaction location. The reaction progress can be explained by four essential phenomena, which are assumed from [11,17,30,38,39]:

I. Transport of the reaction partners (reducing gases CO, H_2) with the gas flow and diffusion through the fluid film to the macroscopic interface of the iron ore particle.

   The diffusion through the fluid film can be determined by the partial pressure difference.

II. Transport of the reaction partners by diffusion phenomena through macro- and micropores to the reaction front and evacuation of the reaction products (oxidized gases CO_2, H_2O).

   Diffusion in macro- and micropores may be assumed to take place in the steady state for short time spans (i.e. a few seconds to several minutes, depending on the reduction stage). Porosity and grain boundaries highly increase the diffusion of solid state species. The temperature dependence of diffusion in macropores is higher than in micropores.

III. Reaction of the reducing gases and solid oxides at the phase boundary.

   During reduction of hematite ($FeO_{1,5}$) to wuestite ($FeO_{1.05}$) only ca. 1/3 of the total removable oxygen is reduced, whereas during the reduction step from wuestite ($FeO_{1.05}$) to metallic iron ca. 2/3 has to be eliminated. So, the final reduction step to Fe is slower than the former steps. In order to simplify the process with regard to kinetics, the last step can be solely taken into account, because the margin of error is small. Additionally it can be assumed, that porous iron is formed during reduction and during the entire process, the reducing gas has access to a portion of the oxide surface. The reaction kinetics of pure H_2 is one order of magnitude higher compared to pure CO, and with increasing temperature, the rate of the chemical reaction increases (regarding the Arrhenius Law).

IV. Formation of new solid phases (lower iron oxides or metallic iron) resulting from the removal of oxygen and the subsequent transport phenomena.

   The iron oxides hematite ($FeO_{1.5}$), magnetite ($FeO_{1.33}$) and wuestite ($FeO_{1.05}$) feature a close-packed oxygen-ion structure with tetrahedral and octahedral interstices. These interstices are occupied with Fe^{2+} and Fe^{3+} ions. During transformation from hematite to magnetite, the oxygen ions have to be redistributed from the hexagonal to

the face-centered cubic structure. The transformation from magnetite to wuestite refers no rearrangement of oxygen ions, here only the ratio iron/oxygen is changing.

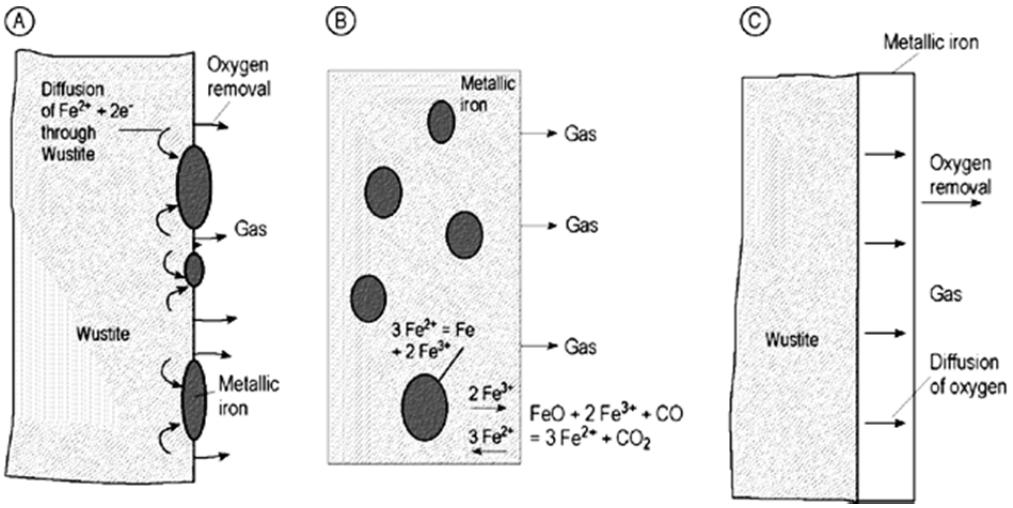

Figure 22: Reduction morphology of wuestite reduced to metallic iron [21]
A) Formation of iron nuclei at the surface
B) Formation of nuclei within the iron oxide lattice
C) Formation of a metallic surface

The formation of new phases depends on the nucleation and new surfaces are formed, which requires energy. The type of nucleus formation is depending on the oxide-structure and the reduction force of the gas mixture. Regarding the final and slowest reduction step from wuestite to iron, three different reduction types are observable (cf. Figure 22):

A represents the formation of lense-shaped segregations of iron at the wuestite surface. B shows the formation of spherical or lense-shaped segregations within the iron oxide lattice. In both cases, a porous wuestite structure is a precondition. C represents the formation of a dense iron layer at the oxide's surface, resulting from a dense wuestite structure. This layer is a barrier for the reduction gas. In this case, the reduction of the wuestite depends on the diffusion of the oxygen-ions through the iron layer. Due to the low solubility of oxygen in metallic iron, the diffusion velocity of oxygen in iron is very slow and hence, reduction type C is slower than A and B.

3.3.2 Reduction mechanisms of iron ore solid-state reduction

The phenomenas discussed above can be split into a sequence of sub-steps to illustrate the whole reduction sequence (cf. Figure 23), corresponding to [4,28,38,40-43]:

1) Mass transfer of the gas species (reducing gases CO, H_2) from the gas stream through the laminar layer (fluid film) of the iron oxides to the interface (I)

2) Diffusion of the reducing gas through macro- and micropores (cracks, pores and grain boundaries are filled) (II)
3) Adsorption of the gas molecules at the oxide's sufaces
4) Phase boundary reaction: oxygen is removed from the crystal's surface by the reductants, building iron iones and leaving vacancies, which are balanced by solid state diffusion (III)

$$H_2 + O^{2-} \leftrightharpoons H_2O + 2e^- \quad (3\text{-}26)$$

$$CO + O^{2-} \leftrightharpoons CO_2 + 2e^- \quad (3\text{-}27)$$

$$Fe^{2+} + 2e^- \leftrightharpoons Fe^0 \quad (3\text{-}28)$$

5) Desorption of the gaseous reaction products CO_2 and H_2O
6) Solid phase diffusion of the solid reaction products to the nuclei; nucleation and growth of the solid products (IV)
7) Diffusion of the gaseous reaction products through micro- and macropores (II)
8) Mass transfer of the gas species through the laminar layer to the gas stream (I)

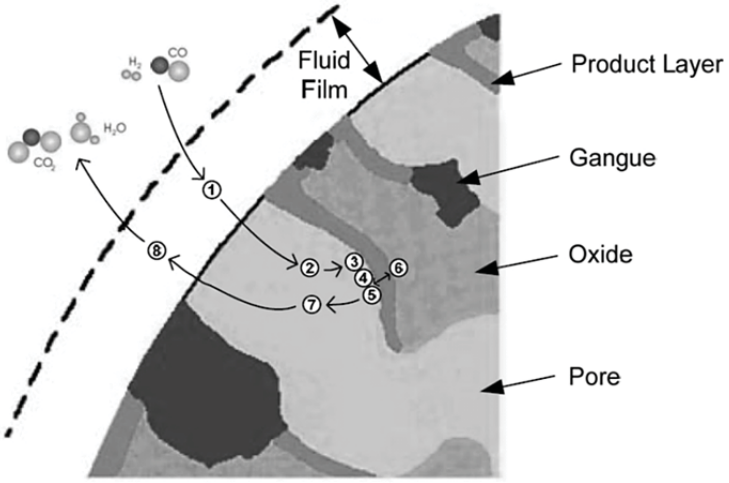

Figure 23: Reduction mechanisms of a porous iron ore particle reduced by a gaseous reductant [28,44]

3.3.3 The rate limiting step – control types

The slowest step in the reaction process phenomena determines the overall reaction rate and becomes the rate limiting or rate controlling step [16,17,28,45]. Based on the assumption, that the chemical reaction is highly temperature sensitive, this reaction seems to be the rate controlling step at lower temperatures. As the reaction rate accelerates exponentially with increasing temperature, the mass transfer mechanisms are assumed to be the rate controlling steps at high temperature [46,47]. Regarding this limiting step, a series of control types can be differentiated [17]:

- Phase controlled reaction (also known as transport controlled reaction):

The reaction kinetics are extensively faster than the transfer of the reductants or reaction products. An additional differentiation is possible regarding the determining phase (metal-phase or slag-phase).

- Reaction controlled total-reaction (also phase boundary controlled reaction):

  The transfer of the reductants or reaction products is substantially faster than the mass transfer of the phase boundary reaction.

- Mixed controlled total-reaction:

  Is the indication for a reaction type, where kinetics of the phase boundary reaction are approximately as fast as the transfer of reductants or reaction products.

More detailed informations regarding reaction kinetics, especially kinetics of iron ore reduction, can be found in [16,17,28,45-47].

3.4 Sticking – procedural problems in reduction processes

During the indirect reduction of iron ores, mainly iron ore fines in a fluidized bed, different procedural problems can occur. An unrequested activity during reduction is the so-called “sticking”. Sticking describes the agglutination, or also agglomeration of reduced iron ore particles at temperatures above 600 °C [4]. Sticking causes insufficient mass transfer between reduction gas and solid phase, which can lead to an agglomerated fixed bed with gas flow channels and from there to a breakdown of the fluidized bed. This involves a longer residence time as well as a lower throughput rate with lower quality of the DRI [48-50]. To avoid or minimize sticking, many different parameters (and their interaction) have to be considered:

- Temperature
- Composition and velocity of the reducing gas
- Consistency of the iron ore
- Grain size
- Particle surface
- Impurities and additives
- Reduction sequences

To gain a better understanding of the impacts of these parameters, different kinds of sticking have to be differentiated. However, according to different authors [50-52], the segregation of metallic iron is a precondition for sticking. The segregation type also plays an important role [52-56]. Regarding Gudenau et al., three possible types of sticking can be identified [4]:

- **Type 1 sticking** [50,52,57]:

  Type 1 sticking occurs at temperatures above 600 °C. The generated whiskers can interlock and agglomerate, mainly during reduction with CO and H_2 (H_2 only in

conjunction with sulfur). Conditions: good diffusion and low reduction rate. Segregation mode: Fibrous iron segregations (“whiskers”)

- **Type 2 sticking** [50,52,57-59]:

  Type 2 sticking is caused by the higher activity of the fresh segregated iron compared to the previously segregated iron. The reason is the higher adhesion-force between the iron ore particles, caused by the higher activity. Thereby the particles agglomerate, especially at high temperature and reduction rate. Due to the high reduction rate in presence of hydrogen, this type is dominating in H_2-rich gas mixtures.

- **Type 3 sticking** [50,57]:

  At temperatures above 850 °C liquid phases can occur. Low melting eutectica lead to an agglomeration of the iron ore particles. Regarding Fang [50] this type is present at RD`s above 33 %, because FeO is a precondition for this type of sticking. Anyhow, this statement is doubtful, because FeO is present at RD’s from about 11 %. In a fluidized bed for direct reduction of iron ore fines, usually high quality ores with low impurities are used. Hence, type 3 sticking is unusual.

Because of the interaction of the different parameters, sticking is very difficult to predict. Langston [60] proposes the following formula:

$$S = A \cdot \frac{B}{C} \tag{3-29}$$

S……. sticking grade

A…… adhesion-force on the surface of the particles

B……. contact area between two particles at collision

C…….. impulse of the particles caused by the gas velocity

Furthermore it can be stated, that all conditions which benefit a fibrous growth of the iron layer, also benefit type 1 sticking.

Influence of the reduction gas:

The two main sticking mechanisms during reduction with a CO-rich gas mixture are type 1 and type 2 sticking [50,52]. Under these conditions many ores build whiskers at temperatures between 650 °C and 900 °C. Also type 2 sticking can occur.

During reduction with H_2-rich gas mixtures, type 1 sticking only occurs in presence of sulfur. Reason is the adsorption of sulfur on the wuestite-surface and the difficult oxygen reduction caused by this. There are less nucleation areas and whisker growth arises. The main sticking mechanism during H_2 reduction is type 2 sticking [50,52,57], because the reduction rate and hence the percentage of freshly segregated iron increases. Adding just small amounts of H_2 to a CO/CO_2-mixture, dense segregation increases and the formation of whiskers decreases [61].

Influence of temperature:

Sticking mainly occurs at temperature ranges from 600 and increases up to a temperature of 900 °C [62]. Below 850 °C sticking only occurs at RDs above 33 % [50,51,63]. The fact, that metallic segregation is a pre-condition for sticking confirms this theory. Above 900 °C sticking is overlayed with recrystallization activities. The reduction degree for the appearance of sticking is influenced by the reduction temperature. For example: a certain iron ore type can be reduced at 700°C with reduction degrees up to 54 %, while at 800 °C sticking problems occur at reduction degrees of 36 %. So, the reduction degree at which sticking begins, decreases with increasing temperature [64].

Influence of iron ore and iron ore type:

Magnetite shows a stronger tendency of dense iron segregation than hematite. On the other hand, hematite shows a higher rate of crystal defects, which increases the fibrous iron segregations and causes sticking [65]. Also iron ore minerals show significant differences: some ores can be reduced up to a rate of 94 % at about 850 ° C without difficulty, while others have massive problems at reduction degrees of about 70 % [51,63,66].

Influence of grain size:

The smaller the iron ore particles are, the higher the tendency of sticking. At small grain sizes, the probability of a sufficient collision time (for agglomeration) increases due to the larger surface area [67,68]. The fine particles also have less kinetic energy [64].

Influence of flow rate:

The rejection-force between the particles increases in proportion to the flow rate. A higher amount of segregated metallic iron is necessary for the agglomeration. Hence, at higher flow rates the starting point of sticking moves to higher reduction degrees and higher temperatures [64].

Influence of additives:

Additives can be enclosed in the iron ore mineral (as gangue), or they can be added into the reduction process. Their influence on sticking is versatile. In dissolved condition, additives influence the segregation behavior, because diffusion and nucleation energy is changing [69].

- MgO: the complete dissolubility of MgO in wuestite leads to MgO-poor segregations on the particle surface [64,70]. The consistent nucleation on the surface assists the dense iron segregation and reduction degrees up to 94 % are possible.
- CaO leads to fibrous segregations (opposite to MgO). The segregation time decreases in presence of CaO [71], but the fast whisker growth causes sticking problems [72].
- SiO_2 has a small dissolubility in wuestite and fayalite segregates [73]. Fayalite leads to a reduction slowdown in presence of H_2 [71], while reduction rate increases in presence of CO.
- Coal (char): According to Fang and Komatina [52,74], a mixed fluidized bed of iron ore and coal is an effective method to prevent sticking. Also higher coal quantity in the in the mixed bed increases the recuction velocity.

These factors offer the possibility of influencing the sticking behaviour. In this fact the interaction of the different factors is important. Table 2 shows the possibilities of influencing the sticking behavior.

Table 2: Possibilities of influencing the sticking behavior

Material specific influences		**Comments**	**References**
Grain size ↓	**S** ↑	Higher specific surface area and surface atoms	[64,67,68]
Gangue ↑	**S** ↑ **S** ↓	Low melting eutecticas Less iron atoms on surface	[50,75-77]
Angular shape of grains ↑	**S** ↑	Increased hooking tendency of grains due to whiskers	[78]
Hematitic ore ↑ Magnetitic ore↑	**S** ↑ **S** ↓	Hematite: fibrous iron segregations Magnetite: dense iron segregations	[65]
Procedural influences			
Temperature ↑	**S** ↑	Below a certain temperature no sticking occurs. The initial point of sticking decreases with increasing temperature.	[50,51,62-64]
Flow rate ↑	**S** ↓	Better rejection of particles	[50,60,64]
Reduction velocity ↑	**S** ↑	Higher iron activity, higher adhesion force between the ore particles	[50,52,57,58]
Compositioin of reduction gas	**S** ↑↓	Different segregation types, different kinds of sticking	[50,52,57,61]
Additives	**S** ↑↓	Influence on the segregation behaviour	[52,64,69-71,73,74,79-81]
Multi-stage reduction	**S** ↓	At the beginning dense segregation; final reduction without sticking possible	[67,82]

4 Characterization of raw and reduced iron ores – phenomenological investigations

Many techniques nowadays can be employed to characterize the properties of iron ores. Some of these physical and chemical methods are rather simple and some of them complicated, but almost associated with experimental errors and implicit assumptions. To select the proper technique for every specific application, the method has to be chosen carefully. In this chapter, the applied methods for characterizing the raw and reduced iron ores within the research work are explained.

4.1 Methods for iron, iron oxide and elementary analysis

For the characterization as well as for the determination of the process behavior of iron ores in raw and reduced states, a series of chemical and physical methods can be applied. The most important methods are: titration, spectrometry, complexometry, potentiometry, gravimetry, and photometry.

Table 3: Chosen methods for the chemical characterization of raw and reduced iron ores

	Elements and oxides	method
Raw iron ore	Fe_{met},	Bromine methanol method
	Fe^{+2}, Fe^{3+} (calculated)	Zimmermann-Reinhard method
	Fe_{tot}	Calculated
	Fe, SiO_2, Mn, CaO, MgO, Al_2O_3, P, TiO_2, K_2O	XRF
	LOI	TGA
Reduced samples	Femet,	Bromine methanol
	Fe^{+2}, Fe^{3+} (calculated)	Zimmermann-Reinhard method
	C	Spark spectrometry

The chosen method for the determination of iron and its valences (oxides) is the titration. In order to determine the gangue elements- and oxides, the X-Ray-Fluorescence Analysis (XRF or RFA respectively) was applied. To define the loss on chemically bound water and volatiles, the Loss On Ignition (LOI) is defined by means of the thermo-gravimetric analysis (TGA). In Table 3, the applied methods for the chemical characterization of raw and reduced iron ores are defined.

4.1.1 Titrimetric analysis of iron and iron oxides

The classical titrimetric analysis is described by the type of endpoint-identification or by the character of the chemical mechanisms. The endpoint can be identified by a colour change or by precipitation in the equivalence point. For detection of this point, an indicator is used in most cases. To determine the iron content, mainly manganometry is used, which is a method of oxidation- and reduction analysis. In some cases, also complex-forming analysis or physical methods can be applied [83].

Zimmerman-Reinhardt-method for the determination of Fe^{2+} and Fe^{3+}

The Zimmermann-Reinhandt-method enables the direct titration of iron ores and iron alloys. The so called Zimmermann-Reinhardt-solution is a mixture of manganese-sulfate-solution, phosphoric acid and sulphuric acid. Additions like cobalt, copper, lead, chrome, titanium and arsenic are unproblematic, whereas antimony causes problems during analysis [83,84].

At the beginning, the Fe^{3+}-ions are reduced to Fe^{2+} by Sn^{2+}. The surplus tin is then precipitated with with Hg^{2+} into a sparingly soluble chloride. During the subsequent titration with the Zimmermann-Reinhardt-solution, the Fe^{2+} is converted to Fe^{3+} by the strong oxidizing permanganate ion. The Mn is then reduced to Mn^{2+} from oxidation state +7. The chemical equation is [84,85]:

$$MnO_4^- + 5\ Fe^{2+} + 8\ H^+ + 5\ e^- \leftrightarrow Mn^{2+} + 5\ Fe^{3+} + 4\ H_2O \qquad (4\text{-}1)$$

Fe^{2+} reacts with MnO_4^- to Fe^{3+} in a molar ratio of 5:1. Accordingly, the equivalent substance quantity is:

$$n(Fe^{2+}) = n\left(\frac{1}{5}KMnO_4\right) \qquad (4\text{-}2)$$

The equivalence point is reached, when the red-purple colour of MnO_4^- turns to transparent Mn^{2+}. The mass of Fe^{2+} can then be calculated:

$$m(Fe^{2+}) = c\left(\frac{1}{5}KMnO_4\right) \times V_{Eq}\left(\frac{1}{5}KMnO_4\right) \times M(Fe^{2+}) \qquad (4\text{-}3)$$

Here, the $V_{Eq}(KMnO_4)$ is the consumed volume of MnO_4^- until reaching the equivalence point, and $M(Fe^{2+})$ the molar mass of iron. Aditionally, the Fe^{3+} content can be calculated, if the total iron content and the metallic iron content is known.

Bromine-Methanol-method for the determination of metallic iron

The titration with Bromine-Methanol regarding the international standard ISO 5416:2006 is used to determine the mass fraction of metallic iron (Fe_{met}) in Direct Reduced Iron (DRI). This method is applicable to mass fractions of metallic iron between 15 % and 95 % in DRI. The term “metallic iron” means those forms of iron not bonded to oxygen or not present as pyrite [86].

The metallic iron is dissolved by treatment with a bromine-methanol solution defined in the standard ISO 5416:2006. The insoluble residue is separated by filtration. The iron in the filtrate is oxidized to Fe^{2+}, which is titrated with a potassium dichromate solution. By the consumption of solution, the Fe_{met}-content in the DRI can be determined. Other metallic elements, such as chromium, cobalt, manganese, nickel and vanadium, are also dissolved by the bromine-methanol solution but, except for vanadium, they do not interfere with the titration procedure [86].

For analysis, a laboratory sample of minus 160 µm particle size should be used, which has been taken and prepared in accordance with ISO 10835 [87]. The analysis has to be carried out at least in duplicate, independentely, on one air equilibrated test sample [86].

The mass fraction of metallic iron w_{Femet}, expressed as a percentage, is calculated to three decimal places using the equation [86]:

$$w_{Fe_{met}} = \frac{(V - V_0) \cdot 0{,}5585 \cdot F}{m} \cdot \frac{100}{100 - A} \qquad (4\text{-}4)$$

whereas

- V volume, in millilitres, of potassium dichromate solution required for the sample analysis
- V_0 corrected volume, in millilitres, of potassium dichromate solution required for the determination of the blank test value
- m mass, in grams, of the air-equilibrated test portion
- F dilution factor
- A hygroscopic moisture content, expressed as a percentage by mass, of the air-equilibrated test sample determined in accordance with ISO 2596

0,5585 is a multiple of the atomic mass of iron.

The metallization degree, which is an important parameter for the characterization of direct reduced iron, can be calculated with equation (3-24), as discussed before.

4.1.2 X Ray-Fluorescence Analysis

The principle of the X-Ray Fluorescense Analysis is the wavelength-determination of the emmited radiation of a sample, whereas the emmited radiation is defined by the atomic number of the emitting element. The primary energy required to generate X-ray fluorescence has to be high enough to remove an electron from the inner electron shell of an element. The

resulting electron gap is then filled up with and electron of an outer electron shell, which emits the released energy as X-ray quantum (cf. Figure 24). The X-ray spectrum is then easy to identify and is usually descriped by a couple of spectral linies. For the qualitative analysis, the wavelength is important (wavelength-dispersive) and for the quantitative analysis, the intensity of the radiation is measured (energy-dispersive). Here, the intensity of the radiation depends on the amount of simultaneous activated atoms. Depending on the element, determinations down tot he ppm-range are possible [88].

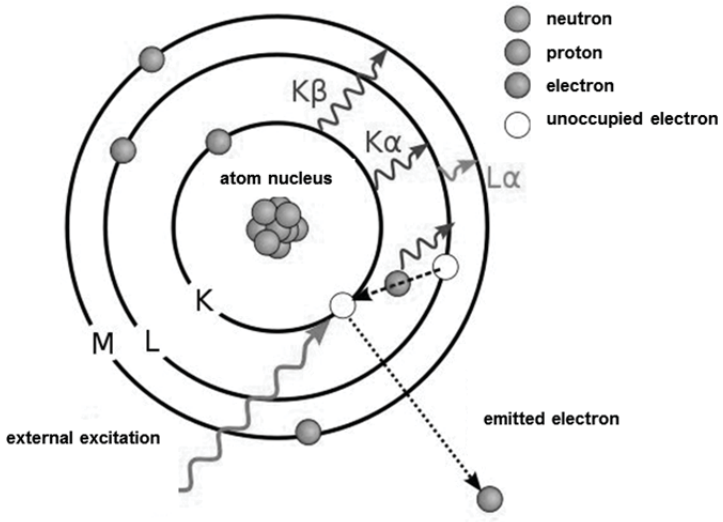

Figure 24: Principle of the X-Ray Fluorescense Analysis, according to [153]

The X-ray fluorescence analysis is suitable for the qualitative and quantitative elementary analysis above the atomic number 9 (fluorine). The radiation of light elements has a longer wavelenght. Hence, it is absorbed very strong by the atmosphere and is difficult to detect [83].

4.1.3 Thermogravimetric analysis

The thermogravimetric analysis is based on the mass change of a sample in dependence on the temperature. Messurements of disintegration- and oxidation-reactions and the monitoring of physical processes like evaporation, sublimation and desorption are all possible. The experimental setup is usually a sensetive scale, an oven and devices to produce desired atmosphere [89]. For the research work, the thermogravimetric analysis was used to quantify the loss on chemically bound water and volatiles of the raw ore.

4.2 Determination of grain size distribution

For the determination of the grain size distribution of a particle collective, many mechanical and optical applications are available, like sieve analysis, imaging techniques or gravity and centrifugal sedimentation. The most commonly used technique for classifying particles, is the sieve analysis.

To determine the grain size distribution, the particle collective has to be sieved through a series of woven–wire screens with standardized mesh size by sifting, swirling, shaking or vibrating [90]. It is recommended to use a sufficient number of screens to create a smooth distribution curve after the analysis. It is also important to use a small enough sample and to ensure that the solid is free-flowing and well dispersed during the sieving sequence. In this context, various standards are applied worldwide.

The sieving technique applied for this research work can be described by the standards DIN 66165 and ISO 4701 [91-93].

4.2.1 Sieving procedure according to DIN 66165 and ISO 4701

The applied method is the sieve analysis by means of dry sieving. The sample mass has to be heated in a drying furnace at 105 °C, removing the moist components. After cooling, the sample is weighted and subsequently sieved by means of a sieve tower, which is fixed on a sieving machine. Therefore, a series of individual woven-wire screens with different mesh sizes between 0.063 and 6.3 mm have to be placed one upon the other. The mesh sizes decrease from the top to the bottom. For the analysis, the sample mass was put on the sieve with the biggest mesh size and the sieving machine was put in a defined oscillating motion. By weighing the residues in the single sieves after the sieving procedure, the grain size distribution was determined.

The sum of the fractional masses of each sieving operation should not differ by more than 1 % for dry sieving. The percentage mass fraction for each mesh size should be calculated as follows:

$$\%\ (size\ fraction) = 100 \cdot \frac{mass\ of\ a\ size\ fraction}{total\ mass\ of\ all\ size\ fractions} \tag{4-5}$$

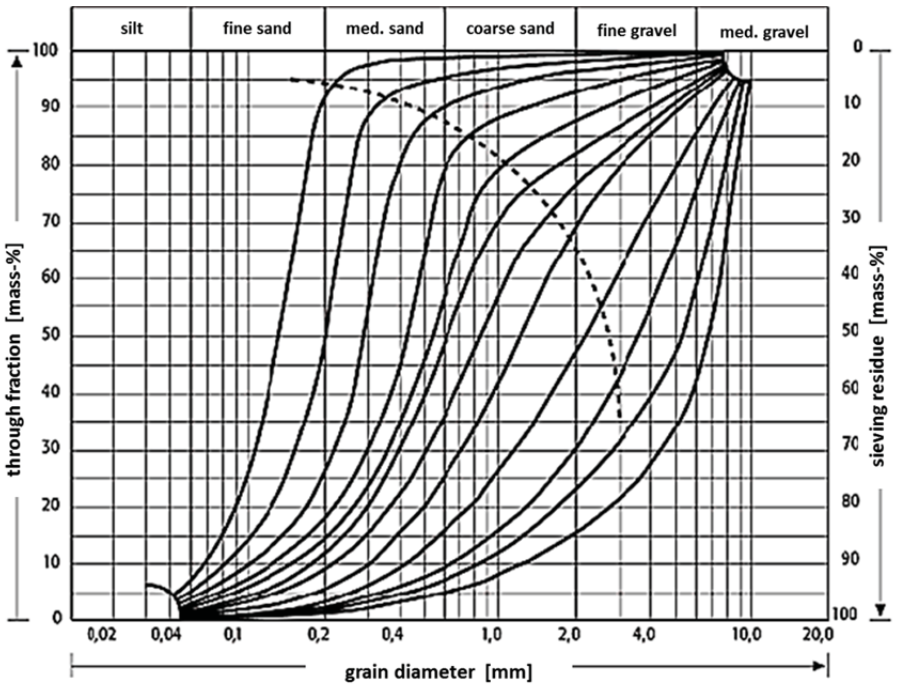

Figure 25: Sieve curves for different bulk materials [154]

When the size analysis is based on sieving several partial samples, the masses of each respective fraction from each sample has to be summed up and calculated corresponding to equation (4-5). The result of such a sieve analysis is commonly plotted in a regular or logarithmic-scale graph with the particle size as abscissa and the cumulative weight percentage as ordinate.

Figure 25 shows characteristic sieve curves of different bulk materials: coarse material on the top right and fine materials bottom left. The mean diameter of the particle collective increases from left to right.

4.3 Determination of the specific surface area (B.E.T.- method)

The B.E.T.-technique is named after its inventors Stephen Brunauer, Paul Hugh Emmet and Edward Teller. The method describes an analysis method of sizing surfaces by means of gas adsorption [94] and can be carried out according to standard DIN ISO 9277:2003-05 [95].

During the measurement of the specific surface area, an equivalent amount of adsorption gas adsorbs at a certain temperature and a certain pressure. Simultaneously the respective amount will be desorbed. The resulting adsorption-isotherme describes the dynamic equilibrium of these activities, which only depends on the pressure. Increasing the pressure, the micro- , meso-, and macro-pores are filled with adsorption gas. Furthermore, on the suface the amount of gas molecules increases and the adsorption gas builds layers. A so called multi-layer adsorption evolves [96].

According to the B.E.T.- equation, the required gas volume V_a can be calculated as follows [94]:

$$\frac{\frac{p}{p_0}}{V_a \cdot \left(1-\frac{p}{p_0}\right)} = \frac{1}{V_m \cdot C} + \frac{C-1}{V_m \cdot C} \cdot \frac{p}{p_0} \qquad (4\text{-}6)$$

whereas V_a is the adsorbed volume, V_m the volume of the monolayer, p the variable pressure and p_0 the vapor pressure above the monolayer. This equation refers to a linear equation y = kx + d and is valid for the following conditions [94,96]:

- Localized adsorption
- Mulitlayer-adsorption
- Homogenity of the solid surface
- Independency of the adsorption heat of the first layer of the degree of coverage
- The adsorption heat is equal to the condensation heat of the adsorption gas as well as the adsorption layers
- Interactions between the gas molecules are negligible

From the linear equation (4-6), a B.E.T.- isotherme can be graphically determined and V_m and C can be calculated with [94,96]:

$$V_m = \frac{1}{d+k} \qquad \textit{and} \qquad C\ \frac{k}{d} + 1 \qquad (4\text{-}7)$$

The specific surface area O_{sp} can be calculated with the Avogadro-constant N_A and the surface a_m of a gas molecule at its specific temperature [94]:

$$O_{sp} = V_m \cdot N_A \cdot a_m \tag{4-8}$$

In the linear equation, the constant C (B.E.T.-constant) is dependent only on the adsorption gas and is approximately [94]:

$$C = \exp \frac{E_1 - E_L}{R \cdot T} \tag{4-9}$$

E_1 is the adsorption enthalpy of the monolayer and E_L the adsorption enthalpy of the additional layers (corresponds tot he condensation enthalpy oft he gas on the surface).

Typical adsoption gases fort he determination of the specific surface of porous materials are: N_2, CO_2, Ar, He, CH_4, C_6H_6 und C_9H_{20}.

4.4 Morphological characterization of raw and reduced ores

The most important method for the petrographical investigation of ores is by microscope. Microscopy can be devided into two subareas: reflected-light microscopy and transmitted light microscopy. For both methods, specially polished sections have to be prepared. Regarding the sample materials, it is important to provide representative specimens, that are not falsified by sample extraction, transport or storage. A documentation of the sample must exist, including sample identification and storage location.

4.4.1 Fundamentals of reflected-light- and transmitted-light microscopy

With a reflected-light microscope, the surface of a polished sample can be determined. The ocular and the objective magnify the surface of the specimen. The total magnification results from the multiplication of both magnification stages. The unpolarized light from the light source is polarized by a polarization filter and is reflected by the surface of the polished section. Depending on the adjustment of the analyzer, the differentiation of inherent colours and interference-colours is possible, which simplifies the investigation of minerals and materials [97].

By means of a transmitted light microscope, the minerals can be studied by means of crossed polarizers. This enables a clear identification of minerals. For these investigations, thin-ground sections with a thickness of just a few µm have to be prepared. The technical construction is similar to the reflected-light microscope, with the difference, that the light source is located beneath the polished section [98].

In Figure 27 a schematic drawing of the reflected-light and the transmitted-light microscopy is shown. The layout of a microscope, which can be used for both methods, is pictured in Figure 26.

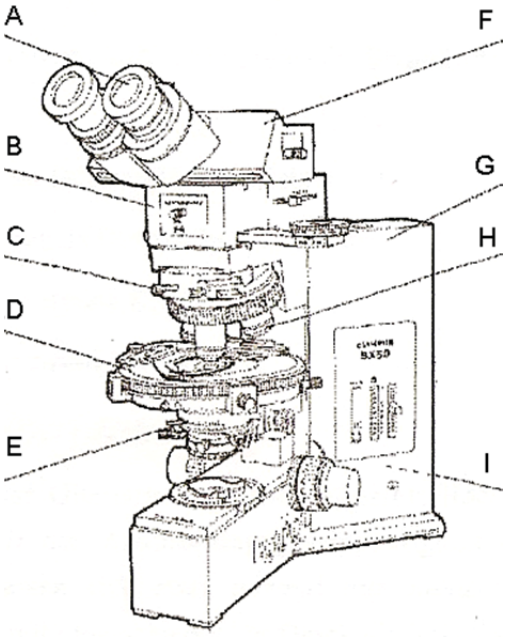

Figure 26: Elements of a reflected- and transmitted-light microscope [97]: A ocular, B polarizer, C objective revolver, D microscope table (turnable), E condenser unit, F lens tube, G stand, H objectives, I lamp housing.

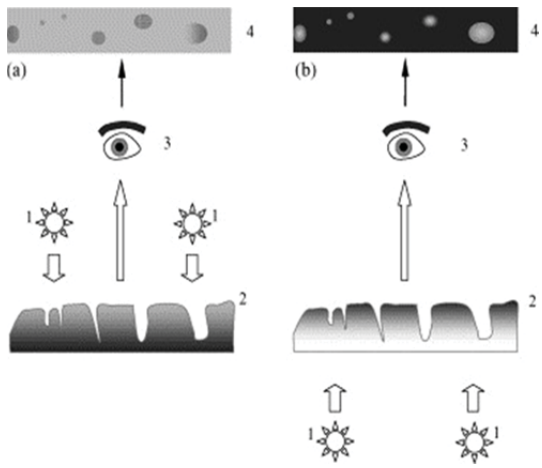

Figure 27: schematic drawing of the transmitted light microscopy (a) and the reflected-light microscopy (b) [155]

Preparation of the polished sections and thin-ground sections

As said before, polished sections and thin-ground sections of the sample material have to be produced to determine the composition of the sample. These specimens have to be completely flat to interprete the phases and crystal structures.

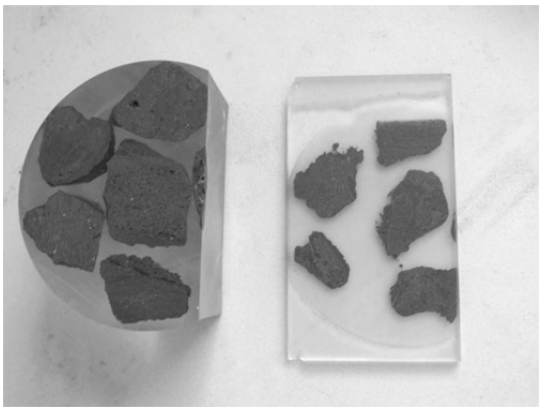

Figure 28: Polished section (left) and thin-ground section (right)

During preparation it is important to avoid modification of the material due to mechanical (breakout, smearing), chemical (dissolution, transformation) or thermal (disintegration) influences. The phases must be retained regarding their characteristics and the polished- and thin-ground sections should be free from cracks and scratches. The specimens for reflected-light microscopy usually are produced with grinding machines, whereas the

specimen for the transmitted-light microscopy have to be grinded manually (because these polished sections have a thickness of just a few µm). This implies referring operating instructions have to be obeyed. In this context, the experience of the metallographer is very important. A standardized methodology has been elaborated in chapter 6.3.2. In Figure 28, an example of a polished section and a thin-ground section is shown.

4.4.2 Characteristics and morphology of raw and reduced ores

All globally traded iron ore consists of various different petrographical types. Depending on the geological and reduction history, every ore shows different structural characteristics (i.e. shape and size of crystals, specific surface, petrographic structures etc.), which influence the reduction behavior in the procees. The mineralogy of most iron ores is rather simple and can be divided into limonite, hematite and magnetite. Additionally, other ore phases can appear, i.e. kenomagnetite, maghemite, pyrite, illmenite and gangue minerals which are intergrown with the iron ore minerals [99]. Sometimes, trace amounts of phyollosilicates, titanium minerals, carbonates, aluminium-hydroxides can be found.

During the reduction process, the iron ore phases and their morphology are changing due to the removal of the oxygen from the crystal lattice in dependence of the mineralogical characteristics and the process conditions. These transformations result in different reduction behavior, which can be advantageous or disadvantageous for the process. In general, the most important phase transformations during reduction of iron ores are shown in Table 4:

Table 4: Phase transformations during reduction

Raw ore		Reduced ore
Limonite (FeOOH)		Magnetite (Fe_3O_4)
Hematite (Fe_2O_3)		Wuestite (FeO)
Magnetite (Fe_3O_4)	→	Iron (Fe)
Silicates		Cementite (Fe_3C)
Carbonates etc.		Silicates
		Carbonates etc.

Based on these facts, it is important to characterize the raw iron ores and their morphological evolution during the reduction sequences, in order to understand the penomenological transactions. Regarding the correlationis between mineralogical properties and reduction behavior of iron ores, a series of authors already performed research studies [1,4,53,56,74,79,82,99-111,111-116].

Below, the morphological characteristics of the most important iron ore modifications in both its natural and reduced forms are described.

Hematite (Fe_2O_3) (cf. chapter 3.1)**:**

The majority of hematite originated through recrystallization of a finely crystalline iron oxide and/or iron hydroxide mud, which was generated by chemical precipitation in the pre-cambrian sea. Depending on the conditions (temperature, pressure, fluids etc.), smaller or larger crystals have been formed through the geological aeons (cf. Figure 29, typical

hematite rich ore) [117]. Some of the ores are composed of a mixture of submicroscopic hematite (H) crystals which are intensely intergrown with limonite (L). The type depicted below originated through dehydration of limonite.

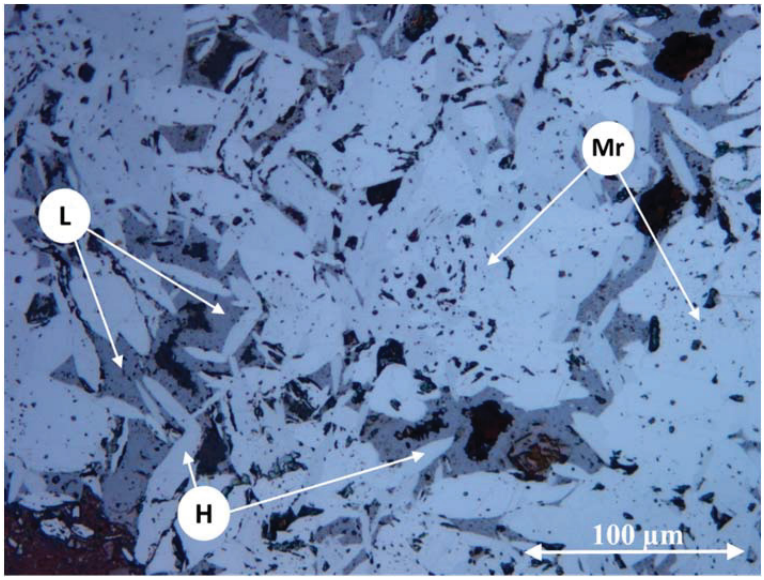

Figure 29: Hematite rich ore with limonite and martite

Hematite can be split into 9 primary subtypes regarding its genesis (martite), crystal size, porosity and shape [117]. Mostly, it occurs in the form of longish plates. From the morphological point of view, hematite crystals can be:

- idiomorphic: defined crystal interface with an angular shape, dense and hardly any pores
- hypidiomorphic: partly defined crystal interface in comparison to idiomorphic
- xenomorphic: irregular with no defined crystal interface; the hematite intergrows with neighbouring crystals and has a porous matrix with a higher specific surface area (well reducible)

with grain sizes ranging from < 10 µm up to a centimeter. The number of pores inside the crystals is very important for the reduction behaviour, because some ores have many intercrystalline pores and some ores show hardly any porosity at all.

Martite (Fe_2O_3 – pseudomorph of hematite after magnetite):

Martite (Mr) is a pseudomorph of hematite after magnetite, which can contain different structures of hematite. The former magnetite had been oxidized to hematite over geological aeons. In some cases, martite forms trellis structures with thin crystal laths following the crystal structure oft he former spinel. Sometimes interfingering crystals can be observed, which have a significantly bigger surface area than the idiomorphic hematite crystals of marite [117].

Limonite ($FeOOH \cdot n\ H_2O$):

Limonite is mainly generated through weathering of the primary iron ore and can usually be found at the surfaces in every iron ore deposit. Hence, the amount of limonite usually

decreases with the depth of the deposit, in contrast to the iron oxide portion. Petrographically, the limonite ores contain a wide variety of structural types and can occur as [117]:

- oolitic ore
- crusts and shells with or without zoning
- massive or non-porous patches
- seam or patch of idiomorphic to hypidiomorphic lepidocrocite crystals
- pseudomorphs after pyrite

In most cases, the limonite is intergrown with hematite and/or magnetite and/or siderite in varying portions. Figure 30 shows a typical limonite (L)-rich ore.

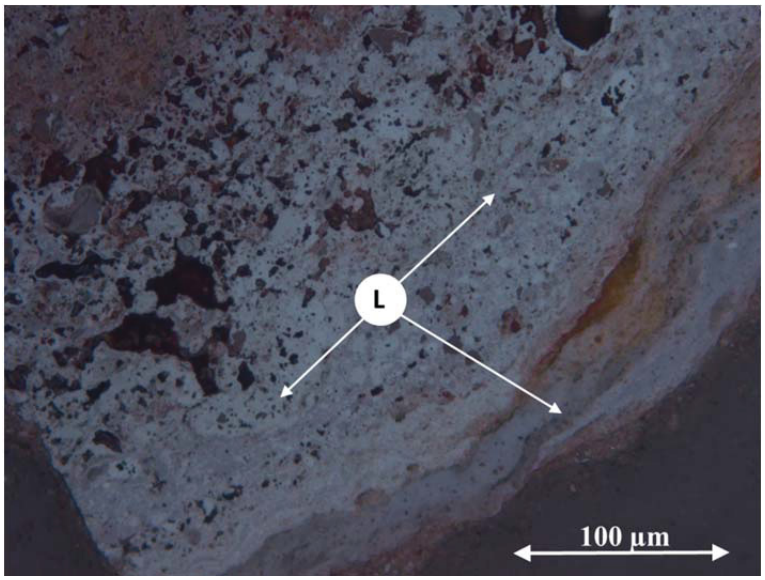

Figure 30: Limonite rich ore

Magnetite (Fe_3O_4) (cf. chapter 3.1)**:**

Magnetite contains less oxygen than hematite and is no stable phase under atmospheric conditions. Most of the magnetite originated from recrystallization of a finely crystalline iron oxide and/or iron hydroxide mud which was generated by chemical precipitation (similar to hematite). It would depend on the oxygen availability and chemical conditions in the rock, whether magnetite or hematite was formed. Temperature and pressure over geological aeons were responsible for the crystal size.

Magnetite can be split into 3 types, depending on porosity, crystal and aggregate size [117]. Magnetite usually occurs in crystal sizes between < 2 µm and cm-range. Similar to hematite, the magnetite crystals can be

- idiomorphic
- hypidiomorphic
- xenomorphic

In most cases, the matrix is very dense and hardly any intercrystalline pores can be found at all (cf. Figure 31). The porosity and specific surface area is very much smaller compared to hematite or limonite. Magnetite can be well identified in the microscope due to the defined grain boundaries.

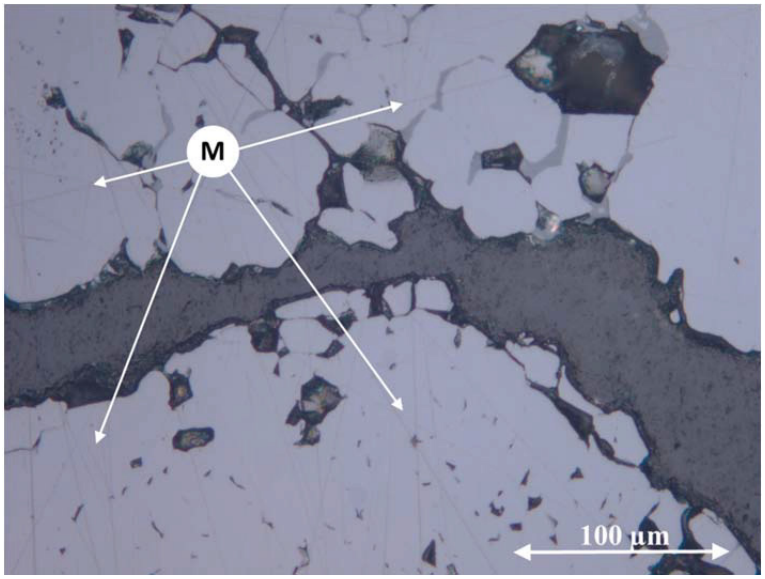

Figure 31: Magnetite ore

Siderite ($FeCO_3$):

Pure siderite is rare but modifications with Mg and Mn are often present, as $(Mg,Fe)CO_3$ or $(Mn,Fe)CO_3$. A deacified siderite can be identified by its ideomorphic and angular shaped appearance. Globally, siderite has no major importance, since the iron content is very low compared to the other iron ores. Figure 32 shows a limonite-rich siderite. The primary carbonate trellis texture is observable, which derived from the former carbonate texture.

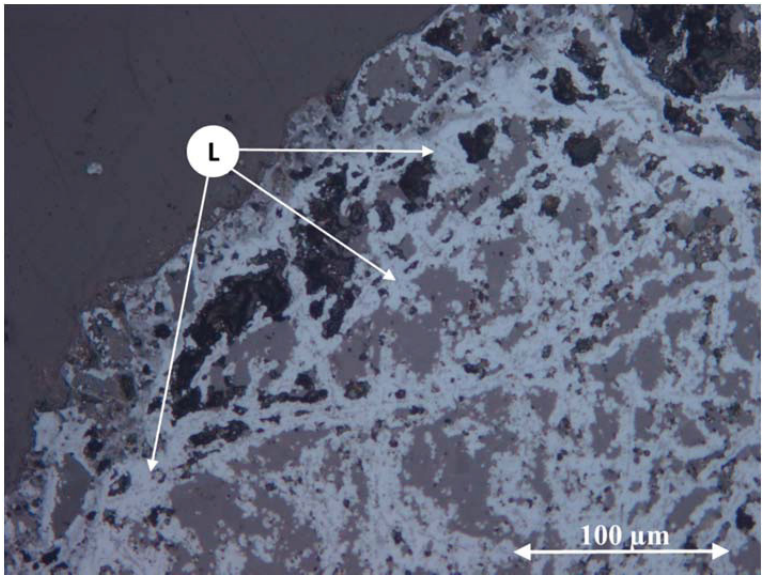

Figure 32: Siderite ore, rich on limonite

Wuestite ($Fe_{1-y}O$) (cf. chapter 3.1)**:**

The mineralogy of the reduced ores is also rather simple. During reduction, limonite portions are dehydrated to hematite. The hematite is first reduced to magnetite, subsequently to wuestite (FeO) and finally to metallic iron (Fe_{met}).

Wuestite (FeO) is the lowest grade oxide and is an intermediate product during reduction, which has already been discussed in chapter 3.1. With decreasing iron content, the vacancy concentration in the wuestite lattice and, hence, the porosity and reducibility increases [118]. It is unstable below 570°C, where it decomposes to Fe and Fe_3O_4. Wuestite is optically isotropic. Under the microscope single grains can only be identified by their grain boundaries. The structure of wuestite depends on the raw ore. Figure 33 shows a reduced limonite rich ore, which has a wuestite matrix with metallic iron scraps.

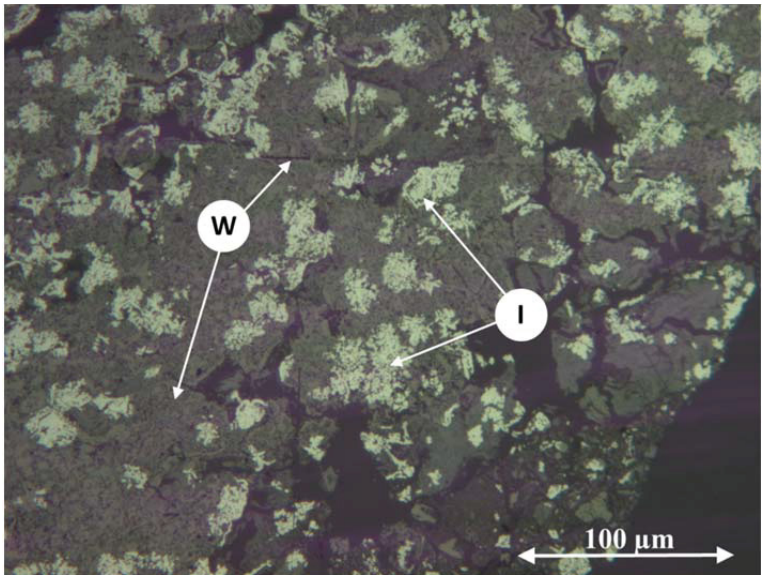

Figure 33: Reduced limonite rich ore, wuestite matrix with iron scraps

Cementite (Fe_3C):

Cementite is also known as tri-iron-carbonate. It has a carbon content of 6.67 % [119]. During reduction in precence of CO and CO_2, carbon can be generated in dependence on the Boudouard-curve (cf. chapter 3.2.3). Over 723 °C to about 1150 °C, γ-iron is soluble for C up to about 2 %. The carbon can be stored in interstitial sites oft he α- or γ-iron. When the iron cools down, Fe_3C is formed below 723 °C. The amount depends on the carbon content. In case of slow cooling, Fe_3C disintegrates into iron and graphite, because Fe_3C is less stable [120].

5 Fundamentals of fluidized bed technology

"Fluidization is the operation, by which solid particles are transformed into a fluidlike state through suspension in a gas or liquid" [121].

Regarding non-catalytic (gas-solid-reaction [10]) fluidized bed technologies, the principle of fluidization can be defined as the "operation, by which a packed bed of solid particles is transformed into a fluid-like state by an upward directed gas stream".

The first technical application of the fluidized bed was the coal gasification by Winkler in 1922 [38,122]. Nowadays fluidized beds are applied for various non-catalytic processes, for example char combustion, roasting of pyrite and blende, aluminium oxide calcination [38] and iron ore reduction. The advantages of this technology are [4,38,123]:

- Good mixture of solid and gas,
- Excellent mass- and heat exchange,
- Consistent temperature distribution throughout the whole reactor loop,
- No hot spots, also in highly exothermic reactions,
- High heat- and energy utilization,
- Better handling of solid matter because of the fluid-like behavior.

However, there are also disadvantages, which have to be considered for the development of fluidized bed technologies [124]:

- Inability to handle sticky material, which could lead to agglomeration and eventually to blockage of the process (i.e. sticking),
- The power dissipation entailed in keeping the bed fluidized.

Based on these properties, fluidized bed technology offers ideal conditions for the processing of fine grained material and enables the reduction of fine ores without prior benefication. In the following section, the fluidization phenomenon and the methodology of dimensioning a fluidized bed for gas-solid processes are discussed.

5.1 The fluidization phenomenon

In general, fluidized systems represent an alternative to fixed-bed applications for gas-solid processes. The best way of illustrating the nature of fluidization is, perhaps, the upward flow of a fluid through a packed bed of solid particles [124]. Depending on the fluid velocity, the packed-bed passes through different states.

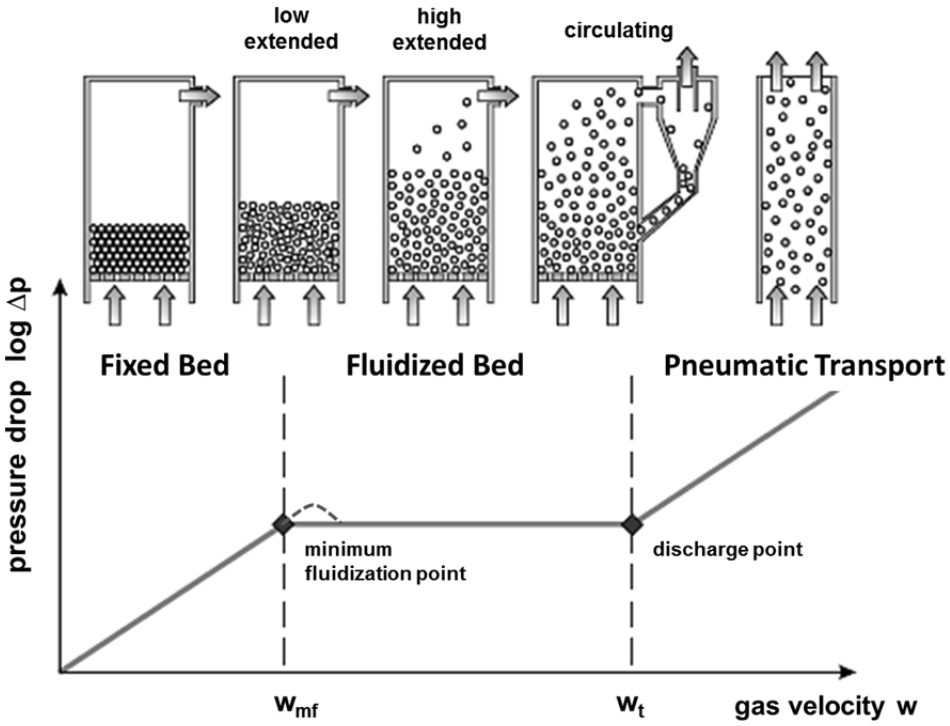

Figure 34: Various forms of a batch of solids contacted by a fluid in dependence on the gas velocity, according to [125]

If a fluid streams upwards through a bed of fine particles at a low flow rate, the fluid merely flows through the void spaces between stationary particles. This is called a “fixed bed” (cf. Figure 34). When the flow rate increases, a corresponding increase in the pressure drop occurs. Particles move apart, start vibrating, move to restricted regions and build an “extended bed” [121,124].

Still increasing the velocity, a certain point is reached, where all particles are just suspended by the upward flowing fluid and the frictional force between particle and fluid is counterbalancing the weight of the particles. In other words, the pressure drop across the bed equals the weight of the bed and the bed attains its loosest possible packing [121,124]. The bed is now at the “minimum fluidization” point and considered to get fluidized. The fluid velocity at this point is called the “minimum fluidization velocity” (w_{mf}).

At the minimum fluidization point w_{mf}, the following equilibrium of force is valid:

$$\text{Gravitational Force } (F_G) = \text{Force by pressure drop } (F_{\Delta p}) \qquad (5\text{-}1)$$

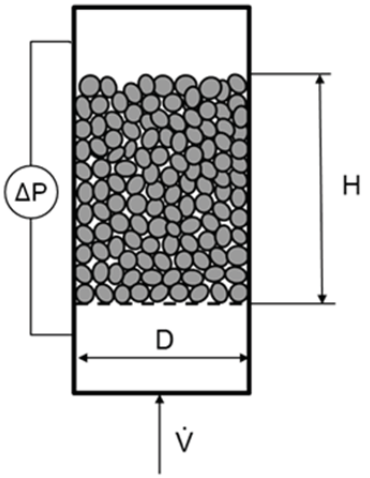

Figure 35: force balance at the Minimum fluidization point [10]

$$F_G = \frac{D^2\pi}{4} \cdot H \cdot (1-\varepsilon) \cdot \rho_s \cdot g \tag{5-2}$$

$$F_{\Delta p} = \Delta p \cdot \frac{D^2\pi}{4} \tag{5-3}$$

$$\Delta p \cdot \frac{D^2\pi}{4} = \frac{D^2\pi}{4} \cdot H \cdot (1-\varepsilon) \cdot \rho_s \cdot g \tag{5-4}$$

$$\frac{\Delta p}{H} = (1-\varepsilon) \cdot \rho_s \cdot g \tag{5-5}$$

At higher flow rates, the bed expands further, the particles become freely expanded in the fluid stream and a “fluidized bed” evolves.

Depending on the fluid velocity, first a homogenous fluidized bed is formed and by increasing the velocity, inhomogenities occur [10]. Hence, different types of fluidization can be distinguished depending on the gas velocity: particulate fluidization, bubbling fluidization, slugging fluidization, turbulent fluidization (cf. Figure 34) [121].

In liquid-solid systems, a velocity increase above w_{mf} results in a smooth expansion of the bed, whereas in gas-solid systems large instabilities with bubbling and channeling of the gas are observed [4,121]. The formation and behavior of bubbles is discussed in [4,45,121,126-132].

The pressure drop across the bed and the flow rate can be described by various models (cf. [90]). The most widely used empirical correlation is the Ergun-correlation [10,90,121,124]:

$$\frac{\Delta_p}{H} = \underbrace{150 \cdot \frac{(1-\varepsilon)^2}{\varepsilon^3} \cdot \frac{\eta \cdot w}{d_p^2}}_{1^{st}\text{ term}} + \underbrace{1{,}75 \cdot \frac{(1-\varepsilon)}{\varepsilon^3} \cdot \frac{w^2 \cdot \rho_f}{d_p}}_{2^{nd}\text{ term}} \tag{5-6}$$

Regarding this equation, Δp depends on the voids fraction ε, the superficial velocity w, the particle diameter d_p, the dynamic viscosity η and the fluid density ρ_f. The Ergun-equation shows, that the drag force of the bed is linear to the superficial velocity (1st term of equation (5-6), but at higher flow rates turbulence occur (2nd term of equation (5-6) [10,90]. So, under laminar flow conditions (Re < 1) the 1st term dominates and in fully turbulent flow (Re > 1000) the 2nd term is dominating [45].

When the fluid velocity increases to the point where particles are discharged, the “terminal velocity” w_t is reached. At this discharge point, the particles are entrained with the fluid stream and a pneumatic transport evolves. For this point, another important equilibrium of force is valid:

Drag Force (F_w) = Gravitational Force (F_G) - Buoyancy Force (F_A) (5-7)

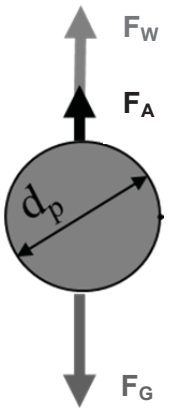

$$F_W = \frac{d_p^2}{4} \cdot \pi \cdot c_w \cdot \rho_f \cdot \frac{w_T^2}{2} \quad (5\text{-}8)$$

$$F_A = \frac{d_p^3}{6} \cdot \pi \cdot \rho_f \cdot g \quad (5\text{-}9)$$

$$F_G = \frac{d_p^3}{6} \cdot \pi \cdot \rho_s \cdot g \quad (5\text{-}10)$$

Figure 36: force balance of a spherical particle at the terminal fluidization point [10]

Whereas d_p is particle diameter, ρ_s the particle density, ρf the fluid density, c_w or also c_d the drag coefficient and w_T the terminal velocity. If the drag force and buoyancy force is higher than the gravity force, the particle is entrained with the fluid stream from the bed.

The minimum fluidization velocity, as well as the terminal velocity, is valid for a defined particle size. For particle size distributions, a representative particle diameter has to be defined for dimensioning a fluidized bed.

5.2 Influence of polydisperse particle collectives on fluidization

In the real process, the grain size distribution of the particles in the bed is not homogeneous. Fine ores consist of a grain size distribution ranging from very fine to coarse material (pellet feed and sinter feed). Regarding the required gas velocity to keep a grain size distribution fluidized, the discharge of the finest fractions is almost unavoidable. For this reason, cyclones are used to separate the finest fractions from the gas stream and recycle these fractions to the fluidized bed.

For the dimensioning of a fluidized bed, a representative particle diameter is important, which represents the average particle size of the whole input material. The mean diameter of the particles can be determined by means of sieve curves, gathered by sieve analyses (for example DIN 66165 and and ISO 4701 [91-93]. For the assembly of a desired grain size distribution for lab scale tests, this standard can also be applied.

As a representative particle diameter for the whole grain size distribution, a mean diameter can be calculated. This average diameter is based on the summation of the reciprocals of the diameters of the individual components of an assemblage [90]. It can be expressed mathematically as [90,121,133,134]:

$$\bar{d} = \frac{1}{\sum \left(\frac{x}{d_p}\right)_i} \quad (5\text{-}11)$$

x is the mass fraction of a class represented by the average diameter (d_p)of the class. This mean diameter is related to the average spherical particle corresponding to the particle surface per unit weight and is similar to the volume-surface-mean or “Sauter-Mean-Diameter” (SMD) [90]. Due to the non-sphericity of most particles, the so called shape factor has to be considered for the calculations. The shape factor φ_s is defined as

$$\varphi_s = \left(\frac{surface\ of\ sphere}{surface\ of\ particle}\right)_{of\ same\ volume} \tag{5-12}$$

With this definition, the shape factor is 1 for spheres and $0 < \varphi_s < 1$ for any other particle shape. Various measures for spericities of different solids are available and typical shape factors for naturally occurring materials would range from about 0.9 to 0.5 [121,124,135]. For including the shape factor into the calculations, the so called effective particle diameter d_{eff} for a grain size distribution can be defined as

$$d_{eff} = \varphi_s \cdot \bar{d} \tag{5-13}$$

The voids fraction ε of particle collectives is defined as the voids between particles in a bulk of dense material with a defined volume [45,133]:

$$\varepsilon = \frac{V_{bed} - V_p}{V_{bed}} \tag{5-14}$$

In a dense packing of a mono disperse system, the voids fraction is between 0.26 (cubic face centered) and 0.32 (cubic close packed). Usually, in a mono disperse system, the voids fraction ε is between 0.35 and 0.5 [136]. Figure 37 for example shows the voids fraction of a two-component mixture. It is usually lower than that of a mono disperse system, because small grains fill in the blanks between large grains.

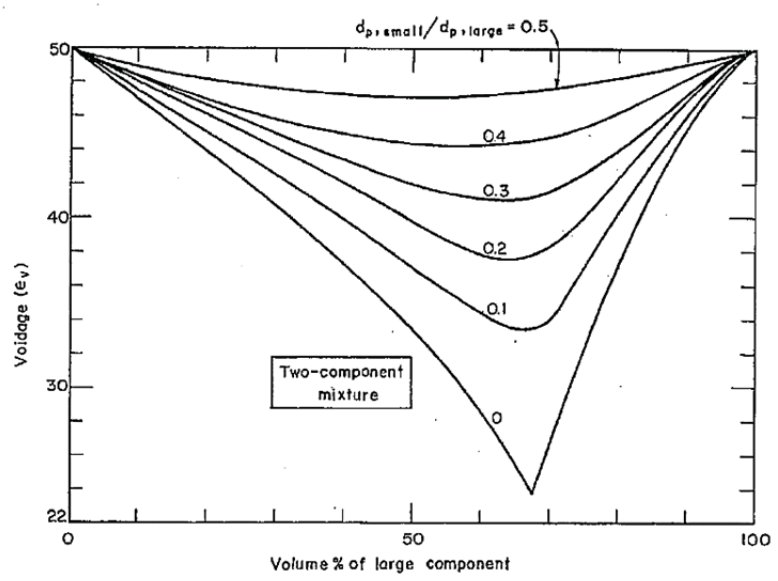

Figure 37: voids fraction of a two-component mixture [137]

5.3 Dimensioning of a gas-solid fluidized bed system

For the dimensioning of a fludized bed system with polydisperse particle collectives, the superficial velocity at the minimum fluidization point (minimum fluidization velocity w_{mf}) and the determination of the discharge point (terminal velocity w_{mf}) are important. After figuring out these velocities, the fluidization conditions can be determined by calculating dimensionless numbers, and the operating region then can be estimated by means of the Reh-diagram [133], developed by L. Reh.

5.3.1 Determination of the minimum fluidization point

As discussed before, the pressure drop across the bed and the flow rate can be described by the equation (5-6):

$$\frac{\Delta_p}{H} = 150 \cdot \frac{(1-\varepsilon)^2}{\varepsilon^3} \cdot \frac{\eta \cdot w}{d_p^2} + 1.75 \cdot \frac{(1-\varepsilon)}{\varepsilon^3} \cdot \frac{w^2 \cdot \rho_f}{d_p}$$

whereas w refers to the minimum fluidization velocity w_{mf}. The particle diameter d_p can be substituted by the effective particle diameter d_{eff} for polydisperse particle collectives (cf. equation (5-13)). The fluid density ρ_f for gas mixtures can be calculated by means of the ideal gas law [138]:

$$p \cdot V = n \cdot R \cdot T \qquad \textit{with} \qquad V = \frac{m}{\rho_g} \qquad \textit{and} \qquad n = \frac{m}{M_g} \tag{5-15}$$

and can be written as

$$\rho_g = \frac{p}{R \cdot T} \cdot M_g \tag{5-16}$$

whereas M_g relates to the molecular weight of the gas mixture and R is the universal gas constant. The dynamic viscosity η of a gas mixture is dependent on temperature and gas composition and can be calculated referring to [139].

Corresponding to equation (5-1), the balance of forces at the minimum fluidization point for gas-solid fluidized bed systems can be expressed as

$$\Delta p \cdot \frac{D^2\pi}{4} = \frac{D^2\pi}{4} \cdot H \cdot (1-\varepsilon) \cdot \rho_s \cdot g - \frac{D^2\pi}{4} \cdot H \cdot (1-\varepsilon) \cdot \rho_g \cdot g \tag{5-17}$$

and reduced to

$$\frac{\Delta p}{H} = (1-\varepsilon) \cdot (\rho_s - \rho_g) \cdot g \tag{5-18}$$

The minimum fluidization velocity w_{mf} can be found by inserting (5-18) into equation (5-6) combined with equation (5-13) and (5-14):

$$(1-\varepsilon)\cdot\left(\rho_s-\rho_g\right)\cdot g = 150\cdot\frac{(1-\varepsilon)^2}{\varepsilon^3}\cdot\frac{\eta\cdot w_{mf}}{d_{eff}^2}+1.75\cdot\frac{(1-\varepsilon)}{\varepsilon^3}\cdot\frac{w_{mf}^2\cdot\rho_g}{d_{eff}} \quad (5\text{-}19)$$

A simplified form of this equation can be obtained by substitution of the constant density and the constant particle diameter by dimensionless numbers. One of these numbers is the Reynolds number, which represents the relationship between inertia force and viscosity force [133]:

$$Re=\frac{d_p\cdot\rho\cdot w}{\eta} \quad (5\text{-}20)$$

Another number is the Archimedes number, which relates to the ratio between buoyancy force and friction force:

$$Ar=\frac{d_p^3\cdot\rho_g\cdot\left(\rho_s-\rho_g\right)\cdot g}{\eta^2} \quad (5\text{-}21)$$

Multiplying equation (5-19) with $\frac{d_{eff}^2\cdot\rho_g}{(1-\varepsilon)\cdot\eta^2}$ the equation can be written as

$$\frac{d_{eff}^3\cdot\rho_g\cdot\left(\rho_s-\rho_g\right)\cdot g}{\eta^2} = 150\cdot\frac{(1-\varepsilon)}{\varepsilon^3\cdot}\cdot\left(\frac{d_{eff}\cdot\rho_g\cdot w_{mf}}{\eta}\right)+\frac{1.75}{\varepsilon^3}\cdot\left(\frac{d_{eff}\cdot\rho_g\cdot w_{mf}}{\eta}\right)^2 \quad (5\text{-}22)$$

and with (Re) and (Ar) reduced to

$$Ar = 150\cdot\frac{(1-\varepsilon)}{\varepsilon^3\cdot}\cdot Re+\frac{1.75}{\varepsilon^3}\cdot Re^2 \quad (5\text{-}23)$$

Based on this equation, the Reynolds number can be calculated by inserting equation (5-21) to equation (5-23) and by solving the quadratic equation. When the Reynolds number is defined, the minimum fluidization velocity w_{mf} can be determined by rearrangement of equation (Re):

$$w_{mf}=\frac{Re\cdot\eta}{d_{eff}\cdot\rho_g} \quad (5\text{-}24)$$

5.3.2 Determination of the discharge point

The discharge point indicates the “terminal velocity” w_t or the force equilibrium, where a particle of a certain size is entrained from the fluidized bed by the gas flow [45]. If the drag force and buoyancy force is higher than the gravity force, the particle is entrained with the fluid stream from the bed. As discussed in chapter 5.1, the force equilibrium can be defined with the equations (5-8) to (5-10). For particle size distributions, the representative particle diameter d_{eff} has to be used and ρ_f is replaced by ρ_g for the gaseous fluid:

$$\frac{d_{eff}^2}{4} \cdot \pi \cdot c_d \cdot \rho_g \cdot \frac{w_t^2}{2} = \frac{d_{eff}^3}{6} \cdot \pi \cdot \rho_s \cdot g - \frac{d_{eff}^3}{6} \cdot \pi \cdot \rho_g \cdot g \quad (5\text{-}25)$$

Multiplying this equation with $\frac{8 \cdot \rho_g}{\eta^2 \cdot \pi}$ results in

$$c_d \cdot \frac{d_{eff}^2 \cdot \rho_g^2 \cdot w_t^2}{\eta^2} = \frac{4}{3} \frac{d_{eff}^3 \cdot \rho_g \cdot (\rho_s - \rho_g) \cdot g}{\eta^2} \quad (5\text{-}26)$$

Replacing the terms by the Reynolds- and Archimedes-number (equations (5-20) and (5-21)), the equation results in

$$c_d \cdot Re^2 = \frac{4}{3} \cdot Ar \quad (5\text{-}27)$$

Table 5: recommended empirical drag correlations, $w=log_{10}(Re)_p$ [90]

$(\mathrm{Re})_p < 0.01$	$C_D = \frac{3}{16} + \frac{24}{(\mathrm{Re})_p}$
$0.01 < (\mathrm{Re})_p \le 20$	$\log_{10}\left[\frac{C_D(\mathrm{Re})_p}{24} - 1\right] = -0.881 + 0.82w - 0.05w^2$
	$C_D = \frac{24}{(\mathrm{Re})_p}\left[1 + 0.1315(\mathrm{Re})_p^{(0.82-0.05w)}\right]$
$20 \le (\mathrm{Re})_p \le 260$	$\log_{10}\left[\frac{C_D(\mathrm{Re})_p}{24} - 1\right] = -0.7133 + 0.6305w$
	$C_D = \frac{24}{(\mathrm{Re})_p}\left[1 + 0.1935(\mathrm{Re})_p^{0.6305}\right]$
$260 \le (\mathrm{Re})_p \le 1500$	$\log_{10} C_D = 1.6435 - 1.1242w + 0.1558w^2$
$1.5 \times 10^3 \le (\mathrm{Re})_p \le 1.2 \times 10^4$	$\log_{10} C_D = -2.4571 + 2.5558w - 0.9295w^2 + 0.1049w^3$
$1.2 \times 10^4 \le (\mathrm{Re})_p \le 4.4 \times 10^4$	$\log_{10} C_D = -1.9181 + 0.6370w - 0.0636w^2$
$4.4 \times 10^4 \le (\mathrm{Re})_p \le 3.38 \times 10^5$	$\log_{10} C_D = -4.3390 + 1.5809w - 0.1546w^2$
$3.38 \times 10^5 \le (\mathrm{Re})_p \le 4 \times 10^5$	$C_D = 29.78 - 5.3w$
$4 \times 10^5 \le (\mathrm{Re})_p \le 10^6$	$C_D = 0.1w - 0.49$
$10^6 < (\mathrm{Re})_p$	$C_D = 0.19 - \frac{8 \times 10^4}{(\mathrm{Re})_p}$

Source: Adapted from Clift et al. (1978).

For calculating the terminal velocity w_T based on this formula, numerous studies are available (e.g. Clift, Levenspiel, Heywood, Allen et al.) [90]. One of these possibilities is the equation by Haider and Levenspiel [90,121]. Therefore, equation (5-27) has to be combined with equation (5-20) and the terminal velocity can be expressed:

$$w_t = \sqrt{\frac{4}{3} \cdot \frac{d_{eff} \cdot (\rho_s - \rho_g) \cdot g}{\rho_g \cdot c_d}} \tag{5-28}$$

By combining equation (5-28) and the recommended drag coefficient correlations by Clift et al. (cf. Table 5) or the equation proposed by Levenspiel (5-29) [121], the terminal velocity can be calculated:

$$c_d = \frac{24}{Re_p} \cdot \left[1 + (8.1716e^{-4{,}0655\varphi}) \cdot Re_p^{0.0964+0.5565\varphi}\right] + \frac{73.29(e^{-5.0748\varphi}) \cdot Re_p}{Re_p + 5.378e^{6.2122\varphi}} \tag{5-29}$$

5.3.3 Definition of the operating point of a fluidized bed

In chapter 5.3.1 and chapter 5.3.2 the gas velocities for minimum fluidization and for the discharge of a particle collective was calculated, hence rendering the possible area of opteration. To define a certain fluidized state, a phase diagram for gas-solid systems can be applied (cf. Figure 38). With this diagram, developed by L. Reh [140], the required gas velocity for the adjustment of a certain fluidized state can be estimated.

As discussed before, the formation of a fluidized bed depends on various parameters, such as flow rate, diameter and shape of particles or density and viscosity of the fluid. These parameters can be combined to dimensionless numbers, which can be correlated in the Reh-diagram [140]. The following dimensionless numbers are important for defining the operating lines in the diagram [10,123,140]:

Reynolds-number: (Ratio: Inertial Force / Viscous Force; function of superficial velocity and particle diameter):

$$Re = \frac{d_p \cdot \rho \cdot w}{\eta} \qquad Re = f(d_p) = f(w) \tag{5-30}$$

Froud-number: (Ratio: Inertial Force / Gravitational Force; function of superficial velocity and particle diameter):

$$Fr = \left(\frac{w^2}{g \cdot d_p}\right)^{\frac{1}{2}} \qquad Fr = f(d_p) = f(w) \tag{5-31}$$

Archimedes-number: (Ratio: Bouyancy Force / Friction Force; function of the particle diameter = dimensionless particle diameter):

$$Ar = \frac{d_p^3 \cdot \rho_g \cdot (\rho_s - \rho_g) \cdot g}{\eta^2} = \frac{1}{K} \qquad Ar = f(d_p) \neq f(w) \tag{5-32}$$

Ljascenko-number: (characteristic number for sedimentation; function of the superficial velocity = dimensionless superficial velocity):

$$Lj = \frac{w^3 \cdot \rho_g^2}{\eta \cdot g \cdot (\rho_s - \rho_g)} = M = \Omega \qquad Lj = f(w) \neq f(d_p) \tag{5-33}$$

Load-factor:

$$n = \frac{\Delta p}{(1-\varepsilon)\cdot(\rho_s - \rho_g)\cdot g} \qquad (5\text{-}34)$$

whereas: n > 1… discharge
n = 1… fluidization of material
n < 1… fixed bed

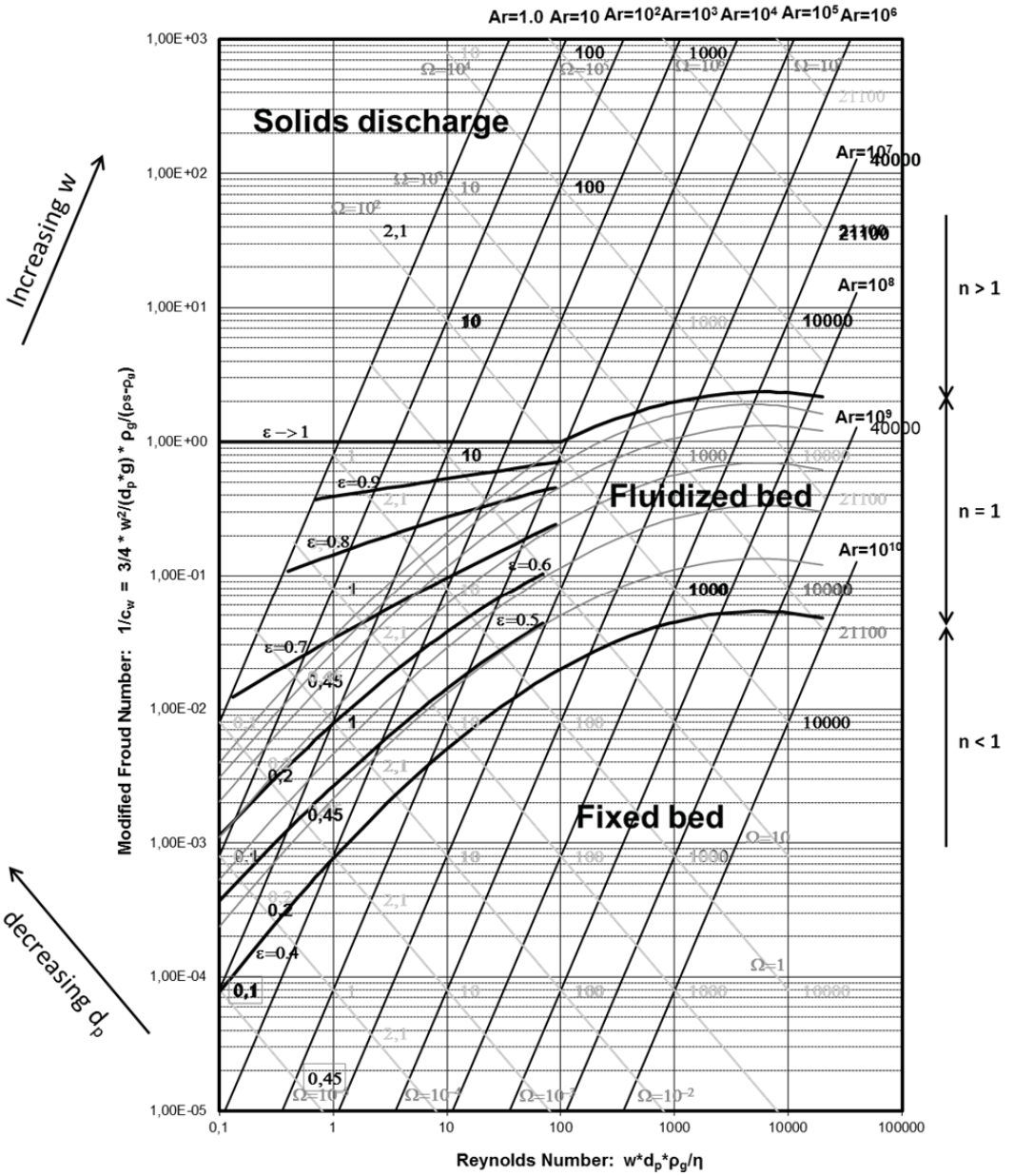

Figure 38: Reh-diagram for gas-solid systems

Porosity: ε is the porosity of the bed, whereas ε = 0.4 is valid for the fluidization point of a bulk of spheric particles and ε = 1 refers to an empty tube.

The x-axis in the diagram is the Re-number, which is calculated with the particle diameter. On the y-axis, the reciprocal of the drag coefficient (a modified Fr-number) is plotted [10,123,140]:

$$\frac{1}{c_w} = \frac{3}{4} \cdot \frac{w^2}{g \cdot d_p} \cdot \frac{\rho_f}{(\rho_s - \rho_f)} = \frac{3}{4} \cdot Fr^2 \cdot \frac{\rho_f}{(\rho_s - \rho_f)} \quad (5\text{-}35)$$

To determine the fluidized bed conditions, an auxiliary grid of lines with constant Ar-number and constant Lj-number is plotted. In the perameters c_w and Re, the particle diameter d_p and the gas velocity w appear coupled, whereas Ar is a function of dp and Lj is a function of w [123,140].

This diagram provides a general scheme for the determination of different fluidized bed systems and their allocation. Hence, related fluidized bed systems can be determined by the knowledge of the operating conditions [140].

Regarding the layout of a gas-solid fluidized bed system, there is another important parameter which has to be considered, the so called “slip”. When the flow rate increases beyond the minimum fluidization velocity, the behavior of the particle velocity increase is not linear. Between gas and solids a relative velocity difference evolves (cf. Figure 39).

In a stationary fluidized bed, the particle and gas velocities are low and the fluidized bed is stable. In a circulating fluidized bed, the gas velocity (and relative velocity) is high and a discharge of particles emerges. Here, the fluidized bed expands across the whole reactor length and the discharged material is recycled into the reactor by means of a cyclone. Because of the high gas velocity and the good gas/solid mixture, a high mass and heat transfer can be generated [38]. In the transport-reactor-system, the gas velocity is on a value, that all particles are discharged from the reactor (pneumatic transport). Because the particles are entrained by the gas stream, the slip decreases. Although there are just three reactor types listed, the band width of fluidized bed applications regarding Figure 39 is tremendous.

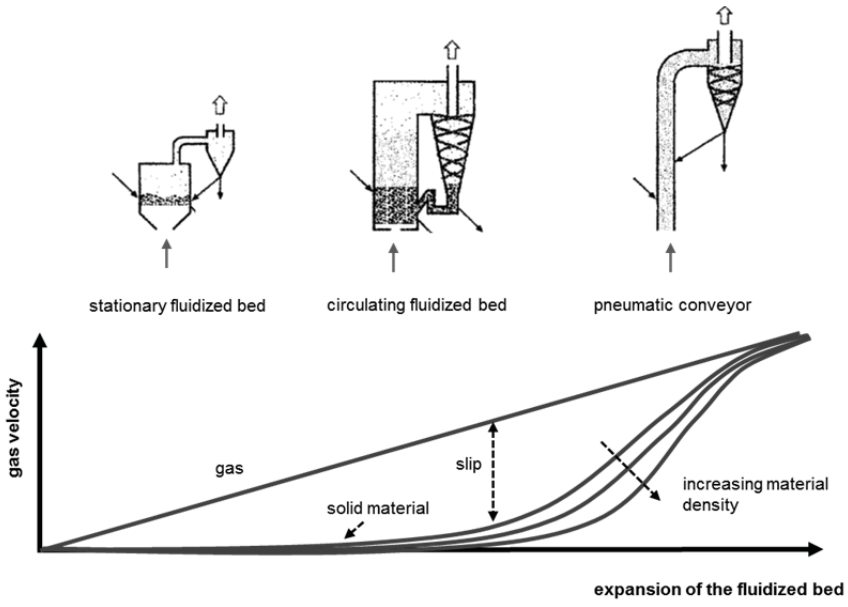

Figure 39: Methodology of fluidized bed systems in dependence on the relative velocity [125]

6 Experimental

6.1 Experimental setup of the fluidized bed reactor installation

The fluidized bed reactor installation was already in progress between 1999 and 2005 at the laboratories of voestalpine for the development of the fluidized bed based iron ore reduction processes FIOR® and FINMET®. In this period, over 200 trials were performed. Due to the development and optimization of the FINMET®- and the new FINEX®-process, the demand for research activities increased again.

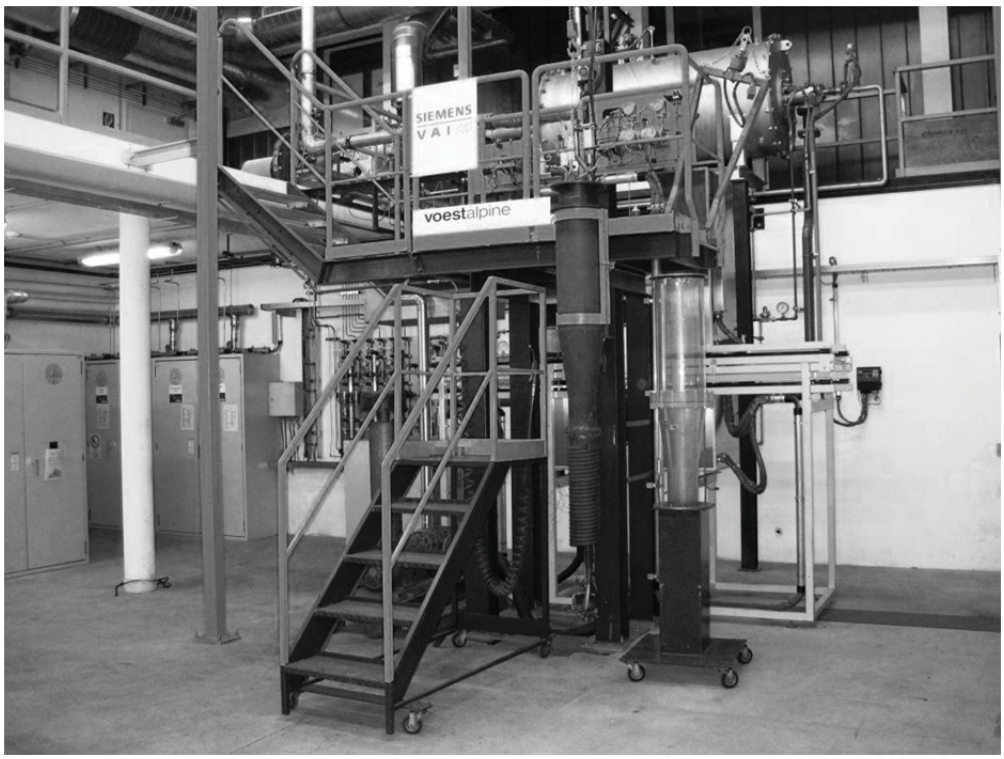

Figure 40: Fluidized bed reactor installation at the Chair of Metallurgy

Within this research work, since July 2009, the facility has been completely rebuild and remodeled in collaboration of Siemens VAI, voestalpine and the Chair of Metallurgy. In June 2010, the installation was successfully set into operation at the Chair of Metallurgy (cf. Figure 40).

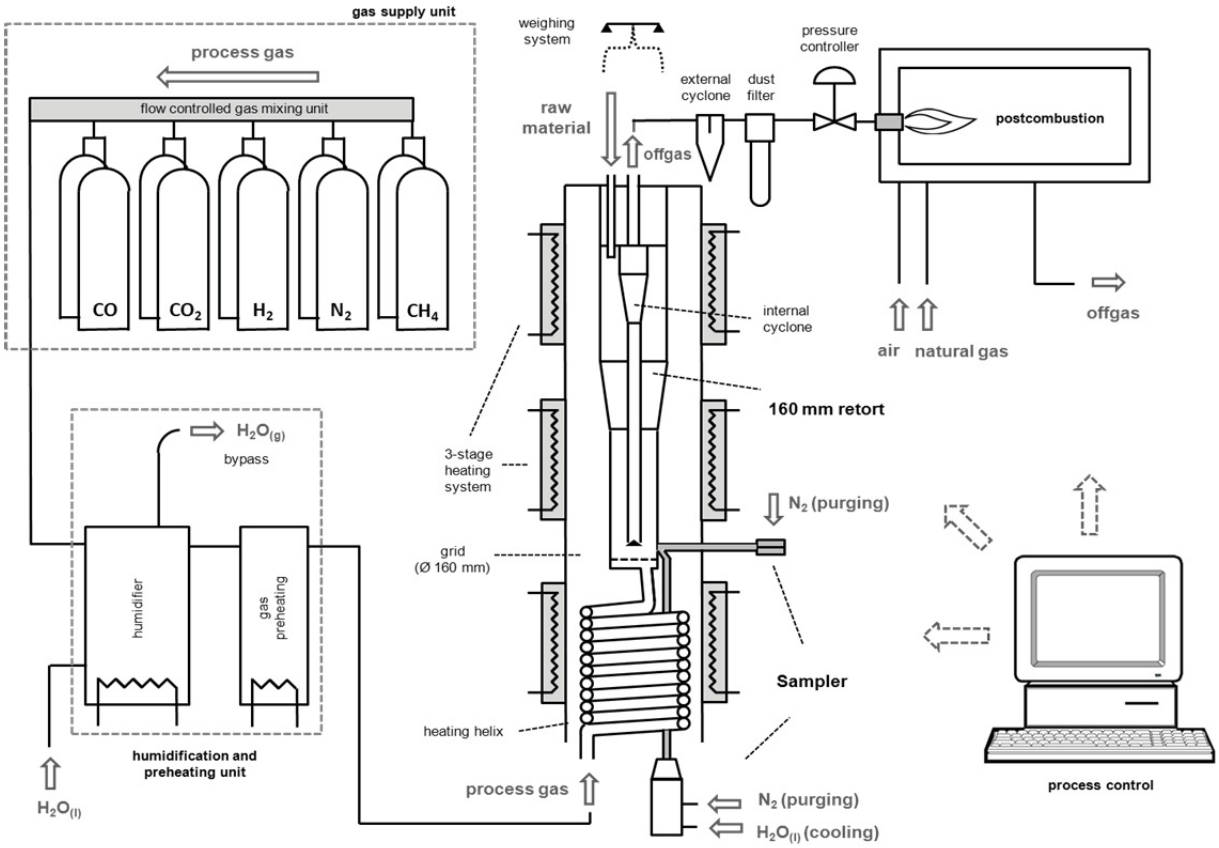

Figure 41: Setup of the fluidized bed reactor installation

The principal assembly of the reactor has already been described by [113]. Figure 41 shows the layout of the fluidized bed reactor installation. In Table 6, the technical details and features are listed. The core part is a retort with a grid diameter of 160 mm and a capacity of up to 5 kg sample mass. The fine ores used for the tests usually have grain size distributions between 0.06 to 4.0 mm. The gas is supplied from gas supply units and a gas mixing unit which operates fully automated by mass flow controllers, and a wide variety of different gas mixtures containing CO, CO_2, H_2, H_2O, N_2 and CH_4 can be realized (cf. Figure 42 and Figure 43). The maximum volume flow rate is up to 700 l_N/min (l_N: liter under standard temperature and pressure). For $H_2O_{(g)}$-enrichment and preheating of the process gas, a humidification unit is installed. The saturated gas mixture flows through a heating helix to the fluidized bed retort. A 3-zone electrical heating system consisting of half pipe shaped heating elements provides the thermal energy for the execution of the reduction tests. The process gas reduces the sample material by building up a fluidized bed above the grid. Fine fractions entrained from the bed are separated and recycled to the fluidized bed by means of an internal cyclone. Dust and finest fractions are discharged to the off-gas system, where the

particles are separated by an external cyclone and a dust filter. Thereafter the gas enters the post combustion chamber, where it is flared by a natural gas burner (cf. Figure 44).

Table 6: Technical facts and features of the fluidized bed reactor installation

Technical details:	
Grid diameter:	160 mm
Sample mass:	up to 5 kg
Grain size distributions:	From 0.06 mm to 4.00 mm
Gas supply (by flow controlers):	up to 700 l_N/min
Gas species:	CO, CO_2, H_2, H_2O, CH_4, N_2
Temperature range:	up to 900 °C
Pressure range:	up to 1.6 bar absolute

Features:

- H_2O gas control by evaporator
- Online weighing system of Fluidized Bed
- Inner Cyclone and Off Gas Dust Filter
- Sampling system
- Fully automated or manual tests
- Cold and hot tests possible

Figure 42: Gas supply unit

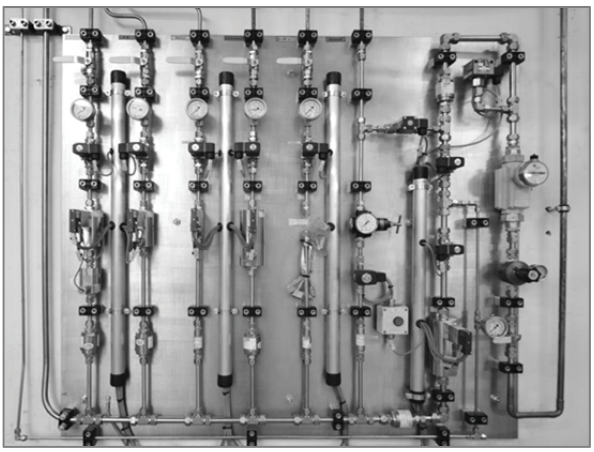

Figure 43: Flow controlled gas mixing unit

The installation is equipped with flow meters, thermocouples and pressure gauge providing the data for the automated control of volume flow, electrical heating and pressure level for the fluidized bed reactor. The retort is attached to a load cell which enables the permanent recording of the weight loss of the fluidized bed material during the reduction. The process automation enables a completely controlled test procedure (cf. Figure 45). The test can be executed fully automated or manually.

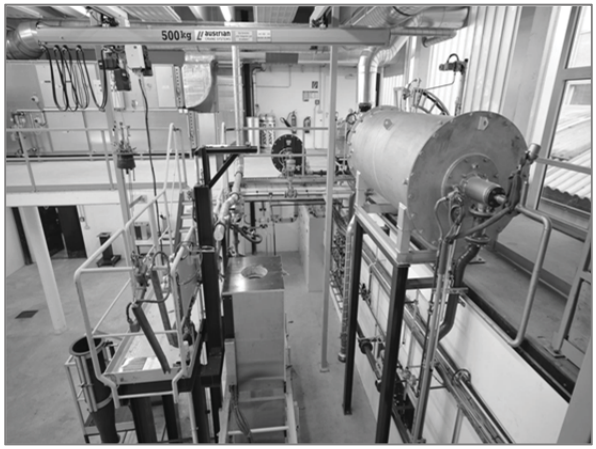

Figure 44: Off-gas system and post combustion

Figure 45: Process automation

To investigate in the morphological behavior and evolution of the sample material during the process, an independent sampling system has been additionally installed in 2012 in the scope of a master thesis (cf. Figure 47) [37].

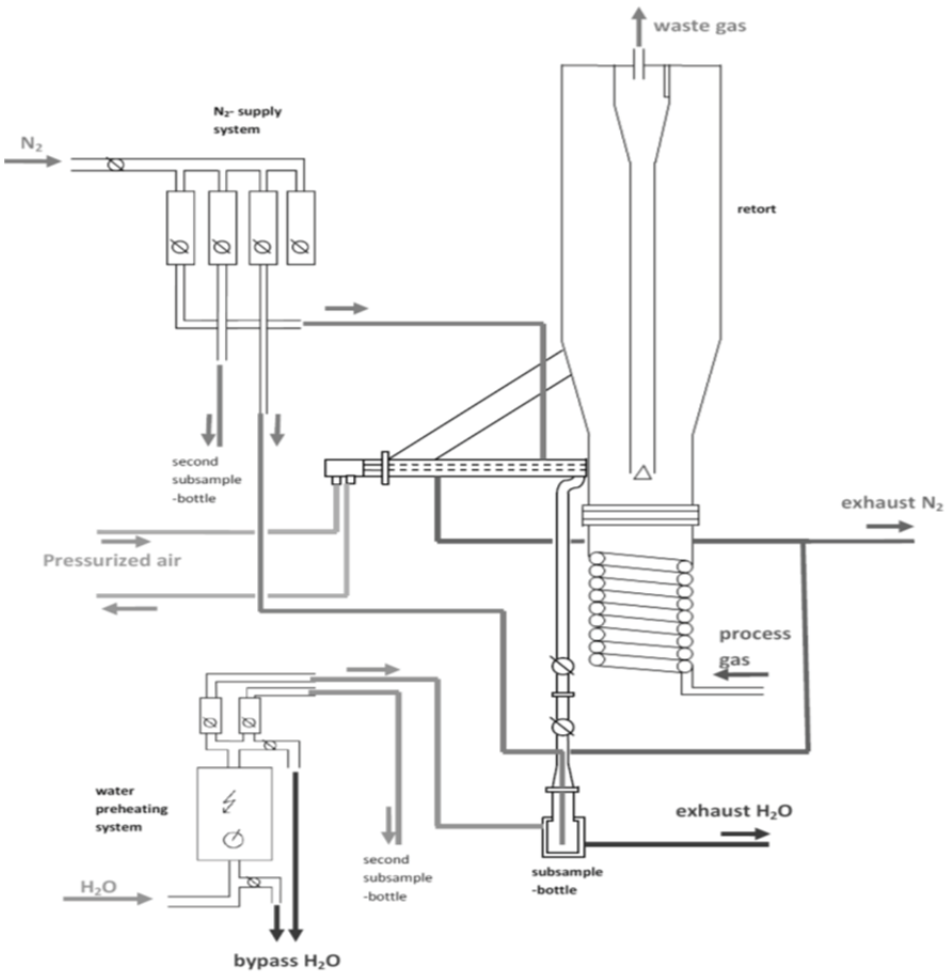

Figure 46: Layout of the sampling system [37]

The system consists of a sampler, flow-controlled nitrogen purging units as well as flow- and temperature-controlled water cooling units. The samples can be extracted directly from the fluidized bed by means of a pneumatically operated locking device. After extracting the sample from the fluidized bed, the material falls through a pipe into a sample container. The whole system is purged with N_2 to avoid reoxidation of the material and additionally, the sample container is cooled with water to assure a fast cooling of the sample mass. The sample container can be exchanged independently from the system, so, various samples can be extracted during the test.

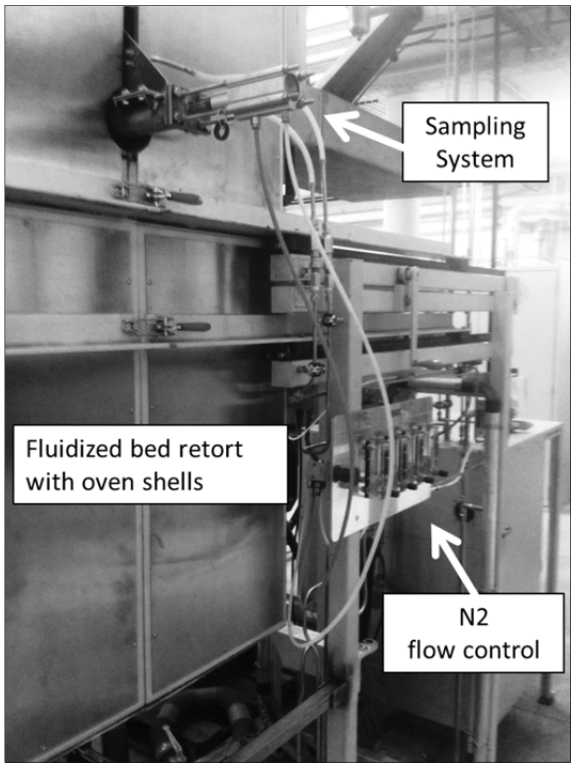

Figure 47: Fluidized bed retort with sampling system

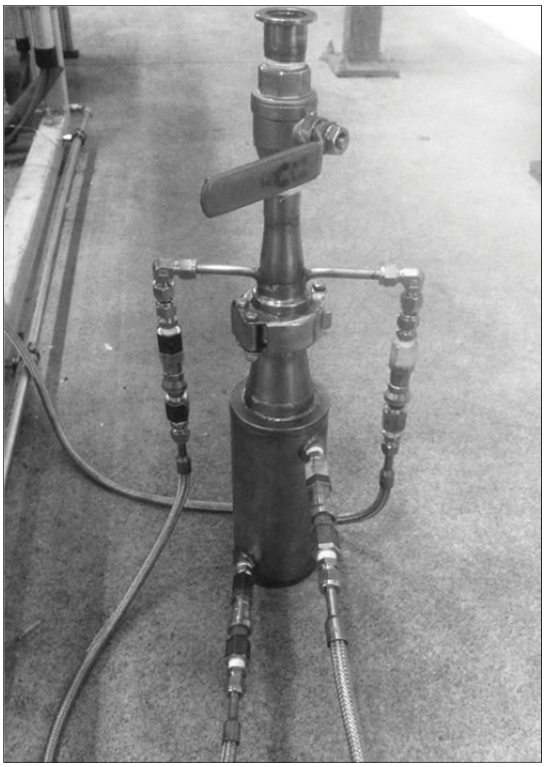

Figure 48: Sample container

Comprising the methodology of process control and the subsequent morphological and chemical analyses of various extracted samples, this new method is an excellent tool for the development of fluidized bed based technologies and for characterizing the process behavior of iron ore fines.

6.2 Experimental procedure and determination of test conditions

Due to thermodynamic and morphologic constraints, fluidized bed reduction processes for the production of direct reduced iron are limited regarding the reduction progress from iron ore to metallic iron. In fluidized bed processes, iron ores are reduced by gas mixtures of CO, CO_2, H_2, H_2O, CH_4 and N_2 at temperatures between 300 °C and 800 °C. In the thermodynamically ideal case, a two-stage fluidized bed reactor with counter current flow of hot reducing gas and cold iron oxide (hematite) can approach the minimum theoretical gas

consumption (cf. Schenk [1]). However, such a system seems to be practically inoperable, since the temperature in the reaction stages would be too low for the chemical reaction kinetics. One measure for raising the temperature is to increase the number of reaction stages to three or four in order to utilize the sensible heat of the reducing gas more efficiently for preheating of the cold iron ore. Optional possibilities would be the increasing of the reducing gas flow and/or to charge pre-heated ore [1]. In the industrial FINEX®-process, the fine iron ore is reduced stepwise in four sequenced fluidized bed reactors. To optimize the process, a three-stage reduction operation should be evaluated and compared to the actually applied four-stage operation. In this chapter, the experimental procedure is described by means of a three-stage fluidized bed operation.

6.2.1 Experimental procedure of a lab scale fluidized bed test

In order to illustrate the reduction process, the thermodynamic conditions and – as an example - the operating points for a sequenced 4-stage reduction can be described by the Baur-Glaessner diagram shown in Figure 49.

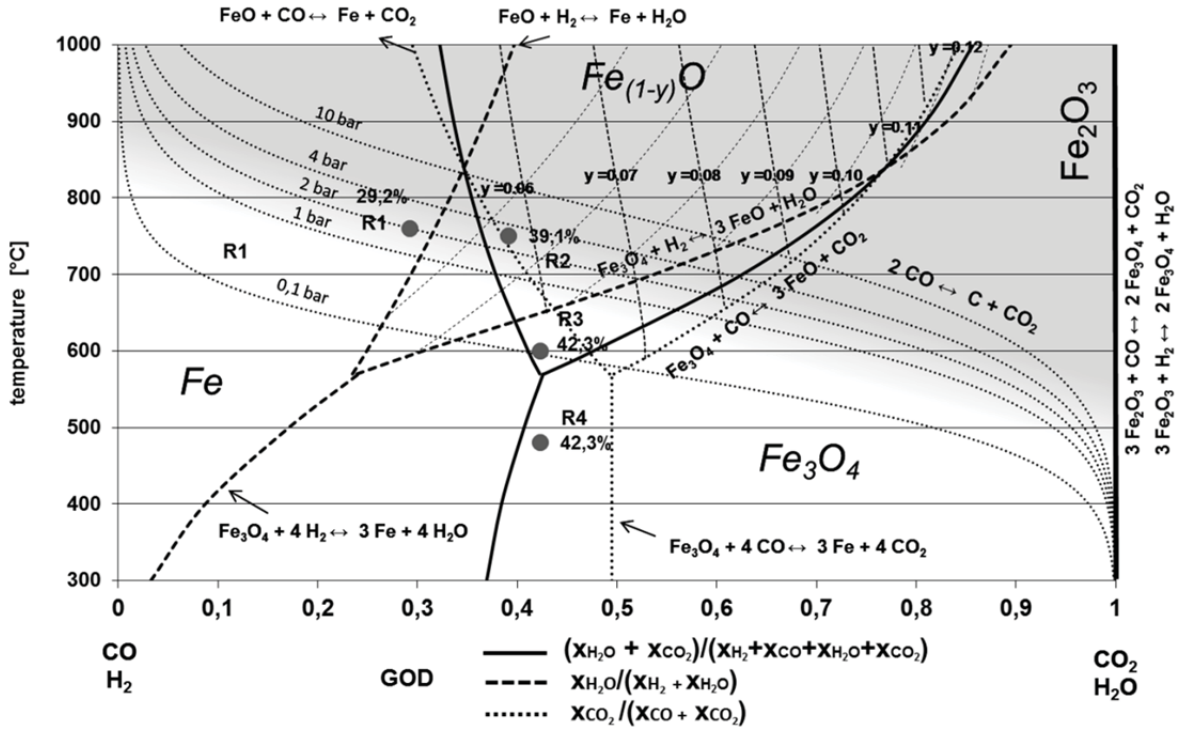

Figure 49: Baur-Glaessner for gas mixtures of H_2, H_2O, CO, CO_2
with operating points of a sequenced 4-stage reduction procedure

These operating points (R1 – R4) are adapted to industrial processes based on coal gasification for the generation of the reducing gas, containing CO, CO_2, H_2, H_2O and N_2. First, the iron ore is reduced by the process gas to magnetite (R4), then to wuestite in two stages (R3/R2) and finally in the stability field of iron to a certain amount of metallic iron (R1). The difference is, that the operation points represent gas mixtures at the discharge of the fluidized bed reactors (cf. Figure 50). In reality, the quality of the gas composition varies with

the height of the bed from conditions at inlet to discharge. The gas at the inlet has a lower GOD, hence the average reducibility of the reducing gas in the bed is stronger in the real process than in the lab tests.

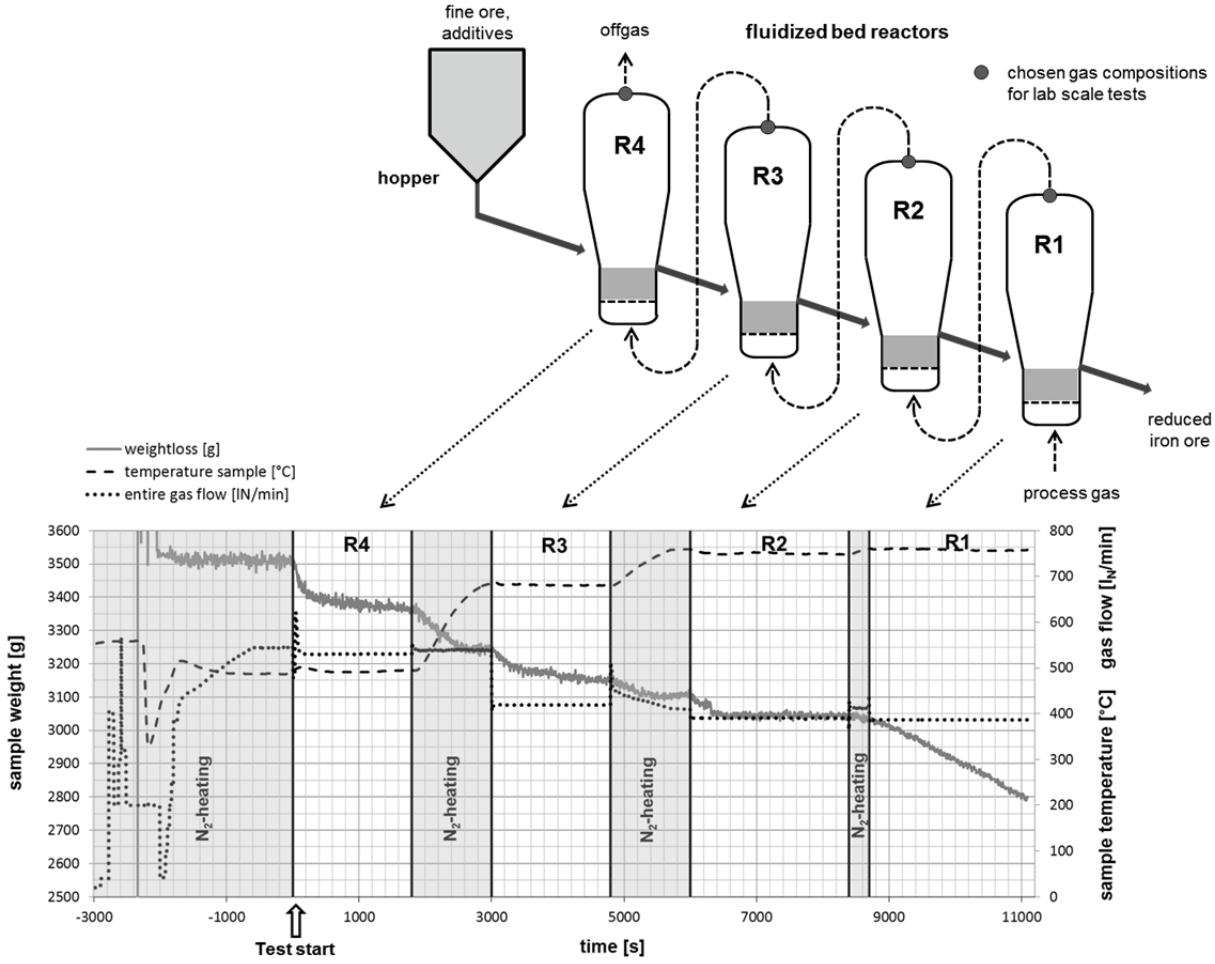

Figure 50: operation mode of a sequenced 4-stage batch lab scale test

The tests are executed in batch mode to guarantee equal conditions such as identical residence time, gas composition and temperature for all particles of the bed material during the operation. Figure 50 shows the operation mode of the batch lab scale tests compared to the industrial reduction process. In real operation, the iron ore flows continuously from a hopper system through the individual reactor stages; the process gas correspondingly moves in a countercurrent flow. The iron ore is progressively reduced in the individual stages at different temperatures and gas compositions i.e. GOD. At lab scale these process conditions can be displayed with a single fluidized bed operated in batch mode by varying temperature and GOD analogous to the real process. A detailed description of the methodology is discussed in chapter 6.3 “Development of a standardized methodology for the classification of fine ores”.

6.2.2 Determination of the test conditions

Based on industrial scale direct- and smelting reduction processes, which rely on coal gasification as a source for the generation of the reducing gas, the test conditions for the fluidized bed tests are determined in this chapter. The values are calculated for a sequenced 3-stage reduction process, adjusted to industrial conditions. First of all, the grain size distribution of the iron ore particle collective and its minimum fluidization point and discharge point has to be calculated. Based on these calculations, the operating point with a certain superficial velocity in the reactor tube can be defined. In the final step, the process conditions of a real industrial application have to be adapted to the conditions of the lab scale fluidized bed facility.

Particle collective and operating range

As discussed in chapter 5.3, the determination of the minimum fluidization point (minimum fluidization velocity w_{mf}) and the discharge point (terminal velocity w_{mf}) is important to define the operating point of a fludized bed system with polydisperse particle collectives. Based on the grain size distribution of iron ore fines in sinter feed quality, the grain size distribution for the lab scale tests was defined (cf. Figure 51 and Table 7) with a spectrum between 0.063 and 4.000 mm. The representative particle diameter or sauter mean diameter can be calculated with equation (5-11) (cf. chapter 5.2):

$$\bar{d} = \frac{1}{\sum\left(\frac{x}{d_p}\right)_i} = \frac{1}{\sum\frac{\Delta Q_{3,i}}{d_{p,i}}} \tag{6-1}$$

Table 7: Grain size distribution for lab scale tests

d_U - d_O [mm]	m_i [g]	$d_{p,i}$ [mm]	$x_i = (m_i/m_{tot}) = \Delta Q_{3,i}$	$\Delta Q_{3,i}/ d_{p,i}$	$Q_{3,i}$
0,000 – 0,063	0,0	0,032	0,000	0,000	0,000
0,063 - 0,125	885,5	0,094	0,253	2,692	0,253
0,125 - 0,250	514,5	0,188	0,147	0,784	0,400
0,25 - 0,50	609,0	0,375	0,174	0,464	0,574
0,5 - 1,0	560,0	0,750	0,160	0,213	0,734
1,0 - 2,8	465,5	1,900	0,133	0,070	0,867
2,8 - 4,0	465,5	3,400	0,133	0,039	1,000
> 4,0	0,0	-	0,000	-	1,000
	Σ = 3500,0		Σ = 1,000	Σ = 4,262	

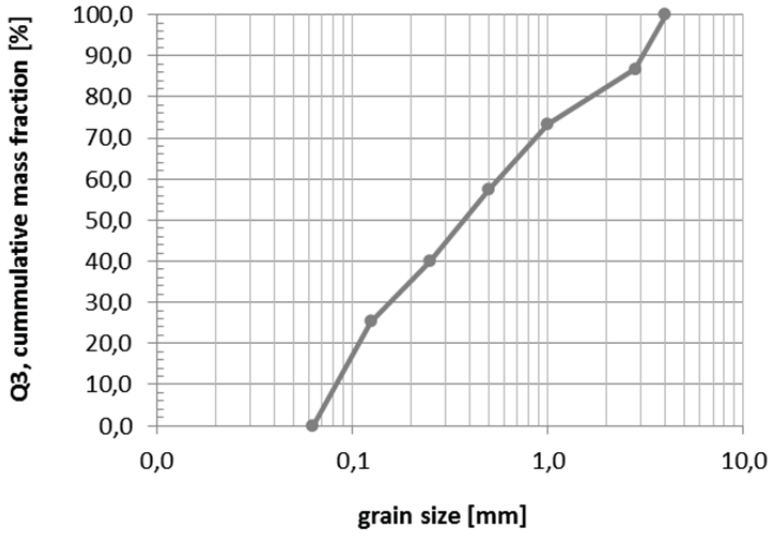

Figure 51: Cummulative grain size distribution

Due to the non spheric nature of most particles, the so called shape factor has to be considered for the calculations (cf. chapter 5.2). Referring to Kunii-Levenspiel, a shape factor of 0,86 for round sand [121] was chosen and the effective particle diameter for the grain size distribution is:

$$d_{eff} = \varphi_s \cdot \bar{d} = 0.86 \cdot 0.2346 = 0.2018\ \text{mm} \qquad (6\text{-}2)$$

For the particle collective, a voids fraction ε of 0.4 was chosen. The density of the ore is 3500 kg/m³ and a pressure of 1.4 bar was chosen, which is the operation pressure of the lab scale facility. Based on the force balance at the minimum fluidization point, the minimum fluidization velocity can be calculated with equations (5-15) to (5-24). The terminal velocity of the particles can be determined by the equations (5-25) to (5-29). In Table 8, w_{mf} and w_T for a 3-stage sequenced fluidized bed system is calculated for maximum, minimum and average grain size fractions.

The flow rates for the fluidization can be determined based on the knowledge about the minimum fluidization and discharge conditions. Regarding Table 8, the terminal velocity of the smaller particles is lower than the minimum fluidization velocity of the bigger particles. That means, that the smaller particles are discharged, before the bigger particles reach the fluidized state.

Hence, the effective particle diameter d_{eff} for the representative grain size of a particle collective is used for the investigations. With d_{eff}, the representative minimum fluidization velocity is 0.02 m/s and the terminal velocity is 1.29 m/s. On the basis of these considerations, a superficial velocity of 0.9 m/s is chosen for the lab scale tests, which is close to the superficial velocity of the industrial plant.

Table 8: Calculation of the minimum fluidization velocity and terminal velocity of a sequenced fluidized bed system (for different grain size fractions)

M_{CO}	28 [g/mol]
M_{CO2}	44 [g/mol]
M_{H2}	2 [g/mol]
M_{H2O}	18 [g/mol]
M_{N2}	28 [g/mol]
M_{CH4}	16 [g/mol]
ε	0,4 [-]
ρ_s	3500 [kg/m³]
d_{SMD}	0,234632 [mm]
φ	0,86 [-]
R	8,3145 [J/molK]
p	1,4 [bar]
d_{max}	4 [mm]
d_{eff}	0,20178 [mm]
d_{min}	0,063 [mm]

Parameter fluidized bed				
gas composition		R1 [%]	R2 [%]	R3 [%]
species	**H_2**	17,7%	16,5%	16,0%
	H_2O	5,6%	7,1%	8,7%
	CO	46,7%	38,9%	36,5%
	CO_2	21,0%	28,5%	29,8%
	CH_4	1,5%	1,6%	1,6%
	N_2	7,5%	7,4%	7,4%
	total dry	94,4%	92,9%	91,3%
	total wet	100,0%	100,0%	100,0%
	GOD	29,2%	39,1%	42,3%
	H_2/H_2O	3,16	2,32	1,84
	CO/CO_2	2,22	1,36	1,22
	T [K]	1033	1023	753
	M_{mix} [g/mol]	26,02	27,37	27,55
	ρ_g [kg/m³]	0,424	0,450	0,616
	η_{dyn}	0,000042	0,000042	0,000034
Minimum fluidization velocity				
Ar	Ar(d_{max})	528164,629	565423,461	1198933,002
	Ar(d_{eff})	67,802	72,585	153,911
	Ar(d_{min})	2,064	2,209	4,684
Re,p	Re,p(d_{max})	115,626	120,366	185,255
	Re,p(d_{eff})	0,048	0,052	0,109
	Re,p(d_{min})	0,001	0,002	0,003
w_{mf}	**w_{mf} (d_{max})**	**2,863**	**2,795**	**2,526**
	w_{mf} (d_{eff})	**0,024**	**0,024**	**0,030**
	w_{mf} (d_{min})	**0,002**	**0,002**	**0,003**
Terminal velocity				
Re,p	Re,p(d_{max})	951,824	983,337	1404,027
	Re,p(d_{eff})	2,630	2,787	5,211
	Re,p(d_{min})	0,107	0,115	0,235
c_d for Re,p	c_d for Re,p(d_{max})	0,777	0,780	0,811
	c_d for Re,p(d_{eff})	13,068	12,458	7,557
	c_d for Re,p(d_{min})	239,065	224,417	113,158
w_T	**w_T(d_{max})**	**23,567**	**22,833**	**19,145**
	w_T (d_{eff})	**1,291**	**1,283**	**1,409**
	w_T (d_{min})	**0,169**	**0,169**	**0,203**

For the choice of the flow rate it should be noted, that the biggest part of the particles should be theoretically fluidized. At the same time, as few small particles as possible should be discharged. Regarding the interpretation of the operating point of a fluidized bed, the fluidized particle spectrum is important. Therefore, the dimensionless Ljascenco-number has to be used (cf. equation (5-33)):

$$Lj = \frac{w^3 \cdot \rho_g^2}{\eta \cdot g \cdot (\rho_s - \rho_g)} = \frac{0.9^3 \cdot 0.424^2}{0.000042 \cdot 9.81 \cdot (3500 - 0.424)} = 0.091 \quad (6\text{-}3)$$

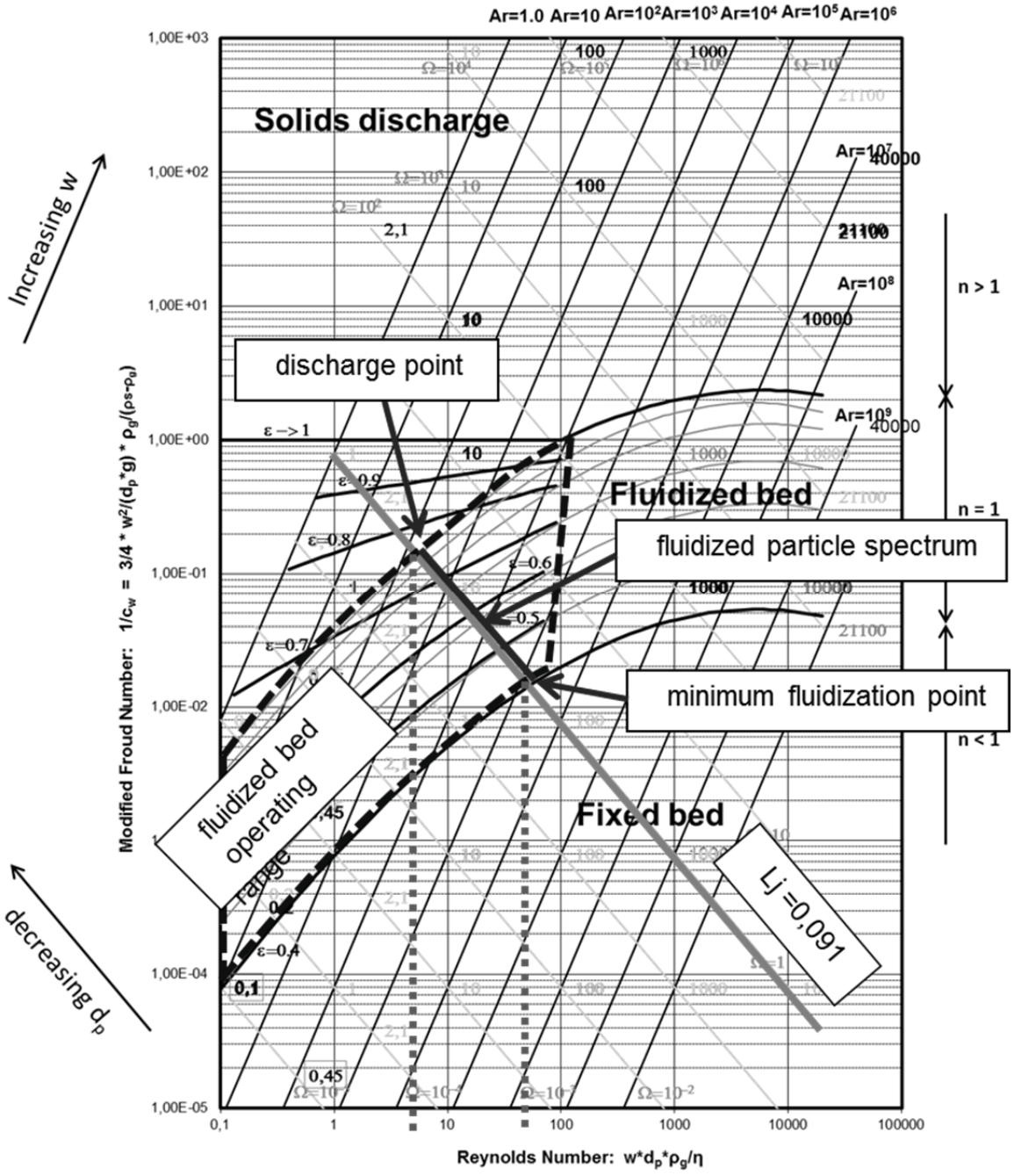

Figure 52: Reh-diagram with fluidized particle spectrum based on the operation conditions

Because of the constant superficial velocity, the fluidized particle spectrum can be determined by plotting the Ljascenco-number into the Reh-diagram (cf. Figure 52). Only a small spectrum of the Ljascenco line represents the fluidized particle spectrum, which is

bounded by the fluidized bed operating region. The intersections of the Ljascenco line with the operation region define the minimum fluidization point and the discharge point. The Reynolds numbers of this operation spectrum can be determined with Re=40 for the minimum fluidization point and Re=4 for the discharge point. By means of equation (5-30), the critical particle diameters $d_{p,max}$ and $d_{p,min}$ can be determined:

$$d_{p,min} = \frac{Re \cdot \eta}{\rho \cdot w} = \frac{4 \cdot 0.000042}{0.424 \cdot 0.9} = 0.44\,mm \tag{6-4}$$

$$d_{p,max} = \frac{Re \cdot \eta}{\rho \cdot w} = \frac{40 \cdot 0.000042}{0.424 \cdot 0{,}9} = 4.40\,mm \tag{6-5}$$

In this juncture, $d_{p,max}$ is the particle size, which is just barely fluidized and $d_{p,min}$ is the particle size which is not yet discharged. In reality, the Ljascenco line is shifting to a lower value because of the influence of particle size distributions. Hence, these critical diameters are decreasing to lower values.

Determination of the gas compositions and flow rates in lab scale dimensions

In order to provide similar process conditions, the gas mixtures and flow rates of an industrial application have to be converted into the conditions of the lab scale test facility. As an example, the calculated conditions of an industrial process are shown in Table 9 and Figure 53.

Table 9: Process conditions of an industrial process

gas composition		R1 [%]	R2 [%]	R3 [%]
species	H_2	17,7%	16,5%	16,0%
	H_2O	5,6%	7,1%	8,7%
	CO	46,7%	38,9%	36,5%
	CO_2	21,0%	28,5%	29,8%
	CH_4	1,5%	1,6%	1,6%
	N_2	7,5%	7,4%	7,4%
	total dry	94,4%	92,9%	91,3%
	total wet	100,0%	100,0%	100,0%
	GOD	29,2%	39,1%	42,3%
	H_2/H_2O	3,16	2,32	1,84
	CO/CO_2	2,22	1,36	1,22
temperature [°C]		760	750	480
pressure [bar]		4	4	4
med. residence time [min]		40	30	30

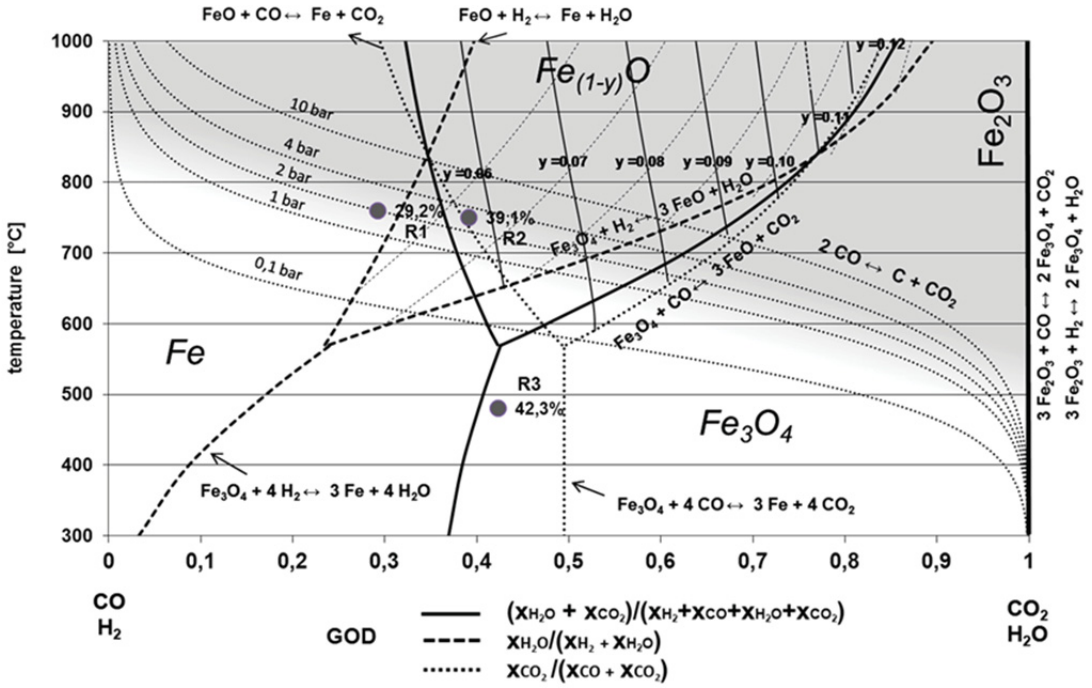

Figure 53: Baur-Glaessner for gas mixtures of H_2, H_2O, CO, CO_2
with Boudouard equilibrium for different pressures and operating points

For the lab scale tests, a specific gas rate of the reacting components of 3000 – 4000 Nm³ per ton is defined (in reality about 800 Nm³/ton). The diameter of the test facility is 160 mm, the operating pressure is 1.4 bar (absolute) and the sample mass is 3.5 kg. The superficial velocity in the industrial plant is about 0.9 m/s. In order to describe the calculation procedure, the conversion of the CO gas flow in Reactor 1 (R1) is illustrated as an example. First of all the total flow rate of the reactive process gas has to be determined:

$$\dot{V}_{pg} = \frac{SGR \cdot m_{sample}}{t} = \frac{4000\ {}^{Nm^3}/_{t} \cdot 0.0035\ t}{40\ min} \cdot 1000 \cdot 60 = 21000\ l_N/h \tag{6-6}$$

With the CH_4 – and N_2-content, the total flow rate is

$$\dot{V}_{tot} = 21000\ {}^{l_N}/_{h} \cdot \frac{H_2 + H_2O + CO + CO_2 + CH_4 + N_2}{H_2 + H_2O + CO + CO_2}[\%] = 23077\ l_N/h \tag{6-7}$$

The gas flow of through the retort with a defined superficial velocity, temperature and pressure (conditions of R1) can be calculated with:

$$\dot{V_{ret}} = \frac{w \cdot A_{ret} \cdot p_{abs} \cdot 273}{(T_{sample} + 273) \cdot p_{atm}} = \frac{0.9\ {}^{m}/_{s} \cdot 0.0196\ m^2 \cdot 1.4\ bar \cdot 273\ K}{(760\ °C + 273\ K) \cdot 1.013\ bar} \cdot 1000 \cdot 3600 = 23202\ l_N/h \tag{6-8}$$

The difference between $\dot{V}_{pg}$ and $\dot{V}_{ret}$ in the test facility is replaced by nitrogen, whereas the relative share of the reactive components H_2, H_2O, CO und CO_2 stays the same. Now, the gas composition and gas flow per minute of the single components can be calculated:

$$CO_{ret}\,[\%] = \frac{\dot{V}_{tot}}{\dot{V}_{ret}} \cdot CO\,[\%] = \frac{23077\ {}^{Nm^3}/_{h}}{23202\ {}^{Nm^3}/_{h}} \cdot 46.7\,\% = 46.4\,\% \tag{6-9}$$

$$\dot{V}_{CO} = \frac{\dot{V}_{ret}\ \cdot\ CO_{ret}}{60}\,[\%] = \frac{23202\ {}^{Nm^3}/_{h}\ \cdot\ 46.4\,\%}{60} \cdot 46.7\,\% = 179.4\ l_N/min \tag{6-10}$$

The process conditions of the single reactors of an industrial application and the calculated conditions for the test facility are shown in Table 10.

Table 10: Calculation between real plant conditions and lab scale conditions

		concentration, temp. plant				concentration test rig				gas flow test rig						
gas composition		R1 [%]	R2 [%]	R3 [%]	R4 [%]	R1 [%]	R2 [%]	R3 [%]	R4 [%]	R1 [Nl/min]	heating [Nl/min]	R2 [Nl/min]	heating [Nl/min]	R3 [Nl/min]	heating [Nl/min]	R4 [Nl/min]
species	H_2	17,7%	16,5%	16,0%	0,0%	17,2%	16,9%	14,3%	0,0%	66,5		66,1		76,1		0,0
	H_2O	5,6%	7,1%	8,7%	0,0%	5,4%	7,3%	7,8%	0,0%	21,0		28,4		41,4		0,0
	CO	46,7%	38,9%	36,5%	0,0%	45,4%	39,9%	32,7%	0,0%	175,4		155,8		173,6		0,0
	CO_2	21,0%	28,5%	29,8%	0,0%	20,4%	29,2%	26,7%	0,0%	78,9		114,2		141,8		0,0
	CH_4	1,5%	1,6%	1,6%	0,0%	0,0%	0,0%	0,0%	0,0%	0,0		0,0		0,0		0,0
	N_2	7,5%	7,4%	7,4%	0,0%	11,6%	6,6%	18,4%	0,0%	45,0		26,0		97,6		0,0
	total dry	94,4%	92,9%	91,3%	0,0%	94,6%	92,7%	92,2%	0,0%	365,7		362,0		489,1		0,0
	total wet	100,0%	100,0%	100,0%	0,0%	100,0%	100,0%	100,0%	0,0%	386,7		390,5		530,5		0,0
	GOD	29,2%	39,1%	42,3%	0,0%	29,2%	39,1%	42,3%	0,0%	29,2%		39,1%		42,3%		0,0%
	H_2/H_2O	3,16	2,32	1,84	0,00	3,16	2,32	1,84	0,00							
	CO/CO_2	2,22	1,36	1,22	0,00	2,22	1,36	1,22	0,00							

6.3 Development of a standardized methodology for the classification of fine ores

In chapter 0 and 6.2.2 the approach for an experimental simulation of an industrially applied fluidized bed process into lab scale fluidized bed conditions was demonstrated. Based on these considerations and calculations, an experimental procedure for the execution of a lab scale test has to be developed. In order to ensure a successful operation of the lab scale fluidized bed reactor at the Chair of Metallurgy, several methodological sequences have to be investigated, especially regarding process reliability and operational safety. Another important fact is the required reproducibility of the test results to realize the comparability between different tests. To meet these requirements, a standardized test procedure for the determination of the process behavior of fine ores was developed. Therefore, a Bachelor thesis was commissioned to contribute this development within the research project [37]. In this chapter, the methodological procedure is summarized.

6.3.1 Fluidized bed test under standardized conditions

Table 10 shows the conditions for the experimental simulation of the industrial process in lab scale dimensions. For the execution of a lab scale test, a standardized test procedure has to be defined. This procedure contains a methodology beginning with the preparation of the test facility and the input materials up to the process control and the evaluation of the results. Prior to the test, accurate test preparation procedure have to be made, involving:

- accuisition and preparation of sufficient sample material in the required grain size spectrum (as discussed in chapter 6.2.2).
- supply of sufficient gas containers of diverse qualities.
- inspection of the operating material to ensure an uninterrupted test progress.
- provision of the protective equipment.
- coordination of all relevant activities relating to a successful test progress.

For the sample preparation of the raw ore, the following procedures have to be executed:

- crushing the iron ore, in case of lumpy burden as feedstock.
- grinding the material, down to the desired grain size fractions.
- screening the finest fractions below 0.063 mm.
- drying the preparated sample.
- sieving the material, in order to extract the different grain size fractions.

The sieved grain size fractions then have to be mixed regarding the defined ratios for the standardized test (cf. Table 7). The sample input mass for a standardized test was defined as 3500 g fine ore. If the origin as well as the chemical and morphological composition of the iron ore is unknown, the mineralogy and chemistry has to be investigated in advance. In Figure 54 the procedure of the sample preparation is shown by means of a flow sheet.

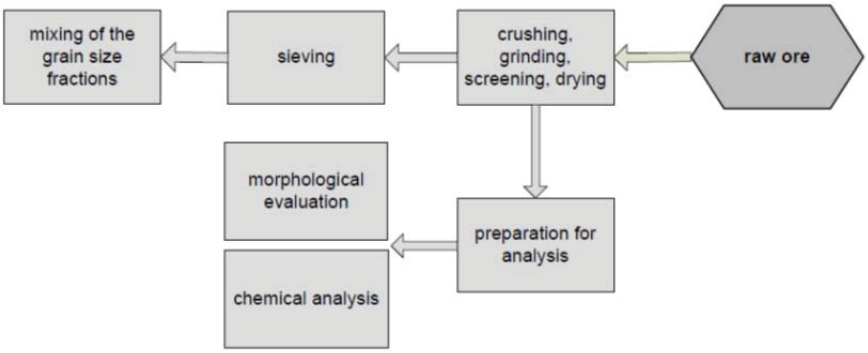

Figure 54: Sample preparation procedure

After the test- and sample preparation procedure, the test itself has to be prepared. For this purpose, all relevant facilities have to be checked whether they function properly, especially the gas pressure values in the gas supply system, the gas alarm device and air conditioning, due to the operation with explosive and toxic gas mixtures. After checking the relevant equipment, the test facility can be assembled. In Figure 55, the test preparation procedure is shown.

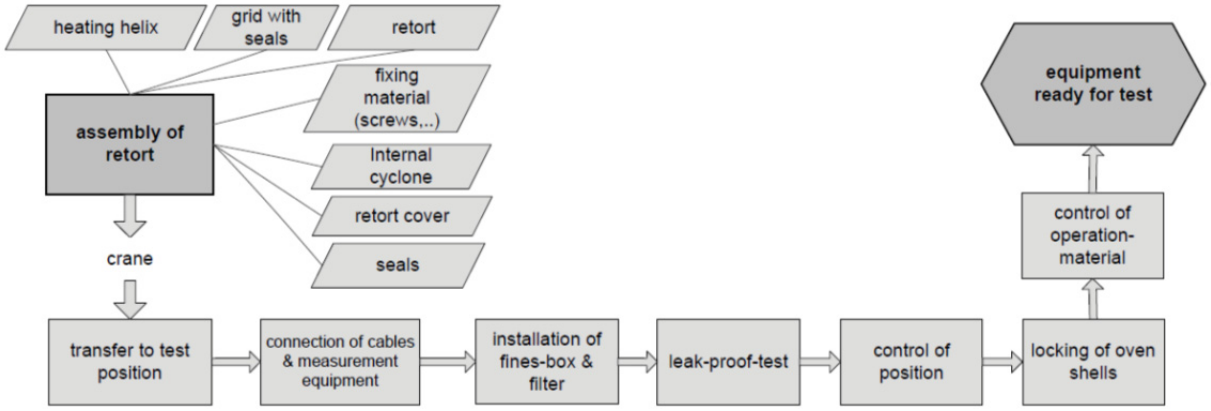

Figure 55: Test prepation procedure

Prior to every test, a leakproof test has to be executed to avoid major accidents. Therefore the fluidized bed retort is pressurized with N_2 up to 1 bar overpressure. If no pressure drop is observable, the retort is ready for the process. Now the weighing mechanism, the off gas system and the sampling system can be connected and checked regarding their operability. If all parts work properly, the fluidized bed facility is ready for process.

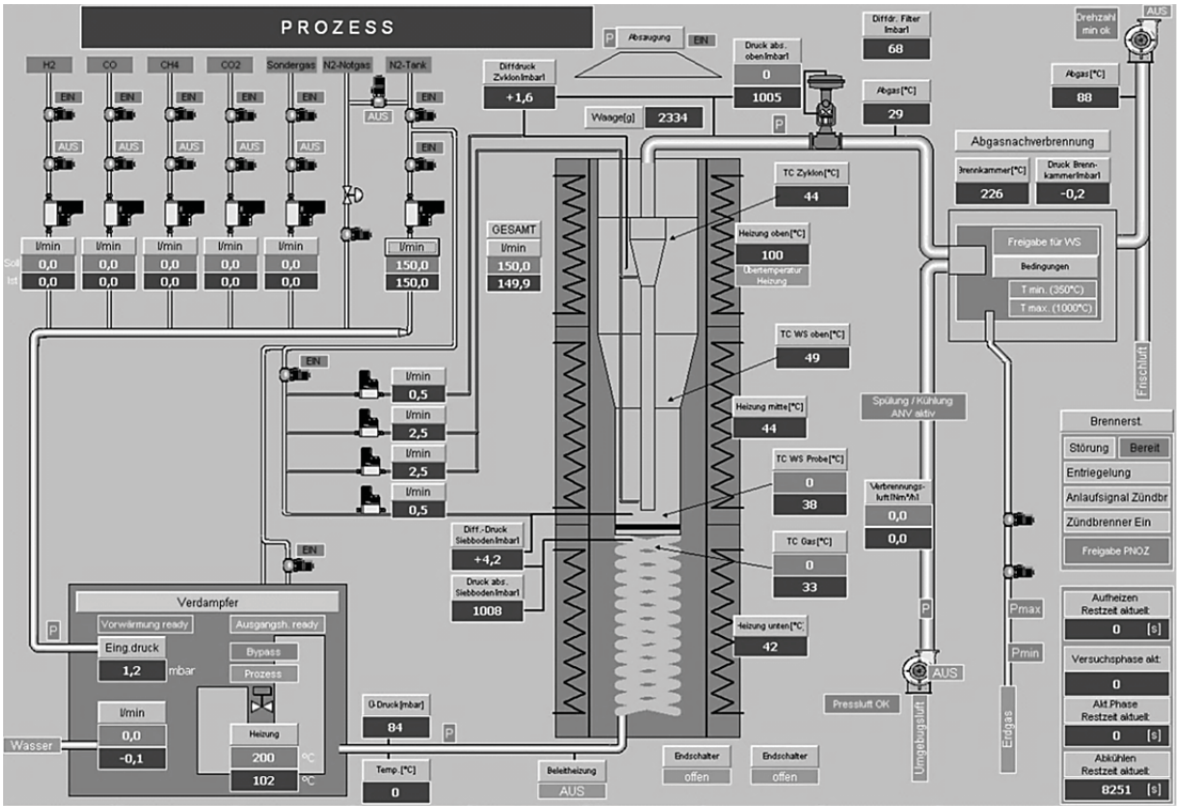

Figure 56: Process visualization

The fluidized bed facility is supplied with electric power by turning on the main control switch and activating the gas supply units. Then, the process automation and the process

data recording can be started. At process visualization, the correct connection and functionality of all components have to be checked. An example of the process visualization is demonstrated in Figure 56, with the fluidized bed retort in the center, the gas supply unit on the top left corner, the humidification and preheating unit on the bottom left and the postcombustion unit on the top right corner. As discussed in chapter 6.1, the tests can be controlled fully automatically or manually. For the automatic execution, a spread sheet for creating a test program is provided in the process visualization system. In this sheet, all relevant process parameters can be defined. In case of urgency, a modification of the parameters during the process is also possible. In Figure 57, the spread sheet for definition of the test program is shown. The program provides the possibility to divide the execution of the test into different phases, wherein different gas compositions, temperatures pressures and residence time can be fixed. After the definition of these parameters, the test can be started.

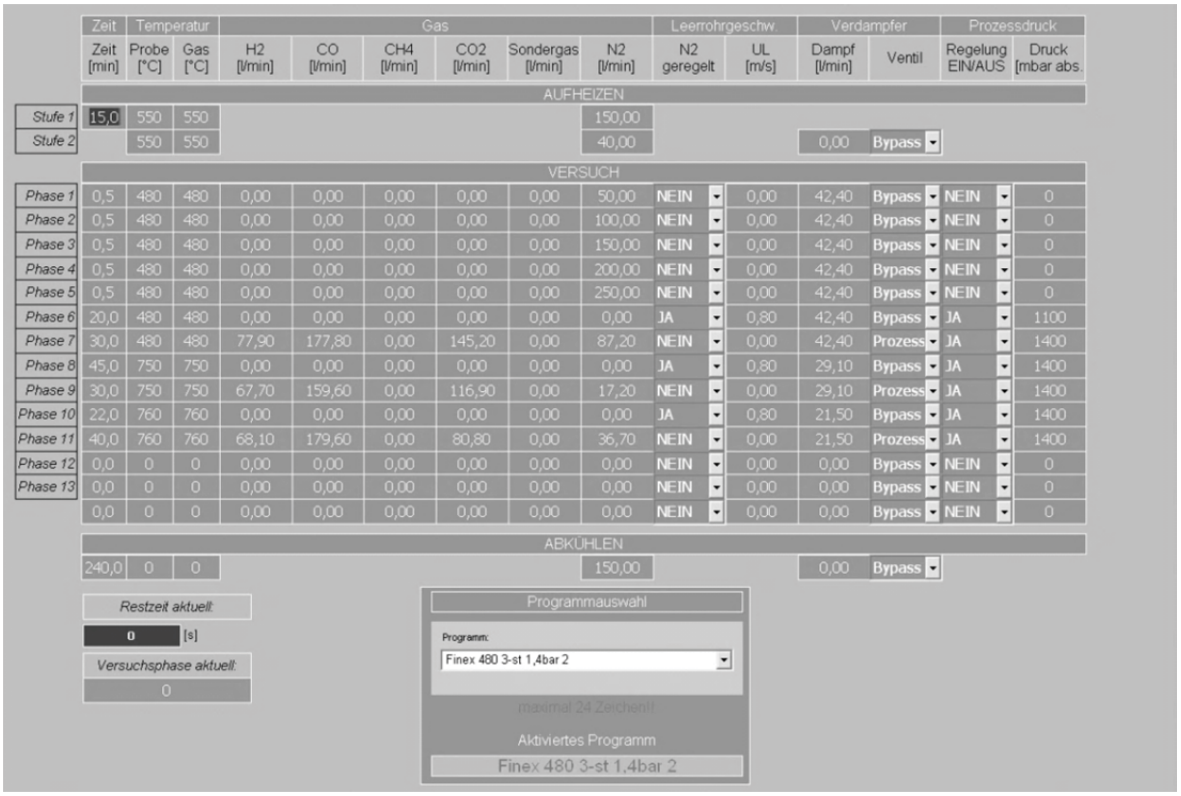

Figure 57: Spread sheet for definition of the test program

In the following section, the methodology of the test procedure is described. Before the test, the dried sample with defined weight and grain size distribution has to be prepared in order to receive reproducible results.

After input of the parameters and start up of the test program, the retort is heated up with N_2 to 550 °C for a system check, with particular regard to pressure loss and leaks. The cold raw material is then filled into the fluidized bed retort which results in temperature drop as displayed in Figure 59 and heated up by the residual heat of the retort to about 500 °C. In this temperature range, chemically bound water and volatile components are calcinated.

Then the temperature is controlled to the desired start value of the process, which represents the temperature of the first reactor stage (here R3).

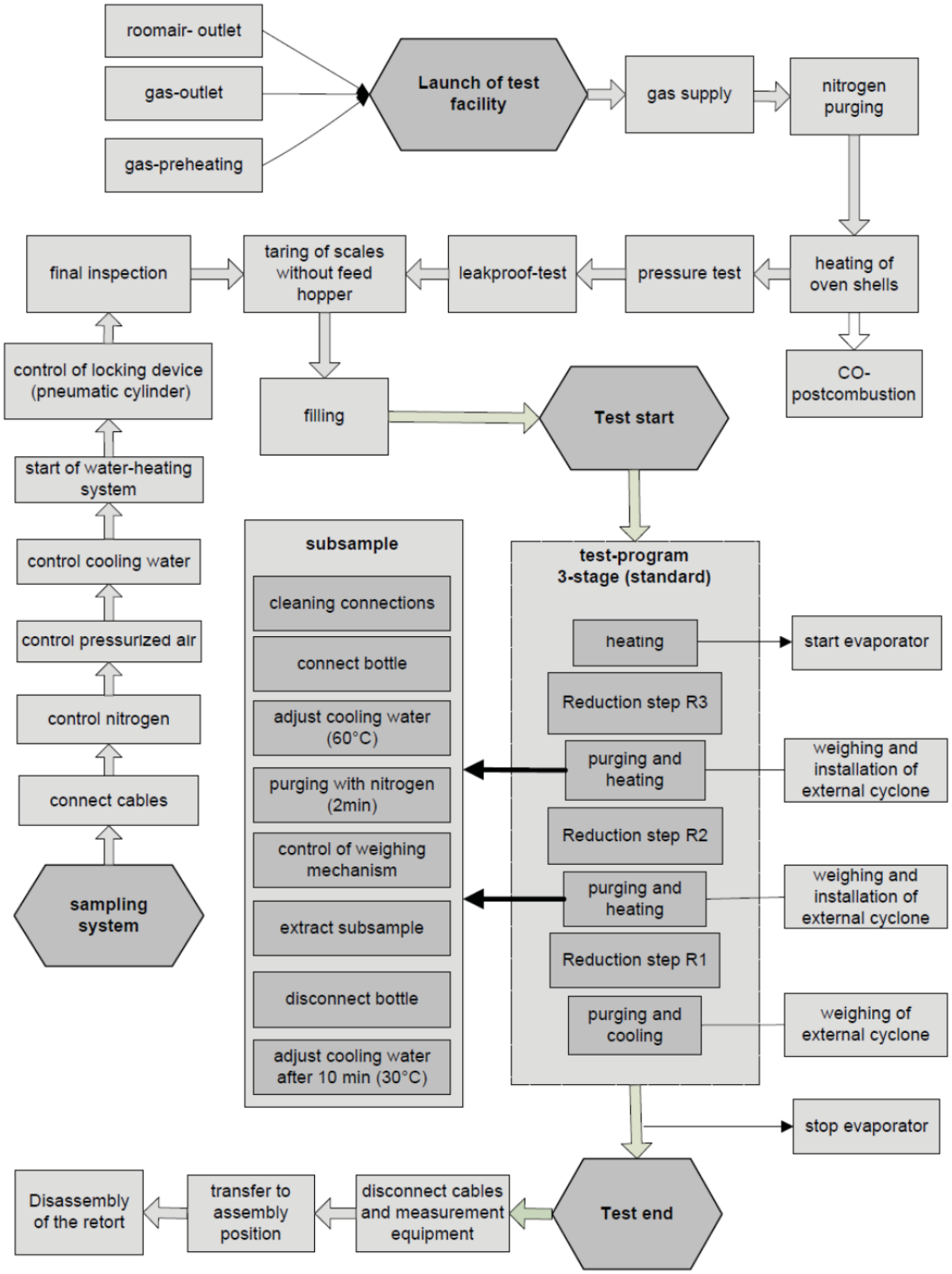

Figure 58: Test procedure

After reaching the start temperature, the gas composition is switched to the process conditions of the reactor. The slight temperature change after switching to process gas is caused by the temperature controller due to a sudden change of the heat capacity of the gases. Between the reduction stages R3 and R2 as well as R2 and R1, the sample is fluidized with N_2 for adjusting the temperature of the next stage. In this transition phase the N_2-flow is adjusted to a defined superficial velocity in order to keep the fluidized bed stable under changing temperature and pressure. Also in these N_2-phases, samples can be taken with the sample system. The diagram in Figure 59 shows a typical weight loss time trend during the entire test time. The weight loss during the N_2 phases is caused by the lifting force during heating of the retort. During the test procedure, the gas supply units and the gas alarm device have to be checked from time to time to ensure the invulnerably operation with the dangerous process gas. In order to receive interpretable results of the tests, the weight loss and the calculated RD-curves of the different reduction phases can be fitted together. This is possible because of the constant temperature and gas flow during the reduction phases.

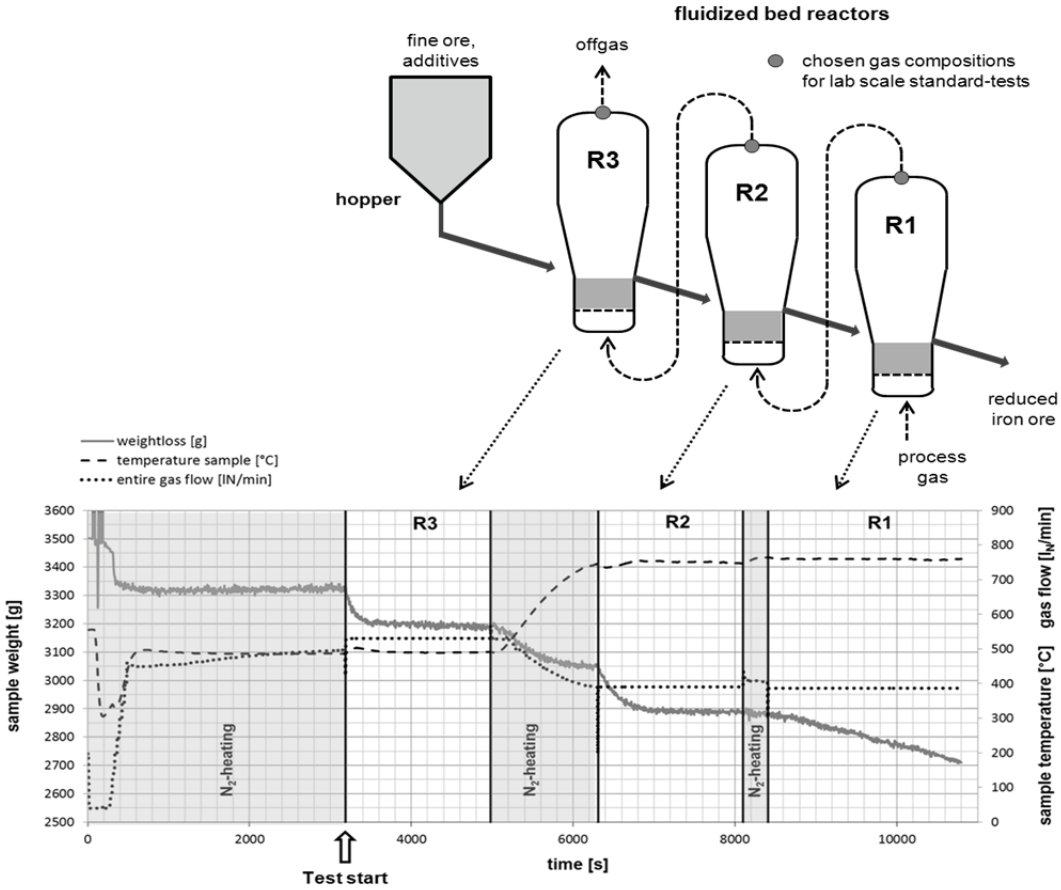

Figure 59: Operation mode of sequenced 3-stage batch lab scale tests

After the test, the reduced material is cooled down to ambient temperature under permanent N_2 flow to avoid reoxidation. At the end of the test procedure, the gas supply system has to be locked and the main power switch has to be turned off. The process data can then be extracted for the determination and interpretation of the test results.

The retort, as well as the sample containers, have to be disassembled for the extraction of the samples. The procedure is shown in Figure 60. The mass of the bed, the mass of the samples and the dust entrained to the external cyclone and dust filter are weighed to evatuate the losses and for the overall mass balance. In reality, the re-weight will be lower than the value determined by the recorded weight loss curve, because it is not possible to extract all the material in the system after the test (i.e. dust losses). One part of the sample is stored as a retain sample. Subsamples are taken from the other part and packed for the chemical and morphological analyses. The rest is then sieved into the grain size fractions to determine the grain size distribution regarding the procedure discussed in chapter 0.

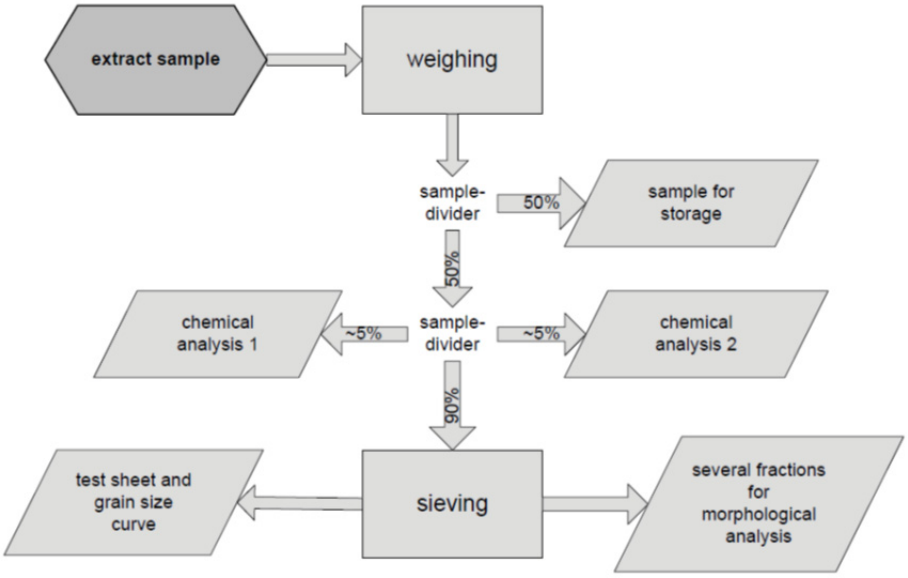

Figure 60: Post-processing of the samples

The bed samples are analyzed in terms of chemical composition (content of Fe_{tot}, Fe_{met}, Fe^{2+} and Fe^{3+} by titrimetic analysis), disintegration (grain size distribution by sieve analysis) and morphological changes (microscopical characterization). The procedures have already been described in chapter 4.

6.3.2 Standardized characterization of raw and reduced samples

In chapter 4.4 the fundamentals of characterization of raw and reduced iron ores was discussed. Based on these fundamentals, an experimental procedure for the characterization of the raw and reduced samples tested in the fluidized bed lab scale tests has to be developed. Within this scope a Bachelor thesis was commissioned to contribute this development within the research project [156]. In this chapter, the methodological procedure is summarized.

Characterization of raw ores

When the sample material arrives in the laboratory, it is weighed and then dried at 105°C to determine the moisture content by means of gravimetry. After the drying procedure, a sample is taken for the elementary analysis and to determine the porosity. These examinations are outsourced to chemical laboratories. From a representative bulk of the fine ores, the grain size distribution is determined. Specimen of every fraction is packed and stored. The fundamentals of the elementary analysis, determination of porosity and determination of the grain size distribution are discuseed in chapter 4. For the morphological analysis, samples have to be prepared. With these samples the morphological characteristics, which have been discussed in chapter 4.4, can be determined.

For the standardized and reproducible determination of the morphological characteristics, the samples have to be prepared according to the following instructions.

Preparation of a polished section:

For a successful investigation of the material by means of the reflected-light method, the most important prerequisite is, that the polished section is completely flat and highly reflective. Under the light microscope, all phases and crystal structures should be observable as authentically as possible (as discussed in chapter 4.4). For the preparation of a polished section, the sieve fractions < 0.063 mm, 0.125 - 0.250 mm and 1.0 - 2.8 mm are used.

First of all, the sample is filled into latex forms and is soused with a resin-hardener agent (i.e. Aralit F and Aradur HY 905 in the ratio 1:1) (cf. Figure 61). The form is placed in a vacuum chamber at a temperature of 120 °C and a residence time of 15 to 20 minutes (cf. Figure 62). Then the form, which is not jet hardened, is placed in a pressure champer and is pressurized with 2 bar for 3 short periods. Finally, the sample is dried in a drying chamber at 120 °C for at least 24 hours. When the sample is hardened, the following grinding and polishing procedure has to be executed:

- Grinding on a 125 µm plate under water with a polishing machine (200 N grinding pressure and 200 rpm) until the sample is flat
- Grinding on a 75 µm plate and a 40 µm plate with Ethylenclyol
- Grinding on a 10 µm plate with a 9 µm diamond suspension (reducing to 100 N grinding pressure and 100 rpm)
- Grinding on a 3 µm plate with a 3 µm diamond suspension
- Grinding on a 1 µm plate with a 1 µm diamond suspension
- Polishing on a OPS-plate

Preparation of a thin-ground section:

For mineral phases, which are not opaque, the transmission-light microscopy can be applied. Therefore, a sample is filled into a form and is soused with a resin-hardener (i.e. Araldit DBF CH and REN HY 956 in the ratio 5:1) and placed in a vacuum chamber at a temperature of 40 °C for 15 minutes. Then the form is placed in a pressure chamber and is pressurized with 2 bar for at least 12 hours. The sample is grinded with different sand papers until the surface is flat and polished with a 15µm powder and a 9µm powder.

Figure 61: Prepared samples in latex forms

Figure 62: Samples in the vacuum chamber

After that, the sample is placed in a drying chamber together with a small glass plate, to heat up these two components to the same temperature. The sample is sticked with the resin-hardener on the small glass plate and is hardened on a heating panel. After the sample is hardened, the resin is sliced off until just a thin layer is left. This layer is then grinded with a 15µ powder down to a thickness of a few µm, which has to be inspected under the microscope during grinding. Achieving the proper thickness, the sample is polished with a 9 µm powder and a second glass plate is sticked on the other side.

Characterization of reduced ores

The reduced samples have to be prepared according to the instructions “preparation of a polished sample”, as discussed before. With these samples the morphological characteristics, wich have been discussed in 4.4, can be determined.

6.4 Interlaboratory test for the accuracy-specification of chemical analyses of iron and iron oxide mixtures

Due to repeating chemical measurement-errors in terms of determining Fe_{tot}, Fe_{met}, Fe^{2+} and Fe^{3+} of the reduced iron ore samples, an interlaboratory test with selected laboratories was carried out. The main target is the verification of the accuracy of the defined measurement value. An interlaboratory test is used to revise accredited laboratories (cf. DIN EN ISO/IEC 17025 [141]). An official interlaboratory tests is very complex and time consuming and, hence, the test executed for this research work is a slimmed-down version. Nevertheless, the gathered data are very important to figure out the accuracy and measurement error of the analyses.

As a result of this test, the analyses could vary widely, which complicates scientific investigations. Reasons for the deviation could be i.e. mistakes during sampling, reactions of the material during transport, methodology of the analysis or human failure. For the interlaboratory test, four different samples containing iron and iron oxides of highest purity were mixed in defined ratios and sent to several laboratories to verify the reliability of the analyses. The interlaboratory test was prepared with the support of a bachelor thesis [157], which was carried out for this project at the Chair of Metallurgy. The results enable statements in terms of accuracy and analysis-error of Fe_{tot}, Fe_{met}, Fe^{2+} and Fe^{3+}.

6.4.1 Specification of sample material

For the investigation, iron oxides and metallic iron with high purity from the companies “Sigma-Aldrich” and “Alfa-Aesar” were used. The prepared samples contained mixtures of FeO as iron(II)-oxide, Fe_3O_4 als iron(II,III)-oxide, as well as metallic iron. In Table 11, the specifications of the sample materials are defined (cf. Figure 63).

Table 11: Definition of high purity materials for the sample preparation

Substance	Producer	Denotation	Purity and iron content
Iron (Fe)	Alfa Aesar	Iron powder, sperical < 10 micron	99,9 % metals basis
Wuestite (FeO)	Sigma Aldrich	Iron(II)oxide powder -- 71,84 g/mol	99,9 % trace metals basis; Fe-content: 76,2 - 79,3 %
Magnetite (Fe_3O_4)	Sigma Aldrich	Iron(II,III)oxide powder -- 231,53 g/mol	99,99 % trace metals basis; Fe-content: 71,3 - 73,4 %

Figure 63: Sample materials

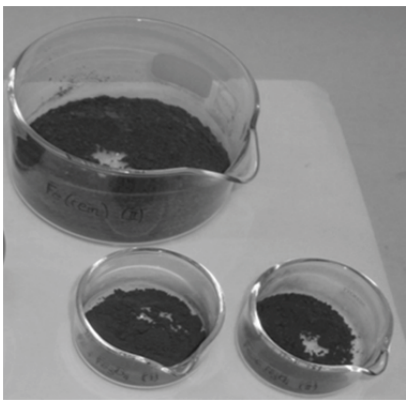

Figure 64: Reactivity test in atmosphere

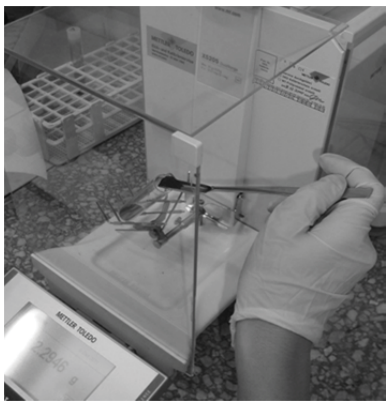

Figure 65: Preparation of the sample mixtures

6.4.2 Reactivity test under atmospheric conditions

In order to verify reactions of the iron and iron oxide materials with the atmosphere, different mixtures of these species were stored at atmospheric conditions. This is important to figure out, whether the material reacts during sample preparation and transport or not. If not, one potentisl error source can be eliminated.

Four samples were prepared: pure Fe, a mixture of Fe/FeO, a mixture of Fe/Fe_3O_4 and a mixture of FeO/Fe_3O_4. After preparation, the samples were stored at atmospheric conditions

(cf. Figure 64) and the weight change was observed over a period of time. For the measurement, an analytical balance with an accuracy of 10^{-5}g from the manufacturer "Mettler-Toledo" was used. In Table 12, the initial weight of each species and the change in weight after 72, 144, 260 hours and after half a year is indicated. All the samples showed no significant increasing or decreasing deviation. Hence, this error source could be eliminated.

Table 12: Oxidation tests with different substance mixtures

Fe		Fe-FeO		Fe-Fe3O4		FeO-Fe3O4	
Initial weight [g]	20,9675	Initial weight [g]	4,0005	Initial weight [g]	4,3455	Initial weight [g]	0,8630
Δm 72h [g]	-0,0089	Δm 72h [g]	-0,0002	Δm 72h [g]	-0,0014	Δm 72h [g]	0,0001
Δm 144h [g]	-0,0201	Δm 144h [g]	-0,0002	Δm 144h [g]	-0,0020	Δm 144h [g]	0,0004
Δm 216 h [g]	-0,0233	Δm 216 h [g]	-0,0002	Δm 216 h [g]	-0,0020	Δm 216 h [g]	0,0006
Δm 1/2 year [g]	-0,0207	Δm 1/2 year [g]	-0,0005	Δm 1/2 year [g]	0,0011	Δm 1/2 year [g]	0,0001
Max. dev. [%]	0,11	Max. dev. [%]	0,01	Max. dev. [%]	0,05	Max. dev. [%]	0,06

6.4.3 Sample preparation for the interlaboratory test

For the interlaboratory test, 4 different samples were prepared according to a defined experimental plan (cf. Table 13). Sample 1 consits of pure Magnetite (Fe_3O_4). Sample 2 consists of a mixture of iron and magnetite (Fe/Fe_3O_4). Sample 3 consists of a mixture of wuestite and magnetite (FeO/Fe_3O_4) and sample 4 is composed of iron, wuestite and magnetite ($Fe/FeO/Fe_3O_4$). The reason for the different sample mixtures was to figure out possible phenomenological differences in dependence on the iron oxide composition. The materials were weighed exactly into a lockable specimen tube (precise up to the 3rd decimal place)(cf. Figure 65). Every sample had a total mass of 4 grams. The same four samples were prepared for every laboratory. Additionally, the samples were packed with a silica gel as desiccant.

Table 13: Definition of the sample mixtures

Sample No.	Species	Mass fraction [%]			Mass/species [g]			Total sample mass [g]
		Fe	FeO	Fe_3O_4	Fe	FeO	Fe_3O_4	
1	Fe_3O_4			100	0	0	4	4
2	Fe,Fe_3O_4	59		41	2,36	0	1,64	4
3	FeO, Fe_3O_4		62	38	0	2,48	1,52	4
4	Fe,Feo,Fe_3O_4	21	54	25	0,84	2,16	1	4

6.4.4 Results and discussion of the interlaboratory test

After being sent to the laboratories, the samples were analyzed regarding the content of Fe_{tot}, Fe_{met}, Fe^{2+} and Fe^{3+}. For the interlaboratory test, 6 well known laboratories were chosen (laboratories A-F). Fe_{met} was analyzed by means of the Bromine-Methanol method, Fe^{2+} by means of the Zimmermann-Reinhardt method. The amounts of Fe^{3+} are calculated values based on the analysis of Fe^{2+}. Hence, the deviation of Fe^{3+} is adequate to the deviation of Fe^{2+}. For the analysis procedure, the following instructions were given to the laboratories:

- Quick analysis after opening the sample tubes
- Sample preparation: grinding and homogenizing
- Determination of Fe_{met} with the Bromine-Methanol method
- Determination of Fe^{2+} with the Zimmermann-Reinhardt method
- Double determination of every sample

The results are illustrated in tables and the deviation of the chemical analyses to the sample composition, as well as the mean value and the standard-deviation is calculated for every sample. The values of the deviation are presented as absolute and percentage deviations. Additionally, the sample compositions and deviations are displayed by means of radar-charts. The dotted lines represent the sample compositions and the solid lines the deviation values. Finally, the total mean value and standard deviation in percentage is illustrated by means of a histogram.

Analysis of Sample 1

Sample 1 consisits of 100 % Fe_3O_4. The analyzed values for total iron content correspond quite well with a mean deviation of 0.47 % and a standard deviation of 0.74 %. Although no metallic iron was present, all laboratories analyzed up to 2.94 % Fe_{met}. The analysis of Fe^{2+} showed extreme deviations from minus 8.52 up to 12.76 % (cf. Table 14 and Figure 66).

Table 14: Chemical analyses and deviations of sample 1

Sample No.			Sample 1							
Prepared sample	Sample specification		Species Fe_3O_4		Fe [%]	FeO [%]	Fe_3O_4 [%] 100		RD = 11,1	
	Chemical composition [%]	Fe_{tot}	72,36	72,36	72,36	72,36	72,36	72,36		
		Fe_{met}	0,00	0,00	0,00	0,00	0,00	0,00		
		Fe^{2+}	24,12	24,12	24,12	24,12	24,12	24,12		
		Fe^{3+}	48,24	48,24	48,24	48,24	48,24	48,24		
Chemical analyses	Laboratories		A	B	C	D	E	F	average	st.dev.
	Results chemical analyses [%]	Fe_{tot}	73,15	73,10	71,50	73,30	73,48	72,48	72,84	**0,74**
		Fe_{met}	2,94	2,10	0,70	2,01	2,23	0,10	1,68	**1,06**
		Fe^{2+}	24,90	24,90	15,60	24,07	30,14	11,36	21,83	**6,95**
		Fe^{3+}	45,35	46,10	55,20	47,22	41,11	61,02	49,33	7,34
Deviations composition vs. chem. allysis	deviation absolute	Fe_{tot}	0,79	0,74	-0,86	0,94	1,12	0,12	**0,47**	**0,74**
		Fe_{met}	2,94	2,10	0,70	2,01	2,23	0,10	**1,68**	**1,06**
		Fe^{2+}	0,78	0,78	-8,52	-0,05	6,02	-12,76	**-2,29**	**6,95**
		Fe^{3+}	-2,89	-2,14	6,96	-1,02	-7,13	12,78	1,09	7,34
	deviation in percentage	Fe_{tot}	1,09	1,02	-1,19	1,30	1,55	0,16	**0,66**	**1,02**
		Fe_{met}	2,94	2,10	0,70	2,01	2,23	0,10	**1,68**	**1,06**
		Fe^{2+}	3,23	3,23	-35,32	-0,20	24,96	-52,90	**-9,50**	**28,81**
		Fe^{3+}	-5,99	-4,44	14,43	-2,12	-14,78	26,49	2,27	15,22

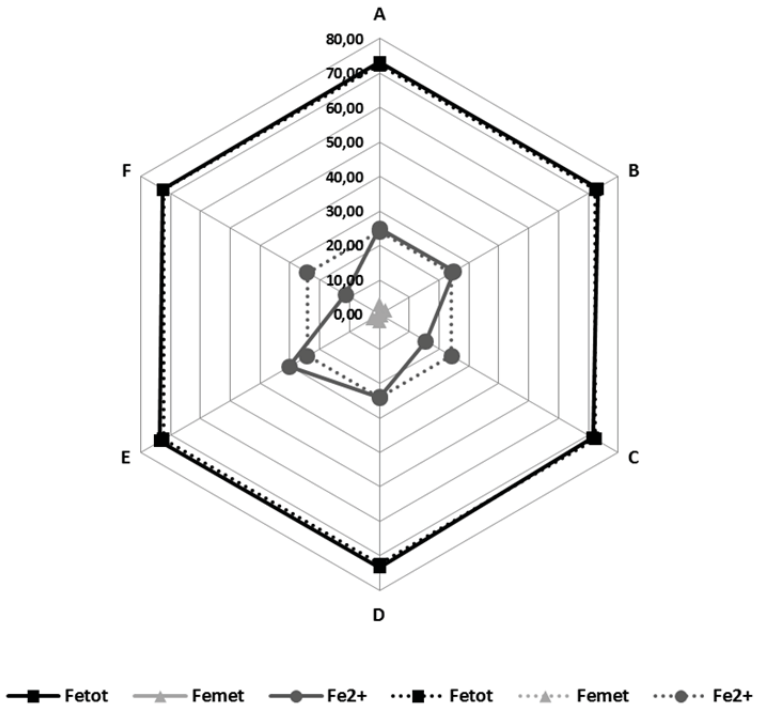

Figure 66: Radar chart of the chemical analyses/deviations of sample 1

Analysis of Sample 2

Sample 2 consisits of 59 % Fe and 41 % Fe_3O_4. Again, the total iron content was analyzed quite well with a mean deviation of -0.79% and a standard deviation of 0.74. Also Fe_{met} shows no substantial deviation, but the standard deviation of 1,91 % is significant. Fe^{2+} again exhibits the greatest deviation with a mean average of -3.95 % (cf. Table 15 and Figure 67). Except for laboratory E, the values of Fe^{2+} are far below the real value.

Table 15: Chemical analyses and deviations of sample 2

Sample No.			Sample 2							
Prepared sample	Sample specification		Species Fe,Fe_3O_4		Fe [%] 59	FeO [%]	Fe_3O_4 [%] 41		RD = 70,3	
	Chemical composition [%]	Fe_{tot}	88,67	88,67	88,67	88,67	88,67	88,67		
		Fe_{met}	59,00	59,00	59,00	59,00	59,00	59,00		
		Fe^{2+}	9,89	9,89	9,89	9,89	9,89	9,89		
		Fe^{3+}	19,78	19,78	19,78	19,78	19,78	19,78		
Chemical analyses	Laboratories		A	B	C	D	E	F	average	st.dev.
	Results chemical analyses [%]	Fe_{tot}	87,60	87,95	87,20	87,35	87,92	89,27	87,88	**0,74**
		Fe_{met}	57,10	58,30	61,70	57,40	56,22	57,70	58,07	**1,91**
		Fe^{2+}	5,61	5,90	3,80	4,81	10,33	5,21	5,94	**2,27**
		Fe^{3+}	24,90	23,70	21,60	25,14	21,37	26,36	23,85	2,02
Deviations composition vs. chem. allysis	deviation absolute	Fe_{tot}	-1,07	-0,72	-1,47	-1,32	-0,75	0,60	**-0,79**	**0,74**
		Fe_{met}	-1,90	-0,70	2,70	-1,60	-2,78	-1,30	**-0,93**	**1,91**
		Fe^{2+}	-4,28	-3,99	-6,09	-5,08	0,44	-4,68	**-3,95**	**2,27**
		Fe^{3+}	5,12	3,92	1,82	5,36	1,59	6,58	4,07	2,02
	deviation in percentage	Fe_{tot}	-1,20	-0,81	-1,66	-1,49	-0,84	0,68	**-0,89**	**0,84**
		Fe_{met}	-3,22	-1,19	4,58	-2,71	-4,71	-2,20	**-1,58**	**3,23**
		Fe^{2+}	-43,27	-40,34	-61,57	-51,35	4,46	-47,32	**-39,90**	**22,96**
		Fe^{3+}	25,89	19,83	9,21	27,11	8,05	33,27	20,56	10,19

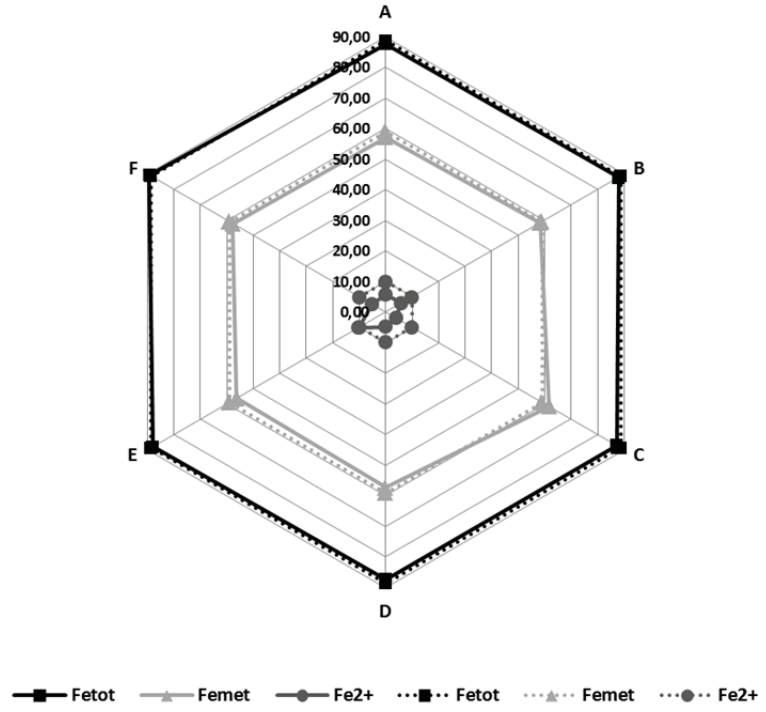

Figure 67: Radar chart of the chemical analyses/deviations of sample 2

Analysis of sample 3

Sample 3 consisits of a mixture of 62 % FeO and 38 % Fe_3O_4. As before, the analyses for total iron content show no big deviation. Although no metallic iron was present, all laboratories analyzed up to 1.5 % Fe_{met}. The mean deviation of Fe^{2+} is -11.8 % and far below the real value with a standard deviation of 2.66 %. All laboratories analyzed a too low Fe^{2+} content (cf. Table 16 and Figure 68).

Table 16: Chemical analyses and deviations of sample 3

Sample No.			Sample 3							
Prepared sample	Sample specification		Species FeO,Fe_3O_4		Fe [%]	FeO [%] 62	Fe_3O_4 [%] 38		RD = 25,2	
	Chemical composition [%]	Fe_{tot}	75,69	75,69	75,69	75,69	75,69	75,69		
		Fe_{met}	0,00	0,00	0,00	0,00	0,00	0,00		
		Fe^{2+}	57,36	57,36	57,36	57,36	57,36	57,36		
		Fe^{3+}	18,33	18,33	18,33	18,33	18,33	18,33		
Chemical analyses	Laboratories		A	B	C	D	E	F	average	st.dev.
	Results chemical analyses [%]	Fe_{tot}	74,45	75,00	74,35	74,50	74,69	76,64	74,94	**0,86**
		Fe_{met}	1,35	0,90	1,35	0,95	1,51	1,10	1,19	**0,25**
		Fe^{2+}	40,80	48,00	45,70	44,58	47,82	46,43	45,56	**2,66**
		Fe^{3+}	32,30	26,10	27,35	28,96	25,36	29,11	28,20	2,51
Deviations composition vs. chem. allysis	deviation absolute	Fe_{tot}	-1,24	-0,69	-1,34	-1,19	-1,00	0,95	**-0,75**	**0,86**
		Fe_{met}	1,35	0,90	1,35	0,95	1,51	1,10	**1,19**	**0,25**
		Fe^{2+}	-16,56	-9,36	-11,66	-12,78	-9,54	-10,93	**-11,80**	**2,66**
		Fe^{3+}	13,97	7,77	9,02	10,63	7,03	10,78	9,87	2,51
	deviation in percentage	Fe_{tot}	-1,64	-0,91	-1,77	-1,57	-1,32	1,25	**-0,99**	**1,14**
		Fe_{met}	1,35	0,90	1,35	0,95	1,51	1,10	**1,19**	**0,25**
		Fe^{2+}	-28,87	-16,32	-20,33	-22,27	-16,63	-19,05	**-20,58**	**4,64**
		Fe^{3+}	76,20	42,38	49,20	57,98	38,34	58,80	53,82	13,67

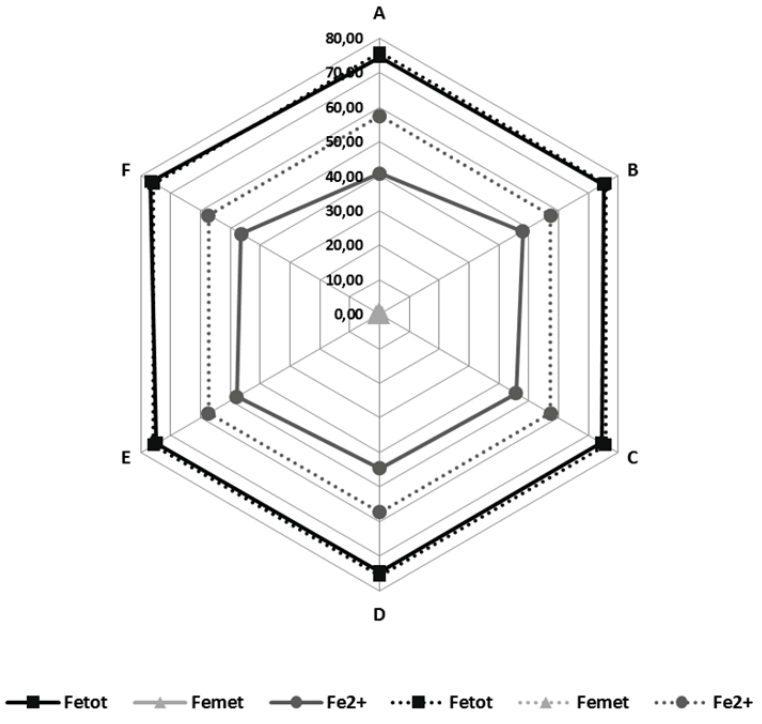

Figure 68: Radar chart of the chemical analyses/deviations of sample 3

Analysis of sample 4

Sample 3 consisits of a mixture of 21 % Fe, 54 % FeO and 25 % Fe_3O_4. Again, the mean deviation of metallic and total iron is below 1 %. Adequate to sample 3, all laboratories analyzed a Fe^{2+} content which was too low (cf. Table 16 and Figure 68). The mean deviation of Fe^{2+} is -7.11 % and far below the real value with a standard deviation of 1.24 %.

Table 17: Chemical analyses and deviations of sample 4

Sample No.			Sample 4							
Prepared sample	Sample specification		Species Fe,FeO,Fe_3O_4		Fe [%] 21	FeO [%] 54	Fe_3O_4 [%] 25		RD = 45,6	
	Chemical composition [%]	Fe_{tot}	81,07	81,07	81,07	81,07	81,07	81,07		
		Fe_{met}	21,00	21,00	21,00	21,00	21,00	21,00		
		Fe^{2+}	48,01	48,01	48,01	48,01	48,01	48,01		
		Fe^{3+}	12,06	12,06	12,06	12,06	12,06	12,06		
Chemical analyses	Laboratories		A	B	C	D	E	F	average	st.dev.
	Results chemical analyses [%]	Fe_{tot}	80,65	79,91	79,70	79,60	80,24	81,530	80,27	**0,73**
		Fe_{met}	22,15	20,30	22,45	20,65	22,01	21,200	21,46	**0,87**
		Fe^{2+}	41,45	42,20	38,90	39,93	41,12	41,770	40,90	**1,24**
		Fe^{3+}	17,05	17,40	18,30	19,00	17,11	18,560	17,90	0,83
Deviations composition vs. chem. allysis	deviation absolute	Fe_{tot}	-0,42	-1,16	-1,37	-1,47	-0,83	0,46	**-0,79**	**0,73**
		Fe_{met}	1,15	-0,70	1,45	-0,35	1,01	0,20	**0,46**	**0,87**
		Fe^{2+}	-6,56	-5,81	-9,11	-8,07	-6,89	-6,24	**-7,11**	**1,24**
		Fe^{3+}	4,99	5,34	6,24	6,94	5,05	6,50	5,84	0,83
	deviation in percentage	Fe_{tot}	-0,51	-1,43	-1,68	-1,81	-1,02	0,57	**-0,98**	**0,90**
		Fe_{met}	5,48	-3,33	6,90	-1,67	4,81	0,95	**2,19**	**4,17**
		Fe^{2+}	-13,66	-12,09	-18,97	-16,81	-14,34	-12,99	**-14,81**	**2,59**
		Fe^{3+}	41,37	44,28	51,74	57,58	41,87	53,90	48,46	6,85

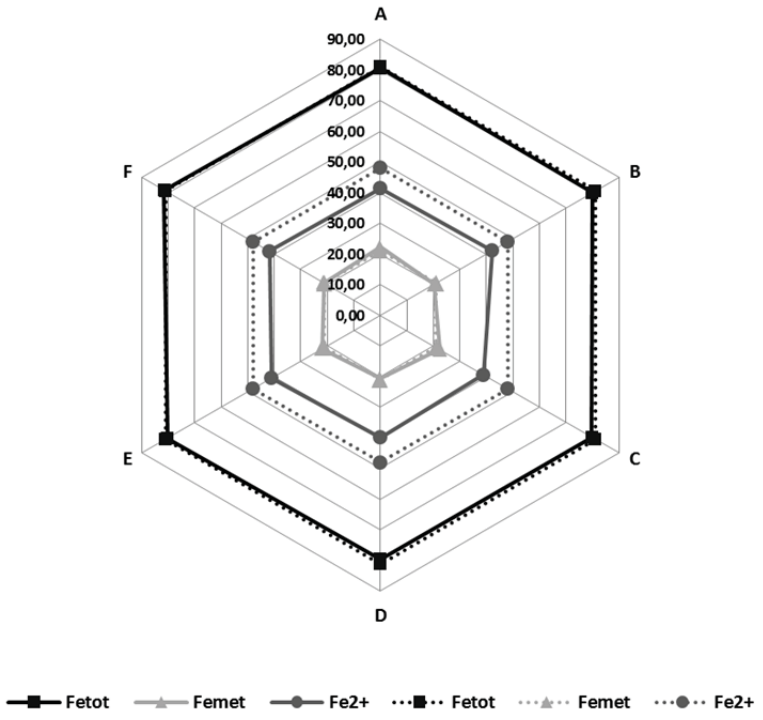

Figure 69: Radar chart of the chemical analyses/deviations of sample 4

Summary

Errors in the sample preparation could be eliminated because sample materials of the highest purity were used and the sample mixtures were weighed with precision (precise up to the 3rd decimal place). Further more, no reaction of the materials with the atmosphere was observed, so reactions with the atmosphere during transport also could be eliminated. The laboratories were instructed to grind/homogenize the samples and to analyze Fe_{met} with the Bromine-Methanol method and Fe^{2+} with the Zimmermann-Reinhardt method. For every sample, a double determination was executed.

The executed analyses of Fe_{tot} delivered favourable results with average deviations and standard deviations of < 0.9 % absolute. Due to the fact, that the total iron content of the pure FeO varies between 76.2 % and 79.3 % (+/- 1.5 % Fe regarding the stoichiometric composition) and the total iron content of Fe_3O_4 varies between 71.3 % and 73.4 % (+/- 1 % regarding the stoichiometric composition), the analyses are reliable. The average deviation of Fe_{tot} of all samples in percentage is -0.55 % with a standard deviation of 1.13 % (cf. Figure 70 and appendix A.5).

Determining Fe_{met} was somewhat less precise with mean deviations of up to 1,7 % and standard deviations of up to 1.9 % absolute. Additionally, although in 2 samples no metallic iron was present, the laboratories detected Fe_{met} amounts up to 3 %. The Bromine-Methanol standard indicates, that metallic iron can be determinated exactly only between 5 and 95 % Fe_{met} absolute. Comprising the variation of the iron content of the raw material up to 1.5 % (cf. Table 11), the analyses are reliable within a certain range, but further investigations are necessary. The average deviation of Fe_{met} of all samples in percentage is 0.87 % with a standard deviation of 2.86 % (cf. Figure 70 and appendix A.5).

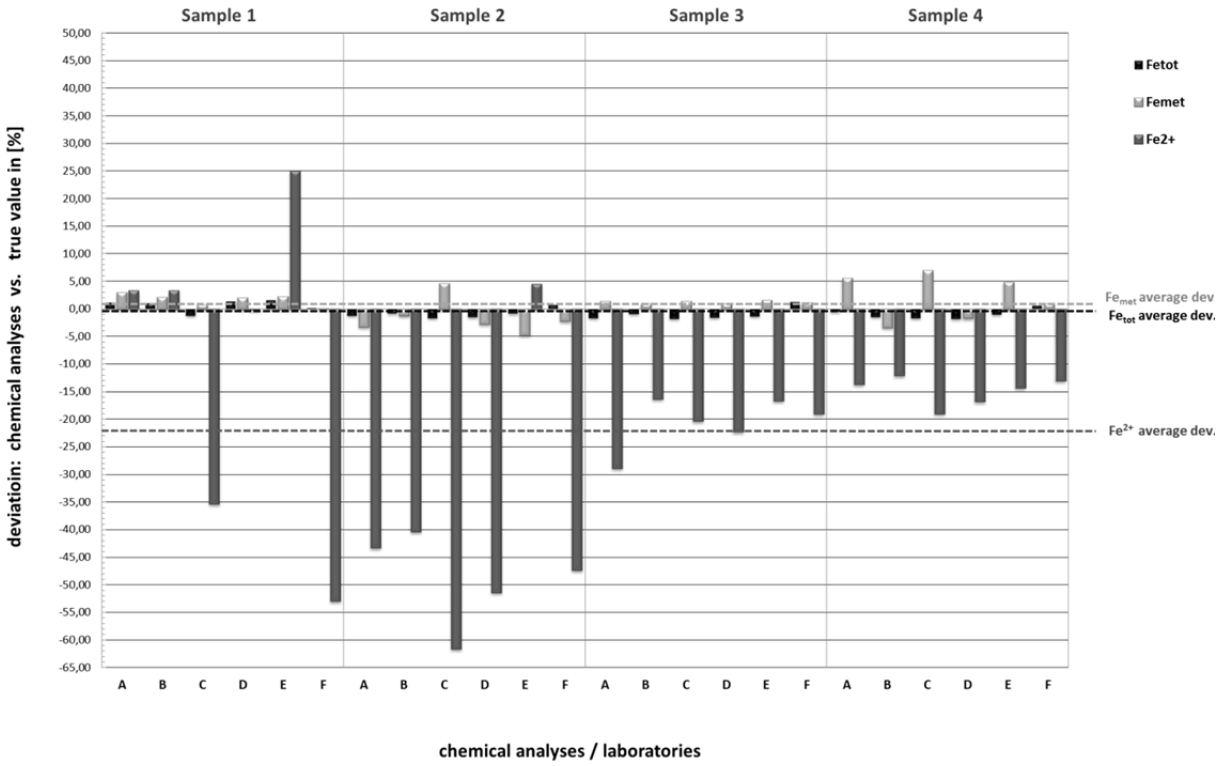

Figure 70: Deviations chemical analyses vs. true value in percentage

The analyses of Fe^{2+} showed extreme deviations up to 16.56 % absolute. In most of the cases, the analyzed Fe^{2+} content was far below the real value. Howewer, despite the variation of the iron content of the raw material up to 1.5 % (cf. Table 11), the results of the analyses are not satisfactory at all. In two cases, the standard deviation was far below the mean deviation, which could be an indicator that the laboratories worked quite well in these two cases, but the method of Fe^{2+} analysis could be doubtful. The average deviation of Fe^{2+} of all samples in percentage is -21.2 % with a standard deviation of 20.51 % (cf. Figure 70 and appendix A.5). Possible explanations for the deviations of Fe^{2+} are:

- Missing experience with the Zimmermann-Reinhardt method
- The reliability of the Zimmermann-Reinhardt method is doubtful

Such deviating measurements could have severe financial and technical consequences. Further investigations in this field are necessary.

7 Fluidized bed test series

Based on industrially applied fluidized bed reduction technologies using coal gasification for the generation of the reduction gas, the reduction behavior of different globally traded fine iron ores was investigated under different process conditions.

In a first approach, the actual industrially applied 4-stage sequenced reduction mode was compared to a more economical 3-stage sequenced mode, and the impacts on the results discussed. Based on these results, in a second series, several 3-stage tests were performed to investigate the variation of temperature in the pre-reduction stage, the variation of gas composition in different stages and the variation of residence time in the final reduction sequence. All tests in these series were executed with the same raw material (hematite ore) and the morphological findings were highlighted. In a third series, the reduction behavior of different ore brands, under the same test conditions, was investigated by means of a standardized 3-stage sequenced reduction mode. Due to the successful installation of a sampling system, the reduction progress can be compared with chemical analyses of extracted samples during the process. Furthermore, the morphological evolution of the sample material during the process is described.

In the field of fine iron ore fines reduction with carbon monoxide- and hydrogen-rich gas mixtures and the subsequent morphological analysis, a series of research has been published [4,53,56,82,100,102-109,111-115,142-145]. Regarding the multi-stage reduction behavior of iron ore fines in the fluidized bed process, the CD-laboratory of the Technical University Vienna did a number of investigations. Based on the process development and optimization of the FINMET®-Technology, a series of scientific work was published with the focus on fluidized bed reduction of iron ore fines under hydrogen-rich gas compositions. Due to the substitution of the pre-reduction shaft of the coal gasification based COREX®-process with fluidized bed cascades for the pre-reduction of fine ores, the FINEX®-process evolved. Therefore, the focus of the research work also expanded towards the reduction of fine ores under CO-rich gas compositions. The main findings of these investigations, which are essential for this research work, are summarized.

Reduction of hematite iron ore fines under H_2-rich gas compositions:

Reduction from hematite to iron (Fe_2O_3→ Fe):

1-stage process (Fe_2O_3→ Fe)

- The pressure change has no influence on RD [105]
- Temperature change: no effect on reduction below 550°C, strong increase between 550 °C and 700 °C [105]
- Gas composition change: Higher concentrations of H_2 → higher reduction rate, weak influence of CO/CO_2. CH_4 up to 6% has no influence [105]
- Rate controlling step: 2 phases: transport, solid state diffusion [105]
- Morphology: grain´s centers are covered with iron layers [105]

2-sequenced process (Fe_2O_3→ Fe_3O_4 → Fe)

- The pre-duction has significant influence on the final RD [109]
- The morphology has significant influence on the final RD [106-108]
- Hematite is better reducible than magnetite [105]
- Magnetite generated in the pre-reduction stage has negative influence on final RD (dense magnetite → dense wuestite) → lower final RD. At low temperatures (350-400 °C) few magnetite generated, at > 500 °C almost all hematite transformed to magnetite [105]
- In final stage wuestite surrounded by iron rims [106-108]
- Wuestite generated in the pre-reduction stage is better reducible and shows a fine pored iron in the final stage (porous wuestite → porous iron) [105-109]
- Pre-reduction in iron phase → wuestite and wuestite-enclaves enclosed by iron occur. Lower specific surface area, lower final RD [105-109]
- Better reduction of hematite relics from 1st stage than magnetite formed in 1st stage → Metallic iron formed from magnetite is denser than iron from hematite relics [108]
- Reduction from wuestite to iron starts on the pore's surfaces and builds iron layers. Further reduction to iron starts at various spots inside the grain [108]
- Higher residence time in R2 increases the final RD [108]

Reduction from hematite to magnetite: Fe_2O_3→ Fe_3O_4

- < 350 °C nearly no magnetite formation, > 400 °C dense magnetite layers [111]
- The reducibility significantly depends on the mineralogy and petrography of a grain. Fine crystals can be reduced faster than coarse jones. Limonite has the highest reducibility, martite and micro platy hematite show a lower reducibility and coarse hematite the lowest [111]
- Between 400 °C and 600 °C: Rate determining step is the phase interface reaction. The magnetite layer thickness is proportional to the reduction time [111]
- At higher temperature, the reduction increases [146]
- By increasing H_2 , the reduction degree increases [146]
- Morphology: dense magnetite with low porosity [146]
- CO-rich gas has a higher reduction rate than H_2-rich [102]

Reduction from hematite to wuestite: Fe_2O_3→ FeO

- H_2-rich higher reduction rate than CO-rich [102]
- With higher temperatures, the reduction degree increases [146]
- increasing H_2 → increasing RD [146]
- H_2-rich higher reduction rate than CO-rich [102]
- high reduction rates at the beginning, similar to 2-step magnetite to wuestite reduction [100]

Reduction of hematite iron ore fines under CO-rich gas compositions

Reduction from hematite to iron (Fe_2O_3→ Fe):

3-sequenced process (Fe_2O_3→ Fe_3O_4 → FeO → Fe)

- The pre-reduction has a significant influence on final RD [103,104]
- The morphology has a significant influence on final RD [103,104,108]
- High Temperature in the pre-reduction stage → porosity↑ and RD↑ [103,104]
- Fe_2O_3→ Fe_3O_4: CO has a higher reduction rate and generates a higher porosity than H_2-rich gas mixtures [102]
- Correlation between ore type and final RD [103,104,108]:
  - many limonite and martite crystals: porous structures at low pre-reduction temperatures and fine porous iron in final RD
  - many coarse hematite crystals: dense magnetite in the magnetite-pre-reduction-field (low porosity), subsequently dense wuestite grains with iron shells in R1 = RD ↓
  - pre-reduction in wuestite-field: finely porous wuestite = finely porous iron scraps in R1
    Influence of pre-reduction conditions on reduced iron ore [103,104]
  - Dense material formed in R3 → final RD ↓ (observed at low pre-reduction temp.)
  - Porous material formed in R3 → final RD↑ (observed at high pre-reduction temp.)
  - Increasing Residence time in R3 → quantity of pores ↑ and RD ↑
- Final RD increases with increasing pre-reduction temperature (continuously increasing prosity). No minimum or maximum values compared to H_2-rich gas compositions [108]
- Longer time in pre-reduction stage → higher final RD (due to higher quantity of pores) [108]

7.1 Investigated iron ores

In the following, the morphology of the different globally traded raw materials for the fluidized bed tests is discussed. The world map in Figure 71 shows the origin of the raw iron ores for the fluidized bed test series.

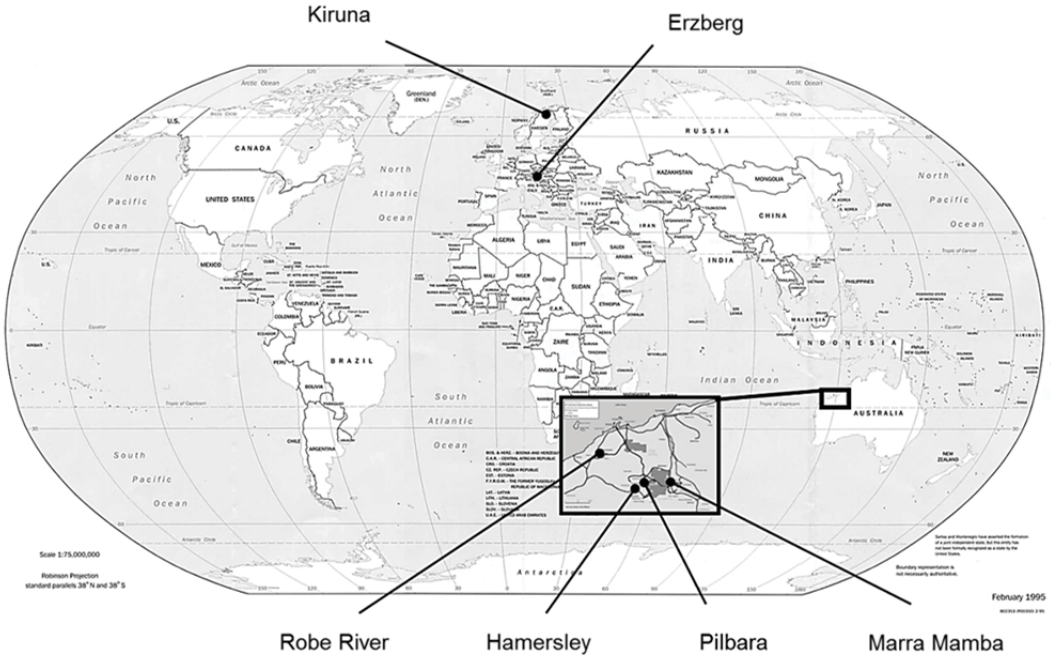

Figure 71: Origin of the raw materials for the fluidized bed lab scale tests

Four of the iron ores come from the iron ore export countriy Australia. From Australia and Brazil, over 70 % of the worldwide traded iron ores originate [147]. Because of the geological differences of the ore deposits, every iron ore brand has its characteristic morphological fingerprint and, hence, different reduction behavior. The morphological characteristics of these ores are investigated in this chapter. As an overview, the chemical composition as well as the specific surface area and pore characteristicx of these six ore brands are shown in Table 18 and Table 19.

Table 18: Chemical analyses of the different iron ore brands

Ore		Hamersley	Kiruna	Robe River	Erzberg	Marra Mamba	Pilbara
Fe tot	[mass-%]	63,60	65,20	56,20	49,40	61,30	61,90
Fe^{2+}	[mass-%]	0,45	20,53	0,29	0,22	0,32	0,42
FeO	[mass-%]	0,58	26,41	0,37	0,28	0,41	0,54
Al_2O_3	[mass-%]	2,07	0,41	2,79	0,52	2,29	2,14
CaO	[mass-%]	0,01	2,24	0,01	4,74	0,01	0,01
K_2O	[mass-%]	0,01	0,19	0,01	0,18	0,02	0,02
MgO	[mass-%]	0,01	0,81	0,01	2,39	0,01	0,01
Mn	[mass-%]	0,17	0,07	0,08	2,80	0,15	0,07
P	[mass-%]	0,07	0,45	0,04	0,04	0,08	0,06
S	[mass-%]	0,01	0,04	<0,001	0,01	0,00	0,00
SiO_2	[mass-%]	3,48	3,30	5,84	2,88	3,89	2,99
TiO_2	[mass-%]	0,12	0,43	0,18	0,03	0,09	0,12
LOI	[mass-%]	3,30	-2,26	10,55	14,39	5,82	6,45
$H2O_{(l)}$ [%]	[mass-%]	0,44	0,00	2,05	4,00	9,77	9,54

Table 19: Specific surface area, external surface area, pore volume and pore diameter of the investigated iron ores

	Hamersley		Kiruna		Siderite		Robe River		Pilbara		Marra Mamba	
Specific surface area [m²/g]												
	coarse	**fine**	**coarse**	**fine**	**coarse**	**fine**	**coarse**	**fine**	**coarse**	**fine**	**coarse**	**fine**
	3,52	6,43	0,05	0,13	66,17	70,56	18,37	23,99	7,89	10,18	5,75	6,23
	3,76	6,93	0,05	0,12	68,93	65,82	17,61	22,14	7,01	10,43	6,28	7,78
	3,51	6,61	0,06	0,15	67,69	67,80	18,45	22,14	8,21	10,40	6,37	7,79
Average	**3,60**	**6,66**	**0,06**	**0,13**	**67,59**	**68,06**	**18,14**	**22,76**	**7,70**	**10,34**	**6,13**	**7,27**
External surface area[m²/g]												
	coarse	**fine**	**coarse**	**fine**	**coarse**	**fine**	**coarse**	**fine**	**coarse**	**fine**	**coarse**	**fine**
	2,64	4,78	measurement not possible		5,51	5,27	11,73	16,30	5,72	7,45	4,09	12,10
	2,30	3,49			4,96	6,20	12,80	15,91	5,11	7,77	4,70	6,11
	2,37	5,12			5,53	5,67	12,92	16,59	3,95	7,84	4,76	6,03
Average	**2,43**	**4,46**			**5,33**	**5,72**	**12,48**	**16,27**	**4,93**	**7,68**	**4,51**	**8,08**
Pore volume [cm³/g]												
	coarse	**fine**	**coarse**	**fine**	**coarse**	**fine**	**coarse**	**fine**	**coarse**	**fine**	**coarse**	**fine**
	0,005	0,009	measurement not possible		0,009	0,008	0,019	0,028	0,010	0,013	0,007	0,023
	0,004	0,007			0,007	0,009	0,019	0,025	0,009	0,014	0,008	0,011
	0,004	0,010			0,008	0,009	0,020	0,026	0,010	0,015	0,008	0,011
Average	**0,004**	**0,009**			**0,008**	**0,009**	**0,019**	**0,026**	**0,010**	**0,014**	**0,008**	**0,015**
Pore diameter [nm]												
	coarse	**fine**	**coarse**	**fine**	**coarse**	**fine**	**coarse**	**fine**	**coarse**	**fine**	**coarse**	**fine**
	3,91	3,83	measurement not possible		3,31	3,90	3,90	3,89	3,91	3,91	5,00	6,71
	3,93	3,83			3,89	3,85	3,89	3,87	3,88	3,90	3,87	3,87
	3,90	3,86			3,90	3,83	3,94	3,87	3,95	3,84	3,91	3,88
Average	**3,91**	**3,84**			**3,70**	**3,86**	**3,91**	**3,88**	**3,91**	**3,88**	**4,26**	**4,82**

Remark: fine fractions: 0,25 - 0,50 mm
coarse fractions: 2,80 - 4,00 mm

7.1.1 Hamersley iron ore

Hamersley iron ore is a hematite rich ore from the Hamersley mining district in Australia. The color is red-brown. The main component of the Hamersley ore is a fine to coarse crystalline hematite from xenomorphic to idiomorphic shape. Large amounts of martite are also present, representing a coarse crystalline and partly trellis textured structure. It also contains small amounts of limonite and magnetite. The limonite in the ore is placed interstitial between the hematite and martite phases, and sporadic, shell shaped agglomerated limonite is present. The magnetite is present only in trace amounts. In Figure 73, the morphology of the ore is shown. A part of the hematite (H) appears as xenomorphic and very dense crystal (white), which is called micro platy hematite (MPH). The LOI is 3.3 %, which derives from the limonite amount of about 10 – 20 %. The gangue consists mainly of the acid phases SiO_2 and Al_2O_3.

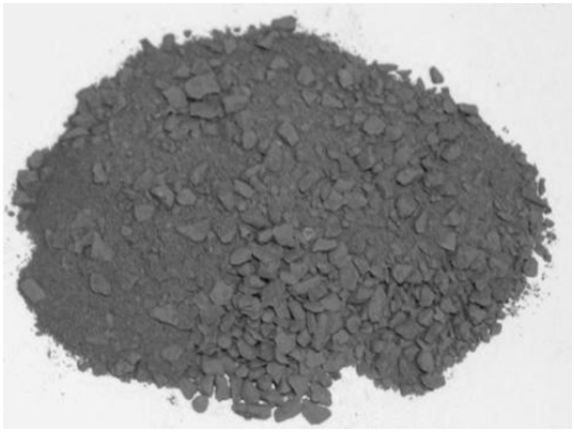

Figure 72: Hamersley iron ore

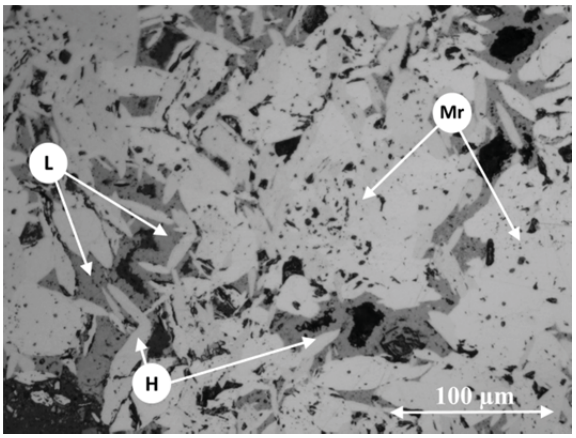

Figure 73: Hamersley iron ore, morphology, 1,0 - 2,8 mm

7.1.2 Kiruna iron ore

Kiruna iron ore is a magnetite rich ore from Sweden, which has a dark grey to black color. The matrix is very dense and shows hardly any pores.

Figure 74: Kiruna iron ore

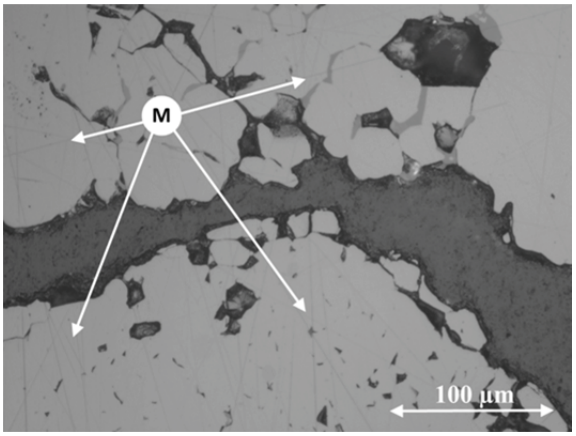

Figure 75: Kiruna iron ore, morphology, 1,0 – 2,8 mm

In Figure 75, the coarse crystalline and dense structure of the magnetite (bright) is shown. No hematite, martite or limonite was observed in the matrix. The magnetite grains can reach a crystal size up to 1 mm. The biggest parts of the crystals are xenomorphic. The gangue consists mainly of CaO and SiO_2. Further components are sulfides (pyrite, marcasite) as well as apathite and ilmenite. The higher sulfur content of the iron ore correlates with the pyrite phases. Apathite is a calcium-phosphate, which is a gangue composite of magnetite ores and ilmenite is a Ti-Fe-mineral [148].

7.1.3 Erzberg iron ore

Erzberg iron ore is a limonite rich ore from central Europe consisting of pseudo morphs of siderite (siderite, which was weathered to limonite) with a few remnants of siderite and ankerite. In principal, the limonite is the favored weathering product of all iron ores and frequently occurs naturally. The color is dark brown. The structure is very porous and finely crystalline with a highly specific surface area. Pores derived from the metamorphosis of the siderite to limonite. The mineralogical composition is approximately 75 % limonite and 25 % hematite, derived from the dehydration of the limonite. The trellis texture derived from the former carbonate crystal lattice is preserved in the matrix (cf. Figure 77). The white areas are limonite crystals and the dark grey areas represent the gangue (quartz). The gangue minerals are quartz, pyrite, chlorite, muscovite, feldspar and calcite. A characteristic of Erzberg iron ore is the high Mn-content.

Figure 76: Erzberg iron ore

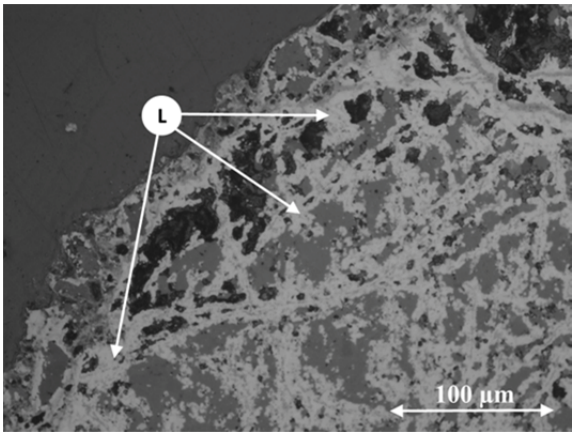

Figure 77: Erzberg iron ore, morphology, 1,0 – 2,8 mm

A lot of the mentioned pores are filled up with Mg-calcite and dolomite, which could be confirmed by means of the Raman-spectroscopy. The main peak is Mg-calcite at a value of 1089 cm^{-1}.

7.1.4 Robe River iron ore

Robe River ore from Australia is a limonite rich ore with a bright red-brown color. It is highly porous and contains finely crystalline limonite aside of some hematite (about 80 % limonite, 20 % hematite).

Figure 78: Robe River iron ore

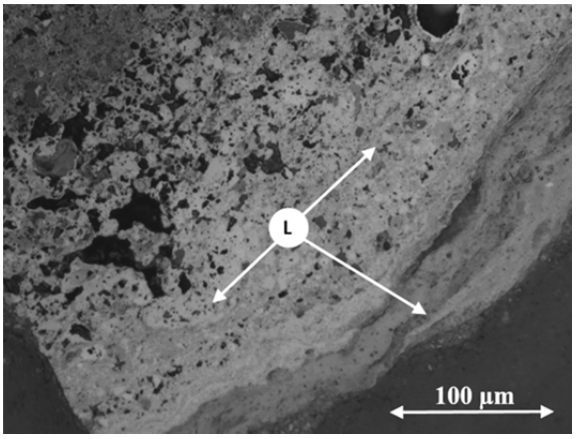

Figure 79: Robe River iron ore, morphology, 1,0 – 2,8 mm

Limonite forms irregular masses and layers, abundant limonite ooids (mineral core with grown shells) can be observed. Most of the very finely crystalline hematite is generated through dehydration of limonite. In Figure 79, the finely porous structure of the ore is shown. The limonite is grown shell shaped on the mineral core. In comparison to the other ores, the amount of gangue is elevated (2.79 % Al_2O_3 and 5.84 % SiO_2. Because of the high LOI of 10.55 %, a limonite amount of 40 – 50 % in the matrix is estimated.

7.1.5 Marra Mamba iron ore

Marra Mamba iron ore is a very porous, limonite-martite rich ore from Australia with orange-brown color and a high specific surface area. The main phases are limonite and martite. The limonite shows very porous masses and layers and is partly dehydrated. The martite is highly porous with a trellis structure. In some martite crystals, magnetite can be found. In Figure 81, the porous structure of the limonitic ore is well recognizable (grey). The martite is white and trellis textured with small grain sizes. The amount of gangue is very low and consists mainly of Al_2O_3 and SiO_2. Compared to other limonite-rich ores the LOI is very low, although the limonite amount in the matrix is very high (60 – 70 %).

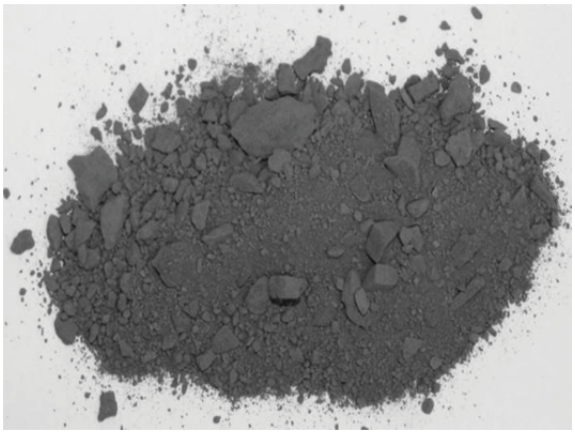

Figure 80: Marra Mamba iron ore

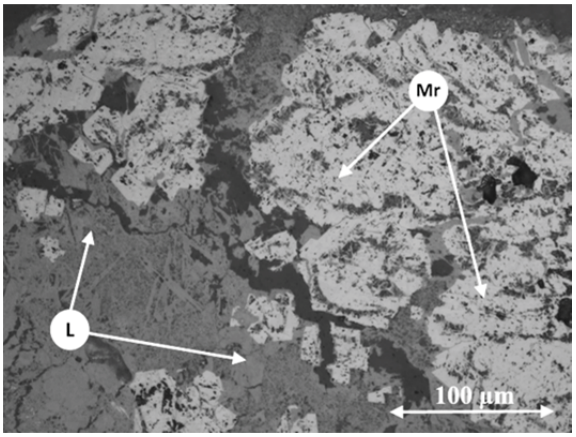

Figure 81: Marra Mamba iron ore, morphology, 1,0 – 2,8 mm

7.1.6 Pilbara iron ore

Pilbara iron ore from Australia is a limonite and martite rich ore with a bright brown color. The limonite is very porous comprising shell structures. The martite is finely crystalline and shows a trellis textured matrix. Partly, intergrowths between limonite and martite are observable and the limonite is accumulated to the martite crystals (cf. Figure 83). Hematite exists in low amounts and forms a very finely crystalline and porous mass derived from dehydration of limonite. Characteristically is the increased occurrence of crusts, which derived from the humidity of the ore. The amount of gangue is very low and consists mainly of Al_2O_3 and SiO_2. In general, the morphological and chemical characteristics of this iron ore are similar to the Marra Mamba iron ore.

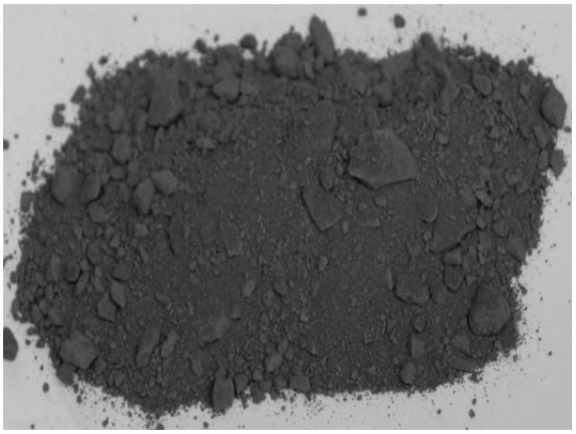

Figure 82: Pilbara iron ore

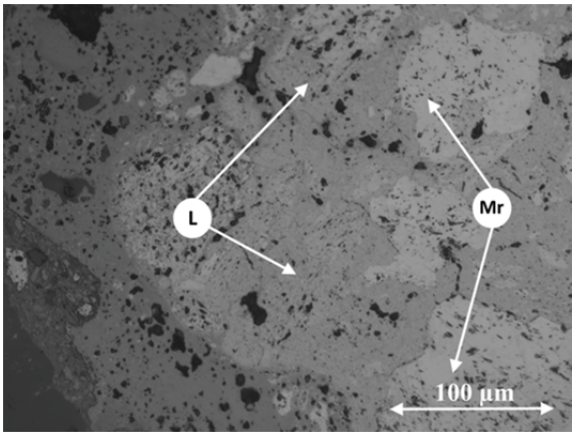

Figure 83: Pilbara iron ore, morphology, 1,0 – 2,8 mm

7.2 Comparison between sequenced 4- and 3-stage reduction tests

In this chapter, the sequenced 4-stage operation mode is compared to a 3-stage reduction mode under different start temperatures with Hamersley hematite-rich iron ore as the input material for all tests. The main issue of this test series is to figure out the process behavior of the iron ore reduced in three and four stages and, accordingly, the evaluation of the necessity of a 4-stage operation.

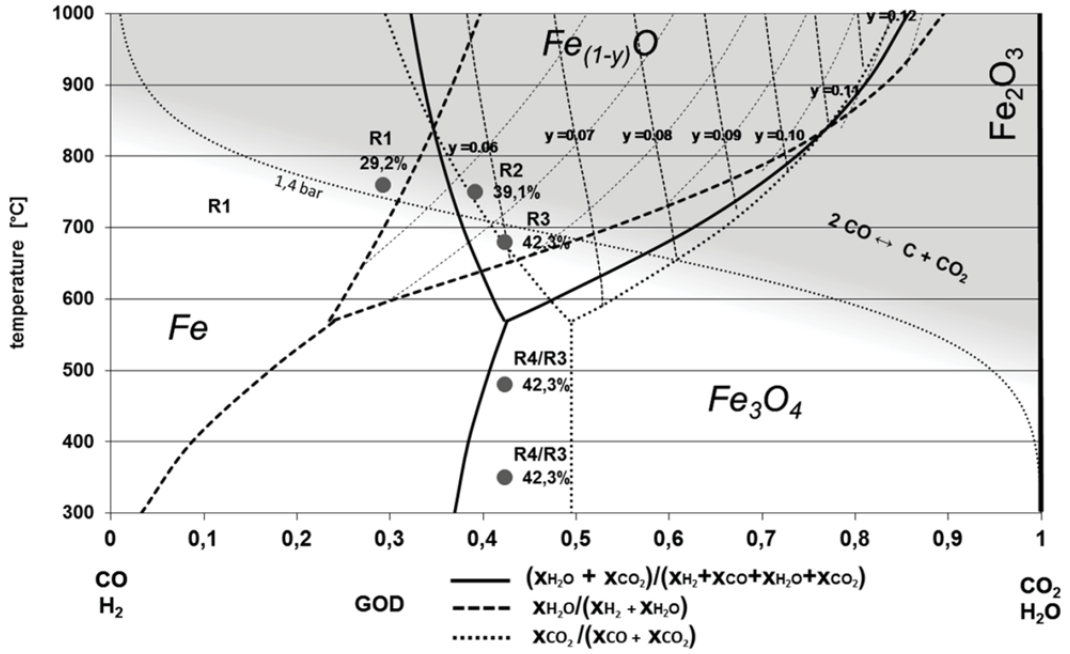

Figure 84: Bauer-Glaessner diagram with operating points of the sequenced 3- and 4-stage tests

Also the variation of the start temperature in the pre-reduction stage (R3 of the 3-stage and R4 of the 4-stage test, variation from 350 °C to 480 °C with the same GOD) is one of the issues of these tests. In the tests the temperatures and GOD's in R2/R1 remain the same (750 °C / 760 °C and 39.1 % / 29.2 %). The additional stage in the 4-stage test is R3 with a process temperature of 680 °C and a GOD of 42.3 %. The process parameters of these tests are shown in Table 20 to Table 23. The calculated gas conditions of the tests are adapted to the gas conditions at the discharge of the fluidized bed cascades of a coal gasification based reduction process. Figure 84 illustrates the variation of operating points of the executed tests.

7.2.1 Sequenced 4- and 3-stage reduction tests with a pre-reduction temperature of 350°C

In this chapter, the 3- and 4-stage tests with a start temperature of 350 °C in the pre-reduction stage are compared. The process parameters and operation points of the 4-stage test are shown in Table 20 and Figure 84, those of the 3-stage test are shown in Table 21 and Figure 84, respectively. The results of the 4-stage test are illustrated in Figure 85 to Figure 88 and the results of the 3-stage test are shown in Figure 89 to Figure 92.

Table 20: test parameter of 4-stage test D with 350°C start temperature

calculation of test parameter:		4-stage 350/680/750/760°C														
		concentration, temp. plant				concentration test rig				gas flow test rig						
gas composition		R1 [%]	R2 [%]	R3 [%]	R4 [%]	R1 [%]	R2 [%]	R3 [%]	R4 [%]	R1 [Nl/min]	heating [Nl/min]	R2 [Nl/min]	heating [Nl/min]	R3 [Nl/min]	heating [Nl/min]	R4 [Nl/min]
species	H2	17.7%	16.5%	16.0%	16.00%	17.6%	16.3%	17.1%	12.8%	**68.1**		**63.5**		**71.8**		**82.1**
	H2O	5.6%	7.1%	8.7%	8.70%	5.6%	7.0%	9.3%	7.0%	**21.5**		**27.3**		**39.0**		**44.6**
	CO	46.7%	38.9%	36.5%	36.50%	46.4%	38.3%	39.1%	29.2%	**179.6**		**149.6**		**163.8**		**187.2**
	CO2	21.0%	28.5%	29.8%	29.80%	20.9%	28.1%	31.9%	23.8%	**80.8**		**109.6**		**133.7**		**152.8**
	CH4	1.5%	1.6%	1.6%	1.60%	0.0%	0.0%	0.0%	0.0%	**0.0**		**0.0**		**0.0**		**0.0**
	N2	7.5%	7.4%	7.4%	7.40%	9.5%	10.4%	2.6%	27.2%	**36.7**		**40.5**		**10.8**		**174.5**
	total dry	94.4%	92.9%	91.3%	91.3%	94.4%	93.0%	90.7%	93.0%	365.2		363.2		380.1		596.6
	total wet	100.0%	100.0%	100.0%	100.0%	100.0%	100.0%	100.0%	100.0%	386.7		390.5		419.2		641.2
	GOD	29.2%	39.1%	42.3%	42.3%	29.2%	39.1%	42.3%	42.3%	29.2%		39.1%		42.3%		42.3%
	H2/H2O	3.16	2.32	1.84	1.84	3.16	2.32	1.84	1.84							
	CO/CO2	2.22	1.36	1.22	1.22	2.22	1.36	1.22	1.22							
temperature [°C]		760	750	680	350					**760**	**0**	**750**	**0**	**680**	**0**	**350**
residence time [min]		40	40	30	30					**40**	**0**	**40**	**0**	**30**	**0**	**30**
spec. gas rate plant [Nm³/t]		810	810	810	810					diameter retort [m]						0.158
supposed gas rate red. [Nm³/t]		4000	4000	3500	4000					cross section retort [m²]						0.020
defined uL retort [m/s]		0.9	0.9	0.9	0.9					absolute pressure [bar]						1.4
flow rate red. comp. [Ndm³/h]		21000	21000	24500	28000					atmospherical pressure [bar]						1.013

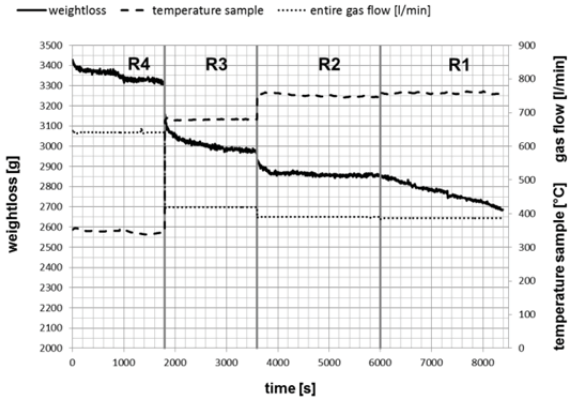

Figure 85: Test D weight loss-curve

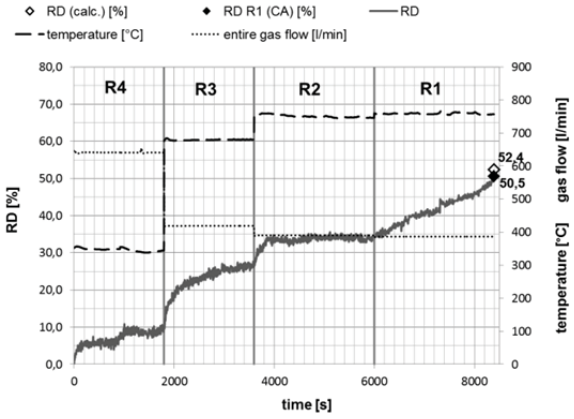

Figure 86: Test D RD-curve and RD-rate

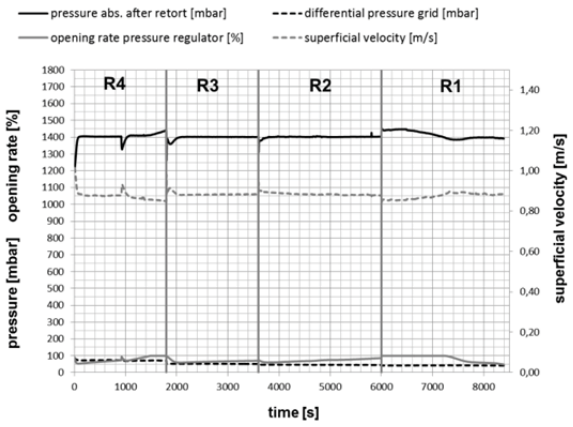

Figure 87: Test D pressure and gas flow

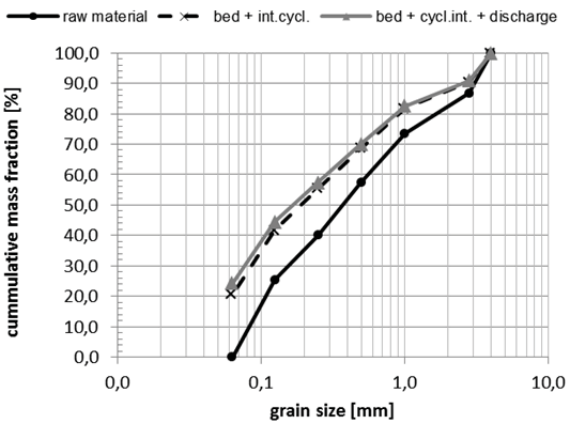

Figure 88: Test D grain size distribution

In the 4-stage test, the reduction from hematite to magnetite in R4 is rather slow and similar to the reduction progress in R3 of the 3-stage test (compare Figure 86 and Figure 90). The fluctuation derives from a small temperature peak during the reduction. The reduction progress from magnetite to wuestite in R3 of the 4-stage test is slower than in R2 of the 3-stage test. The reason is the lower temperature of 680 °C and also the lower GOD in the wuestite field. In R2, the final reduction to wuestite takes part in the first 5 minutes, since most of the ore has already been reduced to wuestite in R3. In both tests, a constant reduction from wuestite to metallic iron during the whole sequence can be observed in R1. Here further reduction potential could possible by prolongation of the residence time.

Regarding the reduction degree-curve and the reduction degree calculated from the chemical analysis and the mass balance, both tests show similar results. As seen in Figure 86 and Figure 90, the RD calculated from the chemical analysis ($RD_{(CA)}$) is 49.9 % for the 3-stage test and 50.5 % for the 4-stage test (MD is 31.3 % and 31.5 % respectively). Also the calculated RD based on the mass balance ($RD_{(calc.)}$) of the whole sample and the discharged material after the test shows similar results. The deviation of the RD-curves compared to the RD's by chemical analysis and mass balance derives from the discharge of finest iron ore and dust during the test, which influences the weight signal and hence the RD. This discharge occurs in every test and varies depending on the input material and the process conditions.

Table 21: test parameter of 3-stage test Test B with 350°C start temperature

calculation of test parameter:		3-stage 350/750/760°C														
		concentration, temp. plant				concentration test rig				gas flow test rig						
gas composition		R1 [%]	R2 [%]	R3 [%]	R4 [%]	R1 [%]	R2 [%]	R3 [%]	R4 [%]	R1 [Nl/min]	heating [Nl/min]	R2 [Nl/min]	heating [Nl/min]	R3 [Nl/min]	heating [Nl/min]	R4 [Nl/min]
species	H2	17.7%	16.5%	16.0%	0.00%	17.6%	17.3%	12.2%	0.0%	**68.1**		**67.7**		**77.9**		**0.0**
	H2O	5.6%	7.1%	8.7%	0.00%	5.6%	7.5%	6.6%	0.0%	**21.5**		**29.1**		**42.4**		**0.0**
	CO	46.7%	38.9%	36.5%	0.00%	46.4%	40.9%	27.7%	0.0%	**179.6**		**159.6**		**177.8**		**0.0**
	CO2	21.0%	28.5%	29.8%	0.00%	20.9%	29.9%	22.6%	0.0%	**80.8**		**116.9**		**145.2**		**0.0**
	CH4	1.5%	1.6%	1.6%	0.00%	0.0%	0.0%	0.0%	0.0%	**0.0**		**0.0**		**0.0**		**0.0**
	N2	7.5%	7.4%	7.4%	0.00%	9.5%	4.4%	30.9%	0.0%	**36.7**		**17.2**		**197.9**		**0.0**
	total dry	94.4%	92.9%	91.3%	0.0%	94.4%	92.5%	93.4%	0.0%	365.2		361.4		598.8		0.0
	total wet	100.0%	100.0%	100.0%	0.0%	100.0%	100.0%	100.0%	0.0%	386.7		390.5		641.2		0.0
	GOD	29.2%	39.1%	42.3%	0.0%	29.2%	39.1%	42.3%	0.0%	29.2%		39.1%		42.3%		0.0%
	H2/H2O	3.16	2.32	1.84	0.00	3.16	2.32	1.84	0.00							
	CO/CO2	2.22	1.36	1.22	0.00	2.22	1.36	1.22	0.00							
temperature [°C]		760	750	350	0					**760**	**0**	**750**	**0**	**350**	**0**	**0**
residence time [min]		40	30	30	0					**40**	**0**	**30**	**0**	**30**	**0**	**0**
spec. gas rate plant [Nm³/t]		810	810	810	0					diameter retort [m]					0.158	
supposed gas rate red. [Nm³/t]		4000	3200	3800	0					cross section retort [m²]					0.020	
defined uL retort [m/s]		0.9	0.9	0.9	0					absolute pressure [bar]					1.4	
flow rate red. comp. [Ndm³/h]		21000	22400	26600	0					atmospherical pressure [bar]					1.013	

Comparing the grain size distributions of the material after the tests, it can be stated, that the material in the 3-stage test was far less disintegrated during the process (cf. Figure 88 and Figure 92). The bold black line in these diagrams represents the defined grain size distribution of the input material. The black dotted line represents the grain size distribution in the fluidized bed (including the internal cyclone) after the test, and the grey line the grain size distribution of the whole re-extracted material after the test (material in fluidized bed and internal cyclone, discharge and rest).

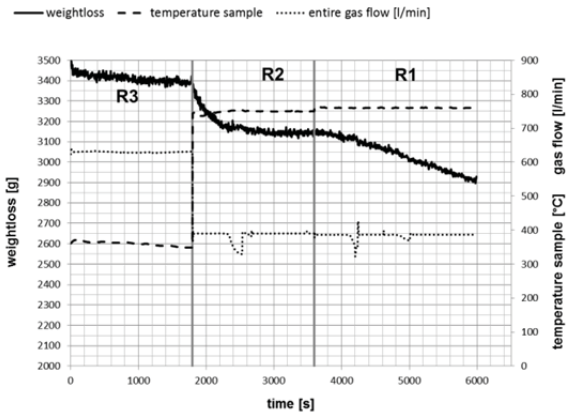

Figure 89: Test B weight loss-curve

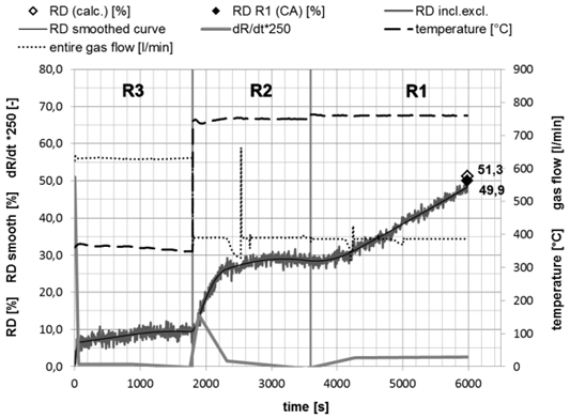

Figure 90: Test B RD-curve and RD-rate

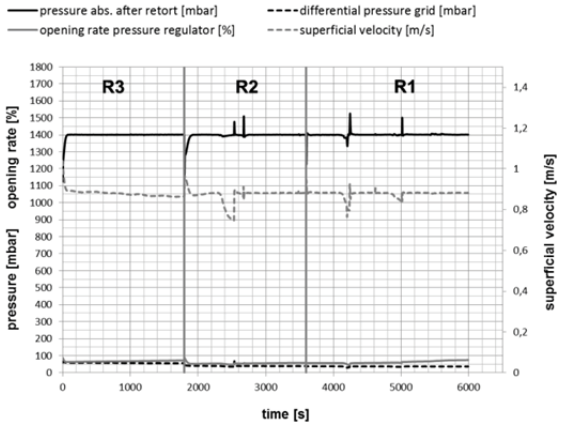

Figure 91: Test B pressure and gas flow

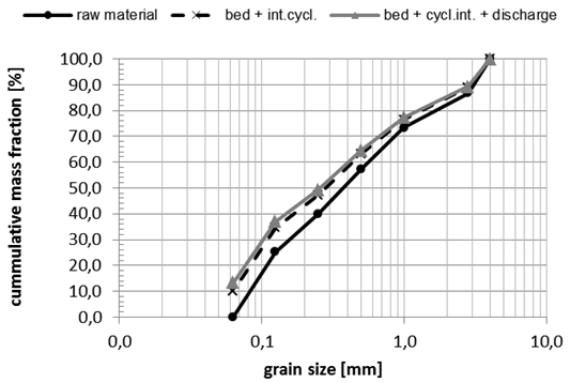

Figure 92: Test B grain size distribution

7.2.2 Sequenced 4- and 3-stage reduction tests with a pre-reduction temperature of 480°C

In this chapter, the 3- and 4-stage tests with a start temperature of 480 °C in the pre-reduction stage, are compared. The process parameters and operation points of the 4-stage test are shown in Table 22 and Figure 84 and the parameters and operation points of the 3-stage test are shown in Table 23 and Figure 84, respectively. The results of the 4-stage test are illustrated in Figure 93 to Figure 96 and the results of the 3-stage test are shown in Figure 97 to Figure 100.

Table 22: test parameter of 4-stage test F with 480°C start temperature

calculation of test parameter:		4-stage 480/680/750/760°C														
		concentration, temp. plant				concentration test rig				gas flow test rig						
gas composition		R1 [%]	R2 [%]	R3 [%]	R4 [%]	R1 [%]	R2 [%]	R3 [%]	R4 [%]	R1 [Nl/min]	heating [Nl/min]	R2 [Nl/min]	heating [Nl/min]	R3 [Nl/min]	heating [Nl/min]	R4 [Nl/min]
species	H2	17.7%	16.5%	16.0%	16.00%	17.6%	16.3%	17.1%	15.5%	**68.1**		**63.5**		**71.8**		**82.1**
	H2O	5.6%	7.1%	8.7%	8.70%	5.6%	7.0%	9.3%	8.4%	**21.5**		**27.3**		**39.0**		**44.6**
	CO	46.7%	38.9%	36.5%	36.50%	46.4%	38.3%	39.1%	35.3%	**179.6**		**149.6**		**163.8**		**187.2**
	CO2	21.0%	28.5%	29.8%	29.80%	20.9%	28.1%	31.9%	28.8%	**80.8**		**109.6**		**133.7**		**152.8**
	CH4	1.5%	1.6%	1.6%	1.60%	0.0%	0.0%	0.0%	0.0%	**0.0**		**0.0**		**0.0**		**0.0**
	N2	7.5%	7.4%	7.4%	7.40%	9.5%	10.4%	2.6%	12.0%	**36.7**		**40.5**		**10.8**		**63.8**
	total dry	94.4%	92.9%	91.3%	91.3%	94.4%	93.0%	90.7%	91.6%	365.2		363.2		380.1		485.9
	total wet	100.0%	100.0%	100.0%	100.0%	100.0%	100.0%	100.0%	100.0%	386.7		390.5		419.2		530.5
	GOD	29.2%	39.1%	42.3%	42.3%	29.2%	39.1%	42.3%	42.3%	29.2%		39.1%		42.3%		42.3%
	H2/H2O	3.16	2.32	1.84	1.84	3.16	2.32	1.84	1.84							
	CO/CO2	2.22	1.36	1.22	1.22	2.22	1.36	1.22	1.22							
temperature [°C]		760	750	680	480					**760**	**0**	**750**	**0**	**680**	**0**	**480**
residence time [min]		40	40	30	30					**40**	**0**	**40**	**0**	**30**	**0**	**30**
spec. gas rate plant [Nm³/t]		810	810	810	810					diameter retort [m]						0.158
supposed gas rate red. [Nm³/t]		4000	4000	3500	4000					cross section retort [m²]						0.020
defined uL retort [m/s]		0.9	0.9	0.9	0.9					absolute pressure [bar]						1.4
flow rate red. comp. [Ndm³/h]		21000	21000	24500	28000					atmospherical pressure [bar]						1.013

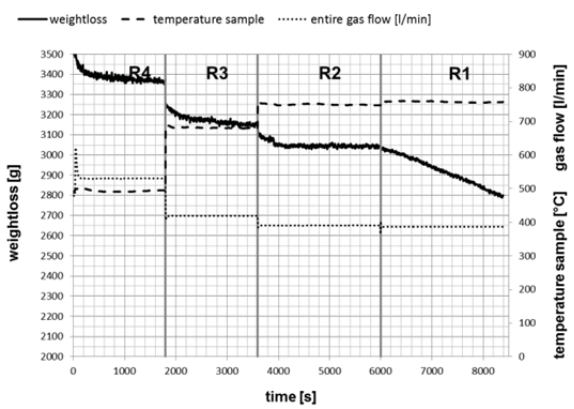

Figure 93: Test F weight loss-curve

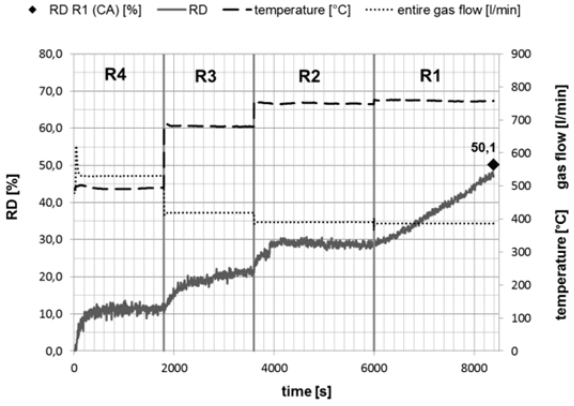

Figure 94: Test F RD-curve and RD-rate

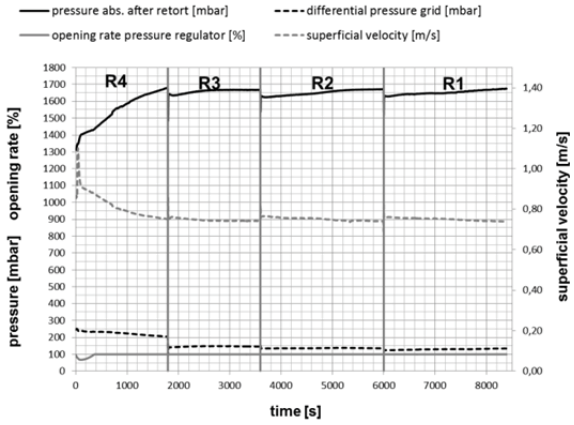

Figure 95: Test F pressure and gas flow

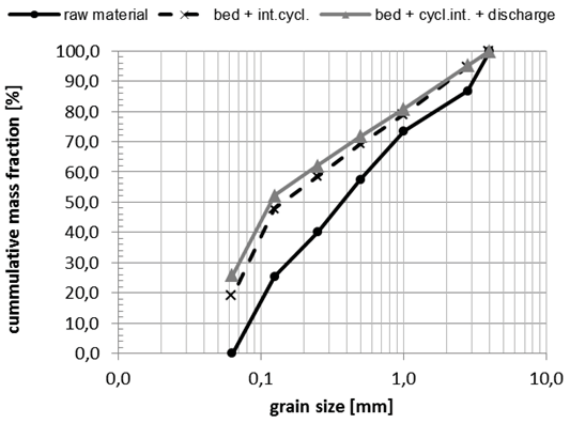

Figure 96: Test F grain size distribution

In the 4-stage test, the reduction from hematite to magnetite in R4 happened relatively quickly and finished within 5 minutes residence time. This was similar to the reduction progress in R3 of the 3-stage test (cf. Figure 94 and Figure 98). In R3 of the 4-stage test at a temperature of 680 °C, the reduction from magnetite to wuestite shows a rather slow inclination, which continues in R2 at 750 °C for about 5 minutes. The reason is the lower temperature of 680 °C and also the lower GOD in the wuestite field in R3 - here, the formation to wuestite has not finished. In comparison, in the 3-stage test, the reduction in R2 at 750 °C (reduction from magnetite to wuestite) was already finished within 15 minutes. In R1 both tests show a constant reduction from wuestite to metallic iron during the whole sequence. Here further reduction potential could be possible by prolongation of the residence time.

Regarding the reduction degree-curve and the reduction degree calculated from the chemical analysis and the mass balance, both tests show similar results. As seen in Figure 94 and Figure 98, the RD calculated from the chemical analysis ($RD_{(CA)}$) is 50.8 % for the 3-stage test and 50.1 % for the 4-stage test and is also similar (MD is 32.2 % and 32.6 % respectively). However, in the 3-stage test the $RD_{(CA)}$ of the chemical analysis seems to be slightly too high compared to the RD-trend the test (cf. Figure 98). In other tests with the same ore and conditions, RDs between 47 % and 49 % were reached. The calculated RD based on the mass balance ($RD_{(calc.)}$) of the 4-stage test could not be calculated because of material losses while the retort was being dismantled after the test.

Comparing the grain size distributions of the material after the tests, it can be stated that the material in the 3-stage test was much less disintegrated during the process than the 4-stage tests (cf. Figure 96 and Figure 100). Although the superficial velocity in the 4-stage test was slightly lower due to a pressure increase during the test, the disintegration of the material was tremendously high compared to the 3-stage test.

Table 23: test parameter of 3-stage test H with 480°C start temperature

calculation of test parameter:		3-stage 480/750/760°C														
		concentration, temp. plant				concentration test rig				gas flow test rig						
gas composition		R1 [%]	R2 [%]	R3 [%]	R4 [%]	R1 [%]	R2 [%]	R3 [%]	R4 [%]	R1 [Nl/min]	heating [Nl/min]	R2 [Nl/min]	heating [Nl/min]	R3 [Nl/min]	heating [Nl/min]	R4 [Nl/min]
species	H2	17.7%	16.5%	16.0%	0.00%	17.6%	17.3%	14.7%	0.0%	**68.1**		**67.7**		**77.9**		**0.0**
	H2O	5.6%	7.1%	8.7%	0.00%	5.6%	7.5%	8.0%	0.0%	**21.5**		**29.1**		**42.4**		**0.0**
	CO	46.7%	38.9%	36.5%	0.00%	46.4%	40.9%	33.5%	0.0%	**179.6**		**159.6**		**177.8**		**0.0**
	CO2	21.0%	28.5%	29.8%	0.00%	20.9%	29.9%	27.4%	0.0%	**80.8**		**116.9**		**145.2**		**0.0**
	CH4	1.5%	1.6%	1.6%	0.00%	0.0%	0.0%	0.0%	0.0%	**0.0**		**0.0**		**0.0**		**0.0**
	N2	7.5%	7.4%	7.4%	0.00%	9.5%	4.4%	16.4%	0.0%	**36.7**		**17.2**		**87.2**		**0.0**
	total dry	94.4%	92.9%	91.3%	0.0%	94.4%	92.5%	92.0%	0.0%	365.2		361.4		488.1		0.0
	total wet	100.0%	100.0%	100.0%	0.0%	100.0%	100.0%	100.0%	0.0%	386.7		390.5		530.5		0.0
	GOD	29.2%	39.1%	42.3%	0.0%	29.2%	39.1%	42.3%	0.0%	29.2%		39.1%		42.3%		0.0%
	H2/H2O	3.16	2.32	1.84	0.00	3.16	2.32	1.84	0.00							
	CO/CO2	2.22	1.36	1.22	0.00	2.22	1.36	1.22	0.00							
temperature [°C]		760	750	480	0					**760**	**0**	**750**	**0**	**480**	**0**	**0**
residence time [min]		40	30	30	0					**40**	**0**	**30**	**0**	**30**	**0**	**0**
spec. gas rate plant [Nm³/t]		810	810	810	0					diameter retort [m]					0.158	
supposed gas rate red. [Nm³/t]		4000	3200	3800	0					cross section retort [m²]					0.020	
defined uL retort [m/s]		0.9	0.9	0.9	0					absolute pressure [bar]					1.4	
flow rate red. comp. [Ndm³/h]		21000	22400	26600	0					atmospherical pressure [bar]					1.013	

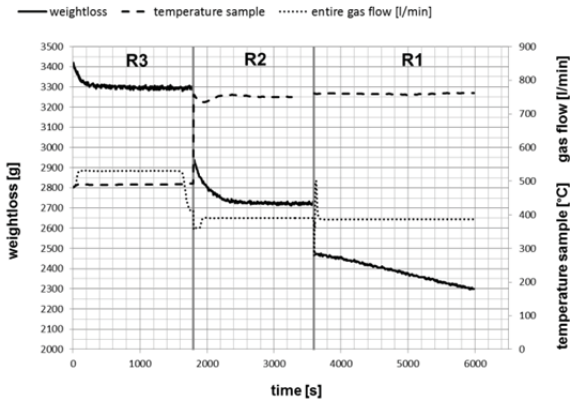

Figure 97: Test H weight loss-curve

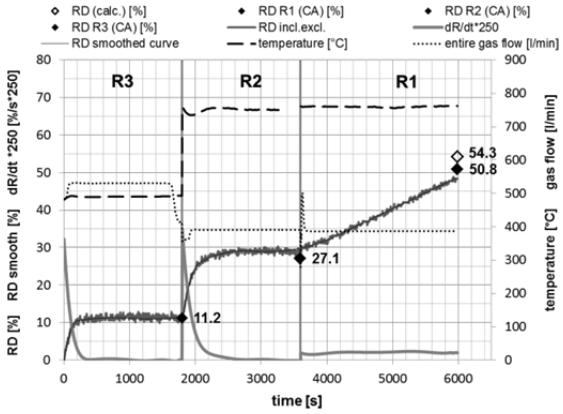

Figure 98: Test H RD-curve and RD-rate

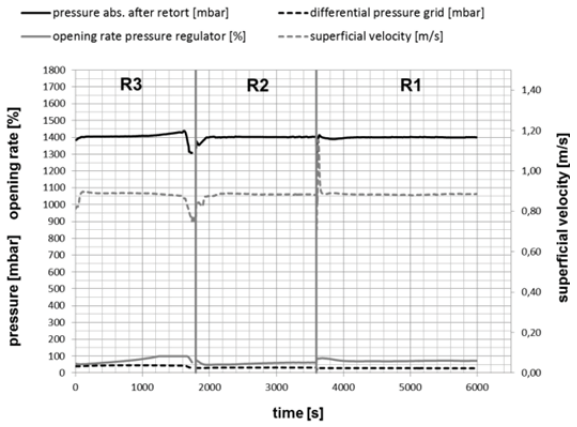

Figure 99: Test H pressure and gas flow

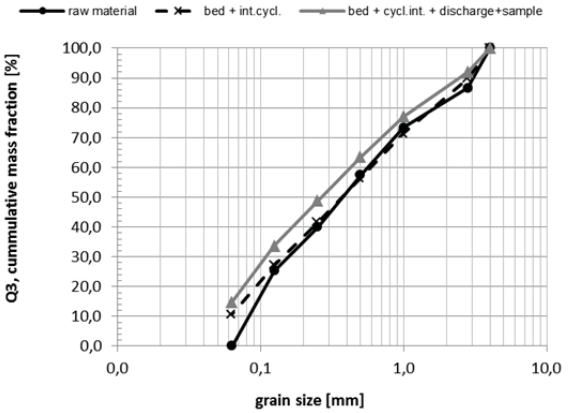

Figure 100: Test H grain size distribution

7.2.3 Morphgological analyses of the sequenced 4- and 3-stage reduction tests

In general it can be summarized that the mineralogical compositions of the reduced samples confirm the degrees of reduction and metallization of the chemical analyses of all tests. The 3-stage test with a start temperature of 350 °C shows some massive and some porous magnetite areas and partly formation of iron scraps. The reduction to magnetite has not completely been finished in the pre-reduction stage. This magnetite is very dense, forming shells around a central hematite relic and could influence the reduction in the following reduction steps.

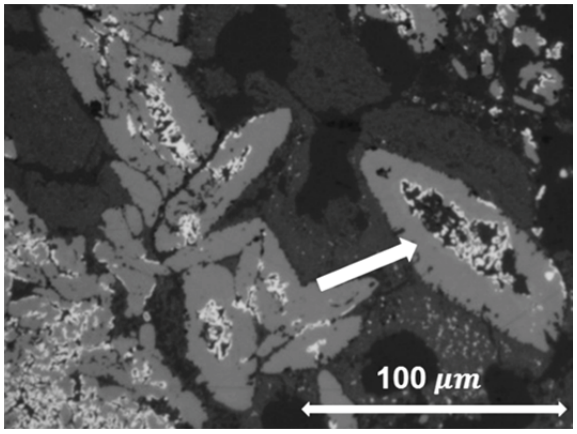

Figure 101: Test B (1 – 2.8 mm)
3-stage 350/750/760 °C

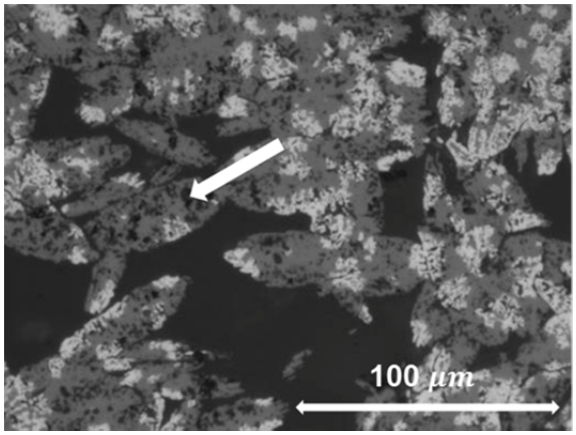

Figure 102: Test D (1 – 2.8 mm)
4-stage 350/680/750/760 °C

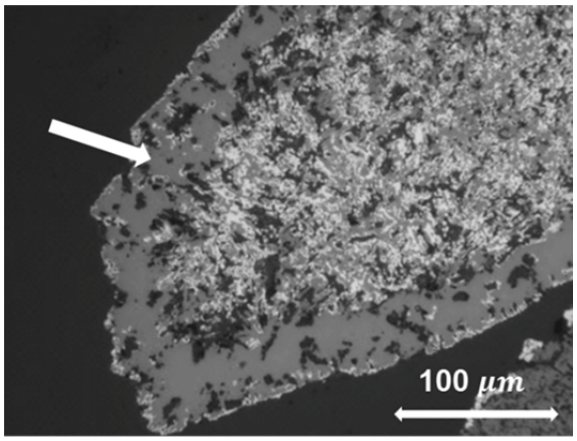

Figure 103: Test H (1 – 2.8 mm)
3-stage 480/750/760 °C

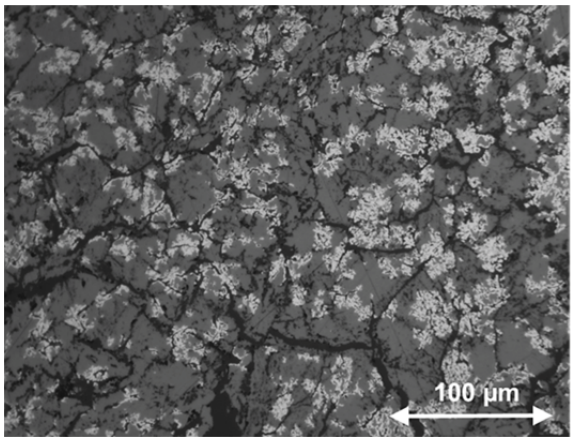

Figure 104: Test F (1 – 2.8 mm)
4-stage 480/680/750/760 °C

Figure 101 shows hematite, which is reduced to wuestite and partly to iron. The former magnetite shells from the first reduction step (hematite to magnetite) comprise dense wuestite shells (mark). The central parts of the former hematite crystals which are not reduced to magnetite in the first stage are well reduced to iron. Finer fractions show a similar morphology, but less coarse wuestite grains (formed from the former coarsely crystalline hematite). The 4-stage test (Figure 102) shows some very porous grains, which were formerly hematite. The hematite was not fully reduced to magnetite during the reduction process. The bright areas represent the metallic iron. The limonite is well reduced. Some dense wuestite areas, derived from dense magnetite of stage 1 were observed. The smaller fractions show a very inhomogeneous reduction. Some grains are well metallized, some grains not.

The 3-stage test with a start temperature of 480 °C shows dense wuestite regions (Figure 103, mark: hematite which was formerly reduced magnetite) and formation of iron scraps. Limonitic fractions of the raw ore were broadly better reduced than the hematite matrix. In general, the grains are reduced non-homogenously. Again, some dense former hematite grains with magnetite shells were observed. The finest fractions are the least reduced, some of the grains are not metallized at all. The 4-stage test with a start temperature of 480 °C also shows dense wuestite regions and formation of iron scraps. The limonitic parts are better

reduced than the hematitic matrix. In general, the grains are reduced inhomogeneously and no surface covering iron shells are present. The finest fractions are poorly reduced and partly metallized.

In summary, the morphology of all tests is similar. The reduction degree is comparable and no surface covering iron layers were observed. In all tests, the finer fractions were non-homogenously reduced. An important fact is the formation of the dense magnetite from former hematite during the reduction process, which was observed in all tests, especially in tests H and F with 480 °C start temperature. It seems that at the higher temperature, denser magnetite was generated because of the more favorable reduction kinetics. The formation of magnetite during the reduction seems to influence the further reduction progress of the iron ore significantly. Comparing the grain size distributions of the material after the tests, the disintegration of the 3-stage tests is similar, as well as the disintegration of the 4-stage tests (cf. Figure 105). The material of the 4-stage tests is much more disintegrated than the material of the 3-stage tests. In this diagram, the grain size distribution curves refer to the whole material which was re-extracted after each test (fluidized bed, internal cyclone, discharge and rest).

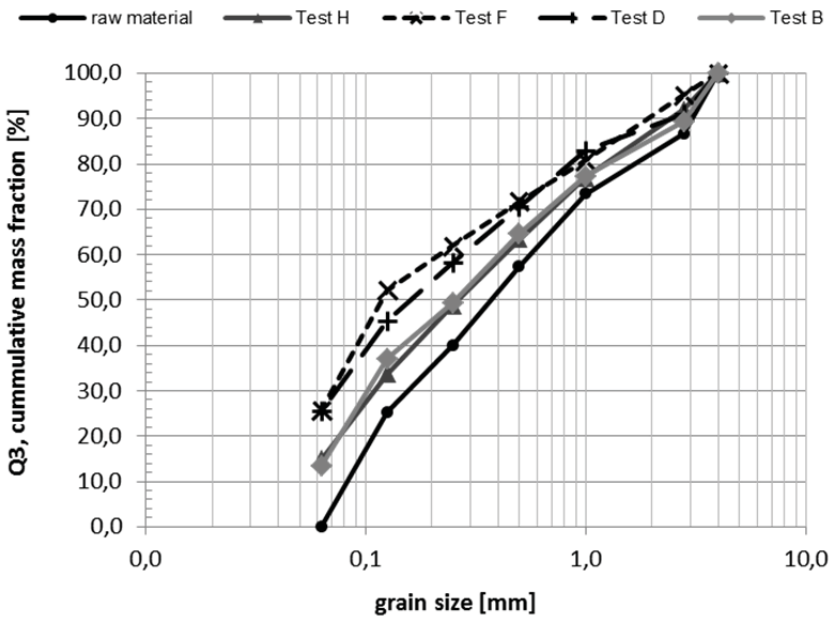

Figure 105: Grain size distribution of the raw material, 3-stage and 4-stage tests

7.2.4 Discussion

Comparing the results of the 3- and 4-stage tests, it can be stated that no major difference of reduction and metallization degree was observed. The final reduction degree is about 50 % for all tests with a metallization degree of approximately 31 %. The reduction degree is comparable and no surface covering iron layers were observed. In all tests, the finer fractions were non-homogenously reduced. An important fact is the formation of the dense magnetite from former hematite during the reduction process, which was observed in all tests, especially in tests C and D with 480 °C start temperature. It seems that at the higher temperature, denser magnetite was generated because of the more favorable reduction

kinetics. The formation of magnetite during the reduction could influence the further reduction progress of the iron ore significantly. Comparing the grain size distributions of the material after the tests, it can be stated, that the material in the 3-stage tests was much less disintegrated during the process, which is a great advantage regarding the process stability in the industrial process, as well as a decreasing in dust. Hence, a sequenced 3-stage operation mode is recommended for the industrial process under the tested conditions.

7.3 Influence of pre-reduction temperature on the reduction behavior in sequenced 3-stage operation

To investigate the influence of the pre-reduction temperature in the first reduction stage on the final reduction degree, 3-stage sequenced fluidized bed tests with different start temperatures were executed and are discussed in this chapter. The operating points of these tests are shown in Figure 106. The temperature in the pre-reduction stage (R3) was varied between 350 °C, 480 °C and 600 °C while the GOD is equal (42.3 %). The second and third reduction stage (R2 and R1) remained the same for all tests (750 °C, 31.1 % GOD in R2 and 760 °C, 29.2 % GOD in R1). The process parameters and results of the 3-stage tests with a start temperature of 350 °C and 480 °C have already been discussed in chapter 7.2 (cf. Table 21 and Table 23). The results were shown in Figure 89 to Figure 92 for the test with 350 °C start temperature and in Figure 97 to Figure 100 for the test with 480 °C start temperature. The process parameters and results for the test with a start temperature of 600 °C are shown in Table 24 and Figure 110 to Figure 113, respectively.

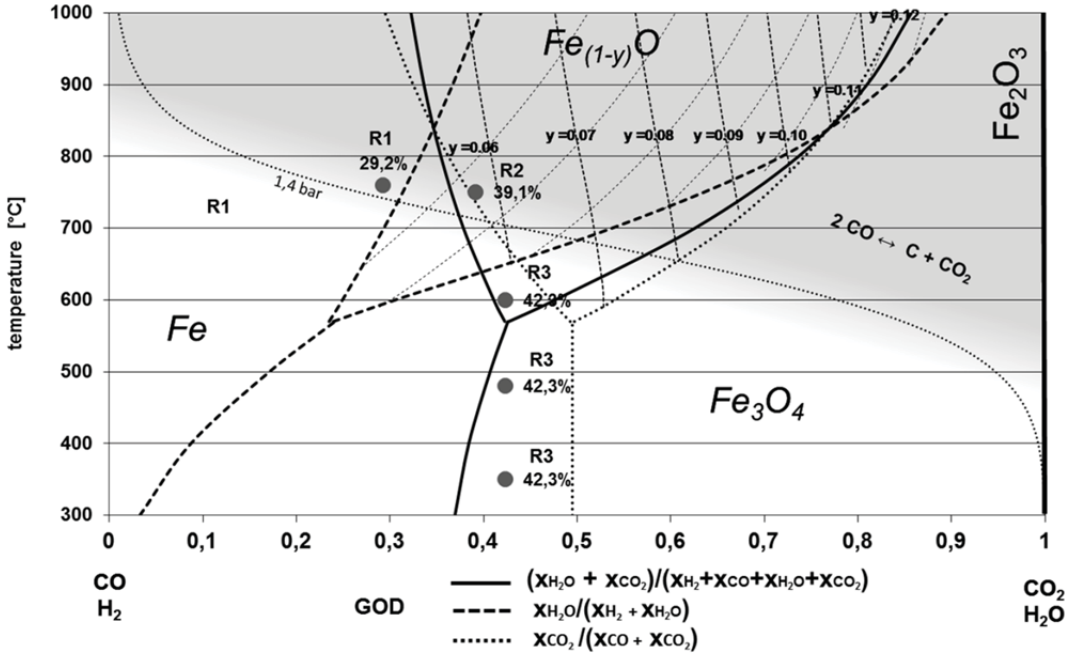

Figure 106: Bauer-Glaessner diagram with operating points of sequenced 3-stage tests with different start temperature in the pre-reduction stage

Literature Review

Regarding the influence of temperature on the reduction behavior of iron ore fines in multi-stage reduction, the following facts are important. During reduction with H_2-rich gas compositions from hematite to metallic iron, Turnhofer [109] found, that magnetite generated in the pre-reduction stage has a negative influence on final RD. At low temperatures (350 – 400 °C) few magnetite is generated and at temperatures above 500 °C almost all hematite is transformed to magnetite. Feilmayr [111] confirmed these findings and added, that below 350 °C, nearly no magnetite is generated and above 400 °C dense magnetite layers are formed (dense magnetite generates dense wuestite, which results in a lower final RD). Furthermore, he stated, that between 400 and 600 °C the rate determining step is the phase interface reaction and that the magnetite layer thickness is proportional to the reduction time. Also Weiss confirmed these findings and, added that the reduction increases with increasing temperature, during hematite reduction to magnetite, as well as during hematite reduction to wuestite [146]. These finding contradict the statements of Habermann [105], who found no effect on reduction below 550°C, but a strong increase between 550°C and 700 °C. In 2-stage reduction tests with pre-reduction at different temperatures in the magnetite, wuestite and iron field (same gas composition) and final reduction in the iron field, the final reduction degree varies in dependence on the pre-reduction temperature (cf. Figure 107). Here, the final reduction degree shows maximum and minimum values.

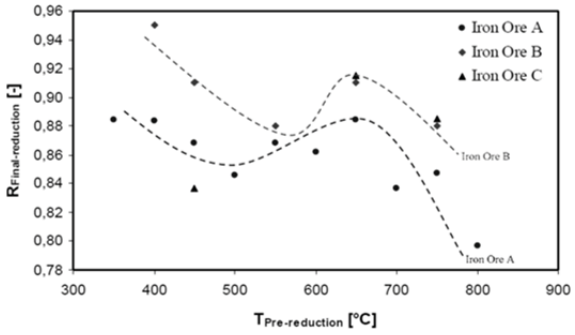

Figure 107: Final reduction degree versus pre-reduction temperature, H_2-rich gas [106]

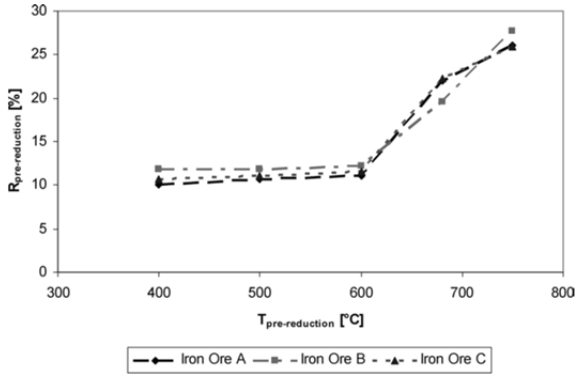

Figure 108: Pre-reduction degree versus pre-reduction temperature [104]

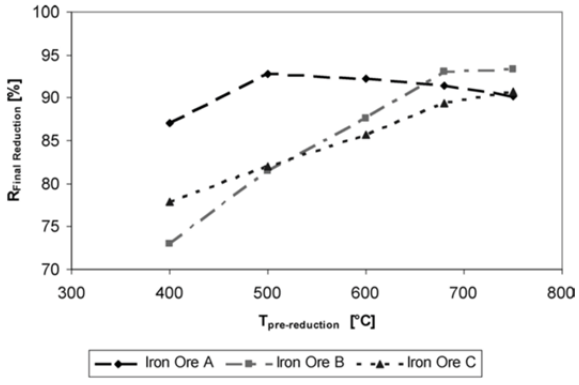

Figure 109: Final reduction degree versus pre-reduction temperature, CO-rich gas [104]

Regarding the reduction under CO-rich gas compositions, Pawlik and Schuster found, that the reduction degree after the reduction in the magnetite field remains almost constant up to 600 °C and increases at higher temperatures (Figure 108). For a 3-stage reduction mode

with pre-reduction in the magnetite and wuestite stability field, they stated that “the final reduction degree increases with increasing pre-reduction temperature [103,104,108]”, which is obviously wrong (cf. Figure 109). In this figure, the final RD in dependence on the pre reduction temperature shows different behaviors for every iron ore.

7.3.1 Sequenced 3-stage reduction tests with start temperatures of 350, 480 and 600 °C in the pre-reduction stage

The 3-stage test with a start temperature of 350 °C shows a slower increase of the RD-curve in R3 compared to the tests with higher temperatures (cf. Figure 90). This could be explained by the inhibited reaction kinetics at low temperatures. The tests with a start temperature of 480 °C and 600 °C (cf. Figure 98 and Figure 111) reached the magnetite state (theoretical RD for Fe_3O_4 is 11.1 %) after a short time and the reduction curve remained stable until the end of R3. In all cases, the magnetite state was almost reached. The operation point of the test with a start temperature of 600 °C is in the lower range of the wuestite field, so theoretically, wuestite should have been formed. Due to the formation of magnetite (cf. curve in Figure 111), the chemical potential for the formation of wuestite seems to be too low at this temperature. In R2, the reduction behaviour is approximately the same for all tests and the wuestite state is almost reached (theoretical RD for $Fe_{(1-y)}O$ is about 30 %). Also in the final stage R1, the RD curves show a similar behaviour for all tests. The RDs by chemical analyses ($RD_{(CA)}$) as well as the metallization degrees have a similar value: 49.9 % and 31.3 % for 350 °C start temperature; 50.8 % and 32.2 % for 480 °C start temperature, 49.5 % and 31,0 % for 600 °C start temperature. The reduction degree of the test with 480 °C start temperature seems a little high. The RDs’ calculated from the mass balance of the whole remaining material after the test ($RD_{(calc.)}$) are higher than the RDs by chemical analysis, because the retrieval of the whole rest material after the test is not possible. The deviation of $RD_{(calc.)}$ is caused by this fact and represents additional information for the interpretation of the tests.

Table 24: test parameter of 3-stage test C with 600°C start temperature

calculation of test parameter:		3-stage 600/750/760°C														
		concentration, temp. plant				concentration test rig				gas flow test rig						
gas composition		R1 [%]	R2 [%]	R3 [%]	R4 [%]	R1 [%]	R2 [%]	R3 [%]	R4 [%]	R1 [Nl/min]	heating [Nl/min]	R2 [Nl/min]	heating [Nl/min]	R3 [Nl/min]	heating [Nl/min]	R4 [Nl/min]
species	H2	17,7%	16,5%	16,0%	0,00%	17,6%	17,3%	17,0%	0,0%	**68,1**		**67,7**		**77,9**		**0,0**
	H2O	5,6%	7,1%	8,7%	0,00%	5,6%	7,5%	9,3%	0,0%	**21,5**		**29,1**		**42,4**		**0,0**
	CO	46,7%	38,9%	36,5%	0,00%	46,4%	40,9%	38,9%	0,0%	**179,6**		**159,6**		**177,8**		**0,0**
	CO2	21,0%	28,5%	29,8%	0,00%	20,9%	29,9%	31,7%	0,0%	**80,8**		**116,9**		**145,2**		**0,0**
	CH4	1,5%	1,6%	1,6%	0,00%	0,0%	0,0%	0,0%	0,0%	**0,0**		**0,0**		**0,0**		**0,0**
	N2	7,5%	7,4%	7,4%	0,00%	9,5%	4,4%	3,1%	0,0%	**36,7**		**17,2**		**14,2**		**0,0**
	total dry	94,4%	92,9%	91,3%	0,0%	94,4%	92,5%	90,7%	0,0%	365,2		361,4		415,2		0,0
	total wet	100,0%	100,0%	100,0%	0,0%	100,0%	100,0%	100,0%	0,0%	386,7		390,5		457,6		0,0
	GOD	29,2%	39,1%	42,3%	0,0%	29,2%	39,1%	42,3%	0,0%	29,2%		39,1%		42,3%		0,0%
	H2/H2O	3,16	2,32	1,84	0,00	3,16	2,32	1,84	0,00							
	CO/CO2	2,22	1,36	1,22	0,00	2,22	1,36	1,22	0,00							
temperature [°C]		760	750	600	0					**760**	**760**	**750**	**750**	**600**	**0**	**0**
residence time [min]		40	30	30	0					**40**	**5**	**30**	**15**	**30**	**0**	**0**
spec. gas rate plant [Nm³/t]		810	810	810	0					diameter retort [m]					0,158	
supposed gas rate red. [Nm³/t]		4000	3200	3800	0					cross section retort [m²]					0,020	
defined uL retort [m/s]		0,9	0,9	0,9	0					absolute pressure [bar]					1,4	
flow rate red. comp. [Ndm³/h]		21000	22400	26600	0					atmospherical pressure [bar]					1,013	

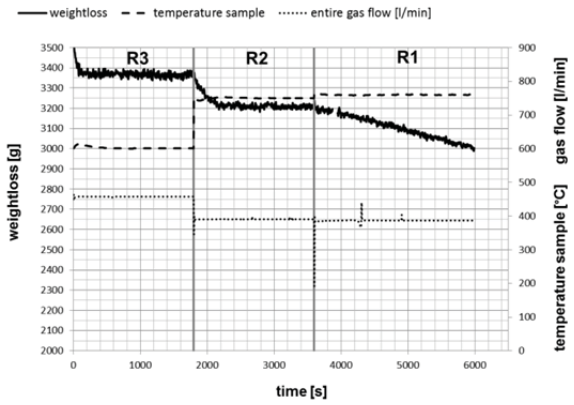

Figure 110: Test C weight loss-curve

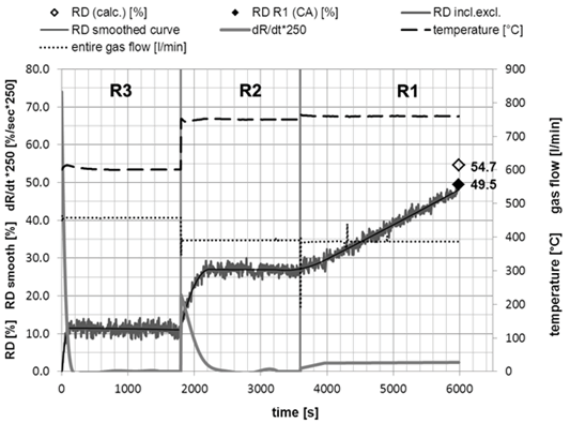

Figure 111: Test C RD-curve and RD-rate

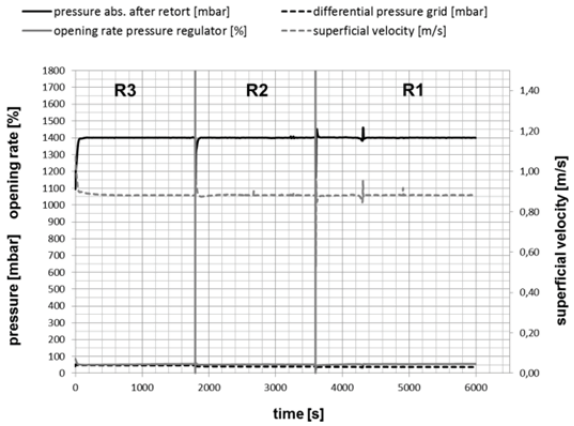

Figure 112: Test C pressure and gas flow

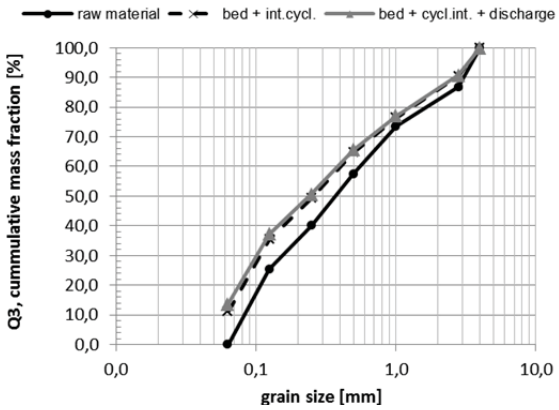

Figure 113: Test C grain size distribution

7.3.2 Morphological analyses of the sequenced 3-stage tests

Regarding the influence of temperature, the morphology of the 3-stage tests with a start temperature of 350 °C and 480 °C has been discussed in chapter 7.2. An important fact was the formation of the dense magnetite from former hematite during the reduction process, which was observed especially in the test with a start temperature 480 °C (cf. Figure 115, dense wuestite generated from dense magnetite). In the test with a start temperature of 350 °C, partly dense and partly porous magnetite was generated during the test (cf. Figure 114, porous wuestite generated from porous magnetite). It seems that with increasing temperature, denser magnetite was generated because of the more favorable reduction kinetics. The test with a start temperature of 600 °C showed a formation of porous magnetite instead of dense magnetite from former hematite (cf. Figure 116), which was observed at lower temperatures. Probably due to the fact, that the operation point is in the lower wuestite field. The formation of dense magnetite in the test with a start temperature of 480 °C could be confirmed by extracting a sample in the magnetite stability field (R3) after installing the sampling system (cf. Figure 117). In case of dense magnetite, iron layers were generated during the process on the grain's surfaces, and in case of porous magnetite, iron scraps were generated within the grains. In dependence on the mineralogical composition of the iron ore, the pre-reduction temperature can influence the magnetite formation and can lead to an inhibited reduction. In general it can be summarized that the mineralogical compositions of

the reduced samples confirm the degrees of reduction and metallization of the chemical analyses of all tests.

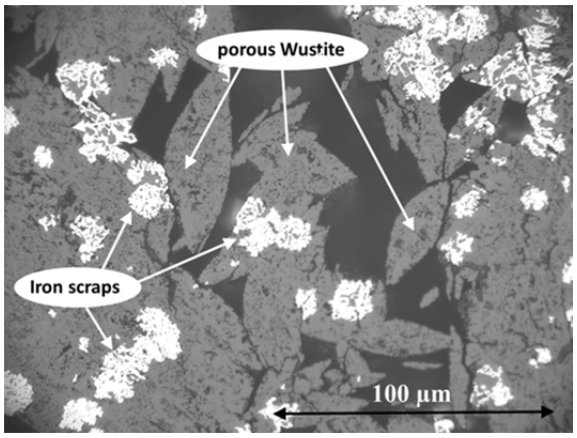

Figure 114: Test B (1 – 2.8 mm)
3-stage 350/750/760 °C

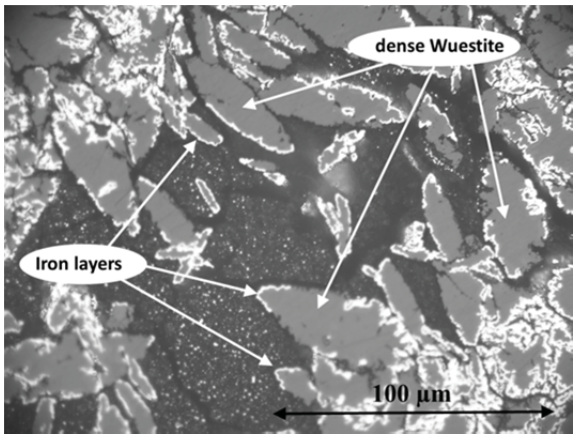

Figure 115: Test H (1 – 2.8 mm)
3-stage 480/750/760 °C

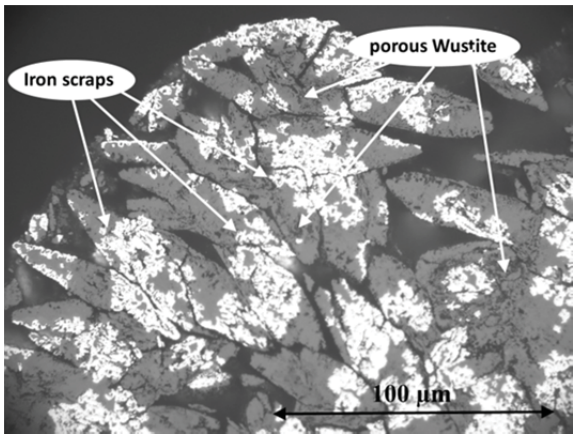

Figure 116: Test C (1 – 2.8 mm)
3-stage 600/750/760 °C

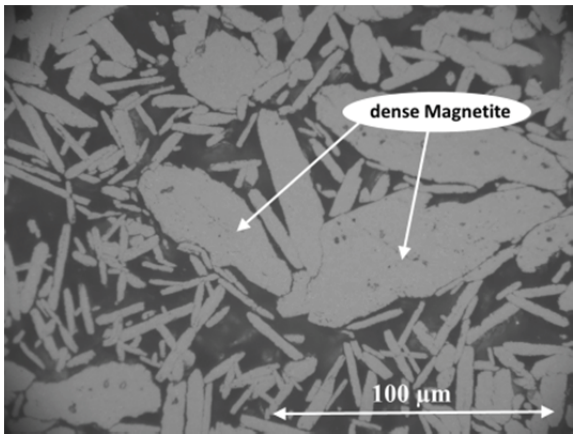

Figure 117: Test H (1 – 2.8 mm)
3-stage 480/750/760 °C

Comparing the grain size distributions of the material after the tests, it can be stated, that the disintegration of the material during the test is nearly equal (cf. Figure 118). In this diagram, the grain size distribution curves refer to the whole material which was re-extracted after each test (fluidized bed, internal cyclone, discharge and rest). The variation of the pre-reduction temperature between 350 °C and 600 °C has low influence on the disintegration behaviour.

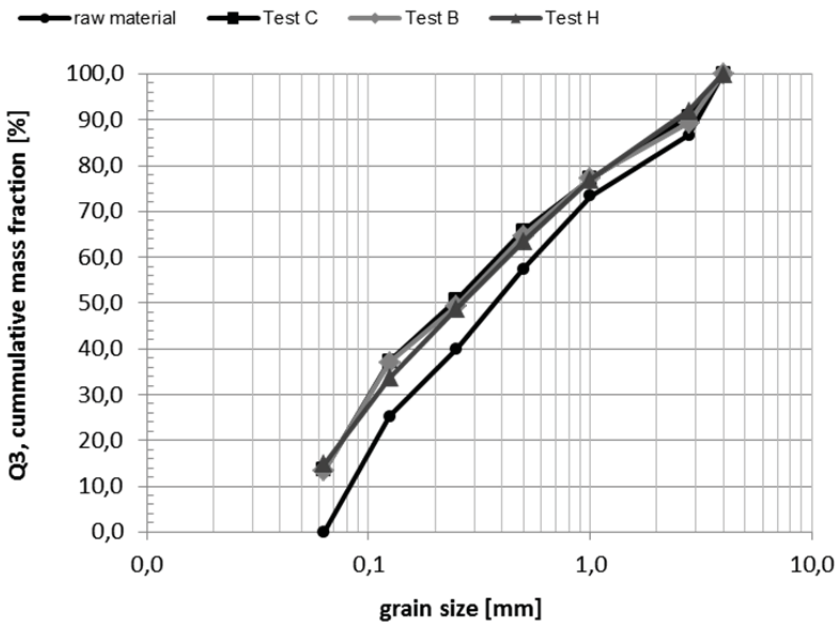

Figure 118: Grain size distribution of the 3-stage tests with different pre-reduction temperature

7.3.3 Discussion

The test with 350 °C start temperature shows a slower increase of the RD-curve in the magnetite field R3, compared to the tests with higher temperatures.The most probable reason is the inhibited reaction kinetics at low temperatures. In the test with 600 °C start temperature, theoretically wuestite should have been formed. Due to the formation of magnetite, the chemical potential for the formation of wuestite seems to be too low at this temperature. In R2 and R1, the RD-curve is nearly similar and also the reduction degrees and metallization degrees of about RD = 50 % and MD = 31 %. As discussed in the previous chapter, the formation of dense magnetite at a start temperature of 350 °C and especially at 480 °C is an important fact, which could influence the further reduction (in dependence on the mineralogical composition of the raw ore). In contrast, at a start temperature of 600 °C porous magnetite instead of dense magnetite was formed, although the operating point was in the lower wuestite area. However, under these process conditions, the formation of the porous magnetite seems to have no big influence on the further reduction behaviour. In general, the variation of the pre-reduction temperature between 350 °C and 600 °C has little influence on the final reduction degree in 3-stage sequenced operation under the mentioned process conditions. Also the disintegration behaviour of the material is nearly equal. The findigns of Thurhofer [109] (negative influence of the magnetite formation due to temperature variation in the pre-reduction field on the final RD) could not be confirmed. Also the findings of Pawlik and Schuster [103,104,108], who found an increasing final RD with increasing pre-reduction temperature, could not be confirmed. This may be caused by the different gas- and temperature conditions in the final reduction stages. Regarding influence of pre-reduction temperature on the final reduction degree, it can be summarized that (under the applied test conditions):

- the magnetite state was reached after the first reduction step R3, independent on the start temperature.
- a start temperature of 350 °C shows a slower increase of the RD-curve in the magnetite field R3, compared to the tests with higher temperatures.
- at a start temperature of 600 °C porous magnetite instead of dense magnetite was formed (although the operating point was in the lower wuestite area), which had no big influence on the further reduction behaviour.
- the type of magnetite, which was generated, had no big influence on the final reduction degree.
- the variation of the pre-reduction temperature between 350 °C and 600 °C had no significant influence on the final reduction degree and grain size distribution.

7.4 Influence of gas composition change on the reduction behavior in sequenced 3-stage operation

In this chapter, sequenced 3-stage tests with changing gas compositions are discussed. As discussed in chapter 6.2, the operating points of all executed tests represent the gas composition at the discharge of the fluidized bed reactors (cf. Figure 50). In reality, the quality of the gas composition is varying with the height of the bed from conditions at inlet to discharge. The gas at the inlet has a lower GOD; hence the average reducibility of the reducing gas in the bed is stronger in the real process than in lab scale. In order to simulate closer real operation conditions, a test with fluctuating gas composition in R1 was executed. Further more, a 3-stage test with pre-reduction-stage in the wuestite field at higher temperatures and two final reduction stages in the iron field with strong reducing gases were executed. The target was to figure out the formation behavior of wuestite at these R3-conditions and afterwards the iron formation behaviour in the subsequent stages (R2 and R1).

In Figure 120, the operating conditions of these tests are shown. The process parameters and results of the 3-stage tests fluctuating gas composition are shown in Table 23 and Figure 120 to Figure 123. The process parameters and results of the 3-stage test with pre-reduction stage in the wuestite field and two iron reduction stages are shown in Table 26 and Figure 124 to Figure 127 .

Literature Review

Regarding the influence of the gas composition on the multi-stage reduction behavior, a few fundamentals are important. Habermann stated that higher concentrations of H_2 in the gas mixture result in a higher reduction rate [105]. The influence of CO/CO_2 in a H_2-rich gas mixture is weak and also additions of CH_4 up to 6% has no influence. Weiss stated the important fact that during the reduction from hematite to magnetite, a CO-rich gas mixture has a higher reduction rate and generates a higher porosity than an H_2-rich gas mixture. On the other hand he found, that during reduction from hematite directly to wuestite, the H_2-rich gas mixture has a higher reduction rate, which increases by increasing the H_2-ratio [102,146]. Pawlik and Schuster stated that a pre-reduction in the wuestite field under CO-rich gas mixtures generates a porous wuestite with excellent reducibility [103,104,108]. Regarding a pre-reduction in the iron-stability field, Turnhofer and Schuster found, that wuestite and

wuestite-enclaves enclosed by iron are generated. This results in a lower specific surface area and a lower final RD [105-109]. Hence, a pre-reduction sequence in the iron stability field is counterproductive for achieving high reduction degrees in the final reduction stage.

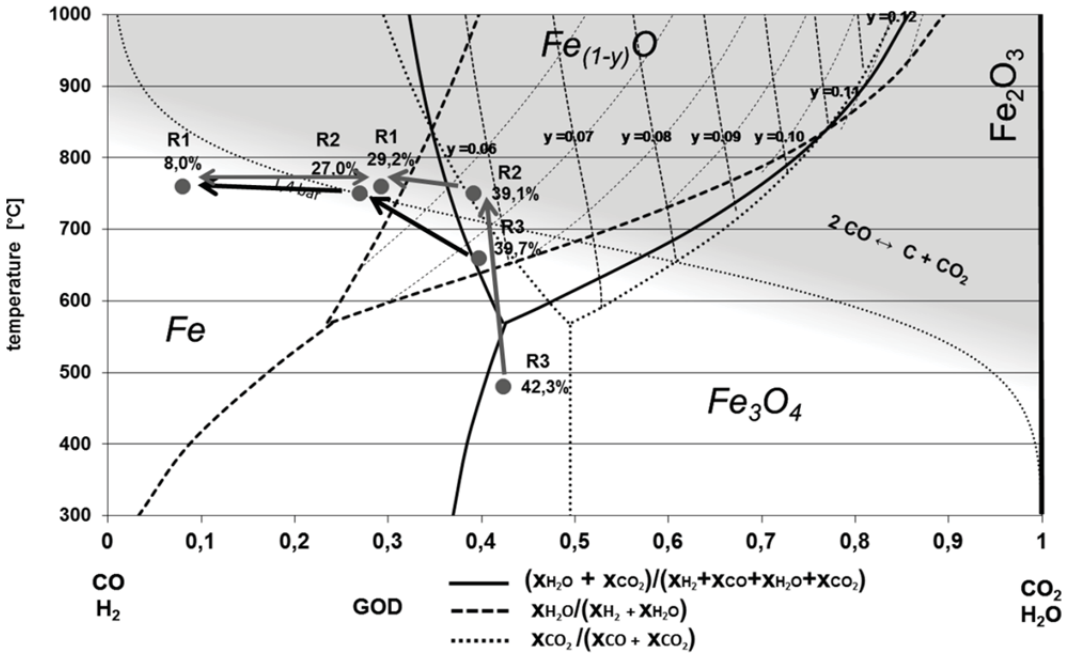

Figure 119: Bauer-Glaessner diagram with operating points of sequenced 3-stage tests with different gas compositions

7.4.1 Sequenced 3-stage reduction test with fluctuating gas composition in R1

The calculated gas conditions of the previous tests were adapted to the gas conditions at the discharge of the fluidized bed cascades of the real process. For simulating real operation conditions, the gas composition in R1 is fluctuating between the composition at the discharge (GOD = 29.2 %) and the composition of the gas inlet (GOD = 8 %) of reactor R1 (cf. Figure 119). This is the gas composition which is closer to the condition that a particle is exposed to during its residence time in R1 of the industrial plant. The fluctuating conditions are as follows: 3 minutes with GOD = 8 % ↔ 7 minutes with GOD = 29.2 %. The residence time in R1 is 40 minutes and other parameters are the same as in test H (42.3 % GOD in R3 and 29.2 % GOD in R1). In Figure 121, the RD-curve with the fluctuating gas composition is readily identifiable. Comparing the RD-curve to the corresponding test H (same process conditions in R3 and R2), a huge gain of reduction degree is evident (78.3 % compared to 50.8 % corresponding to the chemical analysis of the reduced material). It is also observable, that the fluctuation steps with a GOD of 8 % show a significant increase of reduction rate. Though the fluctuating gas composition, the inclinations of the fluctuation steps with 8 % GOD remain almost the same during the sequence. The same is valid for the fluctuation steps with 29.2 % and the sum curve is nearly linear. So, for the formation of metallic iron from wuestite in R1 the reduction potential of the gas mixture is dominant. The grain size distribution shows a strong disintegration of the material (cf. Figure 123).

Table 25: test parameter of 3-stage test G with fluctuating gas composition in R1

calculation of test parameter:		3-stage 480/750/760°C FINEX														
		concentration, temp. plant				concentration test rig				gas flow test rig						
gas composition		R1 [%]	R2 [%]	R3 [%]	R4 [%]	R1 [%]	R2 [%]	R3 [%]	R4 [%]	R1 [Nl/min]	heating [Nl/min]	R2 [Nl/min]	heating [Nl/min]	R3 [Nl/min]	heating [Nl/min]	R4 [Nl/min]
species	H2	17,7%	16,5%	16,0%	0,00%	17,3%	17,1%	16,5%	0,0%	67,1	74,6	66,7		76,8		0,0
	H2O	5,6%	7,1%	8,7%	0,00%	5,5%	7,3%	7,9%	0,0%	21,2	6,4	28,7		41,8		0,0
	CO	46,7%	38,9%	36,5%	0,00%	45,8%	40,3%	33,0%	0,0%	176,9	166,8	157,2		175,2		0,0
	CO2	21,0%	28,5%	29,8%	0,00%	20,6%	29,5%	27,0%	0,0%	79,6	14,6	115,2		143,0		0,0
	CH4	1,5%	1,6%	1,6%	0,00%	0,0%	0,0%	0,0%	0,0%	0,0	0,0	0,0		0,0		0,0
	N2	7,5%	7,4%	7,4%	0,00%	10,8%	5,8%	17,7%	0,0%	41,9	30,2	22,7		93,8		0,0
	total dry	94,4%	92,9%	91,3%	0,0%	94,5%	92,7%	92,1%	0,0%	365,5	286,2	361,8		488,7		0,0
	total wet	100,0%	100,0%	100,0%	0,0%	100,0%	100,0%	100,0%	0,0%	386,7	292,6	390,5		530,5		0,0
	GOD	29,2%	39,1%	42,3%	0,0%	29,2%	39,1%	42,3%	0,0%	29,2%	8,0%	39,1%		42,3%		0,0%
	H2/H2O	3,16	2,32	1,84	0,00	3,16	2,32	1,84	0,00							
	CO/CO2	2,22	1,36	1,22	0,00	2,22	1,36	1,22	0,00							
temperature [°C]		760	750	480	0					760	760	750	750	480	480	0
residence time [min]		40	30	30	0					40	25	30	5	30	0	0
spec. gas rate plant [Nm³/t]		810	810	810	0					diameter retort [m]					0,158	
supposed gas rate red. [Nm³/t]		4000	3200	3800	0					cross section retort [m²]					0,020	
defined ul. retort [m/s]		0,9	0,9	0,9	0					absolute pressure [bar]					14	
flow rate red. comp. [Ndm³/h]		20688	22067,2	26204,8	0					atmospherical pressure [bar]					1013	

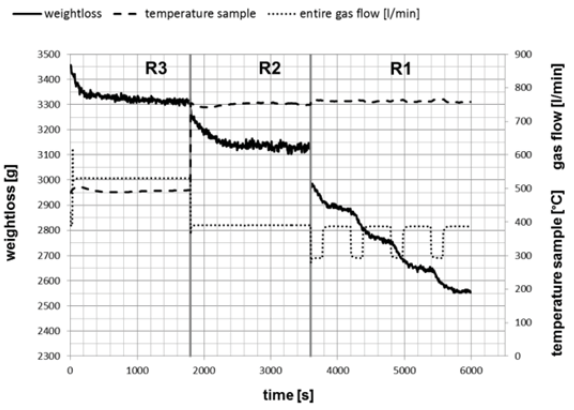

Figure 120: Test G weight loss-curve

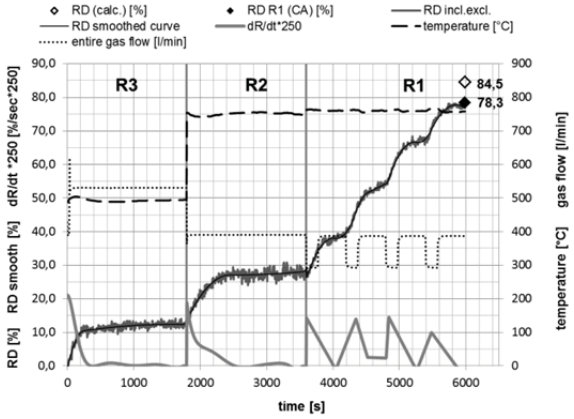

Figure 121: Test G RD-curve and RD-rate

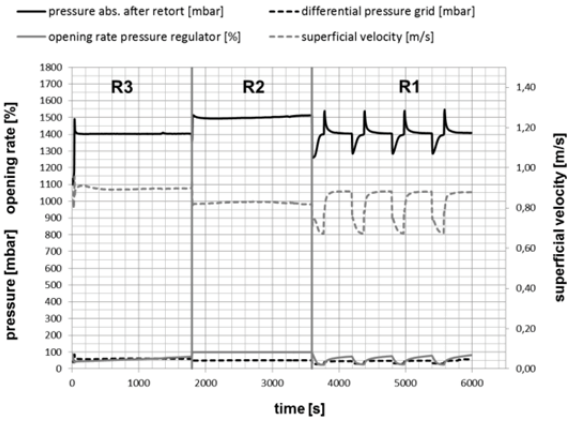

Figure 122: Test G pressure and gas flow

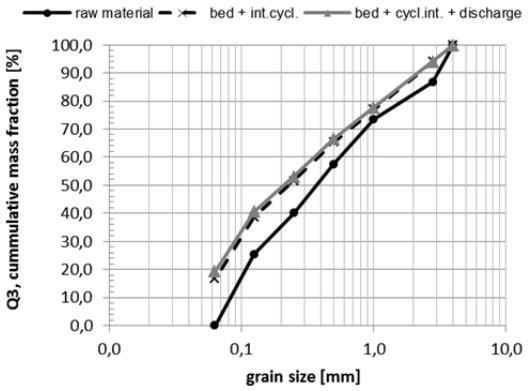

Figure 123: Test G grain size distribution

7.4.2 Sequenced 3-stage reduction test with pre-reduction stage in the wuestite field and two final reduction stages in the iron field

A 3-stage test with high-temperature reduction in the wuestite field and two stages in the iron field was executed to investigate the reduction behaviour under such conditions. In this test, also the reducing gas mixtures are more reducible. The target is to figure out the formation behavior of wuestite at these R3-conditions and afterwards the iron formation behaviour in the subsequent stages (R2 and R1) up to the complete removal of the oxygen. The GODs are as follows: 39.7 % in R3, 27 % in R2 and 8 % in R1. The residence times of the stages are the same as in the test before. In Figure 125, the RD-curve is shown. In R3, the curve shows a strong increase of the curve for 5 minutes until it reaches a smoother, linear inclination. The operating point of R3 is in the wuestite field and, obviously, wuestite is built (theoretical RD is about 30 %). The formation of wuestite has not been finished in R3. In R2, the formation of wuestite continues. Interesting is the unsteadiness of the reduction curve in this stage, which cannot be explained yet, because temperature, pressure and superficial velocity were constant. In R1, the reduction continues again with a very strong inclination, until almost all the oxygen is removed from the iron ore (steady state of the RD curve). The reduction degree based on the chemical analysis is 94.1 %. The grain size distribution after the test shows a strong disintegration of the material.

Table 26: test parameter of 3-stage test A

calculation of test parameter:		3-stage 660/750/760°C FINEX														
		concentration, temp. plant				concentration test rig				gas flow test rig						
gas composition		R1 [%]	R2 [%]	R3 [%]	R4 [%]	R1 [%]	R2 [%]	R3 [%]	R4 [%]	R1 [Nl/min]	heating [Nl/min]	R2 [Nl/min]	heating [Nl/min]	R3 [Nl/min]	heating [Nl/min]	R4 [Nl/min]
species	H2	20,4%	20,0%	16,4%	0,00%	20,4%	20,0%	16,4%	0,0%	**78,9**		**78,1**		**70,0**		**0,0**
	H2O	1,7%	7,4%	9,2%	0,00%	1,7%	7,4%	9,2%	0,0%	**6,7**		**28,8**		**39,5**		**0,0**
	CO	45,7%	44,8%	33,5%	0,00%	45,7%	44,9%	33,5%	0,0%	**176,6**		**175,2**		**143,4**		**0,0**
	CO2	4,0%	16,5%	23,6%	0,00%	4,0%	16,5%	23,6%	0,0%	**15,5**		**64,6**		**100,9**		**0,0**
	CH4	0,0%	0,0%	0,0%	0,00%	0,0%	0,0%	0,0%	0,0%	**0,0**		**0,0**		**0,0**		**0,0**
	N2	28,2%	11,3%	17,4%	0,00%	28,2%	11,2%	17,4%	0,0%	**109,1**		**43,8**		**74,3**		**0,0**
	total dry	98,3%	92,6%	90,8%	0,0%	98,3%	92,6%	90,8%	0,0%	380,0		361,6		388,7		0,0
	total wet	100,0%	100,0%	100,0%	0,0%	100,0%	100,0%	100,0%	0,0%	386,7		390,5		428,2		0,0
	GOD	8,0%	27,0%	39,7%	0,0%	8,0%	27,0%	39,7%	0,0%	8,0%		27,0%		39,7%		0,0%
	H2/H2O	11,80	2,71	1,77	0,00	11,80	2,71	1,77	0,00							
	CO/CO2	11,42	2,71	1,42	0,00	11,42	2,71	1,42	0,00							
temperature [°C]		760	750	660	0					**760**	**760**	**750**	**750**	**660**	**660**	**0**
residence time [min]		40	30	30	0					**40**	**5**	**30**	**10**	**30**	**0**	**0**
spec. gas rate plant [Nm³/t]		4419	3350	3670	0					diameter retort [m]					0,158	
supposed gas rate red. [Nm³/t]		3173	2972	3033	0					cross section retort [m²]					0,020	
defined uL retort [m/s]		0,9	0,9	0,9	0					absolute pressure [bar]					1,4	
flow rate red. comp. [Ndm³/h]		16658,3	20804	21231	0					atmospherical pressure [bar]					1,013	

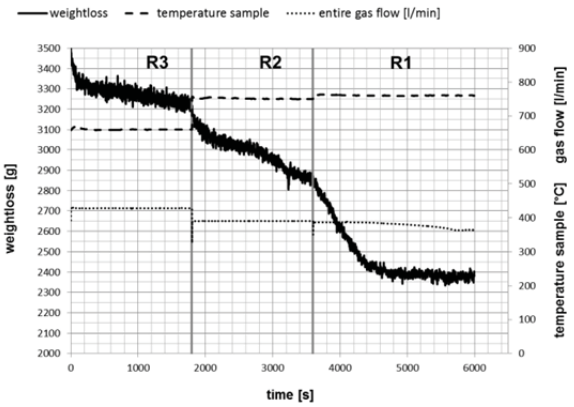

Figure 124: Test A weight loss-curve

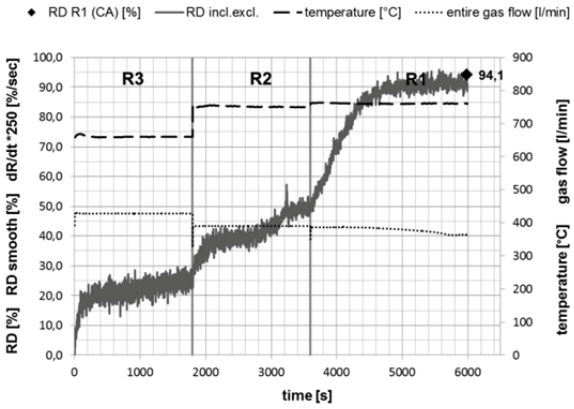

Figure 125: Test A RD-curve and RD-rate

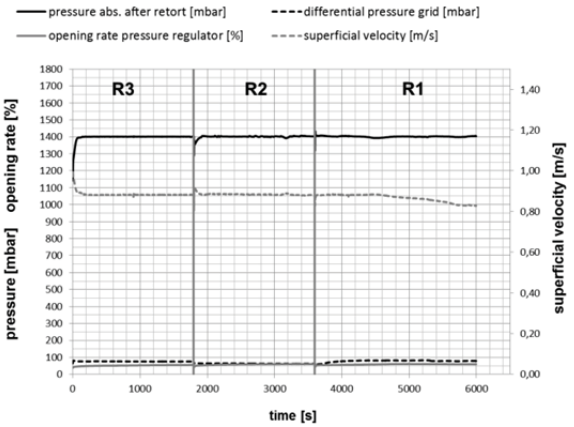

Figure 126: Test A pressure and gas flow

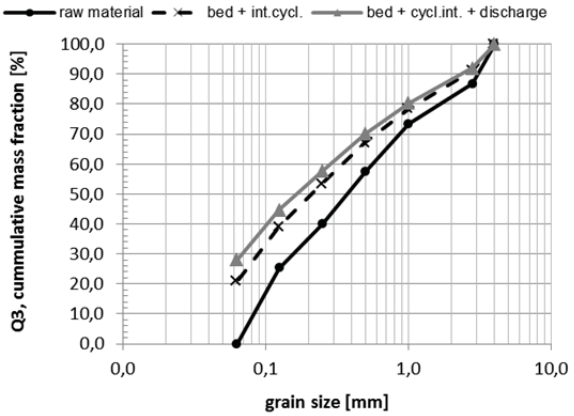

Figure 127: Test A grain size distribution

7.4.3 Morphological analyses of the sequenced 3-stage tests

In Figure 128, the morphology of the 3-stage sequenced test with fluctuating gas composition in R1 is shown. The matrix of the sample is comparable with the other hematite tests. Due to the fluctuation of the gas composition, the metallization increased significantly (white area) and the reduction degree of the chemical analysis can be confirmed. The limonite and martite regions are very well reduced, whereas the micro platy hematite (dense areas) shows hardly any metallization. The morphology of the 3-stage test with the pre-reduction stage in the wuestite field and the final reduction stages in the iron field is shown in Figure 129. This test with a start temperature of 660 °C showed a formation of porous wuestite instead of dense magnetite (and subsequently wuestite) from former hematite (cf. Figure 129).

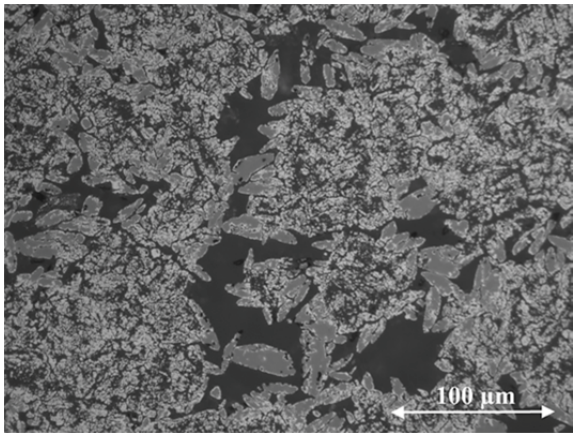

Figure 128: Test G (1 – 2.8 mm)
3-stage 480/750/760 °C

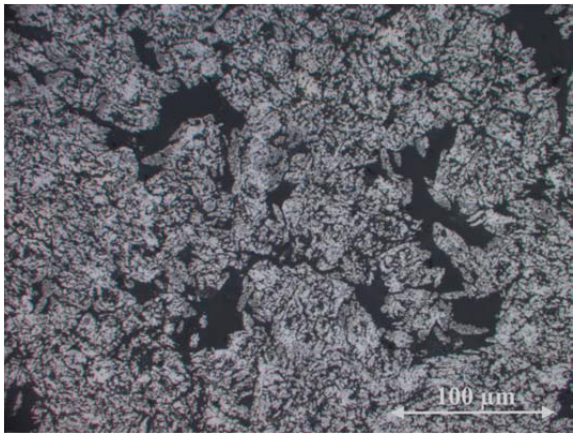

Figure 129: Test A (1 – 2.8 mm)
3-stage 660/750/760 °C

Comparing the grain size distributions of the material after the tests, the disintegration behaviour is quite different (cf. Figure 130). In this diagram, the grain size distribution curves refer to the whole material which was re-extracted after each test (fluidized bed, internal cyclone, discharge and rest). The solid grey line is the grain size distribution for the standardized test with hamersley fine ore, as discussed before. The test with the fluctuating gas composition in R1 shows a slightly higher disintegration and the disintegration behaviour of the test with pre-reduction in the wuestite field and final reduction steps in the iron field is far worse. Comprising the reduction degrees of these three tests, the disintegration increases excessively with increasing RD. This observation is just valid for the executed tests and conditions. With other test conditions, the results may change.

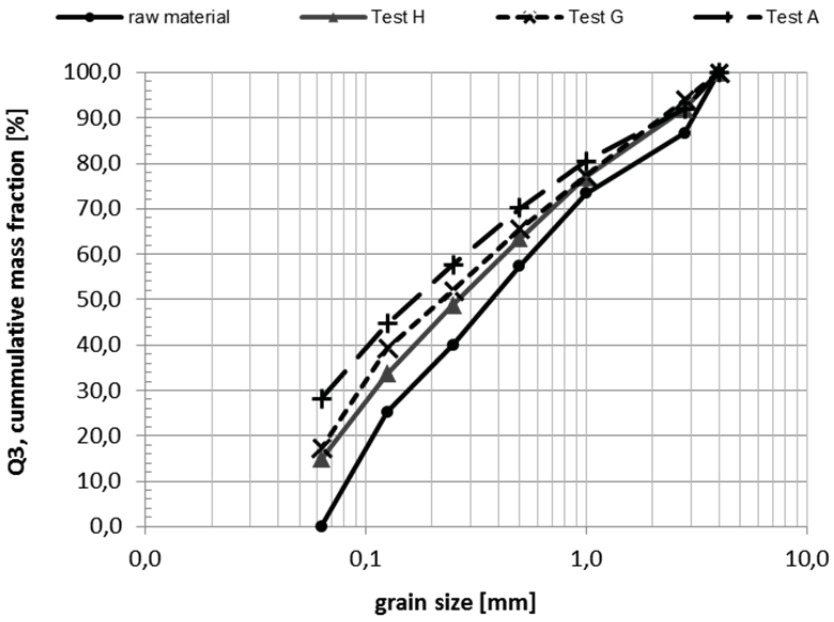

Figure 130: Grain size distribution of the 3-stage tests with different gas compositions

7.4.4 Discussion

In order to simulate closer real operation conditions, a 3-stage test with fluctuating gas composition in R1 was executed. Furthermore, a 3-stage test with pre-reduction-stage in the wuestite field at higher temperatures and two final reduction stages in the iron field with strong reducing gases was executed, to figure out the process behaviour under these conditions.

The 3-stage test with fluctuating gas composition in R1 showed a huge gain of reduction degree in the last sequence (R1) compared to test H (78.3 % compared to 50.8 % corresponding to the chemical analysis of the reduced material). In the fluctuation steps with a GOD of 8 %, a significant increase of reduction rate was observed, whereas the fluctuation steps with a GOD of 29.2 % showed a lower inclination. The inclinations of the fluctuation steps with 8 % and 29.2 % respectively, remained almost the same during the sequence and the sum curve is nearly linear. So, for the formation of metallic iron from wuestite in R1 the reduction potential of the gas mixture is dominant.

The 3-stage test with pre-reduction-stage in the wuestite field at higher temperatures and two final reduction stages in the iron field showed a wuestite formation in R3, which had not completely been finished in this sequence. In sequence R2, in the iron field, iron was generated. The RD-curve soon showed an unsteadiness, which cannot be explained yet, because temperature, pressure and superficial velocity remained constant in this sequence. In R1, the reduction continued with a very strong inclination, until almost all the oxygen was removed from the iron ore. Because of the strong reducing gas mixture, the metallization is very high. From the morphological point of view, whole matrix is very well reduced. The former dense hematite shows a porous structure due to the first reduction step in the wuestite stability field, which also was observed by Pawlik and Schuster [103,104,108]. Only some dense magnetite regions from the original ore are not very well reduced. Compared to the standardized test H, the grain size distributions after the tests showed a rather strong disintegration of the material, especially of test A. Comprising the reduction degrees of these tests, the disintegration increases excessively with increasing RD. This observation is just valid for the executed tests and conditions. With other test conditions, the results may change. Regarding the influence of gas composition on the reduction behaviour under the applied process conditions, it can be stated, that:

- with decreasing GOD, the reduction rate increases extensively.
- for the formation of metallic iron from wuestite, the reduction potential of the gas mixture is dominant.
- the disintegration of the iron ore increases excessively with increasing RD

7.5 Influence of increasing the residence time in the final reduction stage

Due to the findings of the constant reduction in R1 in previous tests, there should be further potential by increasing the residence time in R1. This was tested in test E with a start temperature of 350 °C in the magnetite field. The test conditions are the same as for test B (350/750/760 °C in R3/R2/R1). Only the residence time in R1 was increased from 40 to 60

minutes. In Figure 131, the operating conditions of this test are shown. The process parameters and results of this 3-stage test are shown in Table 27 and Figure 132 to Figure 135.

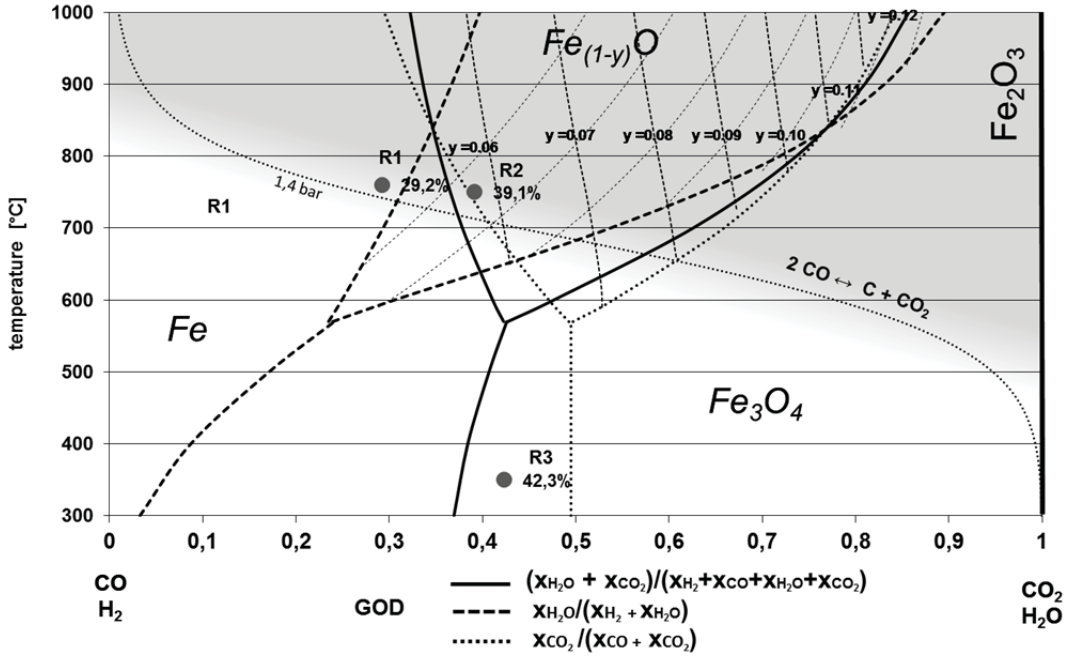

Figure 131: Bauer-Glaessner diagram with operating points of sequenced 3-stage tests with increasing residence time in R1

Literature Review

Regarding the theoretical background of the influence of residence time on the multistage-reduction, the literature is rather rare. Only the influence of the residence time in the reduction sequences R3 and R2 were discussed based on reduction under CO-rich gas compositions. Pawlik [103,104] found, that a longer residence time in the pre-reduction stage R3 leads to an increase of pores in the iron ore matrix and also to a higher final reduction degree. This finding was confirmed by Schuster [108]. Further more he stated that a higher residence time in R2 also increases the final reduction degree. Regarding the influence of residence time in R1 on the reduction behavior, no literature was found.

7.5.1 Sequenced 3-stage reduction test with increased residence time in the final reduction stage with 350°C start temperature

The reduction behaviour in the stages R3, R2 and R1 of the test with 350 °C start temperature in R3 (cf. Figure 133) is similar to the reduction behavior in test B, discussed in chapter 7.2. Increasing the residence time in test E, the reduction in R1 remains constant until reaching the end of the test. According to the chemical analyses, an increase of the residence time in R1 from 40 to 60 minutes results in a rise of reduction degree from 49.9 % (MD = 31,3 %) to 54.6 % (MD = 40.4 %) and still there is further potential for increasing the reduction degree by prolonging the residence time.

Table 27: test parameter of 3-stage test E with 350°C start temperature

calculation of test parameter:		3-stage 350/750/760°C 60 min. R1 FINEX														
		concentration, temp. plant				concentration test rig				gas flow test rig						
gas composition		R1 [%]	R2 [%]	R3 [%]	R4 [%]	R1 [%]	R2 [%]	R3 [%]	R4 [%]	R1 [Nl/min]	heating [Nl/min]	R2 [Nl/min]	heating [Nl/min]	R3 [Nl/min]	heating [Nl/min]	R4 [Nl/min]
species	H2	17,7%	16,5%	16,0%	0,00%	17,4%	17,2%	12,0%	0,0%	**67,4**		**67,0**		**77,1**		**0,0**
	H2O	5,6%	7,1%	8,7%	0,00%	5,5%	7,4%	6,5%	0,0%	**21,3**		**28,8**		**41,9**		**0,0**
	CO	46,7%	38,9%	36,5%	0,00%	46,0%	40,4%	27,4%	0,0%	**177,8**		**157,9**		**176,0**		**0,0**
	CO2	21,0%	28,5%	29,8%	0,00%	20,7%	29,6%	22,4%	0,0%	**79,9**		**115,7**		**143,7**		**0,0**
	CH4	1,5%	1,6%	1,6%	0,00%	0,0%	0,0%	0,0%	0,0%	**0,0**		**0,0**		**0,0**		**0,0**
	N2	7,5%	7,4%	7,4%	0,00%	10,4%	5,4%	31,6%	0,0%	**40,3**		**21,0**		**202,4**		**0,0**
	total dry	94,4%	92,9%	91,3%	0,0%	94,5%	92,6%	93,5%	0,0%	365,4		361,7		599,2		0,0
	total wet	100,0%	100,0%	100,0%	0,0%	100,0%	100,0%	100,0%	0,0%	386,7		390,5		641,2		0,0
	GOD	29,2%	39,1%	42,3%	0,0%	29,2%	39,1%	42,3%	0,0%	29,2%		39,1%		42,3%		0,0%
	H2/H2O	3,16	2,32	1,84	0,00	3,16	2,32	1,84	0,00							
	CO/CO2	2,22	1,36	1,22	0,00	2,22	1,36	1,22	0,00							
temperature [°C]		760	750	350	0					**760**	**760**	**750**	**750**	**350**	**350**	**0**
residence time [min]		60	30	30	0					**60**	**5**	**30**	**35**	**30**	**0**	**0**
spec. gas rate plant [Nm³/t]		810	810	810	0					diameter retort [m]					0,158	
supposed gas rate red. [Nm³/t]		6000	3200	3800	0					cross section retort [m²]					0,020	
defined uL retort [m/s]		0,9	0,9	0,9	0					absolute pressure [bar]					1,4	
flow rate red. comp. [Ndm³/h]		20784	22169,6	26326,4	0					atmospherical pressure [bar]					1,013	

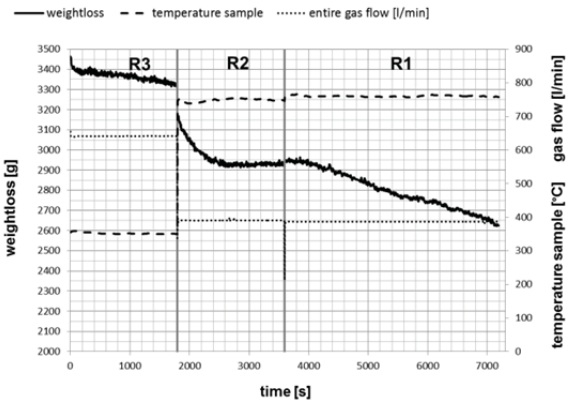

Figure 132: Test E weight loss-curve

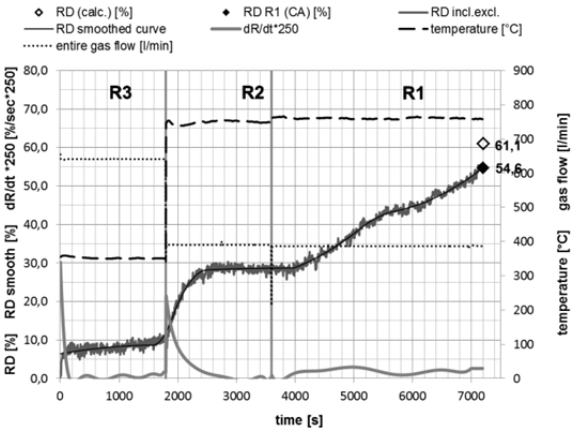

Figure 133: Test E RD-curve and RD-rate

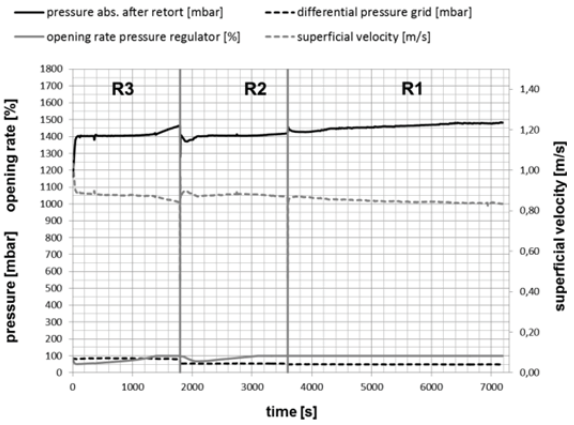

Figure 134: Test E pressure and gas flow

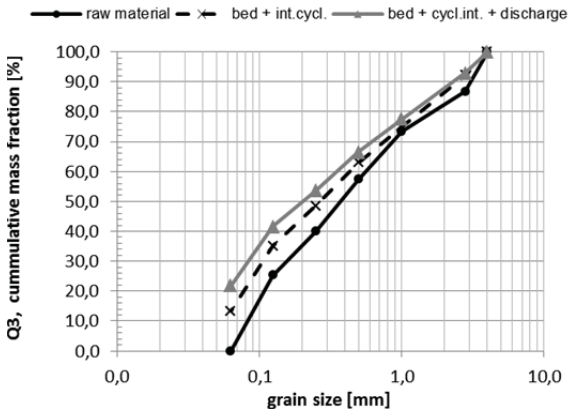

Figure 135: Test E grain size distribution

7.5.2 Morphological analysis

As seen in test B, also in this test dense magnetite is formed around some hematite grains. The martite is very well reduced (white areas in Figure 136), whereas the micro platy hematite and the dense magnetite, which is formed during R3 of the process, are hardly reduced. In Figure 137, a former limonite rich grain is shown. Here, the reduction and metallization is very homogenous. In general, the matrix is comparable with the other hematite tests, especially with test B, but higher metallized.

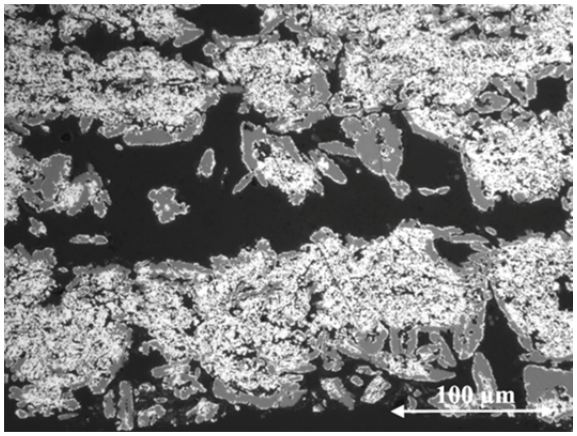

Figure 136: Test E (1 – 2.8 mm)
3-stage 350/750/760 °C

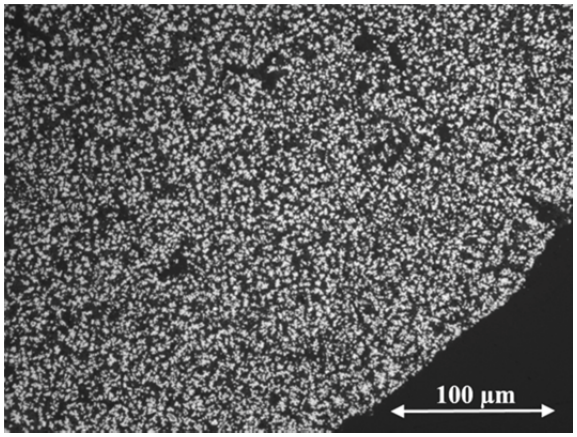

Figure 137: Test E (1 – 2.8 mm)
3-stage 350/750/760 °C

The analysis of the grain size distribution of the tests with 40 and 60 minutes residence time in R1 is compared in Figure 138. In this diagram, the grain size distribution curves refer to the whole material which was re-extracted after each test (fluidized bed, internal cyclone, discharge and rest). Here, the test with 60 minutes residence time shows a stronger disintegration, especially in the finest grain size fractions. The stronger disintegration derives from the increased abrasion time, the particles were exposed to. Also the reduction during this time has an influence (as discussed in chapter 7.4).

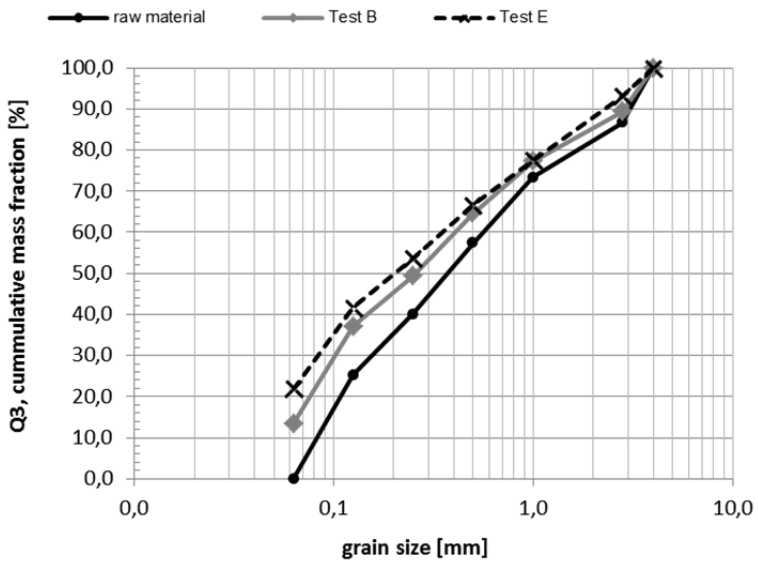

Figure 138: Grain size distribution of the 3-stage tests with 40 and 60 minutes residence time in R1

7.5.3 Discussion

The hypothesis, that an increased residence time in R1 results in a further gain of reduction degree, could be confirmed. The test conditions were the same as for test B, but with an increased residence time from 40 to 60 minutes in R1. According to the chemical analysis, an increase of the resicence time in R1 from 40 to 60 minutes resulted in a rise of reduction degree from 49.9 % (MD = 31.3 %) to 54.6 % (MD = 40.4 %). There is a potential for further gain in reduction degree by increasing of the residence time. The morphological structure is quite the same as in test B, just higher metallized. The grain size distribution after 60 minutes in R1 showed a stronger disintegration than after 40 minutes residence time, especially regarding the finest fractions. The stronger disintegration can be explained with the increased abrasion time, whereas also the reduction during this time plays a role (cf. chapter 7.4). Regarding the influence of residence time on the reduction behavior, it can be stated, that:

- an increased residence time in the final reduction stage R1 results in a higher final reduction degree with a constant inclination of the RD-gradient.
- an increased residence time results in a stronger disintegration of the material.
- the matrix of the material did not change, it is just higher metallized.

7.6 Comparison of different fine ores under the same process conditions

Six globally traded iron ore brands were tested under equal process conditions. After the successful installation of a sampling system, samples were taken after each reduction stage for the chemical and morphological characterization. The sampling system is described in chapter 6.1 and the layout is shown in Figure 46. Depending on the mineralogy and structure of the ore feed, as well as the reduction conditions, various different structural types of magnetite, wuestite and iron were generated and the mineralogical as well as the structural evolution is described.

Based on fluidized bed reduction technologies with reducing gas produced by coal gasification, the reduction behavior of fine iron ores was investigated by means of a sequenced 3-stage reduction process under standardized-conditions. The methodical and thermodynamical specifications were discussed in chapter 6. Results of these investigations were partly published in [149-151]. Additionally, a master thesis was executed within the project of characterization of the different iron ores (cf. [37]). Some of the results are incorporated into this work. The operating points and test parameter of this standardized test are defined in Figure 139 and Table 28. As discussed in chapter 6.2, the calculated gas conditions of the tests are adapted to the gas conditions at the free board of the fluidized bed cascades of the real process. Hence, the average reducibility of the reducing gas in the bed is stronger in the real process than in the lab scale tests.

In chapter 7.1, the morphological characteristics of the iron ore brands have already been discussed. Regarding the theoretical background and findings of other authors regarding the morphological behavior of iron ore fines in a multi-stage reduction process, refer to the introduction of chapter 7. The chemical compositions of the different iron ores can be found

in Table 18. Further informations regarding specific surface area and porosity are listed in Table 19. Table 7 and Figure 51 contain the total mass and grain size distribution of the charged iron ores, which was equal for all tests.

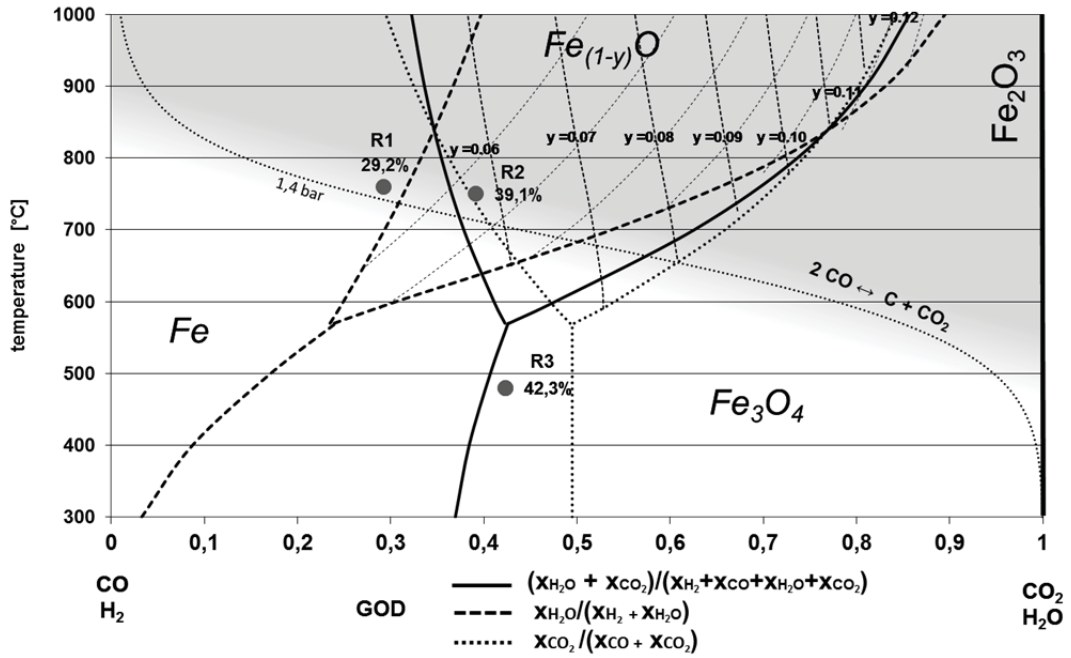

Figure 139: Bauer-Glaessner diagram with operating points of the standardized 3-stage tests

Table 28: Test parameters the 3-stage standard tests

calculation of test parameter:		3-stage 480/750/760°C														
		concentration, temp. plant				concentration test rig				gas flow test rig						
gas composition		R1 [%]	R2 [%]	R3 [%]	R4 [%]	R1 [%]	R2 [%]	R3 [%]	R4 [%]	R1 [Nl/min]	heating [Nl/min]	R2 [Nl/min]	heating [Nl/min]	R3 [Nl/min]	heating [Nl/min]	R4 [Nl/min]
species	H2	17.7%	16.5%	16.0%	0.00%	17.6%	17.3%	14.7%	0.0%	**68.1**		**67.7**		**77.9**		**0.0**
	H2O	5.6%	7.1%	8.7%	0.00%	5.6%	7.5%	8.0%	0.0%	**21.5**		**29.1**		**42.4**		**0.0**
	CO	46.7%	38.9%	36.5%	0.00%	46.4%	40.9%	33.5%	0.0%	**179.6**		**159.6**		**177.8**		**0.0**
	CO2	21.0%	28.5%	29.8%	0.00%	20.9%	29.9%	27.4%	0.0%	**80.8**		**116.9**		**145.2**		**0.0**
	CH4	1.5%	1.6%	1.6%	0.00%	0.0%	0.0%	0.0%	0.0%	**0.0**		**0.0**		**0.0**		**0.0**
	N2	7.5%	7.4%	7.4%	0.00%	9.5%	4.4%	16.4%	0.0%	**36.7**		**17.2**		**87.2**		**0.0**
	total dry	94.4%	92.9%	91.3%	0.0%	94.4%	92.5%	92.0%	0.0%	365.2		361.4		488.1		0.0
	total wet	100.0%	100.0%	100.0%	0.0%	100.0%	100.0%	100.0%	0.0%	386.7		390.5		530.5		0.0
	GOD	29.2%	39.1%	42.3%	0.0%	29.2%	39.1%	42.3%	0.0%	29.2%		39.1%		42.3%		0.0%
	H2/H2O	3.16	2.32	1.84	0.00	3.16	2.32	1.84	0.00							
	CO/CO2	2.22	1.36	1.22	0.00	2.22	1.36	1.22	0.00							
temperature [°C]		760	750	480	0					**760**	**0**	**750**	**0**	**480**	**0**	**0**
residence time [min]		40	30	30	0					**40**	**0**	**30**	**0**	**30**	**0**	**0**
spec. gas rate plant [Nm³/t]		810	810	810	0					diameter retort [m]					0.158	
supposed gas rate red. [Nm³/t]		4000	3200	3800	0					cross section retort [m²]					0.020	
defined uL retort [m/s]		0.9	0.9	0.9	0					absolute pressure [bar]					1.4	
flow rate red. comp. [Ndm³/h]		21000	22400	26600	0					atmospherical pressure [bar]					1.013	

7.6.1 Sequenced 3-stage reduction tests with different globally traded iron ore fines under standardized conditions

In the following, the results of the fluidized bed test series with different iron ore brands are discussed. All tests were carried out under the same process conditions to compare the reduction behavior between the different iron ores. Important for the determination of the reduction behavior are the RD-curve-diagrams. These diagrams represent the reduction degree (RD) gradients of the material during reduction for the different ores (Hamersley: Figure 141; Kiruna: Figure 145, Robe River: Figure 149, Erzberg: Figure 153, Marra Mamba: Figure 157, Pilbara: Figure 161). The dotted lines in these diagrams represent the particular temperature time trends and entire gas flow of each test. The marks represent the RDs' calculated from the chemical analyses of the samples ($RD_{(CA)}$) and the RDs' calculated from the overall mass balance of the reduced material after the test ($RD_{(calc.)}$). Usually $RD_{(calc.)}$ is higher than $RD_{(CA),}$ because the retrieval of the whole rest material after the test is impossible and, hence, this calculated value represents additional information for the interpretation of the tests. The other diagrams provide additional informations regarding the process characteristics of the tests as well as the grain size distributions of the reduced bed material after each test. Regarding the grain size distribution diagrams, the bold black line in these diagrams represents the defined grain size distribution of the input material. The black dotted line represents the grain size distribution in the fluidized bed (including the internal cyclone) after the test, and the grey line the grain size distribution of the whole re-extracted material after the test (material in fluidized bed and internal cyclone, discharge and rest).

Hamersley iron ore (Australia, hematite rich ore)

In the first reduction stage R3 in the magnetite field at 480 °C, the reaction is quite fast and finished within about 4 minutes residence time (cf. Figure 141). After that, a steady state is reached, which represents the magnetite phase stability (theoretical RD for Fe_3O_4 is 11.1 %). The accordance with the chemical analysis of 11.2 % is quite good. In the second reduction stage R2 at 750 °C (reduction from magnetite to wuestite), a rather strong inclination of the RD-curve is observable, which decreases continuously after 3 minutes and reaches a steady state after about 10 minutes. The chemical analyisis of the extracted sample after stage R2 indicates a reduction degree of 27.1 %, which is below the value of the RD-curve and also below the theoretical value (the theoretical RD for $Fe_{(1-y)}O$ under the specified process conditions is about 29 %). This can be caused by reoxidation of the extracted samples (high porosity of the ore) and also by the difficulties in analyzing the content of Fe^{2+} (as discussed in chapter 6.4). In R1, at 750 °C in the iron stability field, the RD-gradient increases steadily during the whole reduction sequence and iron is generated until the end of this sequence. The RD calculated based on the final chemical analysis of 50.8 % can be approximately confirmed, but seems to be slightly too high (cf. chapter 7.2.2). The grain size distribution shows a more or less constant disintegration over the whole grain size fractions. Most of the disintegrated material was found in the finest fraction (cf. Figure 143).

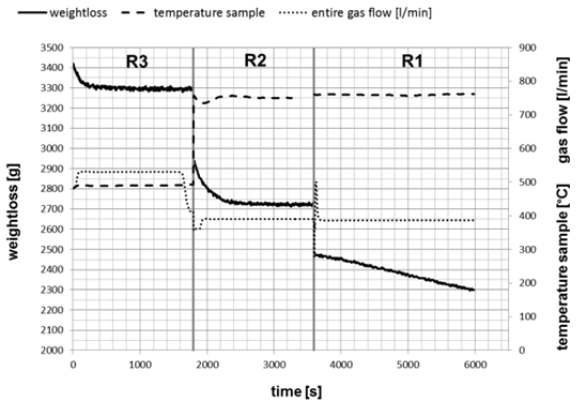

Figure 140: Test H weight loss-curve

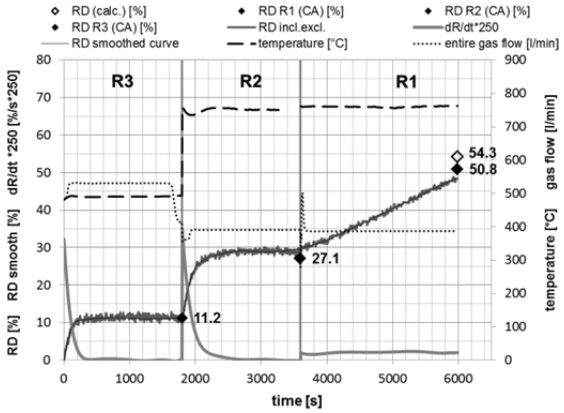

Figure 141: Test H RD-curve and RD-rate

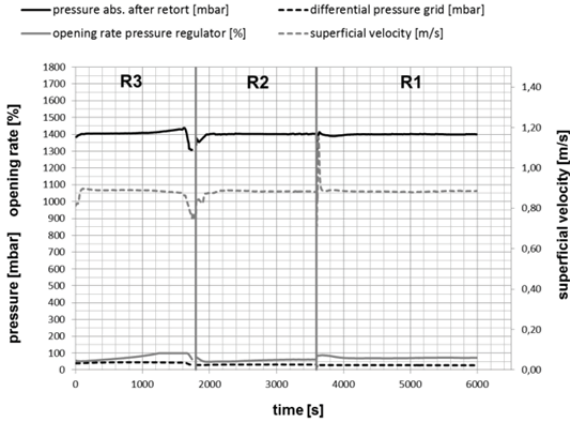

Figure 142: Test H pressure and gas flow

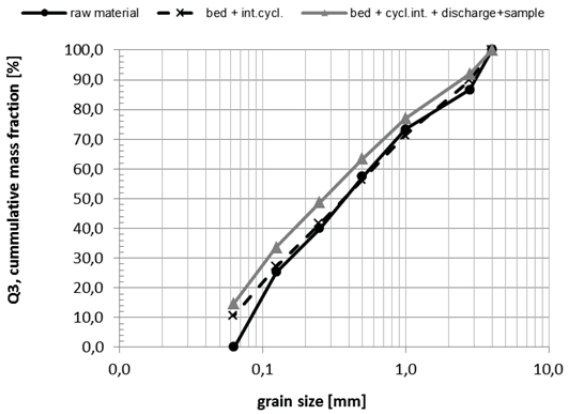

Figure 143: Test H grain size distribution

Kiruna iron ore (Sweden, magnetite rich ore)

The Kiruna ore is a very dense, magnetite-rich ore. In R3 of the test, the RD-curve starts with an RD of about 11 %, which correlates with the theoretical reduction degree of magnetite (Fe_3O_4) of 11.1 %. Due to the fact, that the curve shows no inclination in this sequence, the magnetite seems to be very pure and, hence, no oxygen removal occurs. Also the chemical analysis of 11,0 % shows a very good accordance. In R2 and R1, the reduction progress is inhibited compared to the ore tests of the limonite- or hematite-rich ores. In R2 low amounts of wuestite were formed. The theoretical reduction degree of wuestite is about 29 % under these process conditions and the complete wuestite formation is not reached by far. That means, that a part of the matrix after R2 consists of wuestite, and part is still magnetite, which did not transform. The reduction degree of 22.3 % by chemical analysis confirms this finding. Also in the iron field (R1), the reduction is inhibited and the final reduction degree by chemical analysis is just 27.4 %. The RD-trend in R1 is not valid, because of a temperature fluctuation. Here, the chemical analysis is more reliable. In an additional test under the same conditions, a final RD of 30.6 % was reached based on the chemical analysis. The grain size distribution shows a rather strong and constant disintegration over the whole fractions (cf. Figure 147).

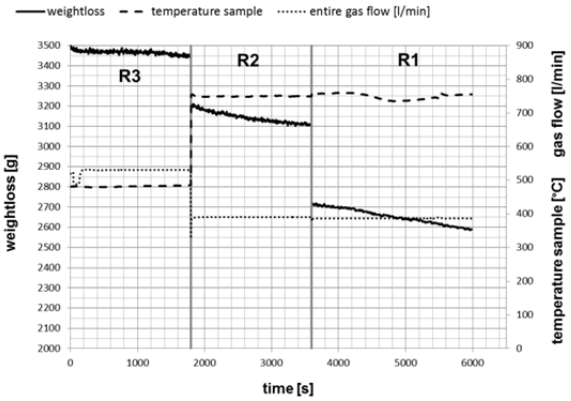

Figure 144: Test I weight loss-curve

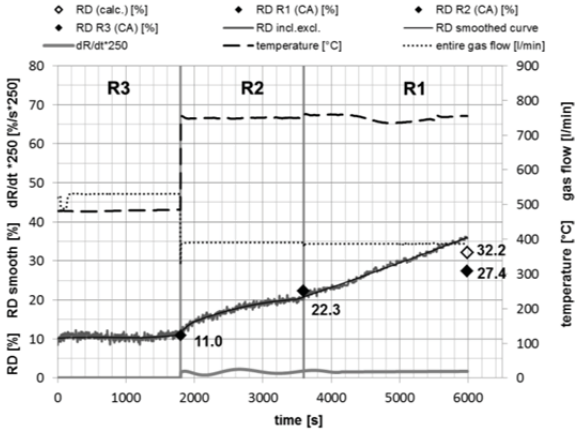

Figure 145: Test I RD-curve and RD-rate

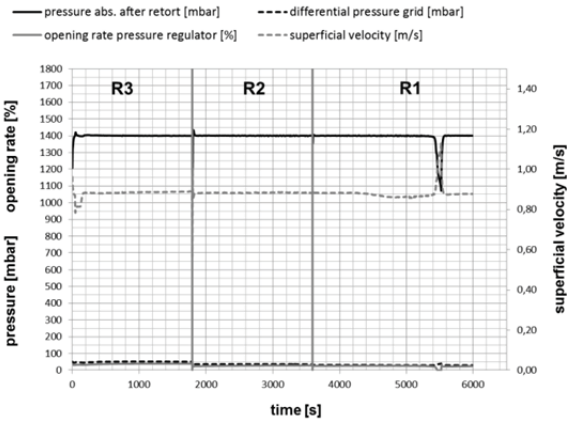

Figure 146: Test I pressure and gas flow

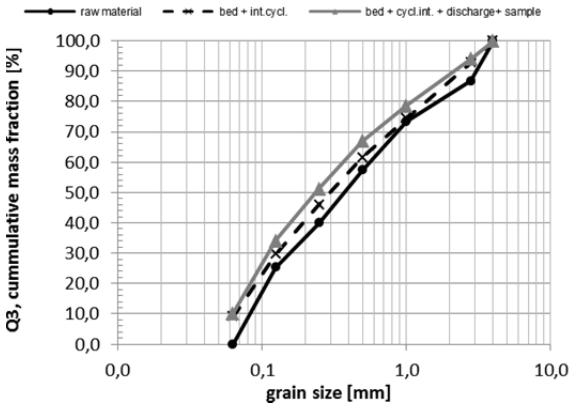

Figure 147: Test I grain size distribution

Robe River iron ore (Australia, limonite rich ore)

The limonite rich Robe River ore shows a very fast reduction in the first reduction stage R3 to magnetite. The magnetite stage is reached within a residence time of 2 minutes. The reduction degree of 9.8 % based on the chemical analysis seems to be too low. Because of the fast reduction to magnetite and the completely even RD-curve during this sequence, the theoretical RD for magnetite of 11.1 % should almost have been reached. In sequence R2, the RD-trend shows a strong inclination at the beginning, which continuously decreases from 3 minutes onwards and comes to a steady state after about 7 minutes. The chemical analyzed RD-value of 20.2 % is obviously too low. The theoretical RD for $Fe_{(1-y)}O$ under the specified process conditions is about 29 % and also the RD-curve is much higher. Reasons could be a strong reoxidation of the sample material after the test or the problems with the determination of Fe^{2+}, discussed in chapter 6.4. Hence, the RD-curve is more reliable and the reduction degree in R2 should be round about 29 % (RD-trend). In R1, in the iron stability field, the RD-trend shows a constant inclination at the beginning of the reduction sequence and decreases slightly till the end of this sequence. The RD calculated based on the chemical analysis of 47.7 % has a good accordance with the value for R1 of the RD-trend. The grain size distribution shows a moderate and constant disintegration over the whole grain size spectrum (cf. Figure 151).

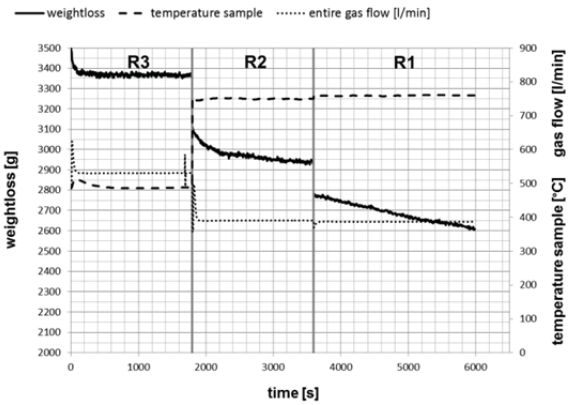

Figure 148: Test J weight loss-curve

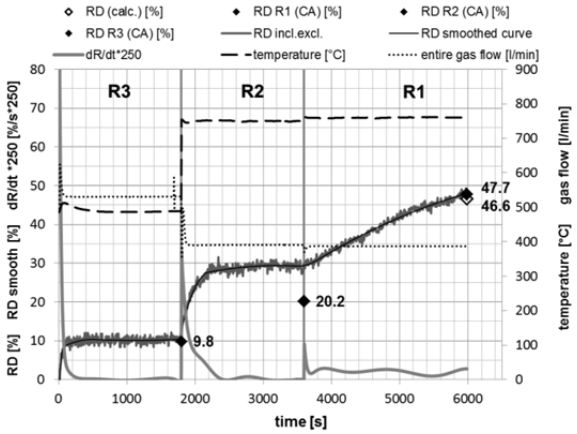

Figure 149: Test J RD-curve and RD-rate

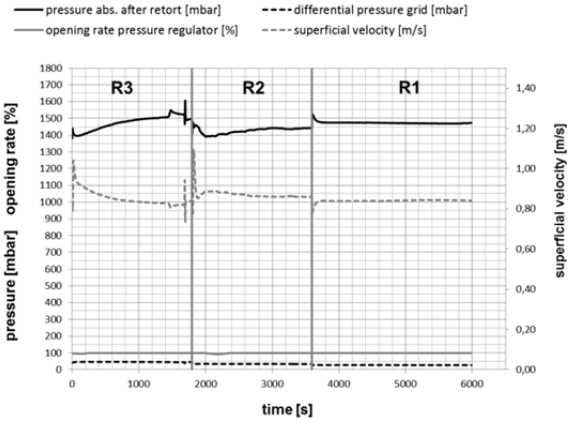

Figure 150: Test J pressure and gas flow

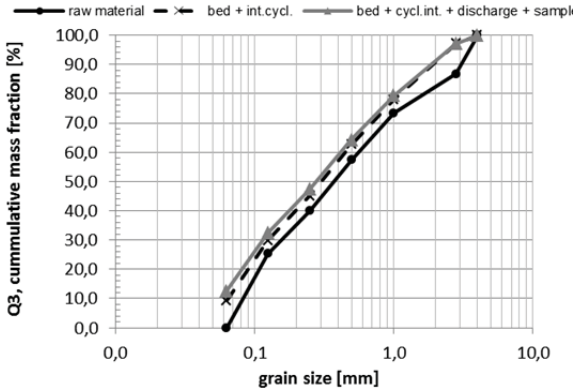

Figure 151: Test J grain size distribution

Erzberg iron ore (Austria, limonitic siderite ore)

The Erzberg iron ore consists of a limonite matrix formed from pseudomorphoses after siderite. In the reduction stage R3, the formation of magnetite occurs almost abruptly. Within about 1 minute, the magnetite state is reached. Anyhow, there is a weak inclination of the RD-curve until the end of the sequence, which is not observed with the other ores. Possible reasons could be carbonate reactions of the siderite or residual magnetite in the grain's centers. The reduction might be inhibited by diffusion. In sequence R2, again the reduction rate at the beginning of the sequence is very strong. The RD-curve shows a steep incline, which decreases after 2 minutes and reaches an almost steady state after only 5 minutes. Again, the chemical analysis of the RD after the sequence R2 seems to be too low. Because of this very porous iron ore, a rather strong reoxidation was observed after the test, which may be the reason for the too low value of 26.4 %. Again, the RD-trend is more reliable in this case. During the iron formation in R1, the RD-curve shows a rather steep and steady incline at the beginning of the sequence, which decreases continuously after about 15 minutes. The RD calculated based on the chemical analysis of 53.1 % shows a good accordance with reading of the RD-trend. The grain size distribution shows little disintegration and the material seems to be very stable. The disintegrated material was found in the finest fraction (cf. Figure 155).

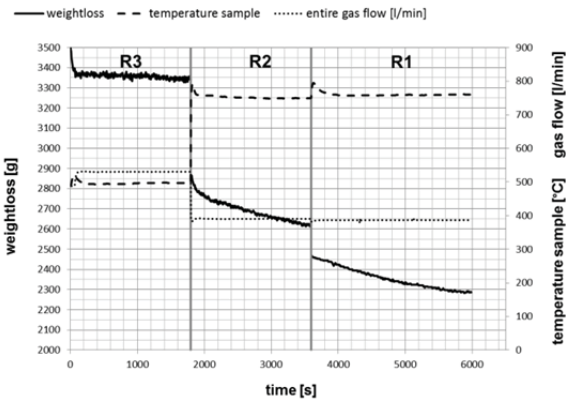

Figure 152: Test K weight loss-curve

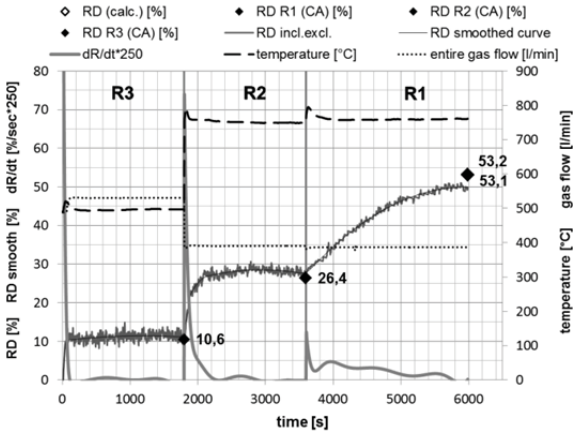

Figure 153: Test K RD-curve and RD-rate

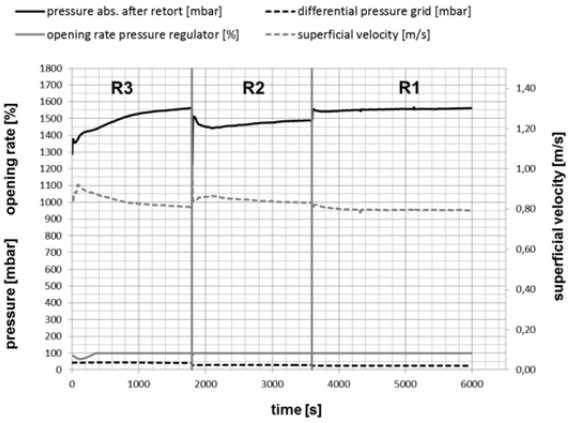

Figure 154: Test K pressure and gas flow

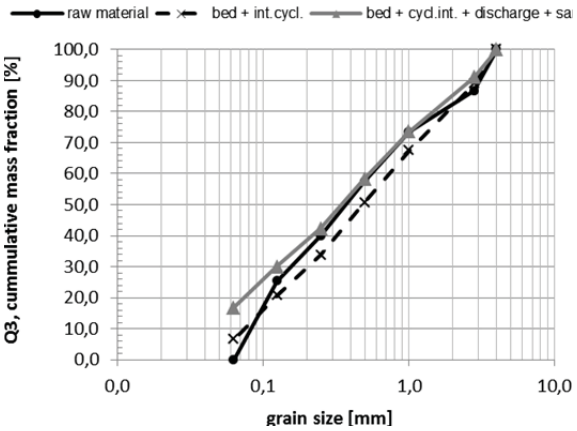

Figure 155: Test K grain size distribution

Marra Mamba iron ore (Australia, limonite-martite rich ore)

In the first reduction stage (R3), there is a strong inclination of the RD-trend, until it reaches a steady state within about 4 minutes residence time, which represents the magnetite phase (theoretical RD for Fe_3O_4 is 11.1 %). The chemical analyses of 10.5 % confirms the reduction degree of the process data. In stage R2, wuestite is formed with a rather strong inclination of the RD-curve at the beginning, which decreases after 3 minutes and reaches an almost steady state after 15 minutes. (theoretical RD for $Fe_{(1-y)}O$ under the specified process conditions is about 29 %). Obviously, the chemical analyses of the ores after R2 are too low. This can be caused by reoxidation of the extracted samples (high porosity of the limonite-rich ore) and also by the difficulties in analyzing the content of Fe^{2+}, as discussed before. Hence, the value for R2 of the RD-trend is more reliable in this case. In R1, the reduction degree increases steadily during the whole reduction sequence and iron is generated. The RD calculated based on the final chemical analysis of 46.7 % can be approximately confirmed. The grain size distribution shows, that this ore is rather unstable compared to the others. The ore disintegrates in the biggest parts into lower grain size fractions below 0.5 mm (cf. Figure 159).

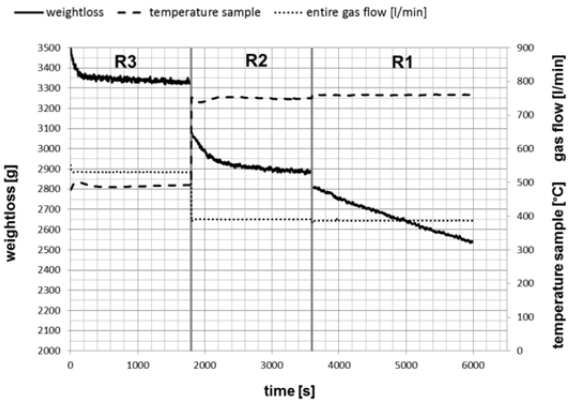

Figure 156: Test L weight loss-curve

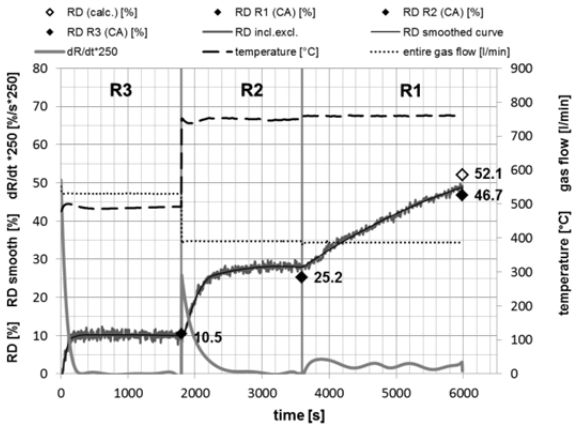

Figure 157: Test L RD-curve and RD-rate

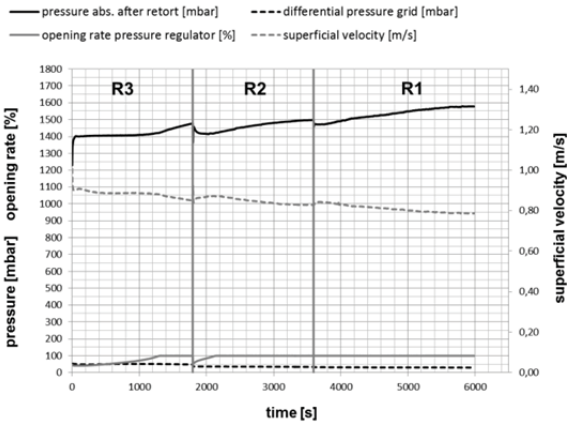

Figure 158: Test L pressure and gas flow

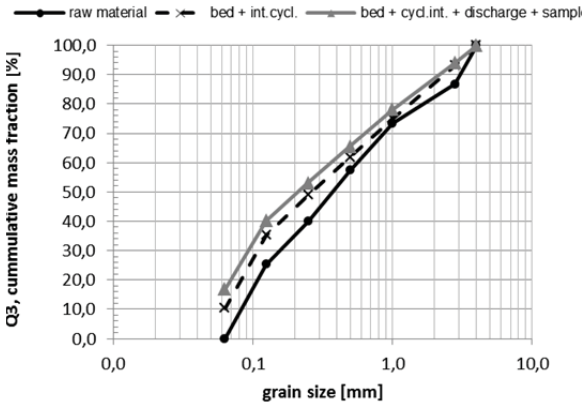

Figure 159: Test L grain size distribution

Pilbara iron ore (Australia, limonite-martite rich ore)

The Pilbara iron ore shows a strong reaction in the first reduction stage R3, and the RD-trend reaches a steady state (magnetite, theoretical RD for Fe_3O_4 is 11.1 %) within about 3 minutes residence time. The chemical analysis of 11.6 % confirms the value for R3 from the RD-trend, but seems to be slightly too high. In the second reduction stage, the Pilbara ore shows a very strong inclination of the RD-curve and after about 10 minutes residence time, the wuestite state is reached. Again, the chemical analysis of the material after the wuestite formation showed a doubtful result of 23.7 %. The theoretical RD for $Fe_{(1-y)}O$ under the specified process conditions is about 29 %, and again the value for R2 from the RD-trend is more reliable. In R1, during the formation of iron, the inclination of the RD-trend is stronger at the beginning and decreases after a while, until it reaches a reduction degree of about 49 %, which correlates quite good with the chemical analysis of 48,6 %. The pressure in the second half of the final reduction sequence was very high because of the discharge of fine material and plugging of the dust filter. The consequence was a lower superficial velocity in the fluidized bed. The occurrence could have slightly influenced the reduction behavior. The grain size distribution shows that this ore is rather unstable and the ore disintegrates in the biggest parts into lower grain size fractions below 0.5 mm (cf. Figure 163). The behavior of this ore is comparable to the Marra Mamba ore.

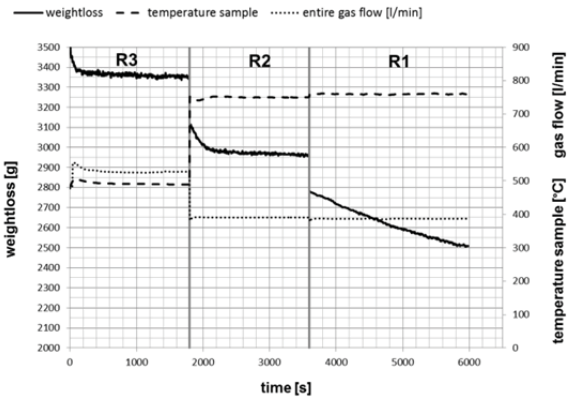

Figure 160: Test M weight loss-curve

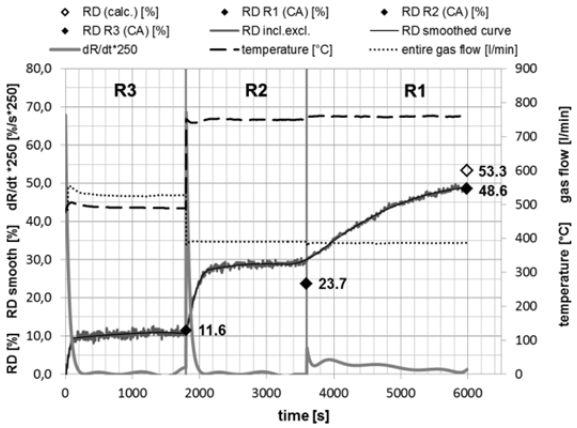

Figure 161: Test M RD-curve and RD-rate

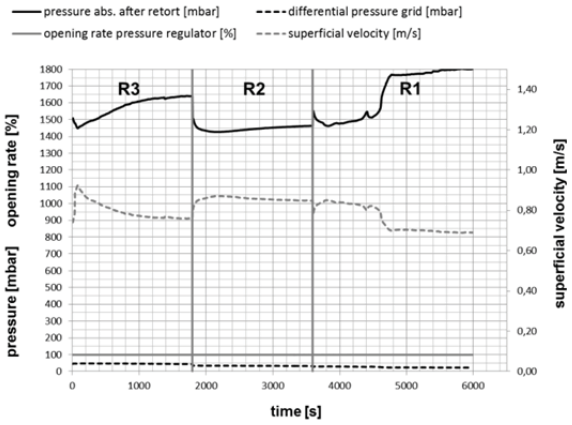

Figure 162: Test M pressure and gas flow

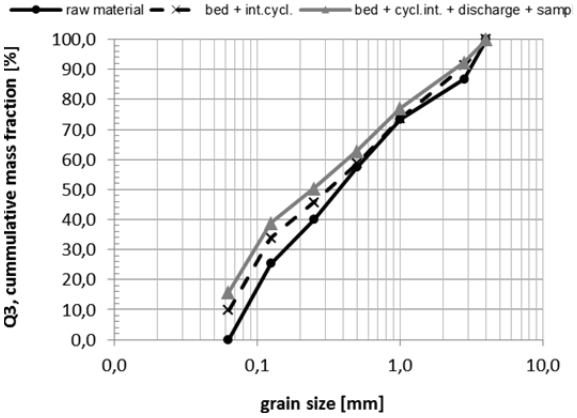

Figure 163: Test M grain size distribution

7.6.2 Morphological evolution of the different iron ore fines

In this chapter, the morphological evolution of the different iron ore brands during the reduction process in the fluidized bed is discussed. The process conditions were the same for all tests and also the samples were extracted under standardized conditions. Hence, the results allow statements regarding the reduction behavior of each ore in every single reduction sequence and, furthermore, the results can be compared. For the determination of the single reduction sequences, the chemical analyses of each reduction step are pointed out, together with the calculated reduction- and metallization degrees. In conjunction with the process data of the fluidized bed tests of the different ores (as discussed in 7.6.1), the morphological evolution can be compared and determined.

Hamersley iron ore (Australia, hematite rich ore, Test H)

The first iron ore, the Hamersley ore from Australia, is a porous hematite rich ore. Its specific surface area is about 5 m^2/g and because of the high amount of hematite, the ore should be easily reducible, which was confirmed in chapter 7.6.1. In Figure 164 to Figure 167, to the morphological evolution of this hematite rich ore during the reduction process is shown.

In the first reduction sequence R3, shown in Figure 165, the whole matrix was transformed to magnetite within about 4 minutes. No former limonite, hematite or martite relics in the grains' centers can be observed. The dark grey (finely porous) magnetite matrix was formed from limonite and the bright grey (dense) magnetite derived from former dense hematite and martite. An important indicator for the complete transformation to magnetite is the transformation of the very dense micro platy hematite, which can be observed in Figure 165 on the bottom. Because this dense hematite is very hard to reduce, its transformation indicates the transformation of the whole matrix to magnetite. The total iron content after this sequence is 67.3 % with a content of 22 % Fe^{2+}, which is in conjunction with a theoretical value of magnetite (66.6 % Fe_{tot} → 22.2 % Fe^{2+} and 44 % Fe^{3+}). Hence, the chemical analysis confirms the morphological investigations of about 100 % magnetite.

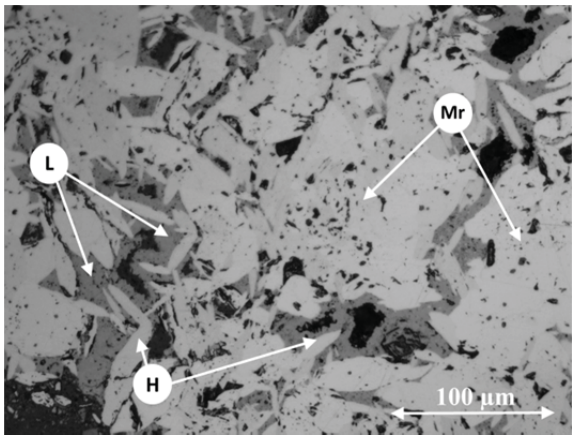

Figure 164: Hamersley raw ore (1 – 2.8 mm) [150]

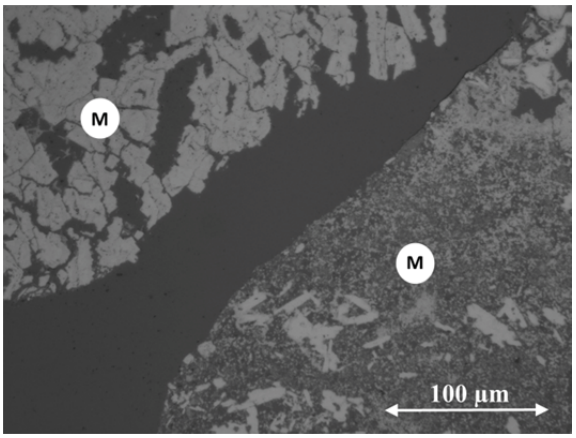

Figure 165: Hamersley after R3 (1 – 2.8 mm) [150]

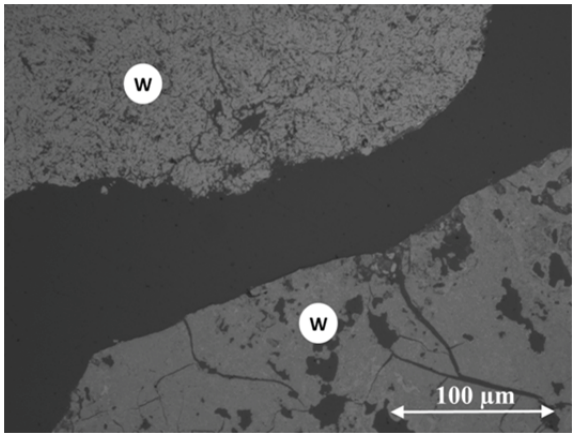

Figure 166: Hamersley after R2 (1 – 2.8 mm) [150]

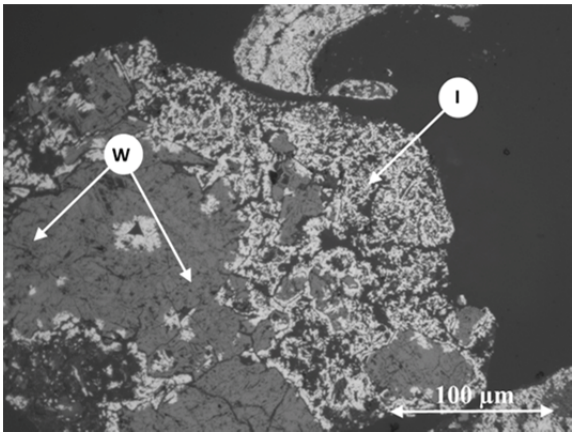

Figure 167: Hamersley after R1 (1 – 2.8 mm) [150]

In the second sequence R2, the magnetite of step R3 was completely reduced to wuestite (cf. Figure 166), and the crude ore structure is well recognizable. Dense wuestite evolved from former dense hematite or micro-platy hematite. Finely porous wuestite derived from former limonite of the raw ore. The finely porous wuestite regions are dark grey and the denser wuestite regions are light grey. Magnetite ore hematite relics were not observed. The former limonite grains show abundant cracks due to contraction (bottom). As discussed in

chapter 7.6.1, the RD calculated by the chemical analysis (Table 29) is too low compared to the reduction curve. Possible reasons are reoxidation of the sample material after the extraction or wrong chemical analysis.

In the last reduction stage R1, in the iron phase equilibrium, parts of the wuestite were transformed into metallic iron. The original matrix of the raw ore is well recognizable after the test. Iron scraps were generated, which appear in different homogeneity and size, depending on the porosity of the former hematite, martite and limonite regions (cf. Figure 166). The generated iron shows no surface covering layers. Former limonite and martite is significantly better metallized, than former hematite. The smaller grain size fractions are reduced more non-homogenously, than the coarser ones. Bigger grain size fractions show more homogenously dispersed iron scraps. Regarding the chemical analysis, the metallization degree is about 32 %, which can be confirmed by the morphological observations. Due to the removal of the oxygen out of the crystal lattice during reduction, the total iron amount increases from 63.6 % to 76.1 % during reduction. The final reduction degree and metallization degree is reasonable compared to the morphological investigations. The RD value for R1 by chemical analysis seems to be slightly too high.

Table 29: Chemical analyses, RD and MD of Hamersley ore during the reduction sequences

	Fe_{tot} [%]	Fe^{2+} [%]	FeO [%]	Fe_{met} [%]	C [%]	RD [%]	MD [%]
RO	63,60	0,45	0,58			0,2	0,0
R3	67,30	22,21	28,55	0,16	0,10	11,2	0,2
R2	70,50	56,45	72,58	0,29	0,12	27,1	0,4
R1	76,10	42,51	54,66	24,50	0,13	50,8	32,2

In general, this ore is well reducible, whereas the different morphological structures of the raw ore are influencing the further reduction behavior. The limonite and martite transform to a porous magnetite, which further forms a porous wuestite and a homogeneous matrix with finely dispersed iron scraps. On the other hand, the dense micro platy hematite generates a very dense magnetite and wuestite, which metallizes very non-homogenously in the final reduction stage. In this case, dense iron nuclei are formed on the grains' surfaces. These findings are generally valid and could also be observed in the morphological investigations of the other ores.

Kiruna iron ore (Sweden, magnetite rich ore, Test I)

In Figure 168 to Figure 171, the morphological evolution of the Kiruna magnetite ore is shown. This ore consists of a very dense magnetite matrix and has a specific surface area of just about 0.1 m²/g. In comparison to hematite or limonite rich iron ores, this is a very small value and this ore is normally difficult to reduce, because the overall reaction surface is very small. This was confirmed in the fluidized bed test (cf. chapter 7.6.1). After the first reduction step in R3, the ore is composed of magnetite still, because in the magnetite phase stability field no reaction occurred and the mineral phases did not change (Figure 169). Due to this fact, this ore consists of pure magnetite. Also the chemical analysis after R3 confirms this finding, because of almost the same values as the raw ore (cf. Table 30). Some grains show cracks along the grain boundaries because of thermal heating and calcination of gangue. The trace amounts of pyrite, ilmentite and apathite from the raw ore still exist. After R2 (Figure 170), the magnetite is just partly reduced to wuestite and the chemical equilibrium is

not reached by far. The theoretical RD for $Fe_{(1-y)}O$ under the specified process conditions is about 29 %. Regarding the chemical analysis, the RD is about 22 %, which can also be confirmed by the RD-trend of the test. Dense wuestite shells of variable thicknesses were formed around the magnetite cores (marks: border between wuestite and magnetite core). The wuestite evolves from the surface of the grains or cracks towards the magnetite core, with a defined reaction front which is clearly observable. This indicates the reaction type of the dense particle model. The phase border between magnetite and wuestite is very bright under the reflected light microscope and contains finely dispersed iron.

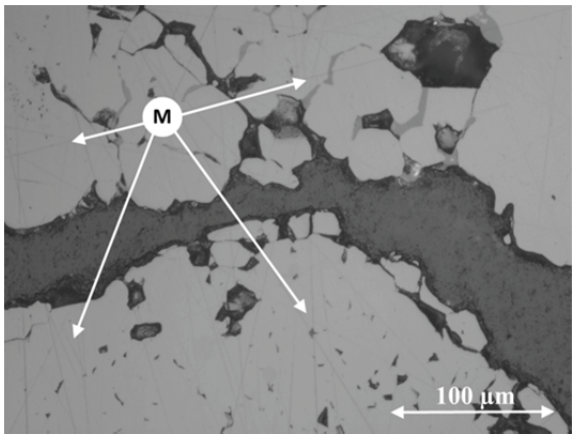

Figure 168: Kiruna raw ore (1 – 2,8 mm) [150]

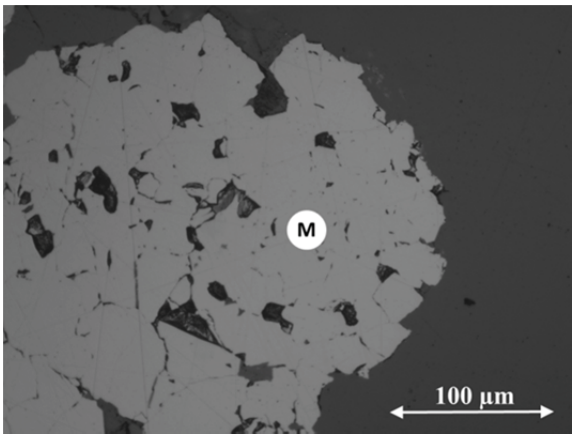

Figure 169: Kiruna after R3 (1 – 2,8 mm) [150]

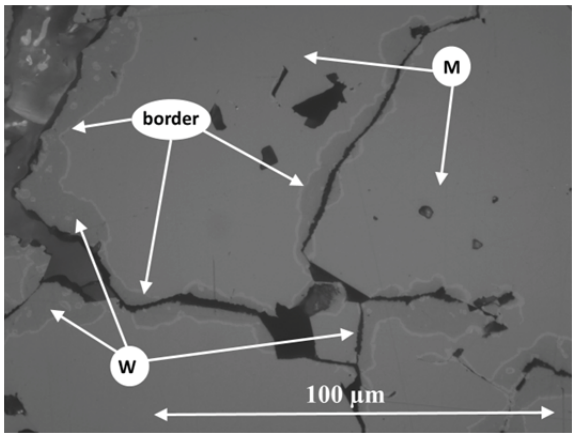

Figure 170: Kiruna after R2 (1 – 2,8 mm) [150]

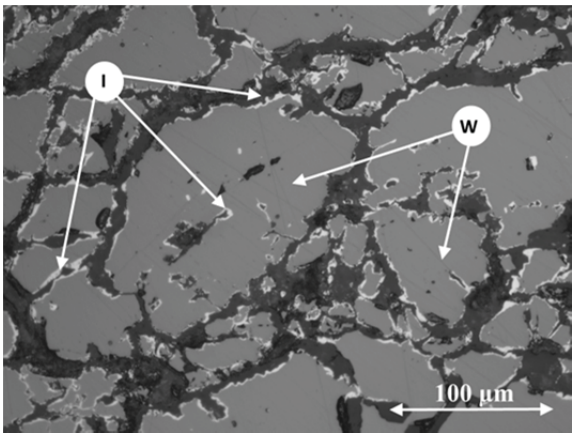

Figure 171: Kiruna after R1 (1 – 2,8 mm) [150]

A possible explanation for this finding could be the degradation of wuestite to magnetite and metallic iron during cooling of the material. Coarse fractions show a high amount of magnetite in the grains' cores. Finest fractions show a matrix, which consists almost of wuestite. Similar to R3, additional cracks were generated. In R1 the reduction again was very weak, In comparison to a hematite or limonite rich ore, the metallization is just 5.5 % instead of about 30 %. This can be confirmed by the morphological investigations. The reduced ore mainly consists of wuestite with iron, formed on the grains' surfaces. In the wuestite grains, sporadic magnetite relics can be observed, which were expected regarding the incomplete reduction to wuestite (refer to the RD-gradient, chapter 7.6.1). Hence, metallic iron is generated before the whole magnetite is transformed into wuestite. Despite the dense structure, hardly any surface covering iron layers were found, except some of the finest

grains. The beginning whisker formation can be observed at the grains surfaces, where iron ions accumulate. No observable change in prosity was detected during the reduction.

Table 30: Chemical analyses, RD and MD of Kiruna ore during the reduction sequences

	Fe_{tot} [%]	Fe^{2+} [%]	FeO [%]	Fe_{met} [%]	C [%]	RD [%]	MD [%]
RO	65,20	20,53	26,41			10,5	0,0
R3	65,10	21,30	27,39	0,06	0,12	11,0	0,1
R2	68,70	45,61	58,64	0,11	0,04	22,3	0,2
R1	69,10	45,31	58,26	3,82	0,04	27,4	5,5

Robe River iron ore (Australia, limonite rich ore, Test J)

In comparison to hematite and magnetite, the morphological evolution of the limonite rich Robe River ore is shown in Figure 172 to Figure 175. This ore is a very finely porous iron ore with a specific surface area of about 20 m²/g, which is much higher than the Hamersley hematite ore or the limonite-martite rich ores from Marra Mamba and Pilbara. This ore should be well-reducible, which was confirmed by the fluidized bed test (chapter 7.6.1). In R3 (cf. Figure 173), the matrix was transformed completely into magnetite. Hardly any hematite relics were found. Due to the removal of the crystal water from the limonite lattice during the preheating sequence, a very finely porous hematite evolved, which led to a very fast reduction of the hematite to magnetite. The magnetite stage was reached within just 2 minutes residence time. The reduction degree by chemical analysis was 9.8 %, which seems to be to low regarding the morphological situation.

Also the RD-trend for R3 shows a fast and almost complete reduction in this sequence (cf. Figure 173). Hence, the theoretical reduction degree of about 11 % should almost have been reached. Crack formation was observed, most probably due to the removal of the crystal water and the thermal stress. These cracks grow in the further reduction sequences. In R2 (cf. Figure 174), all limonite is reduced completely to wuestite and the ooid structures of some grains of the raw ore is still recognizable. No hematite or magnetite relics were found. In comparison to the morphology, the RD of the chemical analysis is far too low. This can also be confirmed by the RD-trend (cf. chapter 7.6.1). Possible reasons are reoxidation of the sample material after the extraction or wrong chemical analysis. At the reduced samples from R1 (Figure 175), a lot of iron scraps are spread all over the finely porous grain and iron layers were partly formed. Dark desiccation and contraction cracks are present all over the grains, whereas dense particle show coarser cracks. The metallization degree of the more dense grains is higher near the surface of the grain compared to the inner grain. Compared to the hematite rich Hamersley ore, the reduction degree is slightly lower. But, as discussed before, the reduction degree by chemical analysis of the Hamersley ore after the test seems to be too high. The total iron amount increases from 61.9 % to 75.5 % during reduction. The final RD and MD by chemical analysis correlate quite well with the morphological analysis and the test data.

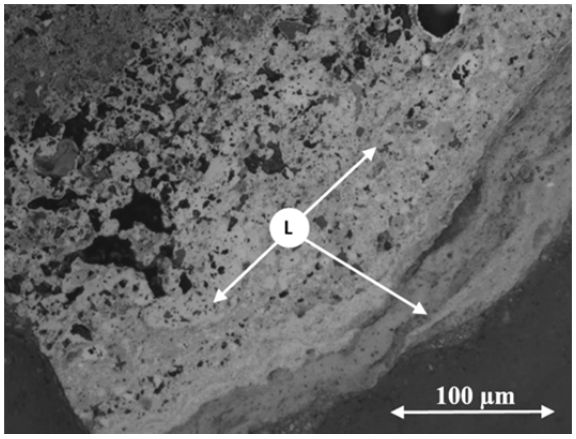

Figure 172: Robe River raw ore (1 – 2.8 mm) [150]

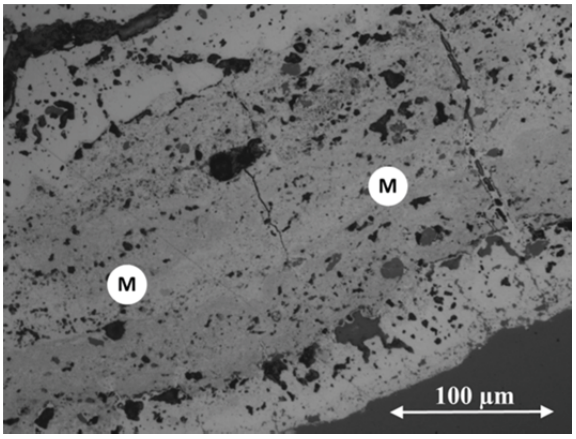

Figure 173: Robe River after R3 (1 – 2.8 mm) [150]

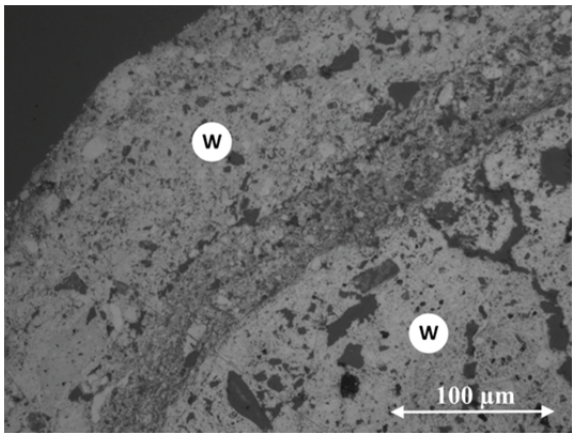

Figure 174: Robe River after R2 (1 – 2.8 mm) [150]

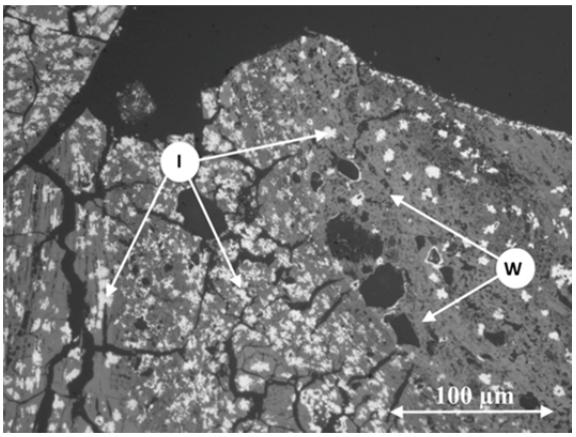

Figure 175: Robe River after R1 (1 – 2.8 mm) [150]

Table 31: Chemical analyses of Robe River ore during the reduction sequences

	Fe_{tot} [%]	Fe^{2+} [%]	FeO [%]	Fe_{met} [%]	C [%]	RD [%]	MD [%]
RO	56,20	0,29	0,37			0,2	0,0
R3	63,40	17,30	22,25	0,46	0,12	9,8	0,7
R2	66,00	39,21	50,41	0,25	0,10	20,2	0,4
R1	71,80	34,31	44,11	22,80	0,06	47,7	31,8

Erzberg iron ore (Austria, limonitic siderite ore, Test K)

Erzberg iron ore from Austria is a very porous limonitic siderite ore. In comparison to other iron ores, the iron content is rather low. The limonite evolved from the former siderite due to weathering and is specified as pseudomorphosis after siderite. The specific surface area of this ore is extremely high and is about 68 m²/g. Hence, this iron ore is fine porous and fine crystalline. Little amounts of siderite remained in the crude ore. The texture of the former carbonate remains preserved during the whole reduction process. Summarized, this ore should be extremely good reducible, which was determined with the fluidized bed test.

The morphological evolution during the reduction process is shown in Figure 176 to Figure 179. In the first reduction sequence R3 (Figure 177), the whole limonite is transformed to magnetite abruptly within one minute (cf. chapter 7.6.1), which can be explained by the extremely high porosity. No limonite or hematite relics were found in the matrix. The chemical analysis confirms this finding with a reduction degree of 10.6 %, which is quite close to the theoretical value, and the carbonate structure is well recognizable. The remaining siderite forms cracks in this sequence because of the calcination of the carbonate. In the second sequence R2, a very porous wuestite is formed and the whole matrix is completely transformed very rapidly within about 5 minutes. The chemical analysis of 26.4 % is again too low, which can be confirmed by the RD-trend (cf. chapter 7.6.1). As discussed before, the reasons could be reoxidation of the sample material after the extraction or wrong chemical analysis. In this sequence the siderite cracks, which were formed by calcination in R3, continue to grow. In the final reduction sequence R1, in the iron phase equilibrium, parts of the wuestite were transformed into metallic iron. The carbonate matrix of the raw ore is well recognizable after the test. In this sequence, a particularly high number of iron scraps were formed, which are dispersed very homogenously. Regarding the chemical analysis, the metallization degree is 35.6 %, which can be confirmed by the morphological observations. The total iron amount increases from 63.6 % to 76.1 % during reduction. The final reduction degree and metallization degree is reasonable compared to the test results and the morphological investigations.

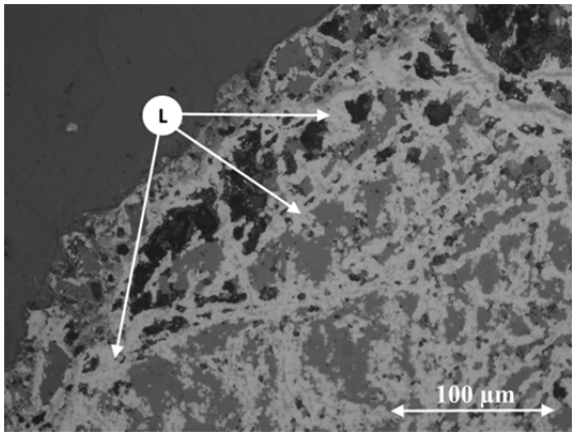

Figure 176: Erzberg raw ore (1 – 2.8 mm)

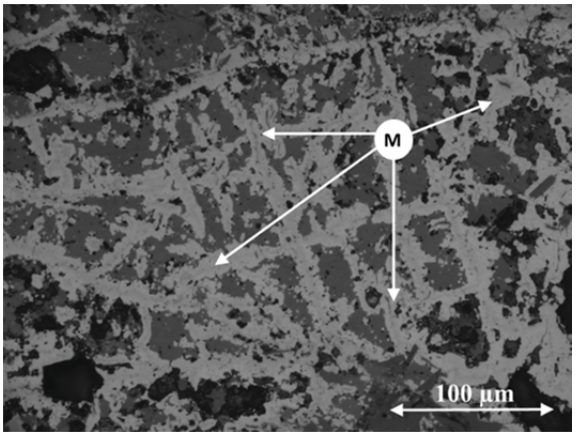

Figure 177: Erzberg after R3 (1 – 2.8 mm)

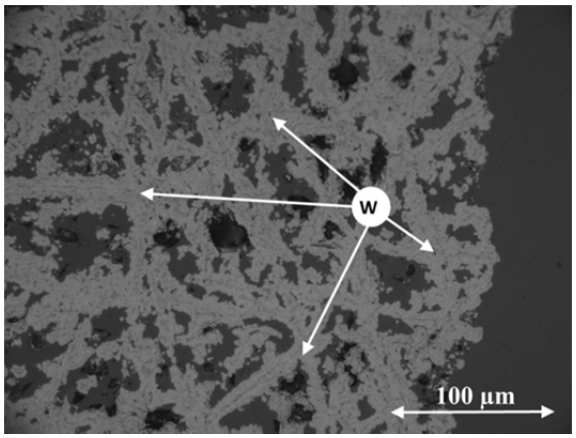

Figure 178: Erzberg after R2 (1 – 2.8 mm)

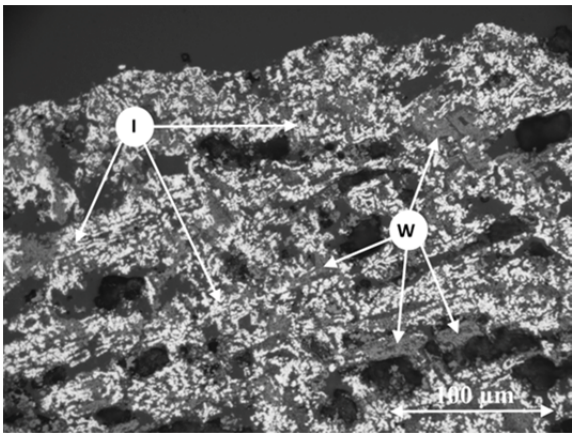

Figure 179: Erzberg after R1 (1 – 2.8 mm)

Table 32: Chemical analyses of Erzberg ore during the reduction sequences

	Fe_{tot} [%]	Fe^{2+} [%]	FeO [%]	Fe_{met} [%]	C [%]	RD [%]	MD [%]
RO	49,40	0,22	0,28			0,1	0,0
R3	55,40	16,30	20,96	0,42	1,68	10,6	0,8
R2	61,00	44,61	57,36	1,24	0,12	26,4	2,0
R1	65,20	34,51	44,37	23,20	0,30	53,2	35,6

Marra Mamba iron ore (Australia, limonite-martite rich ore, Test L)

Marra Mamba iron ore is a very porous limonite-martite rich ore. The high specific surface area of about 7 m^2/g renders it easy to reduce. In the first reduction sequence R3 (Figure 181), the iron oxides are reduced to magnetite very fast and completely within about 4 minutes (cf. chapter 7.6.1). No former limonite, hematite or martite regions are left. The chemical analysis in Table 33 confirms this finding. In the second sequence R2, a finely porous wuestite is built from the magnetite of step R3 (Figure 182). The whole matrix is transformed to wuestite. As discussed in the chapter before, the chemical analysis of this stage can be considered as wrong. The dark grey wuestite was formed from limonite and the bright grey wuestite derives from the martite structure. Because of the material is dehydrated, cracks were observed. In R1, finely dispersed iron scraps were formed, which are spread homogenously. The metallization of the fomer limonite is higher than the metallization of the former martite (cf. Figure 183). No dense iron layers were observed. The original matrix of the raw ore is well recognizable after the test. The smallest fractions are less metallized, and are in most cases surrounded by iron layers. Bigger fractions show homogenously dispersed iron scraps; due to the removal of the oxygen from the crystal lattice during reduction, the total iron amount increases from 61.3 % to 74 % during reduction. The final reduction degree and metallization degree is reasonable, compared to the morphological investigations.

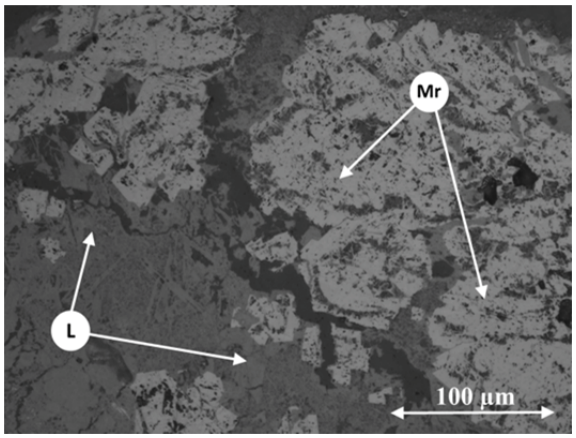

Figure 180: Marra Mamba raw ore (1 – 2.8 mm)

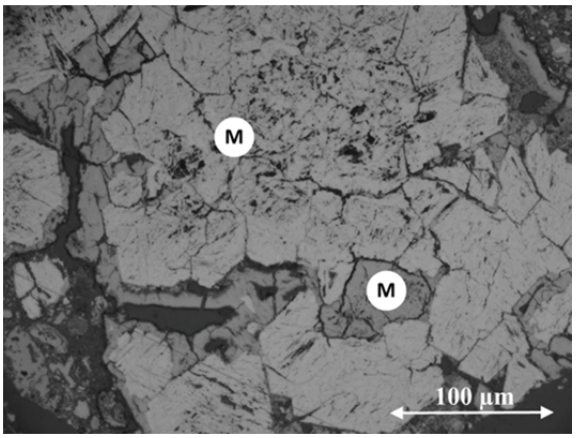

Figure 181: Marra Mamba after R3 (1 – 2.8 mm)

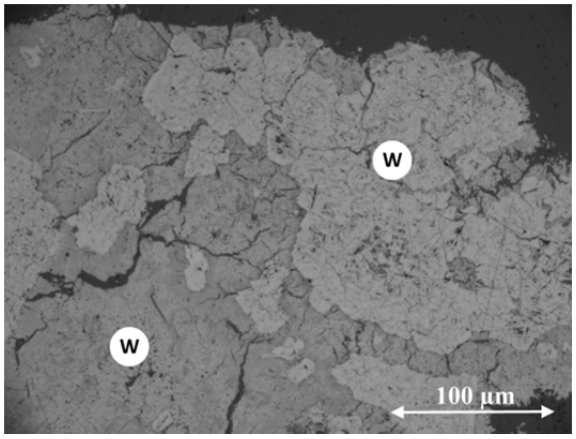

Figure 182: Marra Mamba after R2 (1 – 2.8 mm)

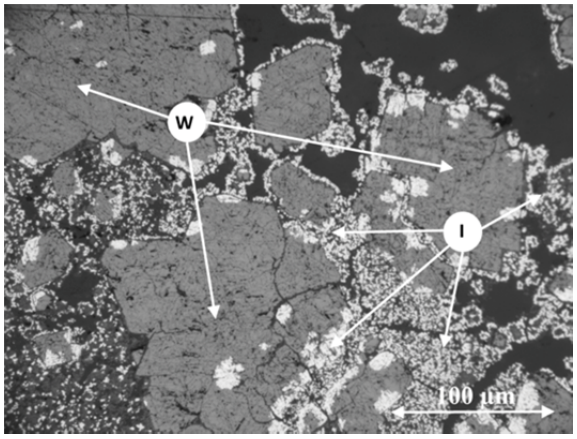

Figure 183: Marra Mamba after R1 (1 – 2.8 mm)

Table 33: Chemical analyses, RD and MD of Marra Mamba ore during the reduction sequences

	Fe_{tot} [%]	Fe^{2+} [%]	FeO [%]	Fe_{met} [%]	C [%]	RD [%]	MD [%]
RO	61,30	0,32	0,41			0,2	0,0
R3	66,10	19,90	25,59	0,31	0,05	10,5	0,5
R2	69,40	51,91	66,74	0,23	0,05	25,2	0,3
R1	74,00	41,11	52,85	20,90	0,03	46,7	28,2

Pilbara iron ore (Australia, limonite-martite rich ore, Test M)

The Pilbara iron ore is a very porous limonite-martite-rich ore with a high specific surface area of about 9 m^2/g. The reducibility of this ore is very good (refer to the previous chapter). Characteristically are the adhesions of very fine material on the grains' surfaces, which remain stuck on the grains during the first two reduction stages. In R3, the whole matrix is converted completely to magnetite, which can be confirmed by the chemical analysis (cf. Figure 185 and Table 34). During the reduction sequence R2, the whole magnetite of R3 was converted to wuestite (cf. Figure 186). The dark grey wuestite was formed from limonite matrix and the bright grey wuestite derives from the martite structure. The RD calculated by the chemical analysis (cf. Table 34) is far too low compared to the morphological state. The reason may also be due to reoxidation of the sample material after extraction or wrong chemical analysis. The RD-trend of R2 (cf. chapter 7.6.1) confirms this finding and is more reliable in this case. In the last reduction step R1, finely dispersed iron scraps were formed, especially in the wuestite matrix derived from former limonite (cf. Figure 187). The matrix of the raw ore is well recognizable after the test, and sporadic iron layers were also observed. Additionally, some adhesions of very fine material of the raw ore are still present. Again, the smaller grain size fractions are reduced less homogenously, than the coarser ones. Due to the removal of the oxygen out of the crystal lattice during reduction, the total iron amount increases from 61.9 % to 75.5 % during reduction. The final RD and MD can be confirmed by the morphological analysis.

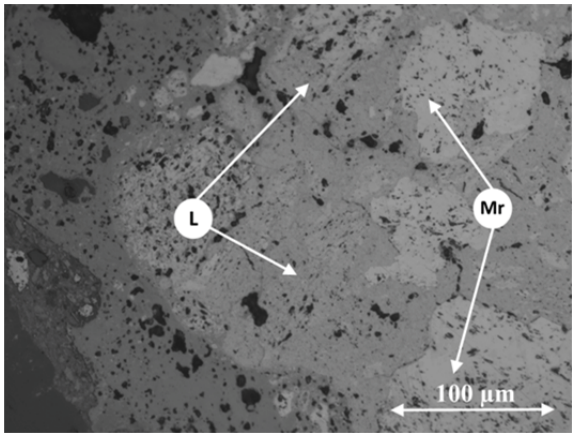

Figure 184: Pilbara raw ore (1 – 2.8 mm)

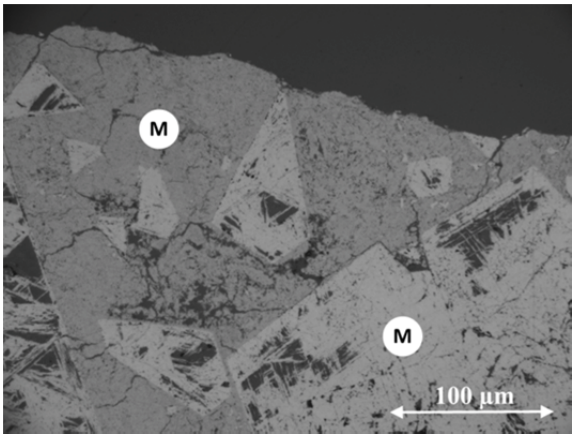

Figure 185: Pilbara after R3 (1 – 2.8 mm)

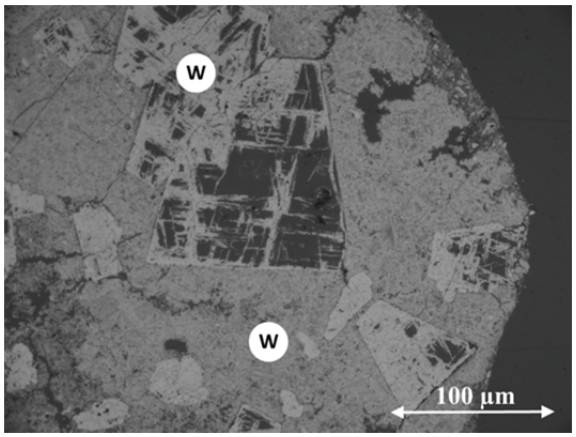

Figure 186: Pilbara after R2 (1 – 2.8 mm)

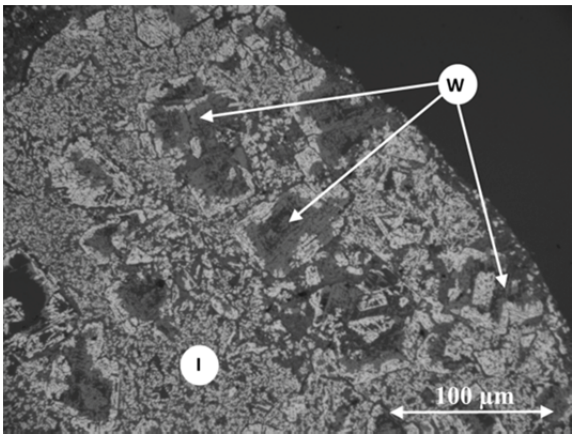

Figure 187: Pilbara after R1 (1 – 2.8 mm)

Table 34: Chemical analyses, RD and MD of Pilbara ore during the reduction sequences

	Fe_{tot} [%]	Fe^{2+} [%]	FeO [%]	Fe_{met} [%]	C [%]	RD [%]	MD [%]
RO	61,90	0,42	0,54			0,2	0,0
R3	66,90	20,97	27,01	0,73	0,07	11,6	1,1
R2	69,40	48,93	63,01	0,13	0,05	23,7	0,2
R1	75,50	39,74	51,18	23,40	0,05	48,6	31,0

7.6.3 Discussion

In general, the iron ores, except of the magnetite ore, were well reducible, whereas the limonite rich ores showed a higher reduction rate. The reduction behavior and the morphological evolution of the iron ores were discussed in chapter 7.6.1 and 7.6.2. For a better interpretation of these results, the behavior of the different iron ores has to be compared in every reduction sequence.

In the first reduction stage (R3), the RD-gradients of the ores showed a strong inclination until they reach a steady state within maximum 5 minutes representing the magnetite phase. The exception is Kiruna ore, which consists of magnetite. In this stage, the reducibility of the limonite rich ores was significantly higher, followed by the limonite-martite rich ores, the hematite rich ore and the magnetite rich ore, which was not reduced at all. Depending on the

raw material structure, different types of magnetie were generated. Limonite and martite phases are transformed into a finely porous magnetite whereas coarse and dense hematite phases transformed to a dense magnetite. The same behavior was observed by Pawlik and Schuster [103,104,108]. Regarding the reduction rate in this sequence, there is a strong dependency on the specific surface area of the raw ore. The ores with the highest specific surface area had a tremendously higher reduction rate (cf. Figure 193). The reduction rates of the ores in R3 can be represented in decreasing order as follows:

Erzberg (limonite) → Robe River (limonite) → Pilbara (limonite-martite) → Marra Mamba (limonite-martite) → Hamersley (hematite) → Kiruna (magnetite)

From the morphological point of view, the reducibility of the different structural iron ore phases can be ordered as follows (beginning with the best):

Limonite → Martite and porous Hematite → dense Hematite → Magnetite

This finding is in good conjunction with the findings of Thurnhofer [110], who also investigated into the reduction behavior of iron ores under CO-rich gas mixtures, but with other gas conditions and pressure.

Also in stage R2, the limonite and hematite rich ores have a similar reduction behavior. The RD-trends show a strong inclination, until they reach a steady state after maximum 10 minutes, which represents the wuestite state (theoretical RD for $Fe_{(1-y)}O$ under the specified process conditions is about 29 %). The chemical analyses of the limonite rich ores after R2 are too low. Due to repetition of these chemical analyses and similar results, the lower RD can be explained on one hand by reoxidation of the sample (since the porosity of the reduced limonite ore and the wuestite formed out of it is high), on the other hand by the problems of the chemical analysis of Fe^{2+} (discussed in chapter 6.4). The RD-trend of the magnetite ore in R2 has a low inclination and the wuestite state is not reached by far. In this stage, the reduction rates of the different iron ores are no longer dependent on the specific surface area of the raw ore. In comparison to R3, here the reduction rates in sequence R2 are listed in decreasing order for the different ores:

Erzberg (limonite) → Pilbara (limonite-martite) → Hamersley (hematite) → Robe River (limonite) → Marra Mamba (limonite-martite) → Kiruna (magnetite)

In the final reduction sequence R1, the wuestite matrix of the iron ores was progressively reduced to metallic iron. In contrast to R3 and R2, the thermodynamic equilibrium was not reached. Hence, only a part of the matrix was transformed to iron. In this sequence an almost linear reaction progress was detected for all ores, with different inclines and final reduction- and metallization degrees. The limonite-rich ores showed a slightly stronger inclination of the RD-gradients at the beginning, which progressively decreased after a while. The Kiruna magnetite ore is the exception, because it was not completely reduced to wuestite in the second reduction step R2 and showed an inhibited behavior. The reached final reduction- and metallization degrees of the different ores after the final sequence R1 are listed in decreasing order, beginning with the highest:

Erzberg (limonite) → Hamersley (hematite) → Pilbara (limonite-martite) → Robe River (limonite) → Marra Mamba (limonite-martite) → Kiruna (magnetite)

Comparing this order with the order in R2, it is obvious, that it is quite similar. Because the chemical analysis of the Hamersley test seems to be slightly too high (cf. to chapter 7.2.2 and 7.6.1), there is a good accordance. Hence, the reduction rate in the first sequence is strongly depending on the specific surface area of the raw ore. In dependence on the process behavior in the first reduction stage and the type of magnetite formation (porous or dense), the behavior of the different iron ores changes in the second sequence and the reduction behavior is no longer dependent on the specific surface area of the raw ore. These new characteristics dominate the reduction behavior until the end of the test. This could be confirmed by the correlations in Figure 188 to Figure 191. In these diagrams, the final reduction degree is correlated to the raw material characteristics: specific surface area, external surface area and pore volume and diameter (cf. Table 19). In contrast to the first reduction sequence, no dependencies could be found any more.

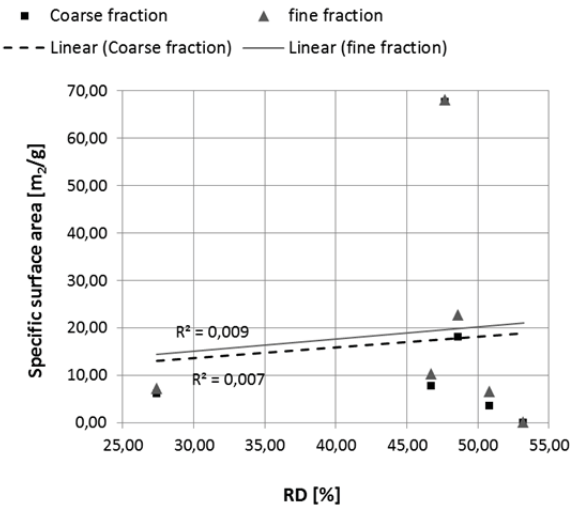

Figure 188: Correlation between specific surface area and final reduction degree

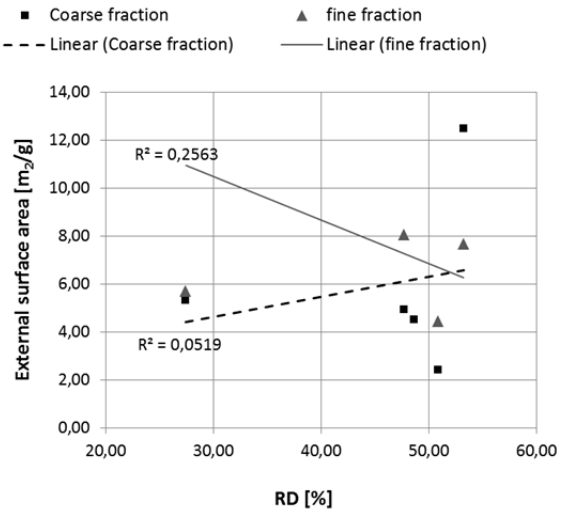

Figure 189: Correlation between external surface area and final reduction degree

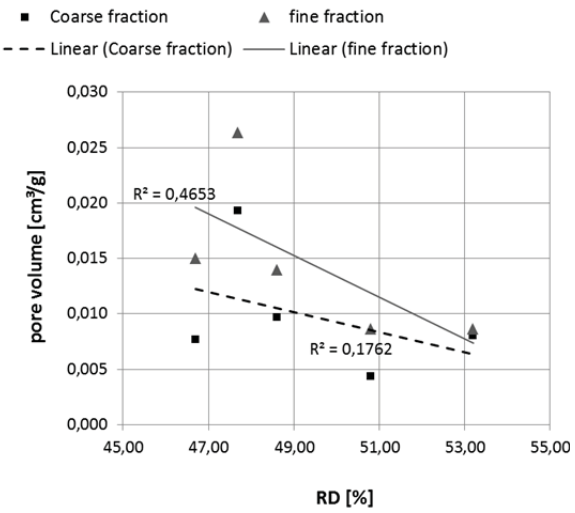

Figure 190: Correlation between pore volume and final reductiton degree

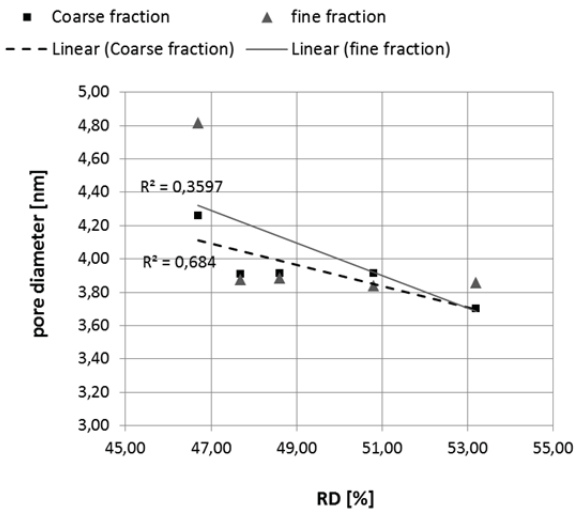

Figure 191: Correlation between pore diameter and final reductiton degree

So it can be stated, that the final reduction- and metallization degree is directly dependent on the type of magnetite, which was generated in reduction sequence R3 in the magnetite phase stability field. This type of magnetite determines the type of wuestite to be formed and, hence, the further reduction behavior of the ore. Additionally it can be stated, that also the amount of magnetite in the raw ore worsens the final reduction- and metallization degree significantly.

Comparing the grain size distributions of the different iron ores after the test, the disintegration behaviour was quite different. In Figure 192, the grain size curves are shown. The bold black line represents the distribution of the input material. As a reference, the $Q3_{50}$-value (the grain size at 50 % of the cumulated grain size curve) is used for the comparison. The stability of the ores in the test in decreasing order is as follows (beginning with the most stalbe):

Erzberg (limonite) → Robe River (limonite) → Hamersley (hematite) → Pilbara (limonite-martite) → Kiruna (magnetite) → Marra Mamba (limonite-martite)

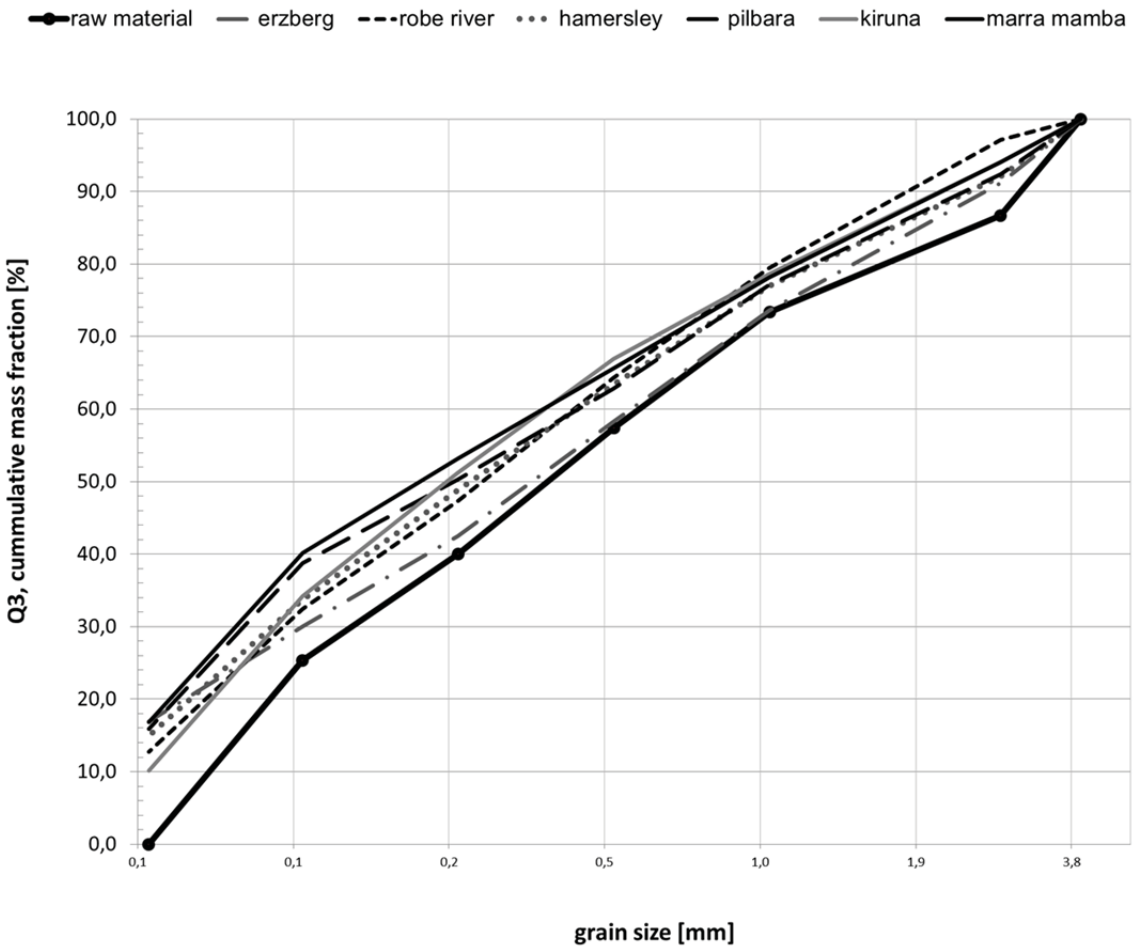

Figure 192: Grain size distribution of the different iron ore brands after the test

Comparing the disintegration behavior of the different ores with the reduction behavior, no dependencies were found. Hence, the disintegration behaviour of the iron ores in a sequenced fluidized bed process is not dependent on the reduction behaviour, but on the mineralogical characteristics of each iron ore.

Summarizing the comparison of the reduction behavior of different iron ores under the same process conditions, it can be stated that:

- the limonite and hematite rich iron ores were well reducible, whereas the limonite rich ores showed a higher reduction rate.
- the magnetite ore was worse reducible, with a final reduction degree far below the limonite and hematite rich ores.
- limonite and martite phases transformed into a finely porous magnetite, whereas coarse and dense hematite phases transformed into a dense magnetite.
- the reduction rate in the first reduction sequence R1 depends strongly on the specific surface area of the raw ore.
- the reduction rate in the second reduction sequence R2 depends on the type of magnetite, which was generated in reduction sequence R1 (in the magnetite phase stability field).
- the amount of magnetite in the raw ore worsens the final reduction- and metallization degree significantly.
- the disintegration behaviour of the iron ores in a sequenced fluidized bed process is not primarily dependent on the reduction behaviour, but on the mineralogical characteristics of each iron ore.
- the mineralogical composition of an iron ore has a significant influence on the reduction behaviour (i. e.: reduction rate, transformation characteristics between the phases, disintegration, final reduction degree).

The chemical composition and mineralogical structure of the raw ore, as well as the structural changes influenced by the process parameters, influence the reduction behavior and the final reduction- and metallization degree significantly.

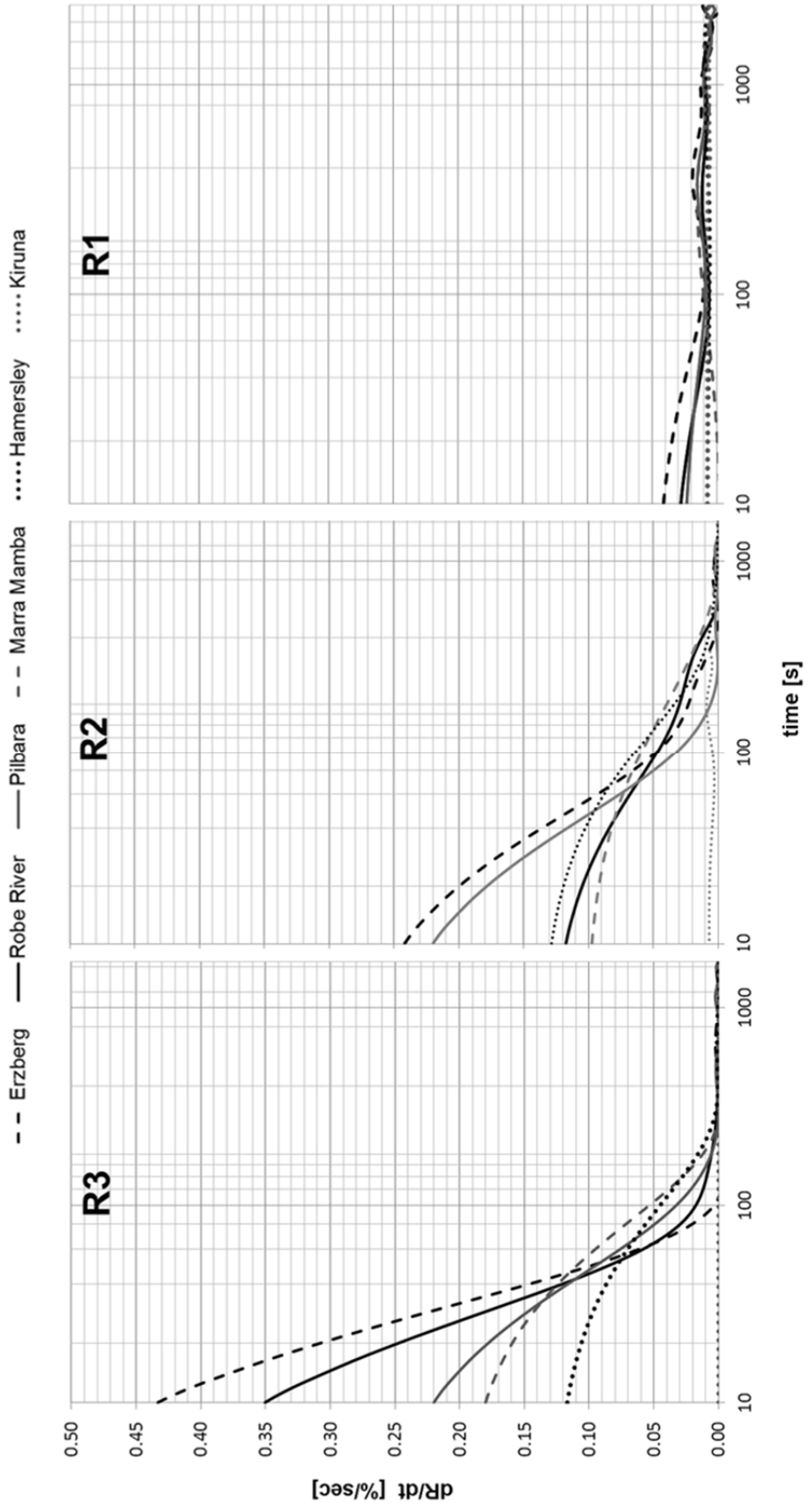

Figure 193: Reduction rates of the different iron ores during the reduction sequences

8 Summary

This research work dealt with the process optimization of fluidized-bed based technologies for iron- and steelmaking and the determination of reduction behavior as well as the mineralogical and petrographical characterization of different iron ores. Therefore a novel lab scale fluidized bed reactor was installed in the laboratories of the Chair of Metallurgy. Based on industrially applied fluidized bed reduction technologies with coal gasification for the generation of the reducing gas, the reduction behavior of different worldwide traded fine iron ores was investigated under different process conditions.

In a first approach, the current industrially applied 4-stage sequenced reduction mode was compared to a more economical 3-stage sequenced mode with the same iron ore as input material (hematite ore). It can be stated, that no big difference of reduction and metallization degree was observed. Additionally, in the 3-stage reduction mode, the iron ore was less disintegrated during the process, which is a huge advantage regarding process stability and dust emissions in the industrial process. Hence, a sequenced 3-stage reduction mode is recommended for industrial applications.

In the second series, defined sequenced 3-stage tests were performed to investigate the variation of temperature in the pre-reduction stage, the variation of gas composition in different stages and the variation of residence time in the final reduction sequence. All tests in these series were executed with the same raw material (hematite ore). The variation of the start temperatures between 350 °C and 600 °C in the pre-reduction stage showed no big influence on the final reduction- and metallization degree in 3-stage sequenced operation under the applied process conditions. Also the disintegration behaviour of the material was almost equal. For a detailed discussion refer to chapter 7.3.3. Regarding the variation of the gas composition and in order to simulate closer real operation conditions, two tests in 3-stage mode with stronger reducing gas compositions were executed: one test with fluctuating gas composition in the final reduction sequence and one with a pre-reduction-stage in the wuestite field and final reduction stages in the iron field. Both tests showed very high reduction degrees, but also excessively increased disintegration of the material. Details are discussed in chapter 7.4.4. Regarding the residence time of the material in the process, it can be stated that hematite- and limonite rich ores showed a substantial potential of decreasing the residence time in R3 (transformation of hematite to magnetite) and R2 (transformation of magnetite to wuestite) under standardized conditions. Increasing the residence time in the final reduction stage R1 (wuestite to iron), showed a considerable gain

in reduction degree with further potential still. The extended residence time resulted in a stronger disintegration of the material, which is a disadvantage for the process and can be explained with the increased abrasion.

In a third test series, the reduction behavior of different globally traded iron ore brands under the same test conditions was investigated by means of a standardized 3-stage sequenced reduction mode. For this purpose, a standardized test methodology was developed. Additionally, a sampling system for the fluidized bed reactor has been installed to extract samples during the reduction process. The chemical, morphological and structural evolution of the material during reduction in the magnetite, wuestite and iron stability field could be characterized. Hematite and limonite ores were well reducible and had a similar process behavior, whereas the limonite rich ores showed a slightly stronger reduction rate at the beginning of the reduction sequences. Magnetite is significantly slower reduced resulting in a worse reduction degree far below of reduced hematite and limonite throughout all steps of the process. Regarding the mineralogical evolution, samples were extracted during the reduction process and have been described in detail in this work (refer to chapter 7.6). Comparing the morphological characteristics of the different iron ores, the finely porous limonite ores as well as the hematite ore was described as being well reducible. The dense magnetite ore, conversely, showed poorer reduction behavior. Comparing the results of the continuously measured process data with the morphological and chemical characterization, the evolution of the reduction progress was thus confirmed and characterized.

Due to recurring chemical measurement-errors (in terms of determination of the reduced iron ore samples), an anonymous interlaboratory test with selected laboratories was carried out. The results render statements and predictions in terms of accuracy and analysis error of Fe_{tot}, Fe_{met}, Fe^{2+} and Fe^{3+}.

The reduction progress of the executed tests could be defined and compared with chemical analyses, morphology and mass balances. Furthermore, compared to prior research work, the facility enabled tests closer to real industrial operation conditions. The tests executed with this new facility provided clear evidence for a better prediction of reducibility of iron ores in the fluidized bed process. Comprising the methodology of process control and the subsequent morphological and chemical analysis of various extracted samples, this new method is an excellent tool for the development of fluidized bed based technologies and for characterizing the process behavior of iron ore fines.

9 Outlook

Based on the results of this work, further investigations are suggested. In order to determine and compare the reduction behavior and the morphological characteristics of iron ore fines under CO- and H_2-rich gas conditions, a series of reduction tests with a smaller lab scale fluidized bed facility should be executed with changing gas- and temperature conditions.

Proposal:

- An iron ore test series for a hematite-rich, a limonite-rich and a magnetite-rich ore, respectively.
- Each iron ore test series should be performed in single-stage reduction as well as sequenced two- and 3-stage reduction with a defined range of operating points.

Therefore, a series of experimental plans has to be worked out and tested. Based on the findings of these test series, tests on the 160 mm fluidized bed retort should be performed to find the optimum process parameters for each iron ore type reduced in two- or three-stage sequenced reduction. Furthermore, a profound understanding of the morphological characteristics of each iron ore type at various process conditions could be engendered.

Regarding the gathered data from the interlaboratory test and the significant inaccuracy of Fe^{2+}-determination by the analytical laboratories, further investigations are suggested. In a first step, the laboratories should be informed about the results, and the potential sources of error should be determined. In a second step, common solutions should be worked out to improve analytical accuracy.

Bibliography

[1] Schenk, J. L., Recent status of fluidized bed technologies for producing iron input material for steelmaking, Particuology 9 (2011), 14-23.

[2] Feinman, J., Direct Reduced Iron- Technology and Economics of Production and Use, The Iron & Steel Society, Warrendale, (1999).

[3] Schmöle, P., Chemical and physical processes in the blast furnace, 1st international seminar - ironmaking in blast furnace plants, Düsseldorf, Germany, March 7th (2012).

[4] Gudenau, H. W., et al., Direktreduktion, Rheinisch-Westfälische Technische Hochschule Aachen, Institut für Eisenhüttenkunde, Aachen, (1997).

[5] Schenk, J. L., Direct Reduction and Smelting Reduction, 1st international seminar - ironmaking in blast furnace plants, Düsseldorf, Germany, March 7th (2012).

[6] MIDREX, World Direct Reduction Statistics, (2012).

[7] W. Grill, C. Böhm, K. Wieder and U. Schmidt, COREX/FINEX - Prepared for present and future ironmaking challenges, International Seminar on Alternative Routes for Ironmaking in India, Kolkata, India, Sept. (2009).

[8] Schenk, J. L. *and W. F. Kepplinger,* Development and Future Potential of the FINEX-Process, 2nd International Congress on the Science and Technology of Ironmaking and 57th Ironmaking Conference, Toronto, Canada, (1997), 1549-1557.

[9] Joo, S.*, et al.,* FINEX - a new process for production of hot metal from fine ore and coal, Scandinavian Journal of Metallurgy 28 (1999), 4, 178-183.

[10] Schenk, J. L., Vorlesungsskriptum zu Spezielle Metallurgische Prozesstechnik, Montanuniversitaet Leoben, Chair of Metallurgy, (2011).

[11] Babich, A., D. Senk, H.W. Gudenau and K. Mavrommatis, Ironmaking, Wissenschaftsverlag Mainz, Aachen, (2008).

[12] Ritz, V., Ionmaking in Blast Furnace Plants: Types and Characteristics of Iron Ore, 1st international seminar - ironmaking in blast furnace plants, Düsseldorf, Germany, March 7th (2012).

[13] ISO Standards development, Technical Comitee TC/102 - Iron ore and direct reduced iron.

[14] Vegman, E. F., Zherebin, N.*, et al.,* Ironmaking, (2004), 774.

[15] Bashforth, G., The manufacture of iron and steel, Chapman & Hall Ltd. 1 (1964), 334.

[16] Feinman, J., D. H. Wakelin (Ed.), The Making Shaping and Treating of Steel 11 (1999), 741-780.

[17] Gudenau, H. W., Materialsammlung zum Praktikum Metallurgie, Rheinisch-Westfälische Technische Hochschule Aachen, Institut für Eisenhüttenkunde, Aachen, (2002).

[18] Tzafaras, N., W. Adlhart and H. Jagodzinski, High temperature investigations of magnetite (Fe_3O_4), Acta Crystallographica Section A37 (1981), 104.

[19] Finger, L. W. and R. M. Hazen, Crystal structure and isothermal compression of Fe_2O_3, Cr_2O_3, and V_2O_3 to 50 kbars, Journal of Applied Physics 51 (1980), 10, 5362-5367.

[20] Schenck, R. and T. Dingmann, Gleichgewichtsuntersuchungen über die Reduktions-, Oxydations- und Kohlungsvorgänge beim Eisen III, Zeitschrift für anorganische und allgemeine Chemie 166 (1927), 113-154.

[21] Bartholomé, E., E. Biekert and H. Hellmann, Ullmanns Encyclopädie der technischen Chemie, Verlag Chemie, 4th ed., Weinheim, (1975).

[22] Senk, D., Material Chemistry of Iron Ore Reduction and Carbon Conversion, 1st international seminar - ironmaking in blast furnace plants, Düsseldorf, Germany, March 7th (2012).

[23] Materialscientist, hematite structure, http://en.wikipedia.org/wiki/File:Hematite, 10th Aug. (2012).

[24] Materialscientist, magnetite structure, http://en.wikipedia.org/wiki/File:Magnetite, 10th Aug. (2012).

[25] Materialscientist, NaCl structure, http://en.wikipedia.org/wiki/File:NaCl, 10th Aug. (2012).

[26] Bogdandy, L. v.*, et al,* Die physikalische Chemie der Eisen und Stahlerzeugung, Course of lectures from „Verein Deutscher Eisenhüttenleute“ and „Haus der Technik Essen", Verlag Stahleisen m. b. H. (1964).

[27] Andronov, V. N., Extraction of ferrous metals from natural and secondary resources, SPbGTU (2007).

[28] Weiss, B., Kinetics of Iron Ore Fines Reduction under Fluidized Bed Conditions at Elevated Pressures, Dissertation, TU Wien, (2008).

[29] Yakushevich, N. F., I. V. Strokina and O. A. Polyakh, Thermodynamic Aspects of Phase-Chemical Equilibria in the Fe-C-O2-H2 System, Steel in Translation 42 (2012), 4, 290-297.

[30] Schenk, J. L., Vorlesungsskriptum zu Eisen- und Stahlmetallurgie I, Montanuniversitaet Leoben, Chair of Metallurgy (2009).

[31] Weiss, B., Empirical reduction diagrams for reduction of iron ores with H_2 and CO gas mixtures considering non-stoichiometries of oxide phases, Ironmaking & Steelmaking 36 (2009), 3, 212-216.

[32] Rist, A. and G. Bonnivard, Revue de Métallurgie 60 (1963), 1, 2737.

[33] Rist, A. and N. A. Meysson, Journal of Metals 19 (1967), 4, 50-59.

[34] Rist, A. and N. A. Meysson, Revue de Métallurgie 63 (1966), 3, 197-200.

[35] Rist, A. and N. A. Meysson, Revue de Métallurgie 63 (1966), 4, 296-312.

[36] Rist, A. and N. A. Meysson, Revue de Métallurgie 61 (1964), 2, 121-145.

[37] Pichler, A., Entwicklung einer Methodik zur Bewertung der morphologischen Veränderung von Feineisenerzen während der Reduktion in einem Wirbelschichtreaktor, Master Thesis, Montanuniversitaet Leoben, Chair of Metallurgy, (2012).

[38] Nuber, D., Fluidatbett-Reduktion mit Erdgas und Kohle, Dissertation, Rheinisch-Westfälische Technische Hochschule Aachen, Institut für Eisenhüttenkunde, (2005).

[39] Bogdandy, L. v. and H. Engell, The Reduction of Iron Ores, Stahleisen, Düsseldorf, (1971).

[40] Habermann, A., Kinetik der Eisenerzreduktion in der Wirbelschicht, Dissertation, TU Wien (2001).

[41] Gudenau H. W., Eisehüttenmännische Verfahrenstechnik - Vom Erz Zum Stahl, Druck- und Verlagshaus Mainz GmbH, Aachen, Germany, (1989).

[42] Steinbach, W., Reduktionskinetik von Feinerzen in der Wirbelschicht, Master Thesis, TU Wien, Institut für Verfahrenstechnik, Brennstofftechnik und Umwelttechnik (1999).

[43] Hofbauer, H., F. Winter, A. Habermann, W. Steinbach, C. Stingland and A. Thurnhofer, Grundsatzuntersuchung zur Wirbelschichtreduktion von Feinerzen, Report, TU Wien, Institut für Verfahrenstechnik, Brennstofftechnik und Umwelttechnik (2001) .

[44] Bogdandy, L. v., H. P. Schulz, I. N. Stranski and B. Würzner, Ber. Bunsenges. phys. Chem. 67 (1963), 958-964.

[45] Geldart, D, Gas Fluidization Technology, John Wiley & Sons, Chichester, New York, Brisbane, Toronto, Singapore, (1986).

[46] Kohl, H. K. and B. Marincek, Über die Reaktionskinetik von Wüstit mit Kohlenmonixid und mit Wasserstoff, Helvetica Chimica Acta 48 (1965), 8, 1857-1867.

[47] Wen, C. Y., Noncatalytic heteroheneours solid-fluid reaction models, Ind. Eng. Chem. 60 (1968), 9, 34-54.

[48] Steffen, R., Direct reduction and smelting reduction - an overview, Steel Research 60 (1989), 3-4, 96-103.

[49] Steinmetz, E., R. Steffen and R. Thielmann, Stand und Entwicklung der Verfahren zur Direktreduktion und Schmelzreduktion von Eisenerzen, Stahl und Eisen 106 (1986), 9, 421-429.

[50] Fang, J., Stickingprobleme im Fluidatbett zur Schmelzreduktion, Dissertation, Rheinisch-Westfälische Technische Hochschule Aachen, Fakultät für Bergbau, Hüttenwesen und Geowissenschaften (1988).

[51] Aran, A. A., Verhinderung von Sticking bei der Eisenreduktion in Fluidatbetten von abgestimmten Erzmischungen, Dissertation, Rheinisch-Westfälische Technische Hochschule Aachen, Institut für Eisenhüttenkunde, (1975).

[52] Fang, J., R. J. De Faria, C. E. R. De Carvalho and P. S. Assis, Research on sticking prevention during reduction in a mixed fluidized bed, 1st International Meeting on Ironmaking, Belo Horizonte, MG, Brasil, 24th-26th Sept. (2001), 284-292.

[53] Gudenau, H. W., M. Hirsch, H. Denecke and R. Degel, Direktreduktion von Feineisenerzen in der Wirbelschicht mit wasserstoffreichem Gas, Stahl und Eisen 117 (1997), 4, 91-99.

[54] Wenzel, W., H. W. Gudenau and A. A. Aran, Reduction of Iron Ores in Multi-Component Fluidised Beds, Klepzig Fachber. 81 (1974), 1, 3-7.

[55] Gudenau, H. W., S. M. Kim, J. Fang and U. Gebel, Smelting reduction by Fluidized Beds, International Conference on New Smelting Reduction and Near Net Shape Casting Technologies for Steel 1 (1990), 149-165.

[56] Gudenau, H. W., J. Hochhaus and R. Degel, Stickingerscheinungen während der Reduktion von Eisenerzen in der Wirbelschicht, 9. Aachener Stahlkolloquium (1994).

[57] Degel, R., Eisenerzreduktion in der Wirbelschicht mit wasserstoffreichen Gasen – Sticking und Ansatzbildung, Dissertation, Rheinisch-Westfälische Technische Hochschule Aachen, Institut für Eisenhüttenkunde, (1996).

[58] Zhang, B., X. Gong, Z. Wang and Z. Guo, Relation between Sticking and Metallic Iron Precipitation on the Surface of Fe_2O_3 Particles Reduced by CO in the Fluidized Bed, ISIJ International 51 (2011), 9, 1403-1409.

[59] Zhong, Y. W., Z. Wang, X. Z. Gong and Z. C. Guo: Sticking behavior caused by sintering in gas fluidisation reduction of haematite, Ironmaking & Steelmaking 39 (2012), 1, 38-44.

[60] Langston, B. G. and F. M. Stephens, Self-agglomerating fluidized-bed reduction, Journal of Metals 12 (1960), 312-316.

[61] Schiller, M., Die Mikromorphologie der Eisenphase als Folge der Reduktion von Eisenoxiden, Dissertation, Rheinisch-Westfälische Technische Hochschule Aachen, Institut für Eisenhüttenkunde, (1987).

[62] Wezel, W. and H. W. Gudenau, Das Sticking bei der Fluidatbettreduktion von Eisenerzen - Der Einfluß der Ausscheidungsart des Eisens, Aufbereitungstechnik (1972), 9, 568-572.

[63] Wortberg, E. J., Die Eisengewinnung mit Elektrolysewasserstoff unter Verwendung von Kernenergie, Dissertation, Rheinisch-Westfälische Technische Hochschule Aachen, (1971).

[64] Ezz, S. Y., Gaseous reduction of fine iron ore in the fluidized state, Transactions of the Metallurgical Society of AIME 218 (1960), 8, 709-715.

[65] Gudenau, H. W., W. G. Burchard and M. Schiller, Ausscheidungsverhalten von Eisen auf Wüstit während der Reduktion, Prozeßkinetik und Prozeßtechnik im Hüttenwesen DFG-Sonderband (1986), 143-154.

[66] Wenzel, W., H. W. Gudenau and A. Aran: Reduction of Iron ore Fluidized beds, Tetsu-To-Hagané 59 (1973).

[67] Eisen, H. P., Einflüsse der Morphologie und der Atmosphäre auf das Sinterverhalten von Eisenpulvern, Dissertation, Rheinisch-Westfälische Technische Hochschule Aachen, (1991).

[68] Hayashi, S. and Y. Iguchi, Morphology of iron reduced from wustite with H_2-H_2O-2S-mixtures, Transactions ISIJ 29 (1989), 596-604.

[69] Nicolle, R. and A. Rist, The mechanism of whisker growth in the reduction of wustite, Metallurgical Transaction B 10 (1979), 3, 429-438.

[70] Bleifuss, R. L., Calcium as a cause of catastrophic swelling of pellets during reduction, Transactions of the Metallurgical Society of AIME 274 (1970), 9, 225-231.

[71] Gebel, U. J., Einfluss von Fremdphasen auf das Ausscheidungsverhalten von Eisen während der Reduktion von Eisenoxid, Dissertation, Rheinisch-Westfälische Technische Hochschule Aachen, (1989).

[72] Möhlmann, H. H., K. Koch and R. G. Ward, Swelling Behaviour During Reduction of Haematite Samples With Additions of Na_2O, K_2O, CaO, MgO or SiO_2, Arch. Eisenhüttenwesen 47 (1976), 11, 647-651.

[73] Hayashi, S. and Y. Iguchi, Influence of gaseous sulfur on hydrogen reduction of wustite added with foreign oxides, ISIJ International 32 (1992), 10, 1066-1075.

[74] Komatina, M. and H. W. Gudenau, The sticking problem during direct reduction of fine ore in the fluidized bed, Association of Metallurgical Engineers Serbia and Montenegro UDC:669.1.094-175-492.3, (2004), 309-328.

[75] Burghardt, O. and H. Kortmann, Prüfung von Einsatzstoffen für die Dirketreduktion, Stahl und Eisen 100 (1980), 24, 1432-1438.

[76] Papst, G., J. Sittard and G. Thaning, Dolomite-Fluxed Iron Ore Pellets for Direct Reduction Process, Skil. Min. Rev. 70 (1981), 393-399.

[77] Mathisson, G., Eisenerzpellets für die Direktreduktion, Stahl und Eisen 100 (1980), 7.

[78] Hayashi, S. and Y. Iguchi, Factors Aftecting the Sticking of Fine Iron Ores during Fluidized Bed Reduction, ISIJ International 32 (1992), 9, 962-971.

[79] Hayashi, S., S. Sawai and Y. Iguchi, Influence of Coating Oxide and Sulfur Pressure on Sticking during Fluidized Bed Reduction of Iron Ores, ISIJ International 33 (1993), 10, 1078-1087.

[80] Möhlmann, H. H., K. Koch and R. G. Ward, Untersuchungen zum Schwellverhalten bei der Reduktion von Hämatitproben mit Zuschlägen an Natrium-, Kalium-, Calcium-, Magnesiumoxid sowie Kieselsäure, Arch. Eisenhüttenwesen 47 (1976), 11, 647-651.

[81] Grandsen, J. F. and J. S. Sheasby, The sticking of iron ore during reduction by hydrogen in a fluidized bed, Canadian Metallurgical Quarterly 13 (1974), 4.

[82] Gudenau, H. W., H. -P Eisen, Y. Qi and G. Steinbeck, Sticking von Feinerz in der Wirbelschicht zur Schmelzreduktion, Stahl und Eisen 111 (1991), 9, 47-52.

[83] Jander, G., K. F. Jander and H. Knoll, Maßanalyse- Theorie Und Praxis Der Klassischen Und Elekrochemischen Titrierverfahren, Sammlung Göschen, Berlin und New York, (1973).

[84] Jander, G., K. F. Jahr, G. Schulze and J. Simon, Maßanalyse, 16th ed., de Gruyter, Berlin, New York, (2003).

[85] Schwalbach, W., Seminar Anorganische Chemie, Quantitative Bestimmung von Eisen nach Reinhardt-Zimmermann, www.biomedizinischechemie.de, (2011).

[86] International Standard ISO 5416, Direct reduced iron - Determination of metallic iron - Bromine-methanol-titrimetic method, (2006).

[87] International Standard ISO 10835:2007, Direct reduced iron and hot briquetted iron – sampling and sample preparation, (2007).

[88] Böcker, J., Spektroskopie, 1st ed., Vogel Buchverlag, Berlin, (1997).

[89] Puxbaum, H. and E. Rosenberg, Vorlesung analytische Chemie I, Montanuniversitaet Leoben, Lehrstuhl für allgemeine und analytische Chemie, (2005).

[90] Yang, W. C., Handbook of fluidization and fluid-particle systems, Siemens Westinghouse Power Corporation (2003).

[91] DIN 66165-1:1987-04, Partikelgrößenanalyse, Siebanalyse, Grundlagen, Beuth (1987).

[92] DIN 66165-2:1987-04, Partikelgrößenanalyse, Siebanalyse, Durchführung, Beuth (1987).

[93] International Standard ISO 4701:2008, Iron ores and direct reduced iron - Determination of size distribution by sieving, (2008).

[94] Brunauer, S., P. H. Emmett and E. Teller, Adsorption of Gases on Molecular Layers, Journal of the American Chemical Society 60 (1938), 2, 309-319.

[95] DIN ISO 9277:2003-05, Bestimmung der spezifischen Oberfläche von Feststoffen durch Gasadsorption nach dem BET-Verfahren, (2003).

[96] Klank, D., Produktgestaltung in der Partikeltechnologie, Frauenhofer-IRB-Verlag, Stuttgart, (2008).

[97] Baumann, L. and O. Leeder, Einführung in Die Auflichtmikroskopie, Deutscher Verlag für Großstoffindustrie GmbH, Leipzig, (1991).

[98] Rantitsch, G., Dünnschliffpräparation, Geowissenschartliche Arbeitsmethoden, Montanuniversitaet Leoben, Chair of Geology, Leoben, (2008).

[99] Morris, R. C. and K.H. Wolf (Ed.), Genesis of Iron Ore in Banded Iron-Formation by Supergene and Supergene-Metamorphic Processes - a Conceptual Model, in: Handbook of Strata-Bound and Stratiform Ore Deposits, 13th ed., Amsterdam, Oxford, New York, Tokyo, (1985), 73-235.

[100] Weiss, B. et al., Structural and morphological changes during reduction of hematite to magnetite and wustite in hydrogen rich reduction gases under fluidised bed conditions, Ironmaking & Steelmaking Vol. 38 (2011), 1, 65-73.

[101] Weiss, B., Charakterisierung der Reaktionskinetik von Hämatit mit H_2-reichen Gasgemischen bei hohem Druck, Master Thesis, TU Wien (2006).

[102] Weiss, B., J. Sturn, S. Schuster, F. Winter and J. L. Schenk, Comparisation of the Reduction Kinetics of Hematite with CO-rich and H_2-rich Gases at Elevated Pressures, SteelSim, Graz, Austria, Sept. (2007).

[103] Pawlik, C., N. Eder, A. Thurnhofer, et al., Characterization of the Reduction of Iron Ore Fines with CO-rich Gases under Pressurized Fluidized Bed Conditions, IFSA, Johannesburg, South Africa, November (2005).

[104] Pawlik, C., et al, Reduction of Iron Ore Fines with CO-rich Gases under Pressurized Fluidized Bed Conditions, ISIJ International 47 (2007), 2, 217-225.

[105] Habermann, A., et al., An experimental study on the kinetics of fluidized bed iron ore reduction, ISIJ International 40 (2000), 10, 935-942.

[106] Schuster, S., C. Pawlik, F. Winter, H. Mali, H. Fischer and J. L. Schenk, Reduction of Iron Ores With CO-rich and H2-rich Gases: A Detailed Evaluation for Industrial Fluidized Bed Processes, AISTech (2006), 1, 297-307.

[107] Schuster, S., et al., Die Direktreduktion von Feinerzen in Druckwirbelschichtreaktoren: Experimentelle Untersuchung und morphologische Betrachtung zur Übertragung auf industrielle Prozesse, Berg und Hüttenmännisches Monatsheft 151 (2006), 11, 462-468.

[108] Schuster, S, C. Pawlik, F. Winter, H. Mali, H. Fischer and J. L. Schenk, Reduction Kinetics of Coarse Hematite Iron Ore in Fluidized Bed Reaktors at Elevated Pressures, FBC Conference, Vienna, Austria, May (2006).

[109] Thurnhofer, A., et al., Iron Ore Reduction in a Laboratory-scale Fluidized Bed Reactor - Effect of Pre-reduction on Final Reduction Degree, ISIJ International 45 (2005), 2, 151-158.

[110] Thurnhofer, A., Memory-Effekte von Eisenerzen bei hohen Drücken und Temperaturen, Dissertation, TU Wien (2004).

[111] Feilmayr, C., et al., Reduction Behavior of Hematite to Magnetite under Fluidized Bed Conditions, ISIJ International 44 (2004), 7, 1125-1133.

[112] Sturn, J., B. Weiss, F. Winter and J. L. Schenk, Kinetic Modeling of Iron Ore Fines Reduction with H_2-rich Gases in Fluidized Beds at Elevated Pressures: From Hematite to Magnetite, AISTech (2008).

[113] Hauzenberger, F., J. Reidetschläger, J. L. Schenk and H. Mali, Methods for Assessing the Properties of Fine Iron Ores for Reduction Processes, BHM 149 (2004), 11, 385-392.

[114] Gudenau, H.W., Eisenerzreduktion in der Wirbelschicht mit wasserstoffreichen Gasen, Europäische Kommission - Technische Forschung Stahl, Luxenburg, (1998).

[115] Hutchings, K. M., J. D. Smith, S. Yoruk and R. J. Hawkins, Reduction of Hematite in a Bubbling Fluidized Bed Using H_2 , CO, and H_2 -CO Mixtures, Ironmaking and Steelmaking 14 (1987), 3, 103-109.

[116] Kang, H. W., W. S. Chung and T. Murayama, Effect of iron ore size on kinetics of gaseous reduction, ISIJ International 38 (1998), 2, 109-115.

[117] Mali, H., Evolution of minerals and structures in the Fior, Finmet and Finex processes, Montanuniversitaet Leoben, Department of Geosciences and Geophysics, (2011).

[118] Kohl, H. K. and H. J. Engell, Über die Reduktion von Wüstit mit Wasserstoff, Archiv für das Eisenhüttenwesen 34 (1963), 411-418.

[119] Hollemann, A. F. and E. Wiberg, Lehrbuch Der Anorganischen Chemie, 101st ed., De Gruyter, Berlin, (1995).

[120] Bargel, H. and G. Schulze, Werkstoffkunde, 7th ed., Springer Verlag, Berlin, Heidelberg, (2000).

[121] Kunii, D. and O. Levenspiel, Fluidization Engineering, 2nd ed., Butterworth-Heinemann, Boston, London, Singapore, Sydney, Toronto, Wellington, (1991).

[122] Fitting, A. and M. Hirsch, Industrielle Anwendung der zirkulierenden Wirbelschicht. Metall 44 (1990), 2, 140-147.

[123] Lehner, M., Vorlesung zu Mechanische Verfahrenstechnik. Montanuniversitaet Leoben, Institut für Verfahrenstechnik des industriellen Umweltschutzes, (2010).

[124] Szekely, J., J. W. Evans and H. Y. Sohn, Gas-Solid Reactions, Academic Press, New York, London, Toronto, Sydney, San Francisco, (1976).

[125] PSRI Fluidization Seminar & Workshop, Puerto Ordaz, Venezuela (1996).

[126] Molerus, O., Fluid-Feststoff-Strömungen - Strömungsverhalten Feststoffbeladener Fluide Und Kohäsiver Schüttgüter, Springer Verlag, Berlin, Heidelberg, New York, (1982).

[127] Gudenau, H. W., Eisehüttenmännische Verfahrenstechnik - Vom Erz Zum Stahl, Druck- und Verlagshaus Mainz GmbH, Aachen, Germany, (1989).

[128] Gottschalk, A., Grundlagen der Wirbelschichttechnologie, Keramische Zeitschrift 39 (1987), 5, 308-308.

[129] Werther, J., Grundlagen der Wirbelschichttechnologie, GVC-Dezembertagung, GVC VDI Gesellschaft Verfahrenstechnik und Chemieingineurwesen (1986), 233-255.

[130] Werther, J. and D. Bellgradt, Feststofftransport und –verteilung in der Wirbelschichtfeuerung, VDI Berichte 601 (1986), 475-490.

[131] Reuter, H., Durchbruch um Blasen im Gas-Feststoff-Fließbett, Chem.-Ing.-Tech. 55 (1983), 2, 87-93.

[132] Muschelknautz, E.*, et al.,* Technik der Gas/Feststoffströmung, VDI-GVC (1981).

[133] Reh, L., Vorlesung zu Mechanische Verfahrenstechnik I, Eidgenössische Technische Hochschule Zürich, Institut für Verfahrenstechnik, Zürich (1998).

[134] International Standard ISO 9276-2:2001, Representation of results of particle size analysis – Part 2: Calculation of average particle sizes, diameters and moments from particle size distribution, (2001).

[135] Themelis, N. J.: Rate phenomena in process metallurgy, Wiley-VCH Verlag GmbH & Co., (1971).

[136] Geiger, G. H. and D. R. Poirer, Transport Phenomena in metallurgy, (1973).

[137] Szekely, J., Fluid Flow Phenomena in Metals Processing, AcademicPress (1979).

[138] Tipler, P. A.: Physik, Spektrum akademischer Verlag, Heidelberg, Berlin, Oxford, (1991).

[139] Verein Deutscher Ingenieure VDI-Gesellschaft Verfahrenstechnik und Chemieingenieurwesen (GVC): VDI-Wärmeatlas - Berechnungsblätter für den Wärmeübergang, (2002), 1510.

[140] Reh, L., Mechanische Verfahrenstechnik, Eidgenössische Technische Hochschule Zürich, Institut für Verfahrenstechnik, Zürich (1998).

[141] DIN EN ISO/IEC 17025:2005, Allgemeine Anforderungen an die Kompetenz von Prüf- und Kalibrierlaboratorien, (2005).

[142] Weiss, B., Charakterisierung der Reaktionskinetik von Hämatit mit H2-reichen Geasgemischen bei hohem Druck, Master Thesis, TU Wien (2006).

[143] Feinman, J., Kinetics of Hydrogen Reduction of Iron Ore in a Batch-fluidized Bed, I&EC Process Design and Development 3 (1964), 3, 241-247.

[144] Chung, U. C., I. O. Lee, H. G. Kim, V. Sahajvalla and W. B. Chung, Degradatioin Characteristics of Iron Ore Fines of a Wide Size Distribution in Fluidized Bed Reduction, ISIJ International 38 (1998), 9, 943-952.

[145] Reifferscheid, M., Y. K. Xie and K. H. Tacke, Hydrogen reduction of iron ore fines in stationary fluidised beds, International Symposium on Global Environmental Iron and Steel Industry, Beijing, China, April (1998).

[146] Weiss, B., et al, Reduction Kinetics of Coarse Hematite in Pressurized Fluidized Beds, Association for Iron & Steel Technology, Warrendale, USA (2007).

[147] Stahlinstitut VDEh, Jahrbuch Stahl 2006 1 (2005) 571.

[148] Hochleitner, R., GU-Kompass: Mineralien, 7th ed., Graefe & Unzer, (1999).

[149] Skorianz, M., H. Mali, J. F. Plaul, J. L. Schenk and C. Thaler, Classification of fine ores regarding their reducibility with tests in a lab scale fluidized bed reactor and petrographical analysis, AISTech, Atlanta, USA, (2012), 531-542 .

[150] Skorianz, M., H. Mali, J. L. Schenk, J. F. Plaul, M. B. Hanel and A. Pichler, Mineralogical and structural evolution of iron ore fines reduced in a lab scale fluidized bed reactor, International Congress on the Science and Technology of Ironmaking ICSTI, Rio de Janeiro, Brazil, (2012), 2347-2359.

[151] Skorianz, M., H. Mali, J. L. Schenk, J. F. Plaul, B. Weiss and M. B. Hanel, Evaluation of reducibility of iron ore fines by reduction tests under fluidized bed conditions and petrographical investigations, Asia Steel Conference, Beijing, China (2012).

[152] Oeters, F., Metallurgie Teil 1: Eisenerzeugung, Verlag Stahleisen mbH, Düsseldorf, Germany, (1982), 63.

[153] Cepheiden, Atom model for EDX, http://de.wikipedia.org/w/index.php?title=Datei: Atom_model_for_EDX_DE., 14. Nov. (2008).

[154] Raupenstrauch, H., Vorlesung zu Brennstoff- und Verbrennungstechnik, Montanuniversitaet Leoben, Lehrstuhl für Thermoprozesstechnik, (2009).

[155] Rud, H. G. Mauschitz and W. Höflinger, Transmitted-light microscopy – a new method for surface structure analysis of cleanable non-woven dust filter media, Journal of Hazardous Materials 144 (2007), 3, 742-746.

[156] Kolb, F., Beitrag zur Entwicklung einer standardisierten Methodik zur Bewertung von rohen und teilreduzierten Eisenerzen, Bachelor Thesis, Montanuniversitaet Leoben, Chair of Metallurgy, to be published in (2013).

[157] Krenn, A., and T. Pfeifer, Bewertung von chemischen Analysemethoden zur Bestimmung von Eisen und Eisenoxid-Phasen mittels Ringversuch, Bachelor Thesis, Montanuniversitaet Leoben, Chair of Metallurgy, to be published in (2013).

Appendix

A.1 Publications and reports (related to the research work)

Contribution to conference proceedings:

Skorianz, M., H. Mali, J. F. Plaul, J. L. Schenk and C. Thaler, Classification of fine ores regarding their reducibility with tests in a lab scale fluidized bed reactor and petrographical analysis, AISTech, Atlanta, USA, (2012), 531-542.

Skorianz, M., H. Mali, J. L. Schenk, J. F. Plaul, M. B. Hanel and A. Pichler, Mineralogical and structural evolution of iron ore fines reduced in a lab scale fluidized bed reactor, International Congress on the Science and Technology of Ironmaking ICSTI, Rio de Janeiro, Brasil, (2012), 2347-2359.

Skorianz, M., H. Mali, J. L. Schenk, J. F. Plaul, B. Weiss and M. B. Hanel, Evaluation of reducibility of iron ore fines by reduction tests under fluidized bed conditions and petrographical investigations, Asia Steel Conference, Beijing, China, (2012).

Presentations at conferences and scientific boards:

Skorianz, M., Classification of fine ores regarding their reducibility with tests in a lab scale fluidized bed reactor and petrographical analysis, VDEh Ausschuss für metallurgische Grundlagen, Leoben, Austria, (2011), July 14th-15th.

Skorianz, M., H. Mali, J. F. Plaul, J. L. Schenk and C. Thaler, Classification of fine ores regarding their reducibility with tests in a lab scale fluidized bed reactor and petrographical analysis, AISTech, Atlanta, USA, (2012), May 7th–10th.

Skorianz, M. and M. Hanel, Development of methods for the evaluation of iron ore reduction behavior for the optimization of ironmaking processes, European Mineral Resources Conference EUMICON, Leoben, Austria, (2012), September 19th–21st.

Skorianz, M., H. Mali, J. L. Schenk, J. F. Plaul, B. Weiss and M. B. Hanel, Evaluation of reducibility of iron ore fines by reduction tests under fluidized bed conditions and petrographical investigations, Asia Steel Conference, Beijing, China, (2012), September 23rd–27th.

Skorianz, M. and M. Hanel, Development of methods for the evaluation of iron ore reduction behavior for the optimization of ironmaking processes, Seminário Técnico Internacional, Universidade Federal de Ouro Preto, Ouro Preto, Brasil, (2012), October 9th–12th.

Skorianz, M., H. Mali, J. L. Schenk, J. F. Plaul, M. B. Hanel and A. Pichler, Mineralogical and structural evolution of iron ore fines reduced in a lab scale fluidized bed reactor, International Congress on the Science and Technology of Ironmaking ICSTI, Rio de Janeiro, Brasil, (2012), October 14th–18th.

Research reports (not accessible):

Karasangabo, A., M. Skorianz and C. Thaler, Characterisation of raw materials for use in the FINEX® process, Chair of Metallurgy, Montanuniversitaet Leoben, Austria, 2010.

Thaler, C., M. Skorianz and J. L. Schenk, Literature and Research Study - Usage of Ultra Fine Ore in the FINEX®-Process, Chair of Metallurgy, Montanuniversitaet Leoben, Austria, 2010.

Gruber, C., N. Voller, E. Bäck and M. Skorianz, Vergleich von Analyseverfahren zur Bestimmung von Eisenoxiden, Chair of Metallurgy, Montanuniversitaet Leoben, Austria, 2011.

Skorianz, M., C. Thaler and J. L. Schenk, Interim Report – Enhancement of Competitiveness of the FINEX® -Technology, Chair of Metallurgy, Montanuniversitaet Leoben, Austria, 2011.

Thaler, C., M. Skorianz, M. Hanel and J. L. Schenk, Final Report – Enhancement of Competitiveness of the FINEX®-Technology - Phase 2, Chair of Metallurgy, Montanuniversitaet Leoben, Austria, 2011.

Schmidt, L., M. Skorianz, M. B. Hanel and J. L. Schenk, The Optimization of Fluidized Bed Reducing Reactor and Technology for the Use of Ultra Fine Ores for FINEX® Process - Interim Report, Chair of Metallurgy, Montanuniversitaet Leoben, Austria, 2012.

A.2 Index of figures

A.3 Index of tables

A.4 Test methodology

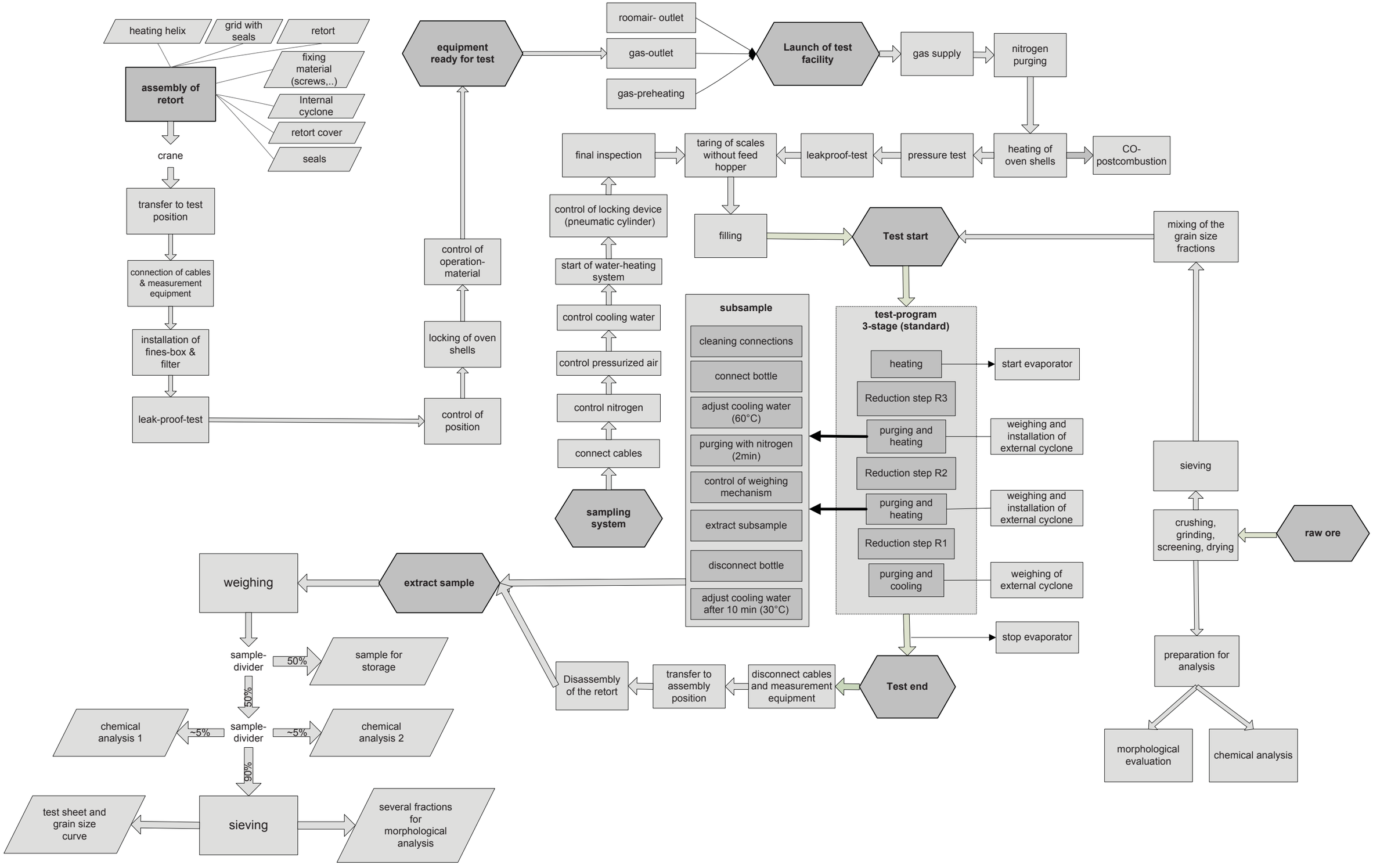
heating helix
grid with seals
retort
fixing material (screws,..)
Internal cyclone
retort cover
seals
assembly of retort
crane
transfer to test position
connection of cables & measurement equipment
installation of fines-box & filter
leak-proof-test
control of position
locking of oven shells
control of operation-material
equipment ready for test
roomair- outlet
gas-outlet
gas-preheating
Launch of test facility
gas supply
nitrogen purging
heating of oven shells
CO-postcombustion
pressure test
leakproof-test
taring of scales without feed hopper
final inspection
control of locking device (pneumatic cylinder)
start of water-heating system
control cooling water
control pressurized air
control nitrogen
connect cables
sampling system
filling
Test start
mixing of the grain size fractions
subsample
cleaning connections
connect bottle
adjust cooling water (60°C)
purging with nitrogen (2min)
control of weighing mechanism
extract subsample
disconnect bottle
adjust cooling water after 10 min (30°C)
test-program 3-stage (standard)
heating
start evaporator
Reduction step R3
purging and heating
weighing and installation of external cyclone
Reduction step R2
purging and heating
weighing and installation of external cyclone
Reduction step R1
purging and cooling
weighing of external cyclone
stop evaporator
Test end
disconnect cables and measurement equipment
transfer to assembly position
Disassembly of the retort
extract sample
weighing
sample-divider
50%
sample for storage
50%
sample-divider
~5%
chemical analysis 1
~5%
chemical analysis 2
90%
sieving
test sheet and grain size curve
several fractions for morphological analysis
sieving
crushing, grinding, screening, drying
raw ore
preparation for analysis
morphological evaluation
chemical analysis

A.5 Interlaboratory test

Sample No.			Sample 1								Sample 2								Sample 3								Sample 4								total deviation average [%]	total st.dev. [%]
Prepared sample	Sample specification		Species Fe_3O_4		Fe [%]	FeO [%]	Fe_3O_4 [%] 100		RD = 11,1		Species Fe,Fe_3O_4		Fe [%] 59	FeO [%]	Fe_3O_4 [%] 41		RD = 70,3		Species FeO,Fe_3O_4		Fe [%]	FeO [%] 62	Fe_3O_4 [%] 38		RD = 25,2		Species Fe,FeO,Fe_3O_4		Fe [%] 21	FeO [%] 54	Fe_3O_4 [%] 25		RD = 45,6			
	Chemical composition [%]	Fe_{tot}	72,36	72,36	72,36	72,36	72,36	72,36			88,67	88,67	88,67	88,67	88,67	88,67			75,69	75,69	75,69	75,69	75,69	75,69			81,07	81,07	81,07	81,07	81,07	81,07				
		Fe_{met}	0,00	0,00	0,00	0,00	0,00	0,00			59,00	59,00	59,00	59,00	59,00	59,00			0,00	0,00	0,00	0,00	0,00	0,00			21,00	21,00	21,00	21,00	21,00	21,00				
		Fe^{2+}	24,12	24,12	24,12	24,12	24,12	24,12			9,89	9,89	9,89	9,89	9,89	9,89			57,36	57,36	57,36	57,36	57,36	57,36			48,01	48,01	48,01	48,01	48,01	48,01				
		Fe^{3+}	48,24	48,24	48,24	48,24	48,24	48,24			19,78	19,78	19,78	19,78	19,78	19,78			18,33	18,33	18,33	18,33	18,33	18,33			12,06	12,06	12,06	12,06	12,06	12,06				
Chemical analyses	Laboratories		A	B	C	D	E	F	average	st.dev.	A	B	C	D	E	F	average	st.dev.	A	B	C	D	E	F	average	st.dev.	A	B	C	D	E	F	average	st.dev.		
	Results chemical analyses [%]	Fe_{tot}	73,15	73,10	71,50	73,30	73,48	72,48	72,84	**0,74**	87,60	87,95	87,20	87,35	87,92	89,27	87,88	**0,74**	74,45	75,00	74,35	74,50	74,69	76,64	74,94	**0,86**	80,65	79,91	79,70	79,60	80,24	81,530	80,27	**0,73**		
		Fe_{met}	2,94	2,10	0,70	2,01	2,23	0,10	1,68	**1,06**	57,10	58,30	61,70	57,40	56,22	57,70	58,07	**1,91**	1,35	0,90	1,35	0,95	1,51	1,10	1,19	**0,25**	22,15	20,30	22,45	20,65	22,01	21,200	21,46	**0,87**		
		Fe^{2+}	24,90	24,90	15,60	24,07	30,14	11,36	21,83	**6,95**	5,61	5,90	3,80	4,81	10,33	5,21	5,94	**2,27**	40,80	48,00	45,70	44,58	47,82	46,43	45,56	**2,66**	41,45	42,20	38,90	39,93	41,12	41,770	40,90	**1,24**		
		Fe^{3+}	45,35	46,10	55,20	47,22	41,11	61,02	49,33	7,34	24,90	23,70	21,60	25,14	21,37	26,36	23,85	2,02	32,30	26,10	27,35	28,96	25,36	29,11	28,20	2,51	17,05	17,40	18,30	19,00	17,11	18,560	17,90	0,83		
Deviations composition vs. chem. allysis	deviation absolute	Fe_{tot}	0,79	0,74	-0,86	0,94	1,12	0,12	**0,47**	**0,74**	-1,07	-0,72	-1,47	-1,32	-0,75	0,60	**-0,79**	**0,74**	-1,24	-0,69	-1,34	-1,19	-1,00	0,95	**-0,75**	**0,86**	-0,42	-1,16	-1,37	-1,47	-0,83	0,46	**-0,79**	**0,73**		
		Fe_{met}	2,94	2,10	0,70	2,01	2,23	0,10	**1,68**	**1,06**	-1,90	-0,70	2,70	-1,60	-2,78	-1,30	**-0,93**	**1,91**	1,35	0,90	1,35	0,95	1,51	1,10	**1,19**	**0,25**	1,15	-0,70	1,45	-0,35	1,01	0,20	**0,46**	**0,87**		
		Fe^{2+}	0,78	0,78	-8,52	-0,05	6,02	-12,76	**-2,29**	**6,95**	-4,28	-3,99	-6,09	-5,08	0,44	-4,68	**-3,95**	**2,27**	-16,56	-9,36	-11,66	-12,78	-9,54	-10,93	**-11,80**	**2,66**	-6,56	-5,81	-9,11	-8,07	-6,89	-6,24	**-7,11**	**1,24**		
		Fe^{3+}	-2,89	-2,14	6,96	-1,02	-7,13	12,78	1,09	7,34	5,12	3,92	1,82	5,36	1,59	6,58	4,07	2,02	13,97	7,77	9,02	10,63	7,03	10,78	9,87	2,51	4,99	5,34	6,24	6,94	5,05	6,50	5,84	0,83		
	deviation in percentage	Fe_{tot}	1,09	1,02	-1,19	1,30	1,55	0,16	**0,66**	**1,02**	-1,20	-0,81	-1,66	-1,49	-0,84	0,68	**-0,89**	**0,84**	-1,64	-0,91	-1,77	-1,57	-1,32	1,25	**-0,99**	**1,14**	-0,51	-1,43	-1,68	-1,81	-1,02	0,57	**-0,98**	**0,90**	**-0,55**	**1,13**
		Fe_{met}	2,94	2,10	0,70	2,01	2,23	0,10	**1,68**	**1,06**	-3,22	-1,19	4,58	-2,71	-4,71	-2,20	**-1,58**	**3,23**	1,35	0,90	1,35	0,95	1,51	1,10	**1,19**	**0,25**	5,48	-3,33	6,90	-1,67	4,81	0,95	**2,19**	**4,17**	**0,87**	**2,86**
		Fe^{2+}	3,23	3,23	-35,32	-0,20	24,96	-52,90	**-9,50**	**28,81**	-43,27	-40,34	-61,57	-51,35	4,46	-47,32	**-39,90**	**22,96**	-28,87	-16,32	-20,33	-22,27	-16,63	-19,05	**-20,58**	**4,64**	-13,66	-12,09	-18,97	-16,81	-14,34	-12,99	**-14,81**	**2,59**	**-21,20**	**20,51**
		Fe^{3+}	-5,99	-4,44	14,43	-2,12	-14,78	26,49	2,27	15,22	25,89	19,83	9,21	27,11	8,05	33,27	20,56	10,19	76,20	42,38	49,20	57,98	38,34	58,80	53,82	13,67	41,37	44,28	51,74	57,58	41,87	53,90	48,46	6,85	**31,27**	**23,63**

Kommentare:

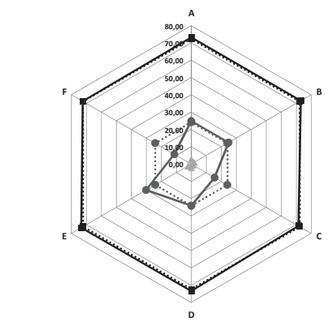

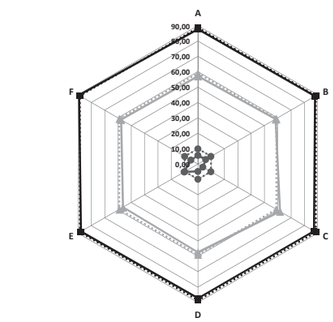

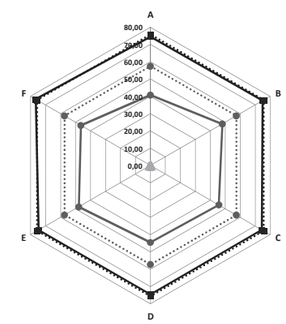

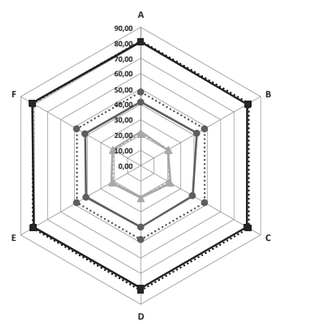

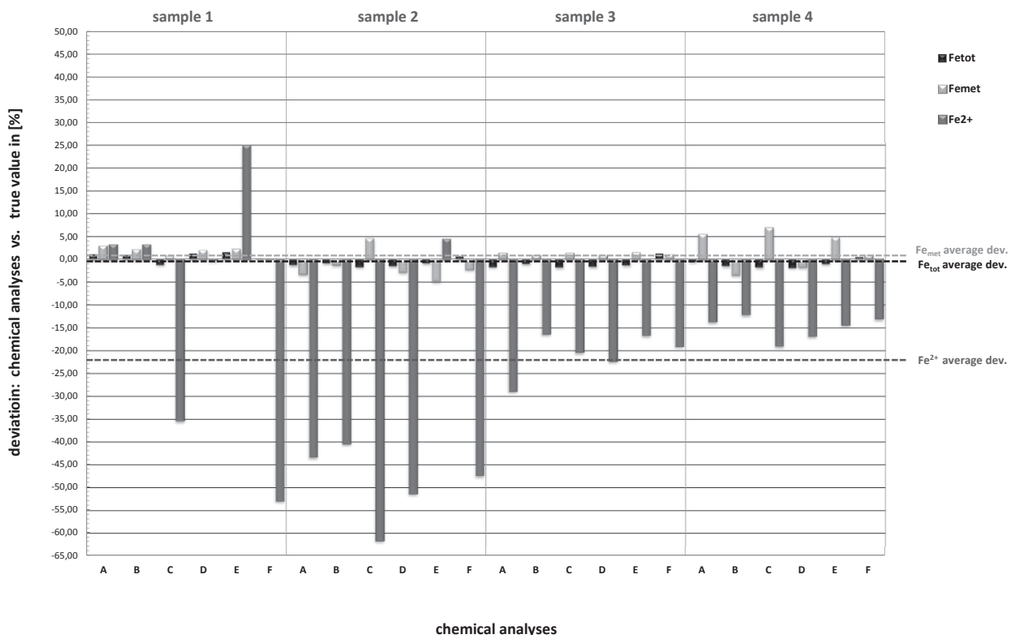

A.6 Test documentation

CHAIR OF METALLURGY
MONTANUNIVERSITAET LEOBEN
PRIMARY METALLURGY
METALLURGICAL PROCESSES

Tel.: +43 3842 402-2201 Fax: DW 2202
Web: http://www.metallurgy.ac.at

160 mm Fluidized Bed Reactor test
Process conditions and test parameter

Test number: **Test A** **Date:**
Customer: Siemens VAI

Kind of test: 3-stage 660/750/760°C FINEX
Target of the test: reduction behaviour of hematite

Test carried out by: Michael Skorianz Dial: 2255
michael.skorianz@unileoben.ac.at

Raw material input

sieves	sieve analyis		input	comments
mesh size [mm]	fraction [%]	cum. [%]	mass [g]	
4-6,3	0		0,0	
2,8-4	13,3	100	465,5	
1,0-2,8	13,3	86,7	465,5	
0,5-1,0	16	73,4	560,0	hamersley fine ore MUL2010/0008
0,25-0,5	17,4	57,4	609,0	
0,125-0,25	14,7	40	514,5	
0,063-0,125	25,3	25,3	885,5	
0-0,063	0	0	0,0	
sum	100,0		3500,0	

chemical analyses

raw material: hamersley fine ore MUL2010/0008			
species	[%]	species	[%]
Fe(tot)	63,60	Na2O	0,00
FeO	0,58	Mn	0,17
Al2O3	2,07	Ni	0,00
SiO2	3,48	Cu	0,00
CaO	0,01	Cr	0,00
MgO	0,01	S	0,01
TiO2	0,12	P	0,07
K2O	0,01	Zn	0,00
V2O5	0,00	LOI (900°	3,30

reduced material						
species	bed Ø [%]	<0,063 [%]	0,25-0,50 [%]	1,0-2,8 [%]	int.cyc. [%]	ex.cyc. [%]
Fe tot	86,8	0,0	0,0	0,0	86,3	0,0
Fe met	79,8	0,0	0,0	0,0	70,8	0,0
FeO	7,0	0,0	0,0	0,0	15,0	0,0
C tot	1,700	0,000	0,000	0,000	0,920	0,000
MD	92,0	0,0	0,0	0,0	82,0	0,0
RD (CA)	94,1	0,0	0,0	0,0	86,5	0,0
RD (cal)	77,1	0,0	0,0	0,0	0,0	0,0
FeOx	0,1	0,0	0,0	0,0	0,0	0,0
Fe bal.	103,4	0,0	0,0	0,0	0,0	0,0

calculation of test parameter: 3-stage 660/750/760°C FINEX

	gas composition	concentration, temp. plant R1 [%]	R2 [%]	R3 [%]	R4 [%]	concentration test rig R1 [%]	R2 [%]	R3 [%]	R4 [%]	gas flow test rig R1 [Nl/min]	heating [Nl/min]	R2 [Nl/min]	heating [Nl/min]	R3 [Nl/min]	heating [Nl/min]	R4 [Nl/min]
species	H2	20,4%	20,0%	16,4%	0,00%	20,4%	20,0%	16,4%	0,0%	**78,9**		**78,1**		**70,0**		**0,0**
	H2O	1,7%	7,4%	9,2%	0,00%	1,7%	7,4%	9,2%	0,0%	**6,7**		**28,8**		**39,5**		**0,0**
	CO	45,7%	44,8%	33,5%	0,00%	45,7%	44,9%	33,5%	0,0%	**176,6**		**175,2**		**143,4**		**0,0**
	CO2	4,0%	16,5%	23,6%	0,00%	4,0%	16,5%	23,6%	0,0%	**15,5**		**64,6**		**100,9**		**0,0**
	CH4	0,0%	0,0%	0,0%	0,00%	0,0%	0,0%	0,0%	0,0%	**0,0**		**0,0**		**0,0**		**0,0**
	N2	28,2%	11,3%	17,4%	0,00%	28,2%	11,2%	17,4%	0,0%	**109,1**		**43,8**		**74,3**		**0,0**
	total dry	98,3%	92,6%	90,8%	0,0%	98,3%	92,6%	90,8%	0,0%	380,0		361,6		388,7		0,0
	total wet	100,0%	100,0%	100,0%	0,0%	100,0%	100,0%	100,0%	0,0%	386,7		390,5		428,2		0,0
	GOD	8,0%	27,0%	39,7%	0,0%	8,0%	27,0%	39,7%	0,0%	8,0%		27,0%		39,7%		0,0%
	H2/H2O	11,80	2,71	1,77	0,00	11,80	2,71	1,77	0,00							
	CO/CO2	11,42	2,71	1,42	0,00	11,42	2,71	1,42	0,00							
temperature [°C]		760	750	660	0					**760**	**760**	**750**	**750**	**660**	**480**	**0**
residence time [min]		40	30	30	0					**40**	**5**	**30**	**10**	**30**	**0**	**0**
spec. gas rate plant [Nm³/t]		4419	3350	3670	0											
supposed gas rate red. [Nm³/t]		3173	2972	3033	0											
defined uL retort [m/s]		0,9	0,9	0,9	0											
flow rate red. comp. [Ndm³/h]		16658,3	20804	21231	0											

diameter retort [m]	0,158
cross section retort [m²]	0,020
absolute pressure [bar]	1,4
atmospherical pressure [bar]	1,013

Baur-Glaessner-Diagram for gas mixtures of H_2, H_2O, CO, CO_2 / process conditions

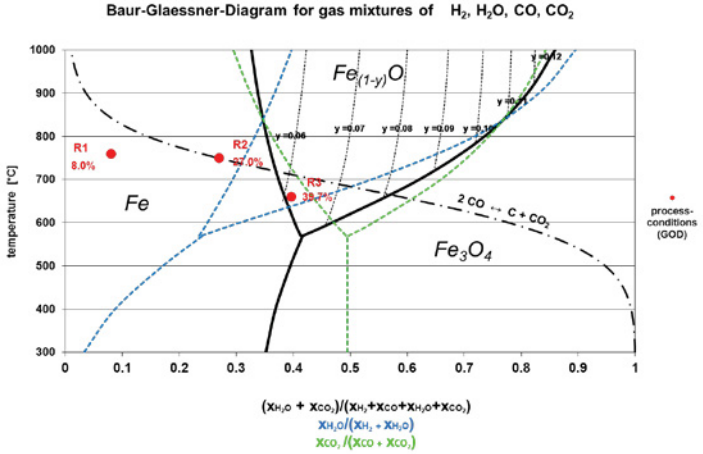

Copyright Chair of Metallurgy

CHAIR OF METALLURGY
MONTANUNIVERSITAET LEOBEN
PRIMARY METALLURGY
METALLURGICAL PROCESSES

Tel.: +43 3842 402-2201 Fax: DW 2202
Web: http://www.metallurgy.ac.at

160 mm Fluidized Bed Reactor test
Test information

Test number: Test A **Date:**
Customer: Siemens VAI

Kind of test: 3-stage 660/750/760°C FINEX
Target of the test: reduction behaviour of hematite

Test carried out by: Michael Skorianz Dial: 2255
michael.skorianz@unileoben.ac.at

Test information and results

Gas supply (reduction phases)

species	gas flow [Ndm³]	content/unit [Ndm³]	unit [pcs]
H2	7601,0	8900,0	**0,85**
H2O	2317,2	0,0	**0,00**
CO	16620,6	5900,0	**2,82**
CO2	5584,3	20300,0	**0,28**
CH4	0,0	12600,0	**0,00**
N2	7904,2	10700,0	**0,74**
sum	**40027,2**		**4,7**

Pressure test at 300 °C

position	200 Nl/min [mbar]	400 Nl/min [mbar]
Δp internal cyclone	2,2	6
p retort outlet	979	1044
Δp grid	15,9	62,1
p before grid	994	1111

Cleaning of grid before test x
Temperature sample after test < 35 °C

Re-weight of input

position	[g]
bed	**2153**
int. cycl.	**259**
ext. cycl. R4	0
ext. cycl. R3	21
ext. cycl. R2	95
ext. cycl. R1	86
sum ext. cycl.	**202**
Filter	27
Rest	10
sum re-weight	**2652**

Test progress: 3-stage 660/750/760°C FINEX

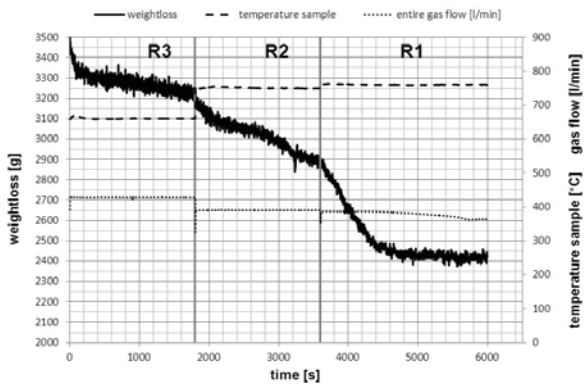

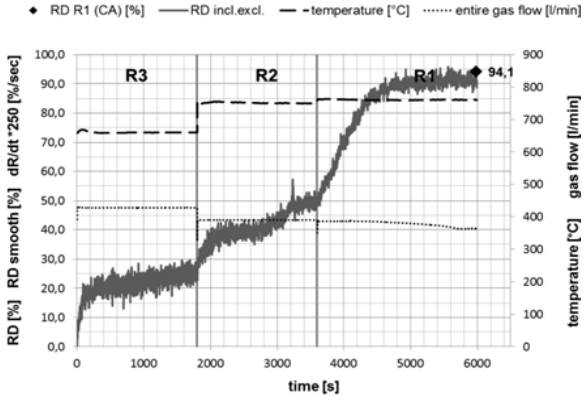

comments

N2-phases without pressure regulation, in the last reactor without pressure control.

test progress ok

Copyright Chair of Metallurgy

CHAIR OF METALLURGY
MONTANUNIVERSITAET LEOBEN
PRIMARY METALLURGY
METALLURGICAL PROCESSES

Tel.: +43 3842 402-2201 Fax: DW 2202
Web: http://www.metallurgy.ac.at

160 mm Fluidized Bed Reactor test
Determination of grain size distribution

Test carried out by: Michael Skorianz Dial: 2255
michael.skorianz@unileoben.ac.at

Date:
Customer: Siemens VAI

kind of sieving: wet dry x
sieving method: three dimensional
standard:
apparatus: RETSCH AS 200
sieves size: 200 x 50 mm
sieving time: 10 min.
interval time: 10 sec.
amplitude: 1,5 mm

Test number: **Test A**

Kind of test:
3-stage 660/750/760°C FINEX
Target of the test: reduction behaviour of hematite
Ore type 1: hamersley fine ore MUL2010/0008
Ore type 2: -
MUL sample number: MUL2010/0008
VASL sample number: 0377/97

sieve analysis - results

sieves	raw material		bed			internal cyclone			bed + internal cyclone			bed + internal cyclone + discharge			summary	
fraction	fraction	cum.	weight	fraction	cum.	weight	fraction	cum.	weight	fraction	cum.	weight	fraction	cum.	fraction change	
[mm]	p3 [%]	Q3 [%]	m [g]	p3 [%]	Q3 [%]	m [g]	p3 [%]	Q3 [%]	m [g]	p3 [%]	Q3 [%]	m [g]	p3 [%]	Q3 [%]	Δp3 [%]	comment
4-6,3	0,0		0,0	0,0		0,0	0,0		0,0	0,0		0,0	0,0		0,0	0
2,8-4	13,3	100,0	211,9	9,8	100,0	0,0	0,0	100,0	211,9	8,8	100,0	211,9	8,0	100,0	-5,3	0
1,0-2,8	13,3	86,7	307,2	14,3	90,2	0,0	0,0	100,0	307,2	12,7	91,2	307,2	11,6	92,0	-1,7	0
0,5-1,0	16,0	73,4	272,6	12,7	75,9	0,0	0,0	100,0	272,6	11,3	78,5	272,6	10,3	80,4	-5,7	0
0,25-0,5	17,4	57,4	331,3	15,4	63,2	0,0	0,0	100,0	331,3	13,7	67,2	331,3	12,5	70,1	-4,9	0
0,125-0,25	14,7	40,0	343,3	15,9	47,8	0,0	0,0	100,0	343,3	14,2	53,4	343,3	12,9	57,7	-1,8	0
0,063-0,125	25,3	25,3	439,6	20,4	31,9	0,0	0,0	100,0	439,6	18,2	39,2	439,6	16,6	44,7	-8,7	0
0-0,063	0,0	0,0	247,1	11,5	11,5	259,3	100,0	100,0	506,4	21,0	21,0	746,0	28,1	28,1	28,1	0
sum	**100**		**2153**	**100**		**259**	**100**		**2412**	**100**		**2652**	**100**		**0**	

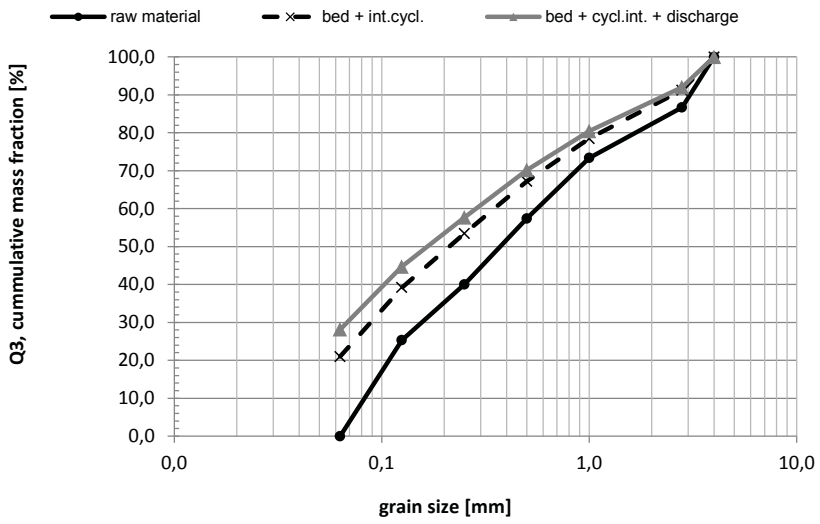

Copyright Chair of Metallurgy

CHAIR OF METALLURGY
MONTANUNIVERSITAET LEOBEN
PRIMARY METALLURGY
METALLURGICAL PROCESSES

Tel.: +43 3842 402-2201 Fax: DW 2202
Web: http://www.metallurgy.ac.at

160 mm Fluidized Bed Reactor test
Process conditions and test parameter

Test number: **Test B** **Date:**
Customer: Siemens VAI

Kind of test: 3-stage 350/750/760°C FINEX
Target of the test: reduction behaviour of hematite

Test carried out by: Michael Skorianz Dial: 2255
michael.skorianz@unileoben.ac.at

Raw material input

sieves	sieve analyis		input	comments
mesh size [mm]	fraction [%]	cum. [%]	mass [g]	
4-6,3	0		0,0	
2,8-4	13,3	100	465,5	
1,0-2,8	13,3	86,7	465,5	
0,5-1,0	16	73,4	560,0	hamersley fine ore MUL2010/0008
0,25-0,5	17,4	57,4	609,0	
0,125-0,25	14,7	40	514,5	
0,063-0,125	25,3	25,3	885,5	
0-0,063	0	0	0,0	
sum	100,0		3500,0	

chemical analyses

raw material: hamersley fine ore MUL2010/0008			
species	[%]	species	[%]
Fe(tot)	63,60	Na2O	0,00
FeO	0,58	Mn	0,17
Al2O3	2,07	Ni	0,00
SiO2	3,48	Cu	0,00
CaO	0,01	Cr	0,00
MgO	0,01	S	0,01
TiO2	0,12	P	0,07
K2O	0,01	Zn	0,00
V2O5	0,00	LOI (900°	3,30

reduced material						
species	bed Ø [%]	R4 [%]	R3 [%]	R2 [%]	int.cyc. [%]	ex.cyc. [%]
Fe tot	76,3	0,0	0,0	0,0	0,0	0,0
Fe met	23,9	0,0	0,0	0,0	0,0	0,0
FeO	54,7	0,0	0,0	0,0	0,0	0,0
C tot	0,070	0,000	0,000	0,000	0,000	0,000
MD	31,3	0,0	0,0	0,0	0,0	0,0
RD (CA)	49,9	0,0	0,0	0,0	0,0	0,0
RD (cal)	51,3	0,0	0,0	0,0	0,0	0,0
FeOx	0,8	0,0	0,0	0,0	0,0	0,0
Fe bal.	99,3	0,0	0,0	0,0	0,0	0,0

calculation of test parameter: 3-stage 350/750/760°C FINEX

	gas composition	concentration, temp. plant R1 [%]	R2 [%]	R3 [%]	R4 [%]	concentration test rig R1 [%]	R2 [%]	R3 [%]	R4 [%]	gas flow test rig R1 [Nl/min]	heating [Nl/min]	R2 [Nl/min]	heating [Nl/min]	R3 [Nl/min]	heating [Nl/min]	R4 [Nl/min]
species	H2	17,7%	16,5%	16,0%	0,00%	17,6%	17,3%	12,2%	0,0%	**68,1**		**67,7**		**77,9**		**0,0**
	H2O	5,6%	7,1%	8,7%	0,00%	5,6%	7,5%	6,6%	0,0%	**21,5**		**29,1**		**42,4**		**0,0**
	CO	46,7%	38,9%	36,5%	0,00%	46,4%	40,9%	27,7%	0,0%	**179,6**		**159,6**		**177,8**		**0,0**
	CO2	21,0%	28,5%	29,8%	0,00%	20,9%	29,9%	22,6%	0,0%	**80,8**		**116,9**		**145,2**		**0,0**
	CH4	1,5%	1,6%	1,6%	0,00%	0,0%	0,0%	0,0%	0,0%	**0,0**		**0,0**		**0,0**		**0,0**
	N2	7,5%	7,4%	7,4%	0,00%	9,5%	4,4%	30,9%	0,0%	**36,7**		**17,2**		**197,9**		**0,0**
	total dry	94,4%	92,9%	91,3%	0,0%	94,4%	92,5%	93,4%	0,0%	365,2		361,4		598,8		0,0
	total wet	100,0%	100,0%	100,0%	0,0%	100,0%	100,0%	100,0%	0,0%	386,7		390,5		641,2		0,0
	GOD	29,2%	39,1%	42,3%	0,0%	29,2%	39,1%	42,3%	0,0%	29,2%		39,1%		42,3%		0,0%
	H2/H2O	3,16	2,32	1,84	0,00	3,16	2,32	1,84	0,00							
	CO/CO2	2,22	1,36	1,22	0,00	2,22	1,36	1,22	0,00							
temperature [°C]		760	750	350	0					**760**	**760**	**750**	**750**	**350**	**480**	**0**
residence time [min]		40	30	30	0					**40**	**5**	**30**	**30**	**30**	**0**	**0**
spec. gas rate plant [Nm³/t]		810	810	810	0											
supposed gas rate red. [Nm³/t]		4000	3200	3800	0											
defined uL retort [m/s]		0,9	0,9	0,9	0											
flow rate red. comp. [Ndm³/h]		21000	22400	26600	0											

diameter retort [m]	0,158
cross section retort [m²]	0,020
absolute pressure [bar]	1,4
atmospherical pressure [bar]	1,013

Baur-Glaessner-Diagram for gas mixtures of H_2, H_2O, CO, CO_2 / process conditions

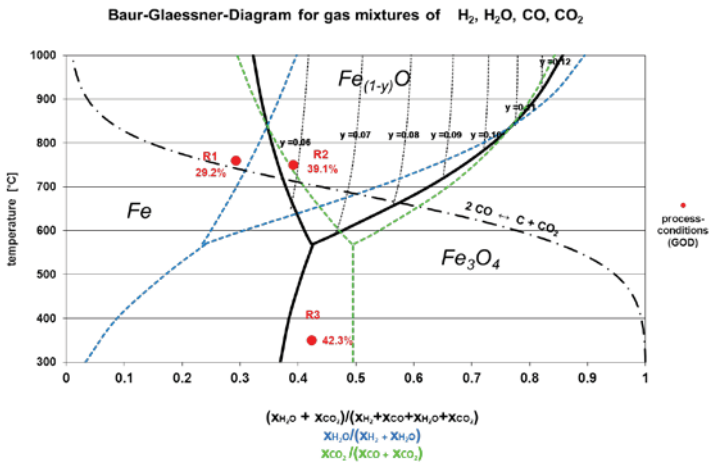

Copyright Chair of Metallurgy

CHAIR OF METALLURGY
MONTANUNIVERSITAET LEOBEN
PRIMARY METALLURGY
METALLURGICAL PROCESSES

Tel.: +43 3842 402-2201 Fax: DW 2202
Web: http://www.metallurgy.ac.at

160 mm Fluidized Bed Reactor test
Test information

Test number: **Test B** **Date:**
Customer: Siemens VAI

Kind of test: 3-stage 350/750/760°C FINEX
Target of the test: reduction behaviour of hematite

Test carried out by: Michael Skorianz Dial: 2255
michael.skorianz@unileoben.ac.at

Test information and results

Gas supply (reduction phases)

species	gas flow [Ndm³]	content/unit [Ndm³]	unit [pcs]
H2	7092,3	8900,0	**0,80**
H2O	3006,9	0,0	**0,00**
CO	17306,9	5900,0	**2,93**
CO2	11093,8	20300,0	**0,55**
CH4	0,0	12600,0	**0,00**
N2	7918,6	10700,0	**0,74**
sum	**46418,6**		**5,0**

Pressure test at 300 °C

position	200 Nl/min [mbar]	400 Nl/min [mbar]
Δp internal cyclone	3	7,1
p retort outlet	1000	1033
Δp grid	9,7	34
p before grid	1013	1074

Cleaning of grid before test x
Temperature sample after test 0 °C

Re-weight of input

position	[g]
bed	**2708**
int. cycl.	**83**
ext. cycl. R4	0
ext. cycl. R3	7
ext. cycl. R2	4
ext. cycl. R1	61
sum ext. cycl.	**72**
Filter	14
Rest	22
sum re-weight	**2899**

Test progress: 3-stage 350/750/760°C FINEX

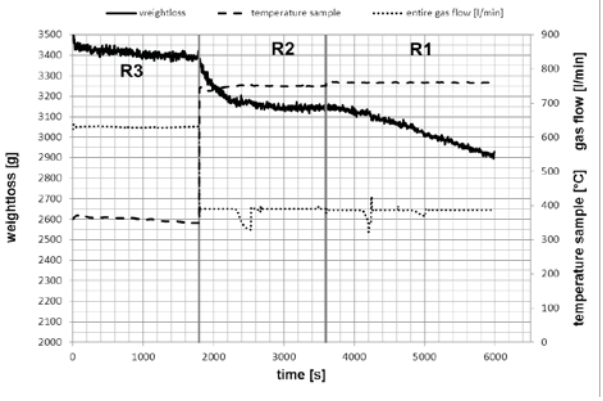

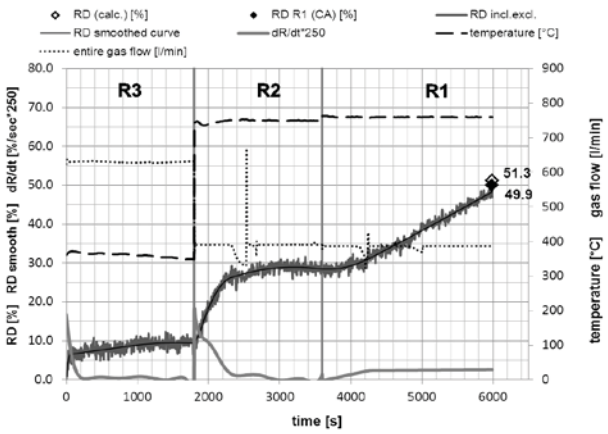

comments

Increase of N2 after filling in steps. Test progress ok

Copyright Chair of Metallurgy

CHAIR OF METALLURGY
MONTANUNIVERSITAET LEOBEN
PRIMARY METALLURGY
METALLURGICAL PROCESSES

Tel.: +43 3842 402-2201 Fax: DW 2202
Web: http://www.metallurgy.ac.at

160 mm Fluidized Bed Reactor test
Determination of grain size distribution

Test carried out by: Michael Skorianz Dial: 2255
michael.skorianz@unileoben.ac.at

Date:
Customer: Siemens VAI

kind of sieving: wet dry x
sieving method: three dimensional
standard:
apparatus: RETSCH AS 200
sieves size: 200 x 50 mm
sieving time: 10 min.
interval time: 10 sec.
amplitude: 1,5 mm

Test number: **Test B**

Kind of test:
3-stage 350/750/760°C FINEX
Target of the test: reduction behaviour of hematite
Ore type 1: hamersley fine ore MUL2010/0008
Ore type 2: -
MUL sample number: MUL2010/0008
VASL sample number: 0377/97

sieve analysis - results

sieves	raw material		bed			internal cyclone			bed + internal cyclone			bed + internal cyclone + discharge			summary	
fraction	fraction	cum.	weight	fraction	cum.	weight	fraction	cum.	weight	fraction	cum.	weight	fraction	cum.	fraction change	
[mm]	p3 [%]	Q3 [%]	m [g]	p3 [%]	Q3 [%]	m [g]	p3 [%]	Q3 [%]	m [g]	p3 [%]	Q3 [%]	m [g]	p3 [%]	Q3 [%]	Δp3 [%]	comment
4-6,3	0,0		0,0	0,0		0,0	0,0		0,0	0,0		0,0	0,0		0,0	0
2,8-4	13,3	100,0	308,9	11,4	100,0	0,0	0,0	100,0	308,9	11,1	100,0	308,9	10,7	100,0	-2,6	0
1,0-2,8	13,3	86,7	349,8	12,9	88,6	0,0	0,0	100,0	349,8	12,5	88,9	349,8	12,1	89,3	-1,2	0
0,5-1,0	16,0	73,4	366,4	13,5	75,7	0,0	0,0	100,0	366,4	13,1	76,4	366,4	12,6	77,3	-3,4	0
0,25-0,5	17,4	57,4	444,2	16,4	62,1	0,0	0,0	100,0	444,2	15,9	63,3	444,2	15,3	64,6	-2,1	0
0,125-0,25	14,7	40,0	356,3	13,2	45,7	0,0	0,0	100,0	356,3	12,8	47,4	356,3	12,3	49,3	-2,4	0
0,063-0,125	25,3	25,3	682,7	25,2	32,6	0,0	0,0	100,0	682,7	24,5	34,6	682,7	23,6	37,0	-1,7	0
0-0,063	0,0	0,0	199,6	7,4	7,4	83,0	100,0	100,0	282,6	10,1	10,1	390,3	13,5	13,5	13,5	0
sum	**100**		**2708**	**100**		**83**	**100**		**2791**	**100**		**2899**	**100**		**0**	

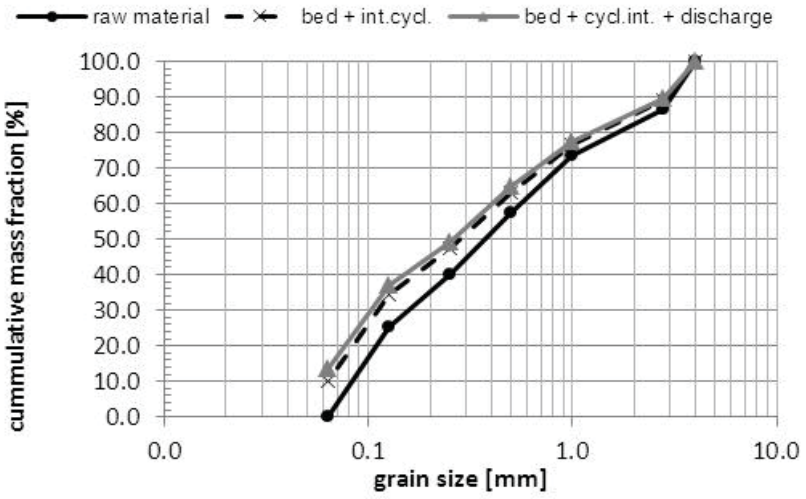

Copyright Chair of Metallurgy

CHAIR OF METALLURGY
MONTANUNIVERSITAET LEOBEN
PRIMARY METALLURGY
METALLURGICAL PROCESSES

Tel.: +43 3842 402-2201 Fax: DW 2202
Web: http://www.metallurgy.ac.at

160 mm Fluidized Bed Reactor test
Process conditions and test parameter

Test number: **Test C** **Date:**
Customer: Siemens VAI

Kind of test: 3-stage 600/750/760°C - FINEX
Target of the test: reduction behaviour of hematite

Test carried out by: Michael Skorianz Dial: 2255
michael.skorianz@unileoben.ac.at

Raw material input

sieves	sieve analyis		input	comments
mesh size [mm]	fraction [%]	cum. [%]	mass [g]	
4-6,3	0		0,0	
2,8-4	13,3	100	465,5	
1,0-2,8	13,3	86,7	465,5	
0,5-1,0	16	73,4	560,0	hammersley fine ore MUL2010/0008
0,25-0,5	17,4	57,4	609,0	
0,125-0,25	14,7	40	514,5	
0,063-0,125	25,3	25,3	885,5	
0-0,063	0	0	0,0	
sum	100,0		3500,0	

chemical analyses

raw material: hammersley fine ore MUL2010/0008			
species	[%]	species	[%]
Fe(tot)	63,60	Na2O	0,00
FeO	0,58	Mn	0,17
Al2O3	2,07	Ni	0,00
SiO2	3,48	Cu	0,00
CaO	0,01	Cr	0,00
MgO	0,01	S	0,01
TiO2	0,12	P	0,07
K2O	0,01	Zn	0,00
V2O5	0,00	LOI (900°	3,30

reduced material						
species	bed Ø [%]	R4 [%]	R3 [%]	R2 [%]	int.cyc. [%]	ex.cyc. [%]
Fe tot	76,1	0,0	0,0	0,0	0,0	0,0
Fe met	23,6	0,0	0,0	0,0	0,0	0,0
FeO	54,1	0,0	0,0	0,0	0,0	0,0
C tot	0,090	0,000	0,000	0,000	0,000	0,000
MD	31,0	0,0	0,0	0,0	0,0	0,0
RD (CA)	49,5	0,0	0,0	0,0	0,0	0,0
RD (cal)	54,7	0,0	0,0	0,0	0,0	0,0
FeOx	0,8	0,0	0,0	0,0	0,0	0,0
Fe bal.	97,9	0,0	0,0	0,0	0,0	0,0

calculation of test parameter: 3-stage 600/750/760°C - FINEX

	gas composition	concentration, temp. plant R1 [%]	R2 [%]	R3 [%]	R4 [%]	concentration test rig R1 [%]	R2 [%]	R3 [%]	R4 [%]	gas flow test rig R1 [Nl/min]	heating [Nl/min]	R2 [Nl/min]	heating [Nl/min]	R3 [Nl/min]	heating [Nl/min]	R4 [Nl/min]
species	H2	17,7%	16,5%	16,0%	0,00%	17,6%	17,3%	17,0%	0,0%	**68,1**		**67,7**		**77,9**		**0,0**
	H2O	5,6%	7,1%	8,7%	0,00%	5,6%	7,5%	9,3%	0,0%	**21,5**		**29,1**		**42,4**		**0,0**
	CO	46,7%	38,9%	36,5%	0,00%	46,4%	40,9%	38,9%	0,0%	**179,6**		**159,6**		**177,8**		**0,0**
	CO2	21,0%	28,5%	29,8%	0,00%	20,9%	29,9%	31,7%	0,0%	**80,8**		**116,9**		**145,2**		**0,0**
	CH4	1,5%	1,6%	1,6%	0,00%	0,0%	0,0%	0,0%	0,0%	**0,0**		**0,0**		**0,0**		**0,0**
	N2	7,5%	7,4%	7,4%	0,00%	9,5%	4,4%	3,1%	0,0%	**36,7**		**17,2**		**14,2**		**0,0**
	total dry	94,4%	92,9%	91,3%	0,0%	94,4%	92,5%	90,7%	0,0%	365,2		361,4		415,2		0,0
	total wet	100,0%	100,0%	100,0%	0,0%	100,0%	100,0%	100,0%	0,0%	386,7		390,5		457,6		0,0
	GOD	29,2%	39,1%	42,3%	0,0%	29,2%	39,1%	42,3%	0,0%	29,2%		39,1%		42,3%		0,0%
	H2/H2O	3,16	2,32	1,84	0,00	3,16	2,32	1,84	0,00							
	CO/CO2	2,22	1,36	1,22	0,00	2,22	1,36	1,22	0,00							
temperature [°C]		760	750	600	0					**760**	**760**	**750**	**750**	**600**	**0**	**0**
residence time [min]		40	30	30	0					**40**	**5**	**30**	**15**	**30**	**0**	**0**
spec. gas rate plant [Nm³/t]		810	810	810	0											
supposed gas rate red. [Nm³/t]		4000	3200	3800	0											
defined uL retort [m/s]		0,9	0,9	0,9	0											
flow rate red. comp. [Ndm³/h]		21000	22400	26600	0											

		diameter retort [m]	0,158
		cross section retort [m²]	0,020
		absolute pressure [bar]	1,4
		atmospherical pressure [bar]	1,013

Baur-Glaessner-Diagram for gas mixtures of H_2, H_2O, CO, CO_2 / process conditions

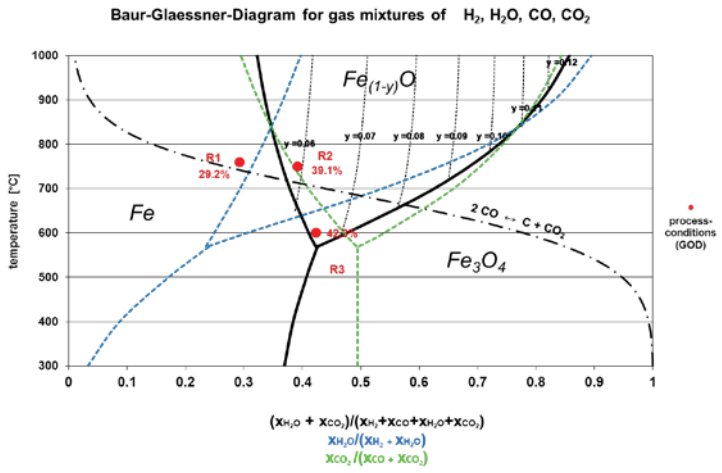

Copyright Chair of Metallurgy

CHAIR OF METALLURGY
MONTANUNIVERSITAET LEOBEN
PRIMARY METALLURGY
METALLURGICAL PROCESSES

Tel.: +43 3842 402-2201 Fax: DW 2202
Web: http://www.metallurgy.ac.at

160 mm Fluidized Bed Reactor test
Test information

Test number: **Test C** **Date:**
Customer: Siemens VAI

Kind of test: 3-stage 600/750/760°C - FINEX
Target of the test: reduction behaviour of hematite

Test carried out by: Michael Skorianz Dial: 2255
michael.skorianz@unileoben.ac.at

Test information and results

Gas supply (reduction phases)

species	gas flow [Ndm³]	content/unit [Ndm³]	unit [pcs]
H2	7092,3	8900,0	**0,80**
H2O	3006,9	0,0	**0,00**
CO	17306,9	5900,0	**2,93**
CO2	11093,8	20300,0	**0,55**
CH4	0,0	12600,0	**0,00**
N2	2410,0	10700,0	**0,23**
sum	**40910,0**		**4,5**

Pressure test at 300 °C

position	200 Nl/min [mbar]	400 Nl/min [mbar]
Δp internal cyclone	3	7,1
p retort outlet	1006	1038
Δp grid	9,6	34,3
p before grid	1020	1081

Cleaning of grid before test -
Temperature sample after test 0 °C

Re-weight of input

position	[g]
bed	**2734**
int. cycl.	**47**
ext. cycl. R4	0
ext. cycl. R3	20
ext. cycl. R2	6
ext. cycl. R1	5
sum ext. cycl.	**31**
Filter	11
Rest	43
sum re-weight	**2866**

Test progress: 3-stage 600/750/760°C - FINEX

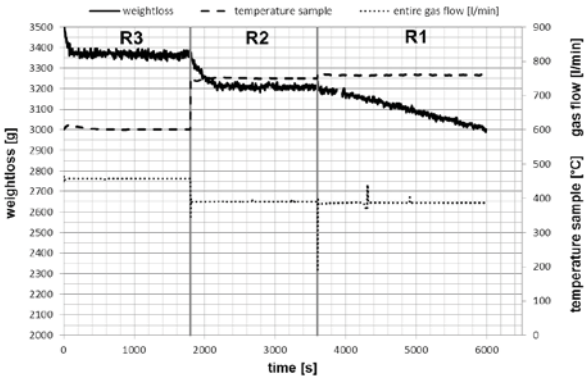

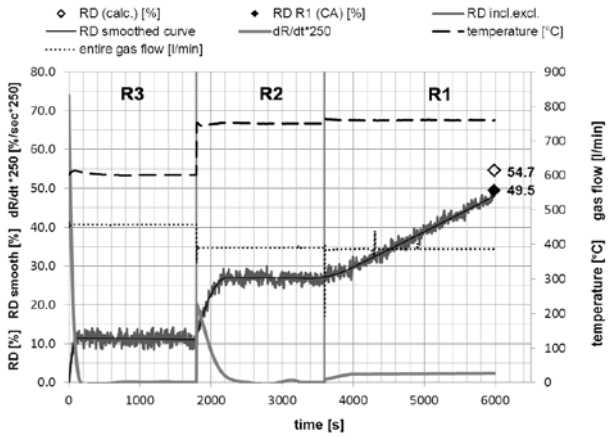

comments

Increase of N2 after filling in steps.

Test progress ok

Copyright Chair of Metallurgy

CHAIR OF METALLURGY
MONTANUNIVERSITAET LEOBEN
PRIMARY METALLURGY
METALLURGICAL PROCESSES

Tel.: +43 3842 402-2201 Fax: DW 2202
Web: http://www.metallurgy.ac.at

160 mm Fluidized Bed Reactor test
Determination of grain size distribution

Test carried out by: Michael Skorianz Dial: 2255
michael.skorianz@unileoben.ac.at

Date:
Customer: Siemens VAI

kind of sieving: wet dry x
sieving method: three dimensional
standard:
apparatus: RETSCH AS 200
sieves size: 200 x 50 mm
sieving time: 10 min.
interval time: 10 sec.
amplitude: 1,5 mm

Test number: **Test C**

Kind of test:
3-stage 600/750/760°C - FINEX
Target of the test: reduction behaviour of hematite
Ore type 1: hammersley fine ore MUL2010/0008
Ore type 2: -
MUL sample number: MUL2010/0008
VASL sample number: 0377/97

sieve analysis - results

sieves	raw material		bed			internal cyclone			bed + internal cyclone			bed + internal cyclone + discharge			summary	
fraction	fraction	cum.	weight	fraction	cum.	weight	fraction	cum.	weight	fraction	cum.	weight	fraction	cum.	fraction change	
[mm]	p3 [%]	Q3 [%]	m [g]	p3 [%]	Q3 [%]	m [g]	p3 [%]	Q3 [%]	m [g]	p3 [%]	Q3 [%]	m [g]	p3 [%]	Q3 [%]	Δp3 [%]	comment
4-6,3	0,0		0,0	0,0		0,0	0,0		0,0	0,0		0,0	0,0		0,0	0
2,8-4	13,3	100,0	265,3	9,7	100,0	0,0	0,0	100,0	265,3	9,5	100,0	265,3	9,3	100,0	-4,0	0
1,0-2,8	13,3	86,7	392,3	14,3	90,3	0,0	0,0	100,0	392,3	14,1	90,5	392,3	13,7	90,7	0,4	0
0,5-1,0	16,0	73,4	326,6	11,9	75,9	0,0	0,0	100,0	326,6	11,7	76,4	326,6	11,4	77,1	-4,6	0
0,25-0,5	17,4	57,4	428,9	15,7	64,0	0,0	0,0	100,0	428,9	15,4	64,6	428,9	15,0	65,7	-2,4	0
0,125-0,25	14,7	40,0	385,3	14,1	48,3	0,0	0,0	100,0	385,3	13,9	49,2	385,3	13,4	50,7	-1,3	0
0,063-0,125	25,3	25,3	678,0	24,8	34,2	0,0	0,0	100,0	678,0	24,4	35,3	678,0	23,7	37,3	-1,6	0
0-0,063	0,0	0,0	257,8	9,4	9,4	47,4	100,0	100,0	305,2	11,0	11,0	389,6	13,6	13,6	13,6	0
sum	**100**		**2734**	**100**		**47**	**100**		**2782**	**100**		**2866**	**100**		**0**	

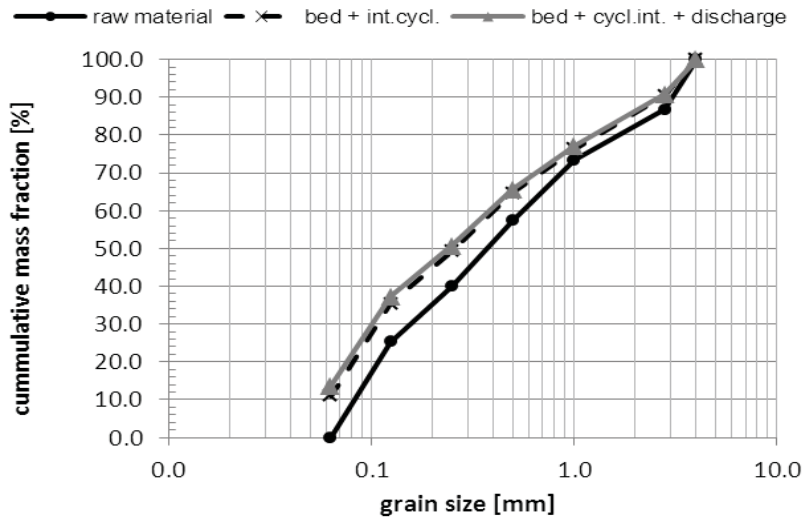

Copyright Chair of Metallurgy

CHAIR OF METALLURGY
MONTANUNIVERSITAET LEOBEN
PRIMARY METALLURGY
METALLURGICAL PROCESSES

Tel.: +43 3842 402-2201 Fax: DW 2202
Web: http://www.metallurgy.ac.at

160 mm Fluidized Bed Reactor test
Process conditions and test parameter

Test number: **Test D** **Date:**
Customer: Siemens VAI

Kind of test: 4-stage 350/680/750/760°C FINEX
Target of the test: reduction behaviour of hematite

Test carried out by: Michael Skorianz Dial: 2255
michael.skorianz@unileoben.ac.at

Raw material input

sieves	sieve analyis		input	comments
mesh size [mm]	fraction [%]	cum. [%]	mass [g]	
4-6,3	0		0,0	
2,8-4	13,3	100	465,5	
1,0-2,8	13,3	86,7	465,5	
0,5-1,0	16	73,4	560,0	hamersley fine ore MUL2010/0008
0,25-0,5	17,4	57,4	609,0	
0,125-0,25	14,7	40	514,5	
0,063-0,125	25,3	25,3	885,5	
0-0,063	0	0	0,0	
sum	100,0		3500,0	

chemical analyses

raw material: hamersley fine ore MUL2010/0008			
species	[%]	species	[%]
Fe(tot)	63,60	Na2O	0,00
FeO	0,58	Mn	0,17
Al2O3	2,07	Ni	0,00
SiO2	3,48	Cu	0,00
CaO	0,01	Cr	0,00
MgO	0,01	S	0,01
TiO2	0,12	P	0,07
K2O	0,01	Zn	0,00
V2O5	0,00	LOI (900°	3,30

reduced material						
species	bed Ø [%]	<0,063 [%]	0,25-0,50 [%]	1,0-2,8 [%]	int.cyc. [%]	ex.cyc. [%]
Fe tot	75,6	0,0	0,0	0,0	0,0	0,0
Fe met	23,8	0,0	0,0	0,0	0,0	0,0
FeO	55,7	0,0	0,0	0,0	0,0	0,0
C tot	0,080	0,000	0,000	0,000	0,000	0,000
MD	31,5	0,0	0,0	0,0	0,0	0,0
RD (CA)	50,5	0,0	0,0	0,0	0,0	0,0
RD (cal)	53,4	0,0	0,0	0,0	0,0	0,0
FeOx	0,7	0,0	0,0	0,0	0,0	0,0
Fe bal.	97,8	0,0	0,0	0,0	0,0	0,0

calculation of test parameter: 4-stage 350/680/750/760°C FINEX

		concentration, temp. plant				concentration test rig				gas flow test rig						
gas composition		R1 [%]	R2 [%]	R3 [%]	R4 [%]	R1 [%]	R2 [%]	R3 [%]	R4 [%]	R1 [Nl/min]	heating [Nl/min]	R2 [Nl/min]	heating [Nl/min]	R3 [Nl/min]	heating [Nl/min]	R4 [Nl/min]
species	H2	17,7%	16,5%	16,0%	16,00%	17,6%	16,3%	17,1%	12,8%	**68,1**		**63,5**		**71,8**		**82,1**
	H2O	5,6%	7,1%	8,7%	8,70%	5,6%	7,0%	9,3%	7,0%	**21,5**		**27,3**		**39,0**		**44,6**
	CO	46,7%	38,9%	36,5%	36,50%	46,4%	38,3%	39,1%	29,2%	**179,6**		**149,6**		**163,8**		**187,2**
	CO2	21,0%	28,5%	29,8%	29,80%	20,9%	28,1%	31,9%	23,8%	**80,8**		**109,6**		**133,7**		**152,8**
	CH4	1,5%	1,6%	1,6%	1,60%	0,0%	0,0%	0,0%	0,0%	**0,0**		**0,0**		**0,0**		**0,0**
	N2	7,5%	7,4%	7,4%	7,40%	9,5%	10,4%	2,6%	27,2%	**36,7**		**40,5**		**10,8**		**174,5**
	total dry	94,4%	92,9%	91,3%	91,3%	94,4%	93,0%	90,7%	93,0%	365,2		363,2		380,1		596,6
	total wet	100,0%	100,0%	100,0%	100,0%	100,0%	100,0%	100,0%	100,0%	386,7		390,5		419,2		641,2
	GOD	29,2%	39,1%	42,3%	42,3%	29,2%	39,1%	42,3%	42,3%	29,2%		39,1%		42,3%		42,3%
	H2/H2O	3,16	2,32	1,84	1,84	3,16	2,32	1,84	1,84							
	CO/CO2	2,22	1,36	1,22	1,22	2,22	1,36	1,22	1,22							
temperature [°C]		760	750	680	350					**760**	**760**	**750**	**680**	**680**	**680**	**350**
residence time [min]		40	40	30	30					**40**	**15**	**40**	**10**	**30**	**30**	**30**
spec. gas rate plant [Nm³/t]		810	810	810	810											
supposed gas rate red. [Nm³/t]		4000	4000	3500	4000											
defined uL retort [m/s]		0,9	0,9	0,9	0,9											
flow rate red. comp. [Ndm³/h]		21000	21000	24500	28000											

		diameter retort [m]	0,158
		cross section retort [m²]	0,020
		absolute pressure [bar]	1,4
		atmospherical pressure [bar]	1,013

Baur-Glaessner-Diagram for gas mixtures of H_2, H_2O, CO, CO_2 / process conditions

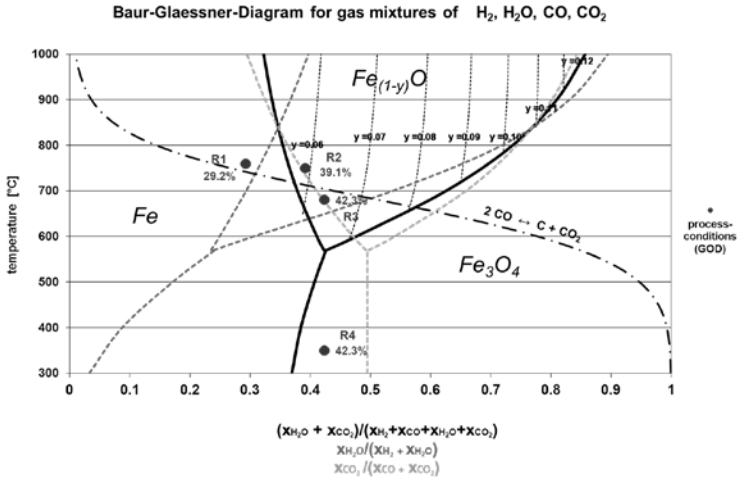

Copyright Chair of Metallurgy

CHAIR OF METALLURGY
MONTANUNIVERSITAET LEOBEN
PRIMARY METALLURGY
METALLURGICAL PROCESSES

Tel.: +43 3842 402-2201 Fax: DW 2202
Web: http://www.metallurgy.ac.at

160 mm Fluidized Bed Reactor test
Test information

Test number: **Test D** **Date:**
Customer: Siemens VAI

Kind of test: 4-stage 350/680/750/760°C FINEX
Target of the test: reduction behaviour of hematite

Test carried out by: Michael Skorianz Dial: 2255
michael.skorianz@unileoben.ac.at

Test information and results

Gas supply (reduction phases)

species	gas flow [Ndm³]	content/unit [Ndm³]	unit [pcs]
H2	9876,9	8900,0	**1,11**
H2O	4463,5	0,0	**0,00**
CO	23698,1	5900,0	**4,02**
CO2	16211,5	20300,0	**0,80**
CH4	0,0	12600,0	**0,00**
N2	8648,4	10700,0	**0,81**
sum	**62898,4**		**6,7**

Pressure test at 300 °C

position	200 Nl/min [mbar]	400 Nl/min [mbar]
Δp internal cyclone	2,6	6,6
p retort outlet	960	993
Δp grid	12,4	43
p before grid	974	1041

Cleaning of grid before test x
Temperature sample after test 0 °C

Re-weight of input

position	[g]
bed	**2650**
int. cycl.	**49**
ext. cycl. R4	47
ext. cycl. R3	33
ext. cycl. R2	9
ext. cycl. R1	33
sum ext. cycl.	**122**
Filter	12
Rest	45
sum re-weight	**2878**

Test progress: 4-stage 350/680/750/760°C FINEX

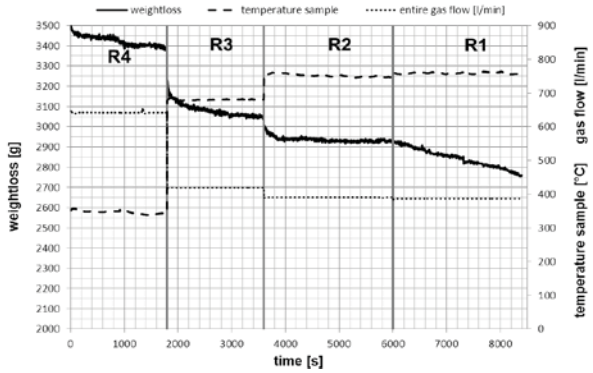

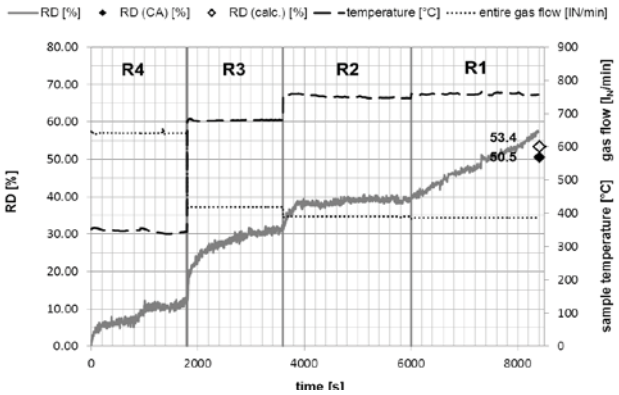

comments

Increase N2 after filling in steps. Test finished

Copyright Chair of Metallurgy

CHAIR OF METALLURGY
MONTANUNIVERSITAET LEOBEN
PRIMARY METALLURGY
METALLURGICAL PROCESSES

Tel.: +43 3842 402-2201 Fax: DW 2202
Web: http://www.metallurgy.ac.at

Determination of grain size distribution - fluidized bed test -

Test carried out by: Michael Skorianz Dial: 2255
michael.skorianz@unileoben.ac.at

Date:
Customer: Siemens VAI

Test number: **Test D**

Kind of test:
4-stage 350/680/750/760°C FINEX
Target of the test: reduction behaviour of hematite
Ore type 1: hamersley fine ore MUL2010/0008
Ore type 2: -
MUL sample number: MUL2010/0008
VASL sample number: 0377/97

kind of sieving: wet dry x
sieving method: three dimensional
standard:
apparatus: RETSCH AS 200
sieves size: 200 x 50 mm
sieving time: 10 min.
interval time: 10 sec.
amplitude: 1,5 mm

sieve analysis - results

sieves	raw material		bed			internal cyclone			bed + internal cyclone			bed + internal cyclone + discharge			summary	
fraction	fraction	cum.	weight	fraction	cum.	weight	fraction	cum.	weight	fraction	cum.	weight	fraction	cum.	fraction change	
[mm]	[%]	[%]	[g]	[%]	[%]	[g]	[%]	[%]	[g]	[%]	[%]	[g]	[%]	[%]	[%]	comment
4-6,3	0,0		0,0	0,0		0,0	0,0		0,0	0,0		0,0	0,0		0,0	0
2,8-4	13,3	100,0	259,2	9,8	100,0	0,0	0,0	100,0	259,2	9,6	100,0	259,2	9,0	100,0	-4,3	0
1,0-2,8	13,3	86,7	232,7	8,8	90,2	0,0	0,0	100,0	232,7	8,6	90,4	232,7	8,1	91,0	-5,2	0
0,5-1,0	16,0	73,4	354,3	13,4	81,4	0,0	0,0	100,0	354,3	13,1	81,8	354,3	12,3	82,9	-3,7	0
0,25-0,5	17,4	57,4	356,2	13,4	68,1	0,0	0,0	100,0	356,2	13,2	68,6	356,2	12,4	70,6	-5,0	0
0,125-0,25	14,7	40,0	369,1	13,9	54,6	0,0	0,0	100,0	369,1	13,7	55,5	369,1	12,8	58,2	-1,9	0
0,063-0,125	25,3	25,3	571,3	21,6	40,7	0,0	0,0	100,0	571,3	21,2	41,8	571,3	19,8	45,4	-5,5	0
0-0,063	0,0	0,0	507,2	19,1	19,1	49,0	100,0	100,0	556,2	20,6	20,6	735,2	25,5	25,5	25,5	0
sum	**100**		**2650**	**100**		**49**	**100**		**2699**	**100**		**2878**	**100**		**0**	

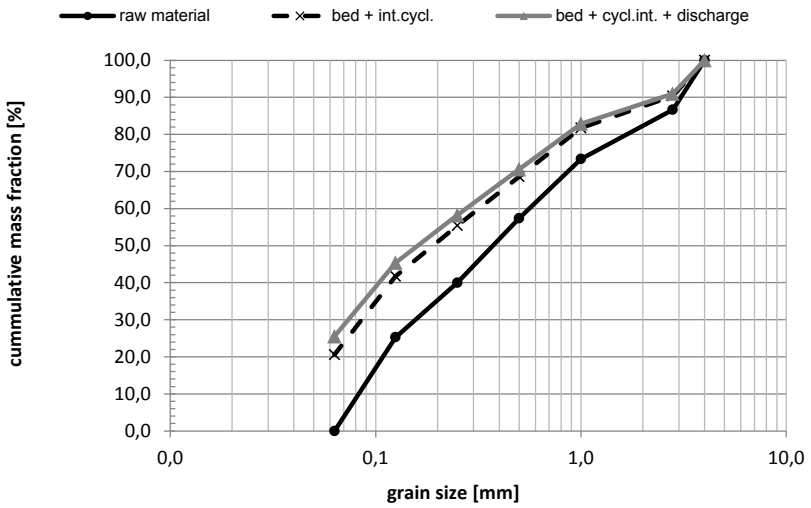

analysis according to DIN 66165
Copyright Chair of Metallurgy

CHAIR OF METALLURGY
MONTANUNIVERSITAET LEOBEN
PRIMARY METALLURGY
METALLURGICAL PROCESSES

Tel.: +43 3842 402-2201 Fax: DW 2202
Web: http://www.metallurgy.ac.at

160 mm Fluidized Bed Reactor test
Process conditions and test parameter

Test number: **Test E** **Date:**
Customer: Siemens VAI

Kind of test: 3-stage 350/750/760°C 60 min. R1 FINEX
Target of the test: reduction behaviour of hematite

Test carried out by: Michael Skorianz Dial: 2255
michael.skorianz@unileoben.ac.at

Raw material input

sieves	sieve analyis		input	comments
mesh size [mm]	fraction [%]	cum. [%]	mass [g]	
4-6,3	0		0,0	
2,8-4	13,3	100	460,7	
1,0-2,8	13,3	86,7	460,7	
0,5-1,0	16	73,4	554,2	hammersley fine ore MUL2010/0008
0,25-0,5	17,4	57,4	602,7	
0,125-0,25	14,7	40	509,2	
0,063-0,125	25,3	25,3	876,4	
0-0,063	0	0	0,0	
sum	100,0		3464,0	

chemical analyses

raw material: hammersley fine ore MUL2010/0008			
species	[%]	species	[%]
Fe(tot)	63,60	Na2O	0,00
FeO	0,58	Mn	0,17
Al2O3	2,07	Ni	0,00
SiO2	3,48	Cu	0,00
CaO	0,01	Cr	0,00
MgO	0,01	S	0,01
TiO2	0,12	P	0,07
K2O	0,01	Zn	0,00
V2O5	0,00	LOI (900°	3,30

reduced material						
species	bed Ø [%]	R4 [%]	R3 [%]	R2 [%]	int.cyc. [%]	ex.cyc. [%]
Fe tot	77,1	0,0	0,0	0,0	0,0	0,0
Fe met	30,9	0,0	0,0	0,0	0,0	0,0
FeO	43,3	0,0	0,0	0,0	0,0	0,0
C tot	0,090	0,000	0,000	0,000	0,000	0,000
MD	40,1	0,0	0,0	0,0	0,0	0,0
RD (CA)	54,6	0,0	0,0	0,0	0,0	0,0
RD (cal)	61,1	0,0	0,0	0,0	0,0	0,0
FeOx	0,7	0,0	0,0	0,0	0,0	0,0
Fe bal.	97,2	0,0	0,0	0,0	0,0	0,0

calculation of test parameter: -stage 350/750/760°C 60 min. R1 FINE

	gas composition	concentration, temp. plant R1 [%]	R2 [%]	R3 [%]	R4 [%]	concentration test rig R1 [%]	R2 [%]	R3 [%]	R4 [%]	gas flow test rig R1 [Nl/min]	heating [Nl/min]	R2 [Nl/min]	heating [Nl/min]	R3 [Nl/min]	heating [Nl/min]	R4 [Nl/min]
species	H2	17,7%	16,5%	16,0%	0,00%	17,4%	17,2%	12,0%	0,0%	**67,4**		**67,0**		**77,1**		**0,0**
	H2O	5,6%	7,1%	8,7%	0,00%	5,5%	7,4%	6,5%	0,0%	**21,3**		**28,8**		**41,9**		**0,0**
	CO	46,7%	38,9%	36,5%	0,00%	46,0%	40,4%	27,4%	0,0%	**177,8**		**157,9**		**176,0**		**0,0**
	CO2	21,0%	28,5%	29,8%	0,00%	20,7%	29,6%	22,4%	0,0%	**79,9**		**115,7**		**143,7**		**0,0**
	CH4	1,5%	1,6%	1,6%	0,00%	0,0%	0,0%	0,0%	0,0%	**0,0**		**0,0**		**0,0**		**0,0**
	N2	7,5%	7,4%	7,4%	0,00%	10,4%	5,4%	31,6%	0,0%	**40,3**		**21,0**		**202,4**		**0,0**
	total dry	94,4%	92,9%	91,3%	0,0%	94,5%	92,6%	93,5%	0,0%	365,4		361,7		599,2		0,0
	total wet	100,0%	100,0%	100,0%	0,0%	100,0%	100,0%	100,0%	0,0%	386,7		390,5		641,2		0,0
	GOD	29,2%	39,1%	42,3%	0,0%	29,2%	39,1%	42,3%	0,0%	29,2%		39,1%		42,3%		0,0%
	H2/H2O	3,16	2,32	1,84	0,00	3,16	2,32	1,84	0,00							
	CO/CO2	2,22	1,36	1,22	0,00	2,22	1,36	1,22	0,00							
temperature [°C]		760	750	350	0					**760**	**760**	**750**	**750**	**350**	**350**	**0**
residence time [min]		60	30	30	0					**60**	**5**	**30**	**35**	**30**	**0**	**0**
spec. gas rate plant [Nm³/t]		810	810	810	0											
supposed gas rate red. [Nm³/t]		6000	3200	3800	0											
defined uL retort [m/s]		0,9	0,9	0,9	0											
flow rate red. comp. [Ndm³/h]		20784	22169,6	26326,4	0											

		diameter retort [m]	0,158
		cross section retort [m²]	0,020
		absolute pressure [bar]	1,4
		atmospherical pressure [bar]	1,013

Baur-Glaessner-Diagram for gas mixtures of H_2, H_2O, CO, CO_2 / process conditions

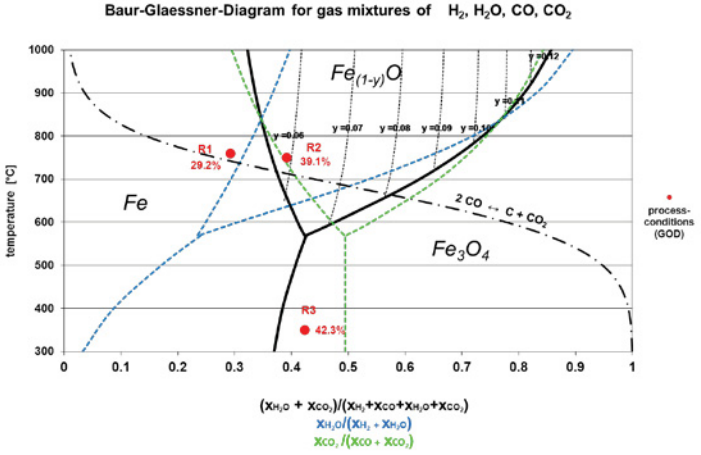

Copyright Chair of Metallurgy

CHAIR OF METALLURGY
MONTANUNIVERSITAET LEOBEN
PRIMARY METALLURGY
METALLURGICAL PROCESSES

Tel.: +43 3842 402-2201 Fax: DW 2202
Web: http://www.metallurgy.ac.at

160 mm Fluidized Bed Reactor test
Test information

Test number: **Test E** **Date:**
Customer: Siemens VAI

Kind of test: 3-stage 350/750/760°C 60 min. R1 FINEX
Target of the test: reduction behaviour of hematite

Test carried out by: Michael Skorianz Dial: 2255
michael.skorianz@unileoben.ac.at

Test information and results

Gas supply (reduction phases)

species	gas flow [Ndm³]	content/unit [Ndm³]	unit [pcs]
H2	8366,9	8900,0	**0,94**
H2O	3402,3	0,0	**0,00**
CO	20684,3	5900,0	**3,51**
CO2	12578,5	20300,0	**0,62**
CH4	0,0	12600,0	**0,00**
N2	9120,7	10700,0	**0,85**
sum	**54152,7**		**5,9**

Pressure test at 300 °C

position	200 Nl/min [mbar]	400 Nl/min [mbar]
Δp internal cyclone	2,7	6,5
p retort outlet	980	1013
Δp grid	9,5	34,1
p before grid	993	1052

Cleaning of grid before test x
Temperature sample after test <35 °C

Re-weight of input

position	[g]
bed	**2453**
int. cycl.	**79**
ext. cycl. vor Start	0
ext. cycl. R3	0
ext. cycl. R2	49
ext. cycl. R1	125
sum ext. cycl.	**174**
Filter	28
Rest	43
sum re-weight	**2776**

Test progress: -stage 350/750/760°C 60 min. R1 FINE

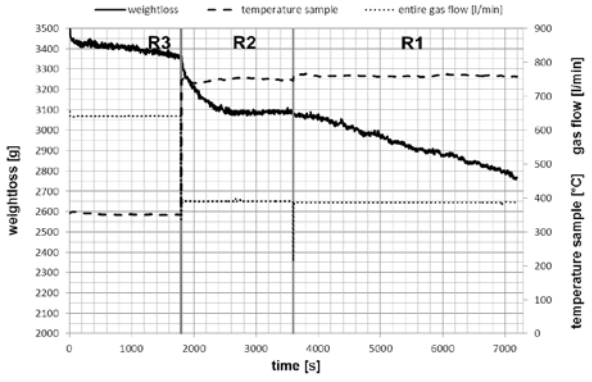

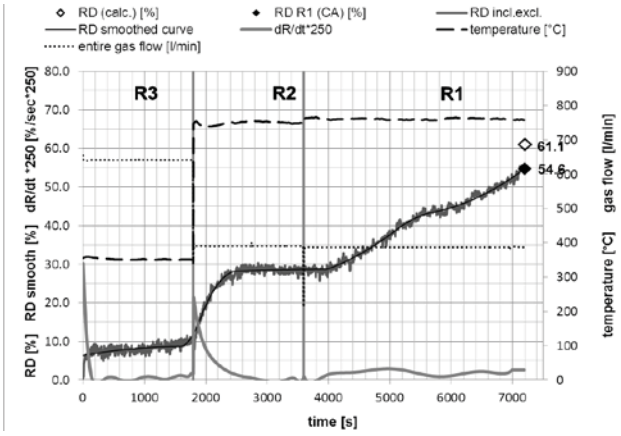

comments

increase N2 after filling in steps.

test progress ok

Copyright Chair of Metallurgy

CHAIR OF METALLURGY
MONTANUNIVERSITAET LEOBEN
PRIMARY METALLURGY
METALLURGICAL PROCESSES

Tel.: +43 3842 402-2201 Fax: DW 2202
Web: http://www.metallurgy.ac.at

160 mm Fluidized Bed Reactor test
Determination of grain size distribution

Test carried out by: Michael Skorianz Dial: 2255
michael.skorianz@unileoben.ac.at

Date:
Customer: Siemens VAI

kind of sieving: wet dry x
sieving method: three dimensional
standard:
apparatus: RETSCH AS 200
sieves size: 200 x 50 mm
sieving time: 10 min.
interval time: 10 sec.
amplitude: 1,5 mm

Test number: **Test E**

Kind of test:
3-stage 350/750/760°C 60 min. R1 FINEX
Target of the test: reduction behaviour of hematite
Ore type 1: hammersley fine ore MUL2010/0008
Ore type 2: -
MUL sample number: MUL2010/0008
VASL sample number: 0377/97

sieve analysis - results

sieves	raw material		bed			internal cyclone			bed + internal cyclone			bed + internal cyclone + discharge			summary	
fraction	fraction	cum.	weight	fraction	cum.	weight	fraction	cum.	weight	fraction	cum.	weight	fraction	cum.	fraction change	
[mm]	p3 [%]	Q3 [%]	m [g]	p3 [%]	Q3 [%]	m [g]	p3 [%]	Q3 [%]	m [g]	p3 [%]	Q3 [%]	m [g]	p3 [%]	Q3 [%]	Δp3 [%]	comment
4-6,3	0,0		0,0	0,0		0,0	0,0		0,0	0,0		0,0	0,0		0,0	0
2,8-4	13,3	100,0	195,9	8,0	100,0	0,0	0,0	100,0	195,9	7,7	100,0	195,9	7,1	100,0	-6,2	0
1,0-2,8	13,3	86,7	436,9	17,8	92,0	0,0	0,0	100,0	436,9	17,3	92,3	436,9	15,7	92,9	2,4	0
0,5-1,0	16,0	73,4	306,7	12,5	74,2	0,0	0,0	100,0	306,7	12,1	75,0	306,7	11,0	77,2	-5,0	0
0,25-0,5	17,4	57,4	366,6	14,9	61,7	0,0	0,0	100,0	366,6	14,5	62,9	366,6	13,2	66,2	-4,2	0
0,125-0,25	14,7	40,0	336,7	13,7	46,8	0,0	0,0	100,0	336,7	13,3	48,4	336,7	12,1	53,0	-2,6	0
0,063-0,125	25,3	25,3	552,6	22,5	33,0	0,0	0,0	100,0	552,6	21,8	35,1	552,6	19,9	40,8	-5,4	0
0-0,063	0,0	0,0	257,5	10,5	10,5	79,0	100,0	100,0	336,5	13,3	13,3	580,6	20,9	20,9	20,9	0
sum	**100**		**2453**	**100**		**79**	**100**		**2532**	**100**		**2776**	**100**		**0**	

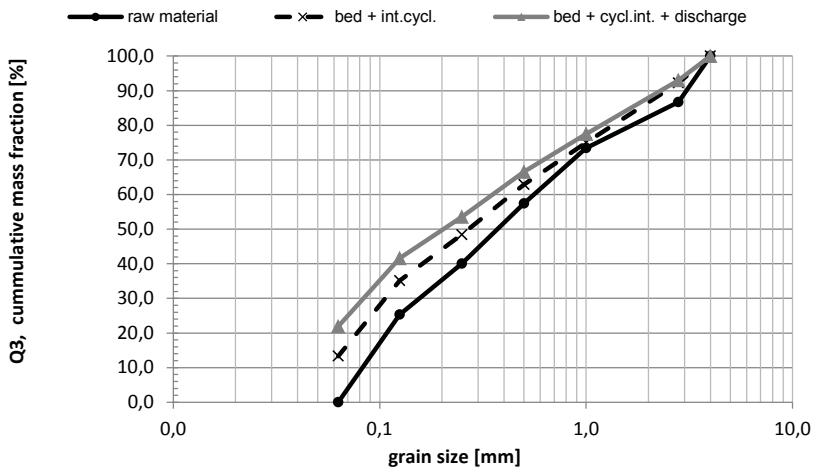

Copyright Chair of Metallurgy

CHAIR OF METALLURGY
MONTANUNIVERSITAET LEOBEN
PRIMARY METALLURGY
METALLURGICAL PROCESSES

Tel.: +43 3842 402-2201 Fax: DW 2202
Web: http://www.metallurgy.ac.at

160 mm Fluidized Bed Reactor test
Process conditions and test parameter

Test number: **Test F** **Date:**
Customer: Siemens VAI

Kind of test: 4-stage 480/680/750/760°C FINEX
Target of the test: reduction behaviour of hematite

Test carried out by: Michael Skorianz Dial: 2255
michael.skorianz@unileoben.ac.at

Raw material input

sieves	sieve analyis		input	comments
mesh size [mm]	fraction [%]	cum. [%]	mass [g]	
4-6,3	0		0,0	
2,8-4	13,3	100	465,5	
1,0-2,8	13,3	86,7	465,5	
0,5-1,0	16	73,4	560,0	hamersley fine ore MUL2010/0008
0,25-0,5	17,4	57,4	609,0	
0,125-0,25	14,7	40	514,5	
0,063-0,125	25,3	25,3	885,5	
0-0,063	0	0	0,0	
sum	100,0		3500,0	

chemical analyses

raw material: hamersley fine ore MUL2010/0008			
species	[%]	species	[%]
Fe(tot)	63,60	Na2O	0,00
FeO	0,58	Mn	0,17
Al2O3	2,07	Ni	0,00
SiO2	3,48	Cu	0,00
CaO	0,01	Cr	0,00
MgO	0,01	S	0,01
TiO2	0,12	P	0,07
K2O	0,01	Zn	0,00
V2O5	0,00	LOI (900°	3,30

reduced material						
species	bed Ø [%]	<0,063 [%]	0,25-0,50 [%]	1,0-2,8 [%]	int.cyc. [%]	ex.cyc. [%]
Fe tot	75,7	0,0	0,0	0,0	0,0	0,0
Fe met	24,7	0,0	0,0	0,0	0,0	0,0
FeO	51,2	0,0	0,0	0,0	0,0	0,0
C tot	0,070	0,000	0,000	0,000	0,000	0,000
MD	32,6	0,0	0,0	0,0	0,0	0,0
RD (CA)	50,1	0,0	0,0	0,0	0,0	0,0
RD (cal)	44,8	0,0	0,0	0,0	0,0	0,0
FeOx	0,7	0,0	0,0	0,0	0,0	0,0
Fe bal.	100,7	0,0	0,0	0,0	0,0	0,0

calculation of test parameter: 4-stage 480/680/750/760°C FINEX

		concentration, temp. plant				concentration test rig				gas flow test rig						
gas composition		R1 [%]	R2 [%]	R3 [%]	R4 [%]	R1 [%]	R2 [%]	R3 [%]	R4 [%]	R1 [Nl/min]	heating [Nl/min]	R2 [Nl/min]	heating [Nl/min]	R3 [Nl/min]	heating [Nl/min]	R4 [Nl/min]
species	H2	17,7%	16,5%	16,0%	16,00%	17,6%	16,3%	17,1%	15,5%	**68,1**		**63,5**		**71,8**		**82,1**
	H2O	5,6%	7,1%	8,7%	8,70%	5,6%	7,0%	9,3%	8,4%	**21,5**		**27,3**		**39,0**		**44,6**
	CO	46,7%	38,9%	36,5%	36,50%	46,4%	38,3%	39,1%	35,3%	**179,6**		**149,6**		**163,8**		**187,2**
	CO2	21,0%	28,5%	29,8%	29,80%	20,9%	28,1%	31,9%	28,8%	**80,8**		**109,6**		**133,7**		**152,8**
	CH4	1,5%	1,6%	1,6%	1,60%	0,0%	0,0%	0,0%	0,0%	**0,0**		**0,0**		**0,0**		**0,0**
	N2	7,5%	7,4%	7,4%	7,40%	9,5%	10,4%	2,6%	12,0%	**36,7**		**40,5**		**10,8**		**63,8**
	total dry	94,4%	92,9%	91,3%	91,3%	94,4%	93,0%	90,7%	91,6%	365,2		363,2		380,1		485,9
	total wet	100,0%	100,0%	100,0%	100,0%	100,0%	100,0%	100,0%	100,0%	386,7		390,5		419,2		530,5
	GOD	29,2%	39,1%	42,3%	42,3%	29,2%	39,1%	42,3%	42,3%	29,2%		39,1%		42,3%		42,3%
	H2/H2O	3,16	2,32	1,84	1,84	3,16	2,32	1,84	1,84							
	CO/CO2	2,22	1,36	1,22	1,22	2,22	1,36	1,22	1,22							
temperature [°C]		760	750	680	480					**760**	**0**	**750**	**0**	**680**	**0**	**480**
residence time [min]		40	40	30	30					**40**	**5**	**40**	**20**	**30**	**20**	**30**
spec. gas rate plant [Nm³/t]		810	810	810	810											
supposed gas rate red. [Nm³/t]		4000	4000	3500	4000											
defined uL retort [m/s]		0,9	0,9	0,9	0,9											
flow rate red. comp. [Ndm³/h]		21000	21000	24500	28000											

diameter retort [m]	0,158
cross section retort [m²]	0,020
absolute pressure [bar]	1,4
atmospherical pressure [bar]	1,013

Baur-Glaessner-Diagram for gas mixtures of H_2, H_2O, CO, CO_2 / process conditions

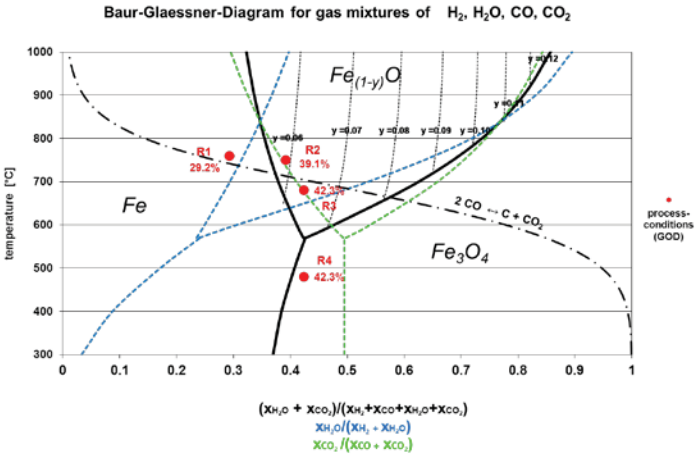

Copyright Chair of Metallurgy

CHAIR OF METALLURGY
MONTANUNIVERSITAET LEOBEN
PRIMARY METALLURGY
METALLURGICAL PROCESSES

Tel.: +43 3842 402-2201 Fax: DW 2202
Web: http://www.metallurgy.ac.at

160 mm Fluidized Bed Reactor test
Test information

Test number: Test F **Date:**
Customer: Siemens VAI

Kind of test: 4-stage 480/680/750/760°C FINEX
Target of the test: reduction behaviour of hematite

Test carried out by: Michael Skorianz Dial: 2255
michael.skorianz@unileoben.ac.at

Test information and results

Gas supply (reduction phases)

species	gas flow [Ndm³]	content/unit [Ndm³]	unit [pcs]
H2	9876,9	8900,0	**1,11**
H2O	4463,5	0,0	**0,00**
CO	23698,1	5900,0	**4,02**
CO2	16211,5	20300,0	**0,80**
CH4	0,0	12600,0	**0,00**
N2	5327,5	10700,0	**0,50**
sum	**59577,5**		**6,4**

Pressure test at 300 °C

position	200 Nl/min [mbar]	400 Nl/min [mbar]
Δp internal cyclone	2,4	6
p retort outlet	957	987
Δp grid	10,9	39,5
p before grid	969	1029

Cleaning of grid before test x
Temperature sample after test < 35 °C

Re-weight of input

position	[g]
bed	**1794**
int. cycl.	**919**
ext. cycl. R4	30
ext. cycl. R3	2
ext. cycl. R2	14
ext. cycl. R1	71
sum ext. cycl.	**117**
Filter	24
Rest	106
sum re-weight	**2960**

Test progress: 4-stage 480/680/750/760°C FINEX

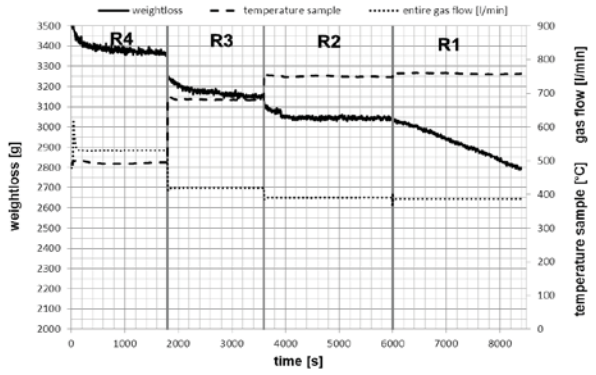

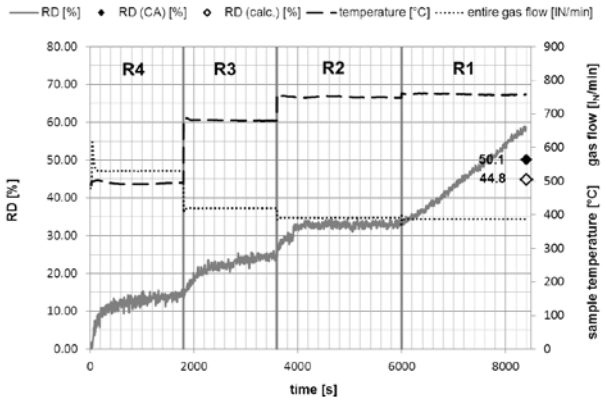

comments

increase N2 after filling in steps. Raw ore fraction 0,063-0,125 wet sieved. Heating after filling 38 minutes. Differential pressure grid from beginning R4 very high (ca. 230 mbar); after R3 and R2 superficial velosity decreased to 0,75 m/s because of high pressure; less discharge into external cyclone.

except elevated pressure, test ok

Copyright Chair of Metallurgy

CHAIR OF METALLURGY
MONTANUNIVERSITAET LEOBEN
PRIMARY METALLURGY
METALLURGICAL PROCESSES

Tel.: +43 3842 402-2201 Fax: DW 2202
Web: http://www.metallurgy.ac.at

Determination of grain size distribution - fluidized bed test -

Test carried out by: Michael Skorianz Dial: 2255
michael.skorianz@unileoben.ac.at

Date:
Customer: Siemens VAI

kind of sieving: wet dry x
sieving method: three dimensional
standard:
apparatus: RETSCH AS 200
sieves size: 200 x 50 mm
sieving time: 10 min.
interval time: 10 sec.
amplitude: 1,5 mm

Test number: **Test F**

Kind of test:
4-stage 480/680/750/760°C FINEX
Target of the test: reduction behaviour of hematite
Ore type 1: hamersley fine ore MUL2010/0008
Ore type 2: -
MUL sample number: MUL2010/0008
VASL sample number: 0377/97

sieve analysis - results

sieves	raw material		bed			internal cyclone			bed + internal cyclone			bed + internal cyclone + discharge			summary	
fraction	fraction	cum.	weight	fraction	cum.	weight	fraction	cum.	weight	fraction	cum.	weight	fraction	cum.	fraction change	
[mm]	[%]	[%]	[g]	[%]	[%]	[g]	[%]	[%]	[g]	[%]	[%]	[g]	[%]	[%]	[%]	comment
4-6,3	0,0		0,0	0,0		0,0	0,0		0,0	0,0		0,0	0,0		0,0	0
2,8-4	13,3	100,0	143,3	8,0	100,0	0,0	0,0	100,0	143,3	5,3	100,0	143,3	4,8	100,0	-8,5	0
1,0-2,8	13,3	86,7	424,1	23,6	92,0	0,0	0,0	100,0	424,1	15,6	94,7	424,1	14,3	95,2	1,0	0
0,5-1,0	16,0	73,4	267,4	14,9	68,4	0,0	0,0	100,0	267,4	9,9	79,1	267,4	9,0	80,8	-7,0	0
0,25-0,5	17,4	57,4	281,9	15,7	53,5	8,0	0,9	100,0	290,0	10,7	69,2	290,0	9,8	71,8	-7,6	0
0,125-0,25	14,7	40,0	282,9	15,8	37,8	6,4	0,7	99,1	289,3	10,7	58,5	289,3	9,8	62,0	-4,9	0
0,063-0,125	25,3	25,3	370,1	20,6	22,0	412,2	44,9	98,4	782,4	28,8	47,9	782,4	26,4	52,2	1,1	0
0-0,063	0,0	0,0	24,2	1,3	1,3	492,3	53,6	53,6	516,6	19,0	19,0	763,6	25,8	25,8	25,8	0
sum	**100**		**1794**	**100**		**919**	**100**		**2713**	**100**		**2960**	**100**		**0**	

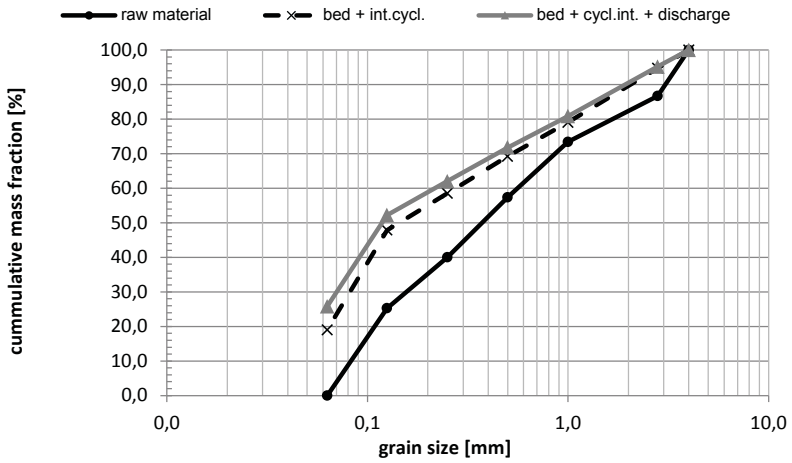

Copyright Chair of Metallurgy

CHAIR OF METALLURGY
MONTANUNIVERSITAET LEOBEN
PRIMARY METALLURGY
METALLURGICAL PROCESSES

Tel.: +43 3842 402-2201 Fax: DW 2202
Web: http://www.metallurgy.ac.at

160 mm Fluidized Bed Reactor test
Process conditions and test parameter

Test number: **Test G** **Date:**
Customer: Siemens VAI

Kind of test: 3-stage 480/750/760°C FINEX
Target of the test: changing gas composition in R1

Test carried out by: Michael Skorianz Dial: 2255
michael.skorianz@unileoben.ac.at

Raw material input

sieves	sieve analyis		input	comments
mesh size [mm]	fraction [%]	cum. [%]	mass [g]	
4-6,3	0		0,0	
2,8-4	13,3	100	458,6	
1,0-2,8	13,3	86,7	458,6	
0,5-1,0	16	73,4	551,7	hamersley fine ore MUL2010/0008
0,25-0,5	17,4	57,4	600,0	
0,125-0,25	14,7	40	506,9	
0,063-0,125	25,3	25,3	872,3	
0-0,063	0	0	0,0	
sum	100,0		3448,0	

chemical analyses

raw material: hamersley fine ore MUL2010/0008			
species	[%]	species	[%]
Fe(tot)	63,60	Na2O	0,00
FeO	0,58	Mn	0,17
Al2O3	2,07	Ni	0,00
SiO2	3,48	Cu	0,00
CaO	0,01	Cr	0,00
MgO	0,01	S	0,01
TiO2	0,12	P	0,07
K2O	0,01	Zn	0,00
V2O5	0,00	LOI (900°	3,30

reduced material						
species	bed Ø [%]	R4 [%]	R3 [%]	R2 [%]	int.cyc. [%]	ex.cyc. [%]
Fe tot	83,7	0,0	0,0	0,0	0,0	0,0
Fe met	59,4	0,0	0,0	0,0	0,0	0,0
FeO	23,8	0,0	0,0	0,0	0,0	0,0
C tot	0,069	0,000	0,000	0,000	0,000	0,000
MD	71,0	0,0	0,0	0,0	0,0	0,0
RD (CA)	78,3	0,0	0,0	0,0	0,0	0,0
RD (cal)	84,5	0,0	0,0	0,0	0,0	0,0
FeOx	0,3	0,0	0,0	0,0	0,0	0,0
Fe bal.	97,0	0,0	0,0	0,0	0,0	0,0

calculation of test parameter: 3-stage 480/750/760°C FINEX

	gas composition	concentration, temp. plant R1 [%]	R2 [%]	R3 [%]	R4 [%]	concentration test rig R1 [%]	R2 [%]	R3 [%]	R4 [%]	gas flow test rig R1 [Nl/min]	heating [Nl/min]	R2 [Nl/min]	heating [Nl/min]	R3 [Nl/min]	heating [Nl/min]	R4 [Nl/min]
species	H2	17,7%	16,5%	16,0%	0,00%	17,3%	17,1%	14,5%	0,0%	**67,1**	**74,6**	**66,7**		**76,8**		**0,0**
	H2O	5,6%	7,1%	8,7%	0,00%	5,5%	7,3%	7,9%	0,0%	**21,2**	**6,4**	**28,7**		**41,8**		**0,0**
	CO	46,7%	38,9%	36,5%	0,00%	45,8%	40,3%	33,0%	0,0%	**176,9**	**166,8**	**157,2**		**175,2**		**0,0**
	CO2	21,0%	28,5%	29,8%	0,00%	20,6%	29,5%	27,0%	0,0%	**79,6**	**14,6**	**115,2**		**143,0**		**0,0**
	CH4	1,5%	1,6%	1,6%	0,00%	0,0%	0,0%	0,0%	0,0%	**0,0**	**0,0**	**0,0**		**0,0**		**0,0**
	N2	7,5%	7,4%	7,4%	0,00%	10,8%	5,8%	17,7%	0,0%	**41,9**	**30,2**	**22,7**		**93,8**		**0,0**
	total dry	94,4%	92,9%	91,3%	0,0%	94,5%	92,7%	92,1%	0,0%	365,5	286,2	361,8		488,7		0,0
	total wet	100,0%	100,0%	100,0%	0,0%	100,0%	100,0%	100,0%	0,0%	386,7	292,6	390,5		530,5		0,0
	GOD	29,2%	39,1%	42,3%	0,0%	29,2%	39,1%	42,3%	0,0%	29,2%	8,0%	39,1%		42,3%		0,0%
	H2/H2O	3,16	2,32	1,84	0,00	3,16	2,32	1,84	0,00							
	CO/CO2	2,22	1,36	1,22	0,00	2,22	1,36	1,22	0,00							
temperature [°C]		760	750	480	0					**760**	**760**	**750**	**750**	**480**	**480**	**0**
residence time [min]		40	30	30	0					**40**	**25**	**30**	**5**	**30**	**0**	**0**
spec. gas rate plant [Nm³/t]		810	810	810	0											
supposed gas rate red. [Nm³/t]		4000	3200	3800	0											
defined uL retort [m/s]		0,9	0,9	0,9	0											
flow rate red. comp. [Ndm³/h]		20688	22067,2	26204,8	0											

			diameter retort [m]		0,158
			cross section retort [m²]		0,020
			absolute pressure [bar]		1,4
			atmospherical pressure [bar]		1,013

Baur-Glaessner-Diagram for gas mixtures of H_2, H_2O, CO, CO_2 / process conditions

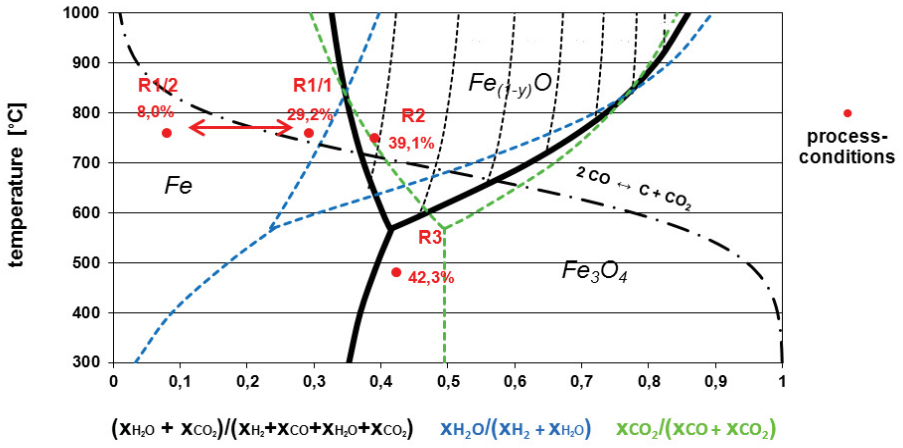

Copyright Chair of Metallurgy

CHAIR OF METALLURGY
MONTANUNIVERSITAET LEOBEN
PRIMARY METALLURGY
METALLURGICAL PROCESSES

Tel.: +43 3842 402-2201 Fax: DW 2202
Web: http://www.metallurgy.ac.at

160 mm Fluidized Bed Reactor test
Test information

Test number: Test G **Date:**
Customer: Siemens VAI

Kind of test: 3-stage 480/750/760°C FINEX
Target of the test: changing gas composition in R1

Test carried out by: Michael Skorianz Dial: 2255
michael.skorianz@unileoben.ac.at

Test information and results

Gas supply (reduction phases)

species	gas flow [Ndm³]	content/unit [Ndm³]	unit [pcs]
H2	6986,9	8900,0	**0,79**
H2O	2962,2	0,0	**0,00**
CO	17049,8	5900,0	**2,89**
CO2	10929,0	20300,0	**0,54**
CH4	0,0	12600,0	**0,00**
N2	5169,6	10700,0	**0,48**
sum	**43097,6**		**4,7**

Pressure test at 300 °C

position	200 Nl/min [mbar]	400 Nl/min [mbar]
Δp internal cyclone	2,4	6,3
p retort outlet	963	1001
Δp grid	11,1	34,5
p before grid	974	1038

Cleaning of grid before test x
Temperature sample after test < 35 °C

Re-weight of input

position	[g]
bed	**2257**
int. cycl.	**260**
ext. cycl. vor Start	0
ext. cycl. R3	13
ext. cycl. R2	8
ext. cycl. R1	4
sum ext. cycl.	**25**
Filter	0
Rest	0
sum re-weight	**2542**

Test progress: 3-stage 480/750/760°C FINEX

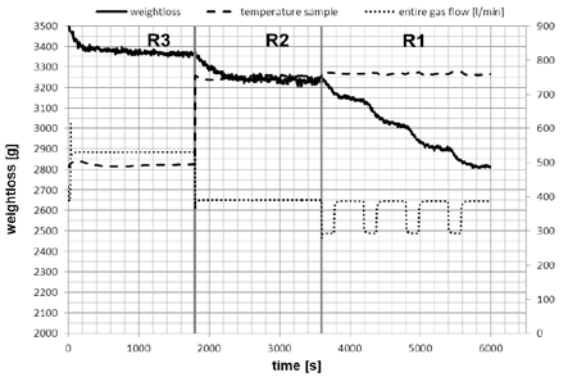

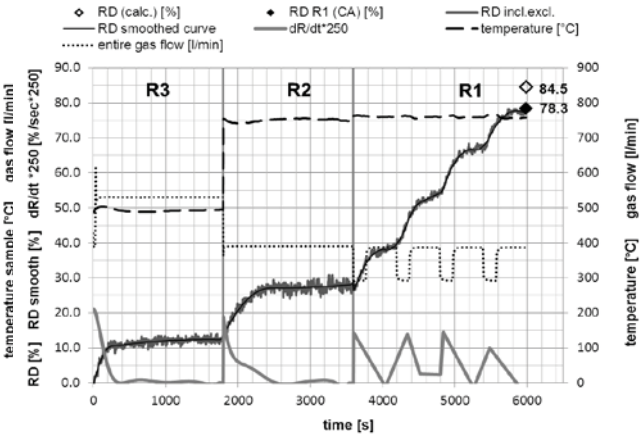

comments

increase N2 after filling without steps. Raw ore fraction 0,063-0,125 wet sieved. Gas composition pulsating in R1. Huge increase of RD (+37,1 %) compared to other tests with similar gas composition.

Pulsating conditions in R1:
alternating 3 min. GOD=8,0 and 7 min GOD=29,0

Test progress ok

Copyright Chair of Metallurgy

CHAIR OF METALLURGY
MONTANUNIVERSITAET LEOBEN
PRIMARY METALLURGY
METALLURGICAL PROCESSES

Tel.: +43 3842 402-2201 Fax: DW 2202
Web: http://www.metallurgy.ac.at

160 mm Fluidized Bed Reactor test
Determination of grain size distribution

Test carried out by: Michael Skorianz Dial: 2255
michael.skorianz@unileoben.ac.at

Date:
Customer: Siemens VAI

kind of sieving: wet dry x
sieving method: three dimensional
standard:
apparatus: RETSCH AS 200
sieves size: 200 x 50 mm
sieving time: 10 min.
interval time: 10 sec.
amplitude: 1,5 mm

Test number: **Test G**

Kind of test:
3-stage 480/750/760°C FINEX
Target of the test: changing gas composition in R1
Ore type 1: hamersley fine ore MUL2010/0008
Ore type 2: -
MUL sample number: MUL2010/0008
VASL sample number: 0377/97

sieve analysis - results

sieves	raw material		bed			internal cyclone			bed + internal cyclone			bed + internal cyclone + discharge			summary	
fraction	fraction	cum.	weight	fraction	cum.	weight	fraction	cum.	weight	fraction	cum.	weight	fraction	cum.	fraction change	
[mm]	p3 [%]	Q3 [%]	m [g]	p3 [%]	Q3 [%]	m [g]	p3 [%]	Q3 [%]	m [g]	p3 [%]	Q3 [%]	m [g]	p3 [%]	Q3 [%]	Δp3 [%]	comment
4-6,3	0,0		0,0	0,0		0,0	0,0		0,0	0,0		0,0	0,0		0,0	0
2,8-4	13,3	100,0	260,4	11,5	100,0	0,0	0,0	100,0	260,4	10,3	100,0	260,4	10,2	100,0	-3,1	0
1,0-2,8	13,3	86,7	393,8	17,4	88,5	0,0	0,0	100,0	393,8	15,6	89,7	393,8	15,5	89,8	2,2	0
0,5-1,0	16,0	73,4	302,3	13,4	71,0	9,8	3,8	100,0	312,1	12,4	74,0	312,1	12,3	74,3	-3,7	0
0,25-0,5	17,4	57,4	318,2	14,1	57,6	12,4	4,8	96,2	330,5	13,1	61,6	330,5	13,0	62,0	-4,4	0
0,125-0,25	14,7	40,0	283,4	12,6	43,5	14,2	5,5	91,5	297,6	11,8	48,5	297,6	11,7	49,0	-3,0	0
0,063-0,125	25,3	25,3	407,9	18,1	31,0	24,6	9,5	86,0	432,5	17,2	36,7	432,5	17,0	37,3	-8,3	0
0-0,063	0,0	0,0	291,1	12,9	12,9	199,0	76,5	76,5	490,1	19,5	19,5	515,1	20,3	20,3	20,3	0
sum	**100**		**2257**	**100**		**260**	**100**		**2517**	**100**		**2542**	**100**		**0**	

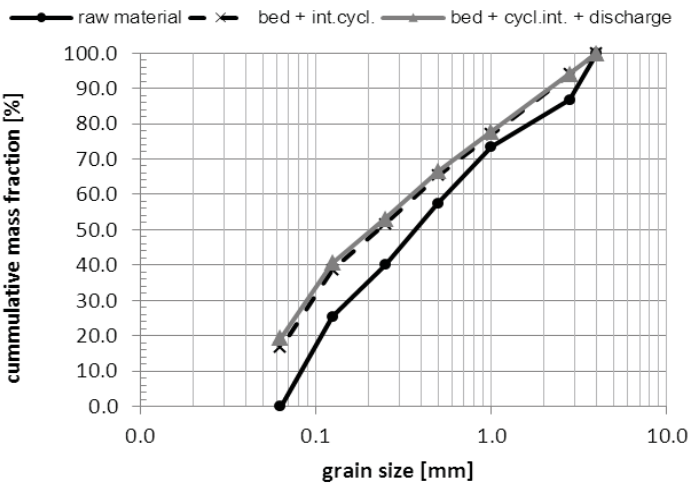

Copyright Chair of Metallurgy

CHAIR OF METALLURGY
MONTANUNIVERSITAET LEOBEN
PRIMARY METALLURGY
METALLURGICAL PROCESSES

Tel.: +43 3842 402-2201 Fax: DW 2202
Web: http://www.metallurgy.ac.at

160 mm Fluidized Bed Reactor test
Process conditions and test parameter

Test number: **Test H** **Date:**
Customer: Siemens VAI

Kind of test: 3-stage 480/750/760°C FINEX
Target of the test: reduction behaviour of hematite

Test carried out by: Michael Skorianz Dial: 2255
michael.skorianz@unileoben.ac.at

Raw material input

sieves	sieve analyis		input	comments
mesh size [mm]	fraction [%]	cum. [%]	mass [g]	
4-6,3	0		0,0	
2,8-4	13,3	100	454,5	
1,0-2,8	13,3	86,7	454,5	
0,5-1,0	16	73,4	546,8	hamersley fine ore MUL2010/0008
0,25-0,5	17,4	57,4	594,6	
0,125-0,25	14,7	40	502,4	
0,063-0,125	25,3	25,3	864,6	
0-0,063	0	0	0,0	
sum	100,0		3417,4	

chemical analyses

raw material: hamersley fine ore MUL2010/0008			
species	[%]	species	[%]
Fe(tot)	63,60	Na2O	0,00
FeO	0,58	Mn	0,17
Al2O3	2,07	Ni	0,00
SiO2	3,48	Cu	0,00
CaO	0,01	Cr	0,00
MgO	0,01	S	0,01
TiO2	0,12	P	0,07
K2O	0,01	Zn	0,00
V2O5	0,00	LOI (900°	3,30

reduced material						
species	bed Ø [%]	R4 [%]	R3 [%]	R2 [%]	int.cyc. [%]	ex.cyc. [%]
Fe tot	76,1	0,0	67,3	70,5	0,0	0,0
Fe met	24,5	0,0	0,2	0,3	0,0	0,0
FeO	54,7	0,0	28,6	72,6	0,0	0,0
C tot	0,134	0,000	0,101	0,117	0,000	0,000
MD	32,2	0,0	0,2	0,4	0,0	0,0
RD (CA)	50,8	0,0	11,2	27,1	0,0	0,0
RD (cal)	54,3	0,0	0,0	0,0	0,0	0,0
FeOx	0,7	0,0	0,0	0,0	0,0	0,0
Fe bal.	98,1	0,0	0,0	0,0	0,0	0,0

calculation of test parameter: 3-stage 480/750/760°C FINEX

		concentration, temp. plant				concentration test rig				gas flow test rig						
gas composition		R1 [%]	R2 [%]	R3 [%]	R4 [%]	R1 [%]	R2 [%]	R3 [%]	R4 [%]	R1 [Nl/min]	heating [Nl/min]	R2 [Nl/min]	heating [Nl/min]	R3 [Nl/min]	heating [Nl/min]	R4 [Nl/min]
species	H2	17,7%	16,5%	16,0%	0,00%	17,2%	16,9%	14,3%	0,0%	**66,5**		**66,1**		**76,1**		**0,0**
	H2O	5,6%	7,1%	8,7%	0,00%	5,4%	7,3%	7,8%	0,0%	**21,0**		**28,4**		**41,4**		**0,0**
	CO	46,7%	38,9%	36,5%	0,00%	45,4%	39,9%	32,7%	0,0%	**175,4**		**155,8**		**173,6**		**0,0**
	CO2	21,0%	28,5%	29,8%	0,00%	20,4%	29,2%	26,7%	0,0%	**78,9**		**114,2**		**141,8**		**0,0**
	CH4	1,5%	1,6%	1,6%	0,00%	0,0%	0,0%	0,0%	0,0%	**0,0**		**0,0**		**0,0**		**0,0**
	N2	7,5%	7,4%	7,4%	0,00%	11,6%	6,6%	18,4%	0,0%	**45,0**		**26,0**		**97,6**		**0,0**
	total dry	94,4%	92,9%	91,3%	0,0%	94,6%	92,7%	92,2%	0,0%	365,7		362,0		489,1		0,0
	total wet	100,0%	100,0%	100,0%	0,0%	100,0%	100,0%	100,0%	0,0%	386,7		390,5		530,5		0,0
	GOD	29,2%	39,1%	42,3%	0,0%	29,2%	39,1%	42,3%	0,0%	29,2%		39,1%		42,3%		0,0%
	H2/H2O	3,16	2,32	1,84	0,00	3,16	2,32	1,84	0,00							
	CO/CO2	2,22	1,36	1,22	0,00	2,22	1,36	1,22	0,00							
temperature [°C]		760	750	480	0					**760**	**760**	**750**	**750**	**480**	**480**	**0**
residence time [min]		40	30	30	0					**40**	**15**	**30**	**35**	**30**	**0**	**0**
spec. gas rate plant [Nm³/t]		810	810	810	0					diameter retort [m]					0,158	
supposed gas rate red. [Nm³/t]		4000	3200	3800	0					cross section retort [m²]					0,020	
defined uL retort [m/s]		0,9	0,9	0,9	0					absolute pressure [bar]					1,4	
flow rate red. comp. [Ndm³/h]		20504,2	21871,1	25971,9	0					atmospherical pressure [bar]					1,013	

Baur-Glaessner-Diagram for gas mixtures of H_2, H_2O, CO, CO_2 / process conditions

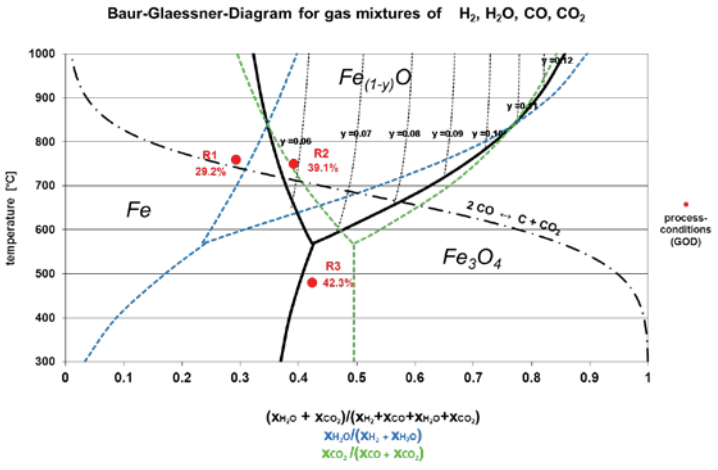

CHAIR OF METALLURGY
MONTANUNIVERSITAET LEOBEN
PRIMARY METALLURGY
METALLURGICAL PROCESSES

Tel.: +43 3842 402-2201 Fax: DW 2202
Web: http://www.metallurgy.ac.at

160 mm Fluidized Bed Reactor test
Test information

Test number: **Test H** **Date:**
Customer: Siemens VAI

Kind of test: 3-stage 480/750/760°C FINEX
Target of the test: reduction behaviour of hematite

Test carried out by: Michael Skorianz Dial: 2255
michael.skorianz@unileoben.ac.at

Test information and results

Gas supply (reduction phases)

species	gas flow [Ndm³]	content/unit [Ndm³]	unit [pcs]
H2	6924,8	8900,0	**0,78**
H2O	2935,9	0,0	**0,00**
CO	16898,3	5900,0	**2,86**
CO2	10831,9	20300,0	**0,53**
CH4	0,0	12600,0	**0,00**
N2	5506,7	10700,0	**0,51**
sum	**43097,6**		**4,7**

Pressure test at 300 °C

position	200 Nl/min [mbar]	400 Nl/min [mbar]
Δp internal cyclone	2,3	5,6
p retort outlet	993	1044
Δp grid	8,3	29,4
p before grid	1002	1076

Cleaning of grid before test x
Temperature sample after test 0 °C

Re-weight of input

position	[g]
bed	**2130**
int. cycl.	**60**
ext. cycl. vor Start	0
ext. cycl. R3	11
ext. cycl. R2	69
ext. cycl. R1	40
sum ext. cycl.	**120**
Filter	6
Rest	32
sum re-weight	**2802**

Test progress: 3-stage 480/750/760°C FINEX

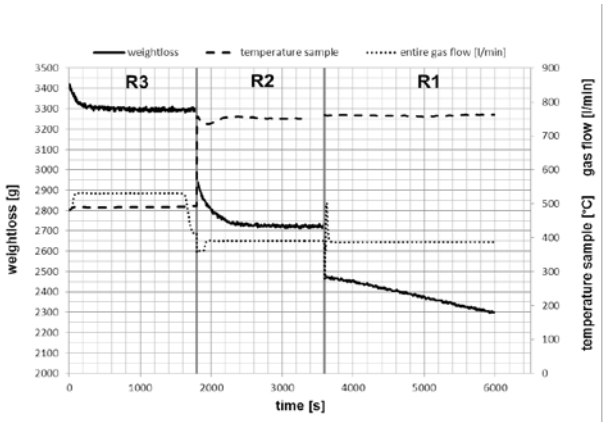

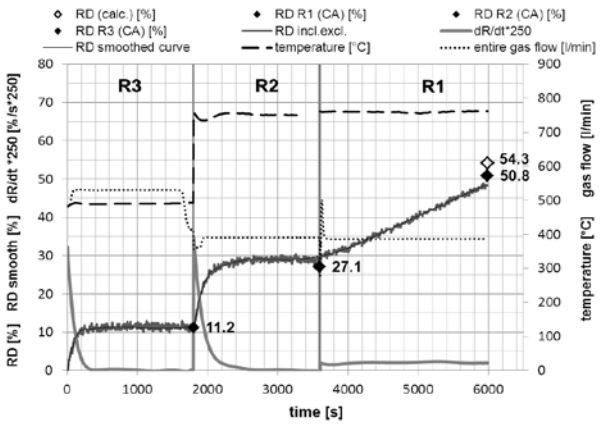

comments

Ore drying 5 h at 105 °C. Increase N2 after filling in steps. Sampling test in N2-phase (480°C, ca. 500 lN/min). 2 short pushes - 80 g sample mass). Restart before test start (overpressure evaporator). R3 ok, finish of R3 breakoff due to CO2 overpressure, valve CO2). Restart and sampling at 480°C in N2-phase. N2 purging of sampling system 3 min, 10 lN/min N2, temperature colling water 60 °C for 10 min, then 30 °C. Heating up to 750°C. R2 ok. Sampling (sampe procedure, 4 short pushes). R1 ok.

test ok

Copyright Chair of Metallurgy

CHAIR OF METALLURGY
MONTANUNIVERSITAET LEOBEN
PRIMARY METALLURGY
METALLURGICAL PROCESSES

Tel.: +43 3842 402-2201 Fax: DW 2202
Web: http://www.metallurgy.ac.at

160 mm Fluidized Bed Reactor test
Determination of grain size distribution

Test carried out by: Michael Skorianz Dial: 2255
michael.skorianz@unileoben.ac.at

Date:

Customer: Siemens VAI

kind of sieving: wet dry x
sieving method: three dimensional
standard:
apparatus: RETSCH AS 200
sieves size: 200 x 50 mm
sieving time: 10 min.
interval time: 10 sec.
amplitude: 1,5 mm

Test number: **Test H**

Kind of test:
3-stage 480/750/760°C FINEX
Target of the test: reduction behaviour of hematite
Ore type 1: hamersley fine ore MUL2010/0008
Ore type 2: -
MUL sample number: MUL2010/0008
VASL sample number: 0377/97

sieve analysis - results

sieves	raw material		bed			internal cyclone			bed + internal cyclone			bed + internal cyclone + discharge			summary	
fraction	fraction	cum.	weight	fraction	cum.	weight	fraction	cum.	weight	fraction	cum.	weight	fraction	cum.	fraction change	
[mm]	p3 [%]	Q3 [%]	m [g]	p3 [%]	Q3 [%]	m [g]	p3 [%]	Q3 [%]	m [g]	p3 [%]	Q3 [%]	m [g]	p3 [%]	Q3 [%]	Δp3 [%]	comment
4-6,3	0,0		0,0	0,0		0,0	0,0		0,0	0,0		0,0	0,0		0,0	0
2,8-4	13,3	100,0	221,5	10,4	100,0	0,0	0,0	100,0	221,5	10,1	100,0	221,5	9,4	100,0	-3,9	0
1,0-2,8	13,3	86,7	403,6	19,0	89,6	0,0	0,0	100,0	403,6	18,4	89,9	403,6	17,2	90,6	3,9	0
0,5-1,0	16,0	73,4	327,6	15,4	70,7	0,0	0,0	100,0	327,6	15,0	71,5	327,6	14,0	73,4	-2,0	0
0,25-0,5	17,4	57,4	324,8	15,3	55,3	0,0	0,0	100,0	324,8	14,8	56,5	324,8	13,8	59,4	-3,6	0
0,125-0,25	14,7	40,0	315,2	14,8	40,0	0,0	0,0	100,0	315,2	14,4	41,7	315,2	13,4	45,6	-1,3	0
0,063-0,125	25,3	25,3	362,1	17,0	25,2	0,0	0,0	100,0	362,1	16,5	27,3	362,1	15,4	32,2	-9,9	0
0-0,063	0,0	0,0	175,1	8,2	8,2	60,0	100,0	100,0	235,1	10,7	10,7	393,1	16,7	16,7	16,7	0
sum	**100**		**2130**	**100**		**60**	**100**		**2190**	**100**		**2348**	**100**		**0**	

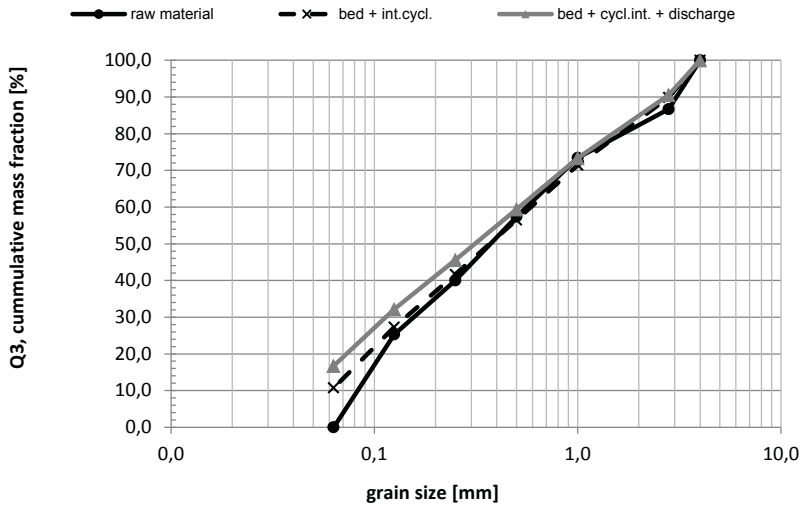

Copyright Chair of Metallurgy

CHAIR OF METALLURGY
MONTANUNIVERSITAET LEOBEN
PRIMARY METALLURGY
METALLURGICAL PROCESSES

Tel.: +43 3842 402-2201 Fax: DW 2202
Web: http://www.metallurgy.ac.at

160 mm Fluidized Bed Reactor test
Process conditions and test parameter

Test number: **Test I** **Date:**
Customer: Siemens VAI

Kind of test: 3-stage 480/750/760°C FINEX
Target of the test: reduction behaviour of magnetite

Test carried out by: Michael Skorianz Dial: 2255
michael.skorianz@unileoben.ac.at

Raw material input

sieves	sieve analyis		input	comments
mesh size [mm]	fraction [%]	cum. [%]	mass [g]	
4-6,3	0		0,0	
2,8-4	13,3	100	465,5	
1,0-2,8	13,3	86,7	465,5	Kiruna Magnetite (Svappavaara Ore); ground, selected
0,5-1,0	16	73,4	560,0	
0,25-0,5	17,4	57,4	609,0	
0,125-0,25	14,7	40	514,5	
0,063-0,125	25,3	25,3	885,5	
0-0,063	0	0	0,0	
sum	100,0		3500,0	

chemical analyses

raw material: Magnetite (Svappavaara Ore); ground, s				reduced material: species	bed Ø	R4	R3	R2	int.cyc.	ex.cyc.
species	[%]	species	[%]		[%]	[%]	[%]	[%]	[%]	[%]
Fe(tot)	65,20	Na2O	0,00	Fe tot	69,1	0,0	65,1	68,7	0,0	0,0
FeO	26,41	Mn	0,07	Fe met	3,8	0,0	0,1	0,1	0,0	0,0
Al2O3	0,41	Ni	0,00	FeO	58,3	0,0	27,4	58,6	0,0	0,0
SiO2	3,30	Cu	0,00	C tot	0,040	0,000	0,119	0,037	0,000	0,000
CaO	2,24	Cr	0,00	MD	5,5	0,0	0,1	0,2	0,0	0,0
MgO	0,81	S	0,04	RD (CA)	27,4	0,0	11,0	22,3	0,0	0,0
TiO2	0,43	P	0,45	RD (cal)	32,2	0,0	0,0	0,0	0,0	0,0
K2O	0,19	Zn	0,00	FeOx	1,1	0,0	0,0	0,0	0,0	0,0
V2O5	0,00	LOI (900°	2,26	Fe bal.	98,8	0,0	0,0	0,0	0,0	0,0

calculation of test parameter: 3-stage 480/750/760°C FINEX

		concentration, temp. plant				concentration test rig				gas flow test rig						
gas composition		R1 [%]	R2 [%]	R3 [%]	R4 [%]	R1 [%]	R2 [%]	R3 [%]	R4 [%]	R1 [Nl/min]	heating [Nl/min]	R2 [Nl/min]	heating [Nl/min]	R3 [Nl/min]	heating [Nl/min]	R4 [Nl/min]
species	H2	17,7%	16,5%	16,0%	0,00%	17,6%	17,3%	14,7%	0,0%	**68,1**		**67,7**		**77,9**		**0,0**
	H2O	5,6%	7,1%	8,7%	0,00%	5,6%	7,5%	8,0%	0,0%	**21,5**		**29,1**		**42,4**		**0,0**
	CO	46,7%	38,9%	36,5%	0,00%	46,4%	40,9%	33,5%	0,0%	**179,6**		**159,6**		**177,8**		**0,0**
	CO2	21,0%	28,5%	29,8%	0,00%	20,9%	29,9%	27,4%	0,0%	**80,8**		**116,9**		**145,2**		**0,0**
	CH4	1,5%	1,6%	1,6%	0,00%	0,0%	0,0%	0,0%	0,0%	**0,0**		**0,0**		**0,0**		**0,0**
	N2	7,5%	7,4%	7,4%	0,00%	9,5%	4,4%	16,4%	0,0%	**36,7**		**17,2**		**87,2**		**0,0**
	total dry	94,4%	92,9%	91,3%	0,0%	94,4%	92,5%	92,0%	0,0%	365,2		361,4		488,1		0,0
	total wet	100,0%	100,0%	100,0%	0,0%	100,0%	100,0%	100,0%	0,0%	386,7		390,5		530,5		0,0
	GOD	29,2%	39,1%	42,3%	0,0%	29,2%	39,1%	42,3%	0,0%	29,2%		39,1%		42,3%		0,0%
	H2/H2O	3,16	2,32	1,84	0,00	3,16	2,32	1,84	0,00							
	CO/CO2	2,22	1,36	1,22	0,00	2,22	1,36	1,22	0,00							
temperature [°C]		760	750	480	0					**760**	**760**	**750**	**750**	**480**	**480**	**0**
residence time [min]		40	30	30	0					**40**	**15**	**30**	**35**	**30**	**0**	**0**
spec. gas rate plant [Nm³/t]		810	810	810	0											
supposed gas rate red. [Nm³/t]		4000	3200	3800	0											
defined uL retort [m/s]		0,9	0,9	0,9	0											
flow rate red. comp. [Ndm³/h]		21000	22400	26600	0											

		diameter retort [m]	0,158
		cross section retort [m²]	0,020
		absolute pressure [bar]	1,4
		atmospherical pressure [bar]	1,013

Baur-Glaessner-Diagram for gas mixtures of H_2, H_2O, CO, CO_2 / process conditions

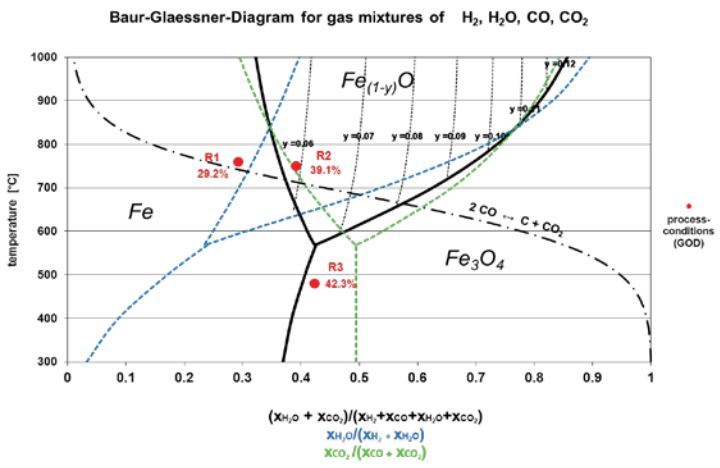

Copyright Chair of Metallurgy

CHAIR OF METALLURGY
MONTANUNIVERSITAET LEOBEN
PRIMARY METALLURGY
METALLURGICAL PROCESSES

Tel.: +43 3842 402-2201 Fax: DW 2202
Web: http://www.metallurgy.ac.at

160 mm Fluidized Bed Reactor test
Test information

Test number: Test I **Date:**
Customer: Siemens VAI

Kind of test: 3-stage 480/750/760°C FINEX
Target of the test: reduction behaviour of magnetite

Test carried out by: Michael Skorianz Dial: 2255
michael.skorianz@unileoben.ac.at

Test information and results

Gas supply (reduction phases)

species	gas flow [Ndm³]	content/unit [Ndm³]	unit [pcs]
H2	7092,3	8900,0	**0,80**
H2O	3006,9	0,0	**0,00**
CO	17306,9	5900,0	**2,93**
CO2	11093,8	20300,0	**0,55**
CH4	0,0	12600,0	**0,00**
N2	4597,6	10700,0	**0,43**
sum	**43097,6**		**4,7**

Pressure test at 300 °C

position	200 Nl/min [mbar]	400 Nl/min [mbar]
Δp internal cyclone	2,3	6
p retort outlet	974	1010
Δp grid	9,5	34,1
p before grid	985	1049

Cleaning of grid before test -
Temperature sample after test 28 °C

Re-weight of input

position	[g]
bed	**2542**
int. cycl.	**163**
ext. cycl. vor Start	0
ext. cycl. R3	20
ext. cycl. R2	16
ext. cycl. R1	3
sum ext. cycl.	**39**
Filter	4
Rest	17
sum re-weight	**3263**

Test progress: 3-stage 480/750/760°C FINEX

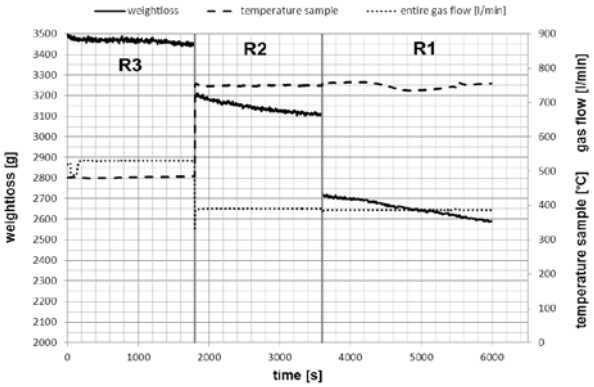

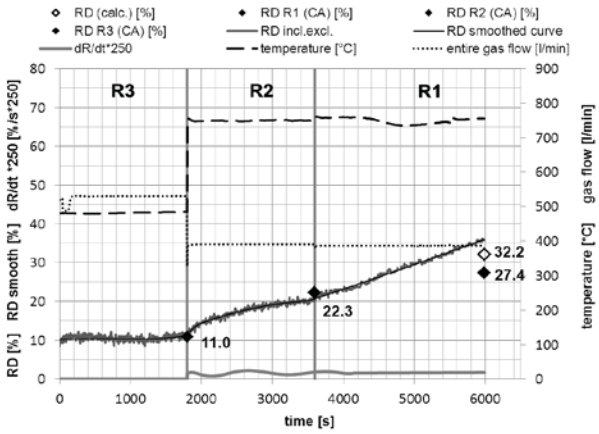

comments

Ore drying 5 h at 105 °C. Increase N2 after filling in steps. Sampling test in N2-phase (480°C, ca. 500 lN/min). 2 short pushes - 80 g sample mass). Restart before test start (overpressure evaporator). R3 ok, finish of R3 breakoff due to CO2 overpressure, valve CO2). Restart and sampling at 480°C in N2-phase. N2 purging of sampling system 3 min, 10 lN/min N2, temperature colling water 60 °C for 10 min, then 30 °C. Heating up to 750°C. R2 ok. Sampling (same procedure, 4 short pushes). R1 ok.

test ok

Copyright Chair of Metallurgy

CHAIR OF METALLURGY
MONTANUNIVERSITAET LEOBEN
PRIMARY METALLURGY
METALLURGICAL PROCESSES

Tel.: +43 3842 402-2201 Fax: DW 2202
Web: http://www.metallurgy.ac.at

160 mm Fluidized Bed Reactor test
Determination of grain size distribution

Test carried out by: Michael Skorianz Dial: 2255
michael.skorianz@unileoben.ac.at

Date:
Customer: Siemens VAI

Test number: **Test I**
Kind of test: 3-stage 480/750/760°C FINEX
Target of the test: reduction behaviour of magnetite
Ore type 1: una Magnetite (Svappavaara Ore); ground, selec
Ore type 2: -
MUL sample number: MUL2010/0001
VASL sample number: -

kind of sieving: wet dry x
sieving method: three dimensional
standard:
apparatus: RETSCH AS 200
sieves size: 200 x 50 mm
sieving time: 10 min.
interval time: 10 sec.
amplitude: 1,5 mm

sieve analysis - results

sieves	raw material		bed			internal cyclone			bed + internal cyclone			bed + internal cyclone + discharge			summary	
fraction	fraction	cum.	weight	fraction	cum.	weight	fraction	cum.	weight	fraction	cum.	weight	fraction	cum.	fraction change	
[mm]	p3 [%]	Q3 [%]	m [g]	p3 [%]	Q3 [%]	m [g]	p3 [%]	Q3 [%]	m [g]	p3 [%]	Q3 [%]	m [g]	p3 [%]	Q3 [%]	Δp3 [%]	comment
4-6,3	0,0		0,0	0,0		0,0	0,0		0,0	0,0		0,0	0,0		0,0	0
2,8-4	13,3	100,0	195,1	7,7	100,0	0,0	0,0	100,0	195,1	7,2	100,0	195,1	7,1	100,0	-6,2	0
1,0-2,8	13,3	86,7	497,2	19,6	92,3	0,0	0,0	100,0	497,2	18,4	92,8	497,2	18,0	92,9	4,7	0
0,5-1,0	16,0	73,4	345,7	13,6	72,8	3,5	2,1	100,0	349,2	12,9	74,4	349,2	12,6	75,0	-3,4	0
0,25-0,5	17,4	57,4	410,0	16,1	59,2	11,2	6,9	97,9	421,2	15,6	61,5	421,2	15,2	62,3	-2,2	0
0,125-0,25	14,7	40,0	408,5	16,1	43,0	32,2	19,7	91,0	440,7	16,3	45,9	440,7	15,9	47,1	1,2	0
0,063-0,125	25,3	25,3	505,1	19,9	27,0	48,3	29,6	71,2	553,4	20,5	29,6	553,4	20,0	31,2	-5,3	0
0-0,063	0,0	0,0	180,3	7,1	7,1	67,9	41,6	41,6	248,2	9,2	9,2	308,2	11,1	11,1	11,1	0
sum	**100**		**2542**	**100**		**163**	**100**		**2705**	**100**		**2765**	**100**		**0**	

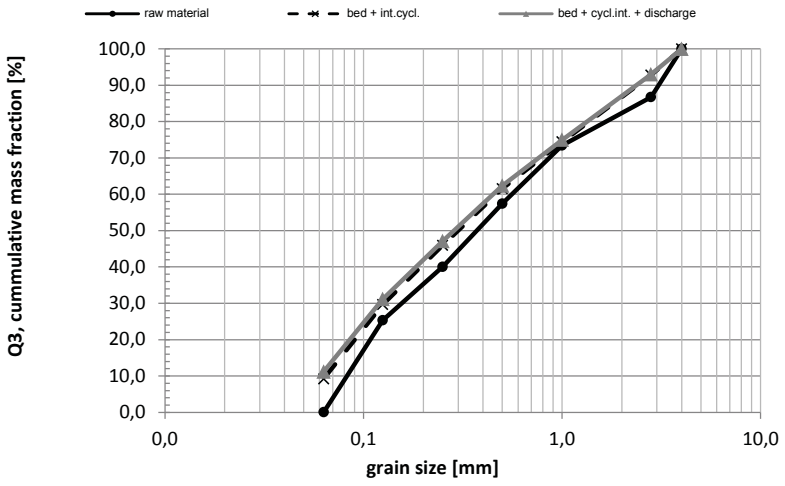

Copyright Chair of Metallurgy

CHAIR OF METALLURGY
MONTANUNIVERSITAET LEOBEN
PRIMARY METALLURGY
METALLURGICAL PROCESSES

Tel.: +43 3842 402-2201 Fax: DW 2202
Web: http://www.metallurgy.ac.at

160 mm Fluidized Bed Reactor test
Process conditions and test parameter

Test number: **Test J** **Date:**
Customer: Siemens VAI

Kind of test: 3-stage 480/750/760°C FINEX
Target of the test: reduction behaviour of limonite

Test carried out by: Michael Skorianz Dial: 2255
michael.skorianz@unileoben.ac.at

Raw material input

sieves	sieve analyis		input	comments
mesh size [mm]	fraction [%]	cum. [%]	mass [g]	
4-6,3	0		0,0	
2,8-4	13,3	100	465,5	
1,0-2,8	13,3	86,7	465,5	
0,5-1,0	16	73,4	560,0	robe river fine ore MUL2010/0007
0,25-0,5	17,4	57,4	609,0	
0,125-0,25	14,7	40	514,5	
0,063-0,125	25,3	25,3	885,5	
0-0,063	0	0	0,0	
sum	100,0		3500,0	

chemical analyses

raw material				reduced material						
robe river fine ore MUL2010/0007				species	bed Ø	R4	R3	R2	int.cyc.	ex.cyc.
species	[%]	species	[%]		[%]	[%]	[%]	[%]	[%]	[%]
Fe(tot)	56,20	Na2O	0,00	Fe tot	71,8	0,0	63,4	66,0	0,0	0,0
FeO	0,37	Mn	0,08	Fe met	22,8	0,0	0,5	0,3	0,0	0,0
Al2O3	2,79	Ni	0,00	FeO	44,1	0,0	22,3	50,4	0,0	0,0
SiO2	5,84	Cu	0,00	C tot	0,061	0,000	0,144	0,091	0,000	0,000
CaO	0,01	Cr	0,00	MD	31,8	0,0	0,7	0,4	0,0	0,0
MgO	0,01	S	0,00	RD (CA)	47,7	0,0	9,8	20,2	0,0	0,0
TiO2	0,18	P	0,04	RD (cal)	46,6	0,0	verwech	0,0	0,0	0,0
K2O	0,01	Zn	0,00	FeOx	0,8	0,0	0,0	0,0	0,0	0,0
V2O5	0,00	LOI (900°	10,55	Fe bal.	100,0	0,0	0,0	0,0	0,0	0,0

calculation of test parameter: 3-stage 480/750/760°C FINEX

		concentration, temp. plant				concentration test rig				gas flow test rig						
gas composition		R1 [%]	R2 [%]	R3 [%]	R4 [%]	R1 [%]	R2 [%]	R3 [%]	R4 [%]	R1 [Nl/min]	heating [Nl/min]	R2 [Nl/min]	heating [Nl/min]	R3 [Nl/min]	heating [Nl/min]	R4 [Nl/min]
species	H2	17,7%	16,5%	16,0%	0,00%	17,6%	17,3%	14,7%	0,0%	**68,1**		**67,7**		**77,9**		**0,0**
	H2O	5,6%	7,1%	8,7%	0,00%	5,6%	7,5%	8,0%	0,0%	**21,5**		**29,1**		**42,4**		**0,0**
	CO	46,7%	38,9%	36,5%	0,00%	46,4%	40,9%	33,5%	0,0%	**179,6**		**159,6**		**177,8**		**0,0**
	CO2	21,0%	28,5%	29,8%	0,00%	20,9%	29,9%	27,4%	0,0%	**80,8**		**116,9**		**145,2**		**0,0**
	CH4	1,5%	1,6%	1,6%	0,00%	0,0%	0,0%	0,0%	0,0%	**0,0**		**0,0**		**0,0**		**0,0**
	N2	7,5%	7,4%	7,4%	0,00%	9,5%	4,4%	16,4%	0,0%	**36,7**		**17,2**		**87,2**		**0,0**
	total dry	94,4%	92,9%	91,3%	0,0%	94,4%	92,5%	92,0%	0,0%	365,2		361,4		488,1		0,0
	total wet	100,0%	100,0%	100,0%	0,0%	100,0%	100,0%	100,0%	0,0%	386,7		390,5		530,5		0,0
	GOD	29,2%	39,1%	42,3%	0,0%	29,2%	39,1%	42,3%	0,0%	29,2%		39,1%		42,3%		0,0%
	H2/H2O	3,16	2,32	1,84	0,00	3,16	2,32	1,84	0,00							
	CO/CO2	2,22	1,36	1,22	0,00	2,22	1,36	1,22	0,00							
temperature [°C]		760	750	480	0					**760**	**760**	**750**	**750**	**480**	**480**	**0**
residence time [min]		40	30	30	0					**40**	**0**	**30**	**0**	**30**	**0**	**0**
spec. gas rate plant [Nm³/t]		810	810	810	0											
supposed gas rate red. [Nm³/t]		4000	3200	3800	0											
defined uL retort [m/s]		0,9	0,9	0,9	0											
flow rate red. comp. [Ndm³/h]		21000	22400	26600	0											

diameter retort [m]	0,158
cross section retort [m²]	0,020
absolute pressure [bar]	1,4
atmospherical pressure [bar]	1,013

Baur-Glaessner-Diagram for gas mixtures of H_2, H_2O, CO, CO_2 / process conditions

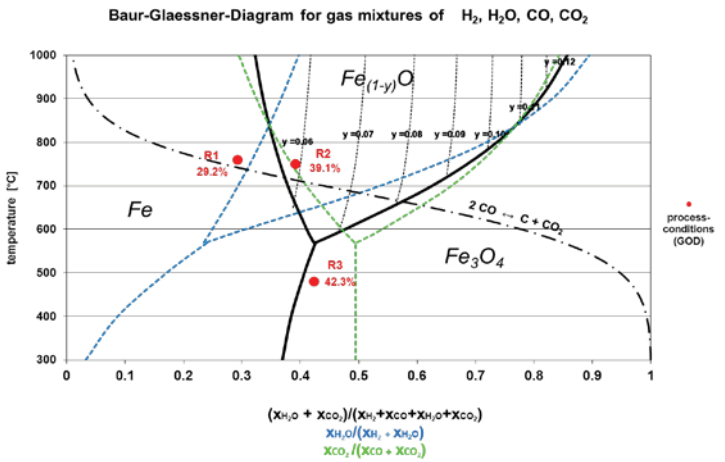

Copyright Chair of Metallurgy

CHAIR OF METALLURGY
MONTANUNIVERSITAET LEOBEN
PRIMARY METALLURGY
METALLURGICAL PROCESSES

Tel.: +43 3842 402-2201 Fax: DW 2202
Web: http://www.metallurgy.ac.at

160 mm Fluidized Bed Reactor test
Test information

Test number: **Test J** **Date:**
Customer: Siemens VAI

Kind of test: 3-stage 480/750/760°C FINEX
Target of the test: reduction behaviour of limonite

Test carried out by: Michael Skorianz Dial: 2255
michael.skorianz@unileoben.ac.at

Test information and results

Gas supply (reduction phases)

species	gas flow [Ndm³]	content/unit [Ndm³]	unit [pcs]
H2	7092,3	8900,0	**0,80**
H2O	3006,9	0,0	**0,00**
CO	17306,9	5900,0	**2,93**
CO2	11093,8	20300,0	**0,55**
CH4	0,0	12600,0	**0,00**
N2	4597,6	10700,0	**0,43**
sum	**43097,6**		**4,7**

Pressure test at 300 °C

position	200 Nl/min [mbar]	400 Nl/min [mbar]
Δp internal cyclone	2,2	5,5
p retort outlet	1019	1108
Δp grid	9	31
p before grid	1028	1149

Cleaning of grid before test -
Temperature sample after test 28 °C

Re-weight of input

position	[g]
bed	**2259**
int. cycl.	**64**
ext. cycl. vor Start	0
ext. cycl. R3	8
ext. cycl. R2	37
ext. cycl. R1	29
sum ext. cycl.	**74**
Filter	11
Rest	42
sum re-weight	**2740**

Test progress: 3-stage 480/750/760°C FINEX

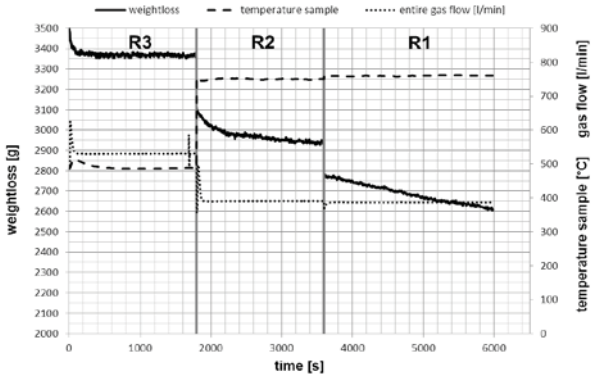

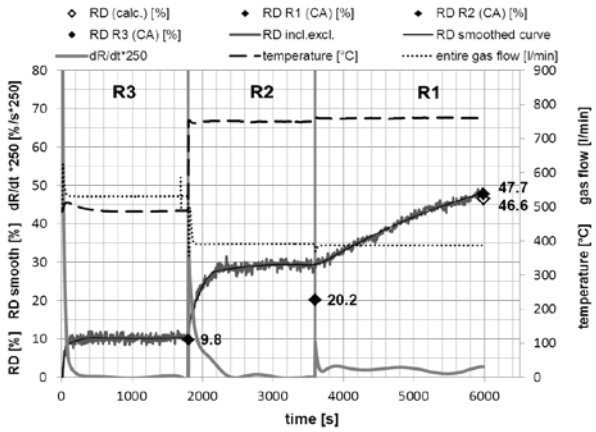

comments

increase N2 after filling in steps.

test progress ok

Copyright Chair of Metallurgy

CHAIR OF METALLURGY
MONTANUNIVERSITAET LEOBEN
PRIMARY METALLURGY
METALLURGICAL PROCESSES

Tel.: +43 3842 402-2201 Fax: DW 2202
Web: http://www.metallurgy.ac.at

160 mm Fluidized Bed Reactor test
Determination of grain size distribution

Test carried out by: Michael Skorianz Dial: 2255
michael.skorianz@unileoben.ac.at

Date:

Customer: Siemens VAI

Test number: **Test J**

Kind of test:
3-stage 480/750/760°C FINEX

Target of the test: reduction behaviour of limonite
Ore type 1: robe river fine ore MUL2010/0007
Ore type 2: -
MUL sample number: MUL2010/0007
VASL sample number: 1154/06

kind of sieving: wet dry x
sieving method: three dimensional
standard:
apparatus: RETSCH AS 200
sieves size: 200 x 50 mm
sieving time: 10 min.
interval time: 10 sec.
amplitude: 1,5 mm

sieve analysis - results

sieves	raw material		bed			internal cyclone			bed + internal cyclone			bed + internal cyclone + discharge			summary	
fraction	fraction	cum.	weight	fraction	cum.	weight	fraction	cum.	weight	fraction	cum.	weight	fraction	cum.	fraction change	
[mm]	p3 [%]	Q3 [%]	m [g]	p3 [%]	Q3 [%]	m [g]	p3 [%]	Q3 [%]	m [g]	p3 [%]	Q3 [%]	m [g]	p3 [%]	Q3 [%]	Δp3 [%]	comment
4-6,3	0,0		0,0	0,0		0,0	0,0		0,0	0,0		0,0	0,0		0,0	0
2,8-4	13,3	100,0	65,1	2,9	100,0	0,0	0,0	100,0	65,1	2,8	100,0	65,1	2,7	100,0	-10,6	0
1,0-2,8	13,3	86,7	446,9	19,8	97,1	0,0	0,0	100,0	446,9	19,2	97,2	446,9	18,2	97,3	4,9	0
0,5-1,0	16,0	73,4	357,8	15,8	77,3	0,0	0,0	100,0	357,8	15,4	78,0	357,8	14,6	79,1	-1,4	0
0,25-0,5	17,4	57,4	405,8	18,0	61,5	0,0	0,0	100,0	405,8	17,5	62,6	405,8	16,6	64,5	-0,8	0
0,125-0,25	14,7	40,0	354,7	15,7	43,5	0,0	0,0	100,0	354,7	15,3	45,1	354,7	14,5	47,9	-0,2	0
0,063-0,125	25,3	25,3	476,8	21,1	27,8	0,0	0,0	100,0	476,8	20,5	29,8	476,8	19,5	33,5	-5,8	0
0-0,063	0,0	0,0	152,0	6,7	6,7	64,0	100,0	100,0	216,0	9,3	9,3	343,0	14,0	14,0	14,0	0
sum	**100**		**2259**	**100**		**64**	**100**		**2323**	**100**		**2450**	**100**		**0**	

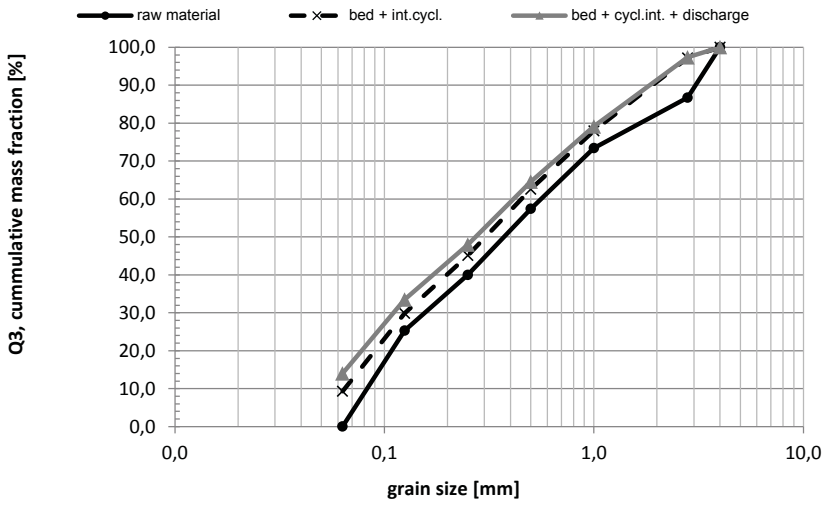

Copyright Chair of Metallurgy

CHAIR OF METALLURGY
MONTANUNIVERSITAET LEOBEN
PRIMARY METALLURGY
METALLURGICAL PROCESSES

Tel.: +43 3842 402-2201 Fax: DW 2202
Web: http://www.metallurgy.ac.at

160 mm Fluidized Bed Reactor test
Process conditions and test parameter

Test number: **Test K** **Date:**
Customer: Siemens VAI

Kind of test: 3-stage 480/750/760°C FINEX
Target of the test: reduction behaviour of siderite (limonitic)

Test carried out by: Michael Skorianz Dial: 2255
michael.skorianz@unileoben.ac.at

Raw material input

sieves	sieve analyis		input	comments
mesh size [mm]	fraction [%]	cum. [%]	mass [g]	
4-6,3	0		0,0	
2,8-4	13,3	100	465,5	erzberg fine ore MUL2010/0009
1,0-2,8	13,3	86,7	465,5	
0,5-1,0	16	73,4	560,0	
0,25-0,5	17,4	57,4	609,0	
0,125-0,25	14,7	40	514,5	
0,063-0,125	25,3	25,3	885,5	
0-0,063	0	0	0,0	
sum	100,0		3500,0	

chemical analyses

raw material: erzberg fine ore MUL2010/0009			
species	[%]	species	[%]
Fe(tot)	49,40	Na2O	0,00
FeO	0,28	Mn	2,80
Al2O3	0,52	Ni	0,00
SiO2	2,88	Cu	0,00
CaO	4,74	Cr	0,00
MgO	2,39	S	0,01
TiO2	0,03	P	0,04
K2O	0,18	Zn	0,00
V2O5	0,00	LOI (900°	14,39

reduced material						
species	bed Ø [%]	R4 [%]	R3 [%]	R2 [%]	int.cyc. [%]	ex.cyc. [%]
Fe tot	65,2	0,0	55,4	61,0	0,0	0,0
Fe met	23,2	0,0	0,4	1,2	0,0	0,0
FeO	44,4	0,0	21,0	57,4	0,0	0,0
C tot	0,297	0,000	1,680	0,123	0,000	0,000
MD	35,6	0,0	0,8	2,0	0,0	0,0
RD (CA)	53,2	0,0	10,6	26,4	0,0	0,0
RD (cal)	53,1	0,0	0,0	0,0	0,0	0,0
FeOx	0,7	0,0	0,0	0,0	0,0	0,0
Fe bal.	98,2	0,0	0,0	0,0	0,0	0,0

calculation of test parameter: 3-stage 480/750/760°C FINEX

		concentration, temp. plant				concentration test rig				gas flow test rig						
gas composition		R1 [%]	R2 [%]	R3 [%]	R4 [%]	R1 [%]	R2 [%]	R3 [%]	R4 [%]	R1 [Nl/min]	heating [Nl/min]	R2 [Nl/min]	heating [Nl/min]	R3 [Nl/min]	heating [Nl/min]	R4 [Nl/min]
species	H2	17,7%	16,5%	16,0%	0,00%	17,6%	17,3%	14,7%	0,0%	**68,1**		**67,7**		**77,9**		**0,0**
	H2O	5,6%	7,1%	8,7%	0,00%	5,6%	7,5%	8,0%	0,0%	**21,5**		**29,1**		**42,4**		**0,0**
	CO	46,7%	38,9%	36,5%	0,00%	46,4%	40,9%	33,5%	0,0%	**179,6**		**159,6**		**177,8**		**0,0**
	CO2	21,0%	28,5%	29,8%	0,00%	20,9%	29,9%	27,4%	0,0%	**80,8**		**116,9**		**145,2**		**0,0**
	CH4	1,5%	1,6%	1,6%	0,00%	0,0%	0,0%	0,0%	0,0%	**0,0**		**0,0**		**0,0**		**0,0**
	N2	7,5%	7,4%	7,4%	0,00%	9,5%	4,4%	16,4%	0,0%	**36,7**		**17,2**		**87,2**		**0,0**
	total dry	94,4%	92,9%	91,3%	0,0%	94,4%	92,5%	92,0%	0,0%	365,2		361,4		488,1		0,0
	total wet	100,0%	100,0%	100,0%	0,0%	100,0%	100,0%	100,0%	0,0%	386,7		390,5		530,5		0,0
	GOD	29,2%	39,1%	42,3%	0,0%	29,2%	39,1%	42,3%	0,0%	29,2%		39,1%		42,3%		0,0%
	H2/H2O	3,16	2,32	1,84	0,00	3,16	2,32	1,84	0,00							
	CO/CO2	2,22	1,36	1,22	0,00	2,22	1,36	1,22	0,00							
temperature [°C]		760	750	480	0					**760**	**760**	**750**	**750**	**480**	**480**	**0**
residence time [min]		40	30	30	0					**40**	**15**	**30**	**30**	**30**	**0**	**0**
spec. gas rate plant [Nm³/t]		810	810	810	0											
supposed gas rate red. [Nm³/t]		4000	3200	3800	0											
defined uL retort [m/s]		0,9	0,9	0,9	0											
flow rate red. comp. [Ndm³/h]		21000	22400	26600	0											

		diameter retort [m]	0,158
		cross section retort [m²]	0,020
		absolute pressure [bar]	1,4
		atmospherical pressure [bar]	1,013

Baur-Glaessner-Diagram for gas mixtures of H_2, H_2O, CO, CO_2 / process conditions

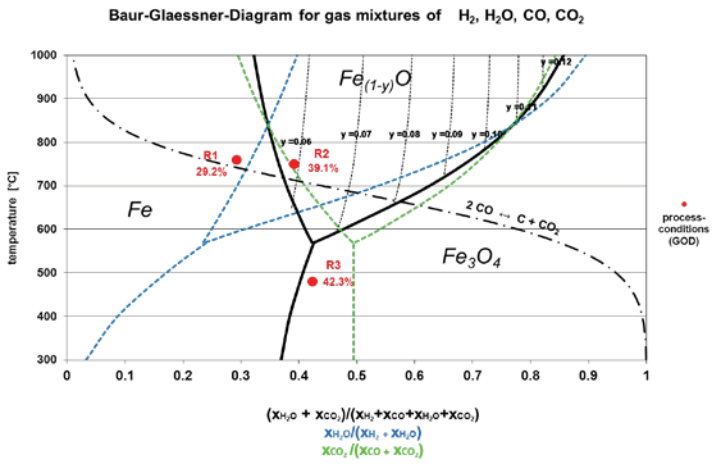

Copyright Chair of Metallurgy

CHAIR OF METALLURGY
MONTANUNIVERSITAET LEOBEN
PRIMARY METALLURGY
METALLURGICAL PROCESSES

Tel.: +43 3842 402-2201 Fax: DW 2202
Web: http://www.metallurgy.ac.at

160 mm Fluidized Bed Reactor test
Test information

Test number: **Test K** **Date:**
Customer: Siemens VAI

Kind of test: 3-stage 480/750/760°C FINEX
Target of the test: reduction behaviour of siderite (limonitic)

Test carried out by: Michael Skorianz Dial: 2255
michael.skorianz@unileoben.ac.at

Test information and results

Gas supply (reduction phases)

species	gas flow [Ndm³]	content/unit [Ndm³]	unit [pcs]
H2	7092,3	8900,0	**0,80**
H2O	3006,9	0,0	**0,00**
CO	17306,9	5900,0	**2,93**
CO2	11093,8	20300,0	**0,55**
CH4	0,0	12600,0	**0,00**
N2	4597,6	10700,0	**0,43**
sum	**43097,6**		**4,7**

Pressure test at 300 °C

position	200 Nl/min [mbar]	400 Nl/min [mbar]
Δp internal cyclone	2,2	5,3
p retort outlet	1011	1085
Δp grid	9,1	31
p before grid	1020	1136

Cleaning of grid before test -
Temperature sample after test 27 °C

Re-weight of input

position	[g]
bed	**1806**
int. cycl.	**223**
ext. cycl. vor Start	0
ext. cycl. R3	9
ext. cycl. R2	167
ext. cycl. R1	84
sum ext. cycl.	**260**
Filter	6
Rest	38
sum re-weight	**2604**

Test progress: 3-stage 480/750/760°C FINEX

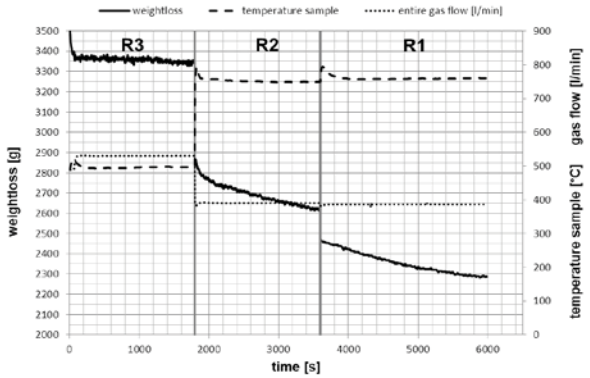

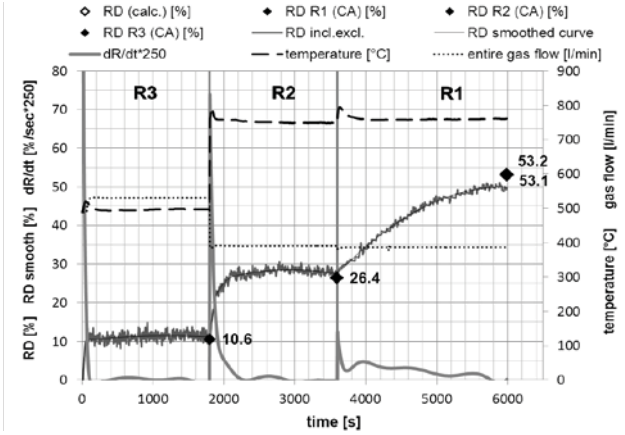

comments

Ore drying 5 h at 105 °C. Restart at beginning, overpressure evaporator. R3 ok. R2 at the beginning temperature increase from 750 to 790°C in 15 seconds and back to 760 in 1 minute (probably strong exothermic ore reaction). In R1 at the beginning also temperature Increase and decrease as in R2. Strong reoxidation of bed material after disassembling.

Sampling after R1 at 480°C in N2-phase. N2 purging of sampling system 3 min, 10 lN/min N2, temperature colling water 60 °C for 10 min, then 30 °C. Sampling after R2 same procedure, ok.

test ok

Copyright Chair of Metallurgy

CHAIR OF METALLURGY
MONTANUNIVERSITAET LEOBEN
PRIMARY METALLURGY
METALLURGICAL PROCESSES

Tel.: +43 3842 402-2201 Fax: DW 2202
Web: http://www.metallurgy.ac.at

160 mm Fluidized Bed Reactor test
Determination of grain size distribution

Test carried out by: Michael Skorianz Dial: 2255
michael.skorianz@unileoben.ac.at

Date:
Customer: Siemens VAI

Test number: **Test K**
Kind of test: 3-stage 480/750/760°C FINEX
Target of the test: reduction behaviour of siderite (limonitic)
Ore type 1: erzberg fine ore MUL2010/0009
Ore type 2: -
MUL sample number: MUL2010/0009
VASL sample number: 0

kind of sieving: wet dry x
sieving method: three dimensional
standard:
apparatus: RETSCH AS 200
sieves size: 200 x 50 mm
sieving time: 10 min.
interval time: 10 sec.
amplitude: 1,5 mm

sieve analysis - results

sieves	raw material		bed			internal cyclone			bed + internal cyclone			bed + internal cyclone + discharge			summary	
fraction	fraction	cum.	weight	fraction	cum.	weight	fraction	cum.	weight	fraction	cum.	weight	fraction	cum.	fraction change	
[mm]	p3 [%]	Q3 [%]	m [g]	p3 [%]	Q3 [%]	m [g]	p3 [%]	Q3 [%]	m [g]	p3 [%]	Q3 [%]	m [g]	p3 [%]	Q3 [%]	Δp3 [%]	comment
4-6,3	0,0		0,0	0,0		0,0	0,0		0,0	0,0		0,0	0,0		0,0	0
2,8-4	13,3	100,0	223,5	12,4	100,0	2,0	0,9	100,0	225,5	11,1	100,0	225,5	9,7	100,0	-3,6	0
1,0-2,8	13,3	86,7	425,9	23,6	87,6	8,8	4,0	99,1	434,7	21,4	88,9	434,7	18,6	90,3	5,3	0
0,5-1,0	16,0	73,4	320,0	17,7	64,0	21,6	9,7	95,2	341,6	16,8	67,5	341,6	14,6	71,7	-1,4	0
0,25-0,5	17,4	57,4	316,1	17,5	46,3	26,9	12,1	85,5	343,1	16,9	50,6	343,1	14,7	57,1	-2,7	0
0,125-0,25	14,7	40,0	239,7	13,3	28,8	23,3	10,4	73,4	263,0	13,0	33,7	263,0	11,3	42,4	-3,4	0
0,063-0,125	25,3	25,3	242,1	13,4	15,5	46,1	20,7	62,9	288,1	14,2	20,8	288,1	12,4	31,1	-12,9	0
0-0,063	0,0	0,0	38,7	2,1	2,1	94,3	42,3	42,3	133,0	6,6	6,6	437,0	18,7	18,7	18,7	0
sum	**100**		**1806**	**100**		**223**	**100**		**2029**	**100**		**2333**	**100**		**0**	

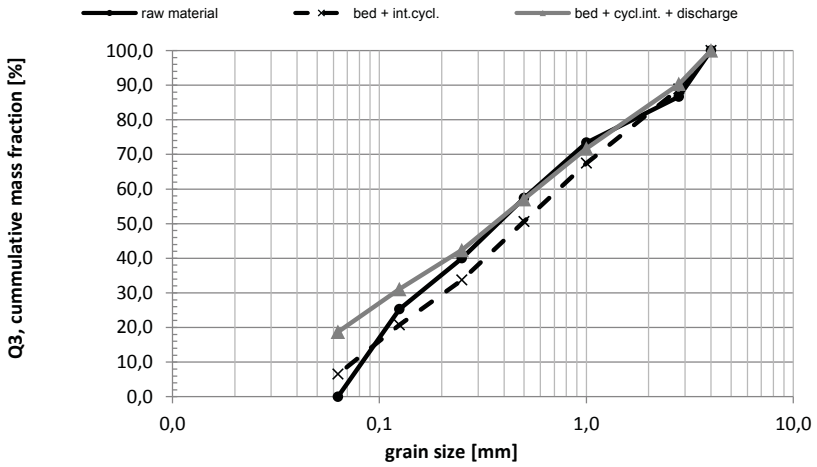

Copyright Chair of Metallurgy

CHAIR OF METALLURGY
MONTANUNIVERSITAET LEOBEN
PRIMARY METALLURGY
METALLURGICAL PROCESSES

Tel.: +43 3842 402-2201 Fax: DW 2202
Web: http://www.metallurgy.ac.at

160 mm Fluidized Bed Reactor test
Process conditions and test parameter

Test number: **Test L** **Date:**
Customer: Siemens VAI

Kind of test: 3-stage 480/750/760°C FINEX
Target of the test: reduction behaviour of hematite (industria

Test carried out by: Michael Skorianz Dial: 2255
michael.skorianz@unileoben.ac.at

Raw material input

sieves	sieve analyis		input	comments
mesh size [mm]	fraction [%]	cum. [%]	mass [g]	
4-6,3	0		0,0	
2,8-4	13,3	100	465,5	MAC.F (marra mamba) MUL2010/0005
1,0-2,8	13,3	86,7	465,5	
0,5-1,0	16	73,4	560,0	
0,25-0,5	17,4	57,4	609,0	
0,125-0,25	14,7	40	514,5	
0,063-0,125	25,3	25,3	885,5	
0-0,063	0	0	0,0	
sum	100,0		3500,0	

chemical analyses

raw material				reduced material						
MAC.F (marra mamba) MUL2010/0005				species	bed Ø	R4	R3	R2	int.cyc.	ex.cyc.
species	[%]	species	[%]		[%]	[%]	[%]	[%]	[%]	[%]
Fe(tot)	61,30	Na2O	0,00	Fe tot	74,0	0,0	66,1	69,4	0,0	0,0
FeO	0,41	Mn	0,15	Fe met	20,9	0,0	0,3	0,2	0,0	0,0
Al2O3	2,29	Ni	0,00	FeO	52,9	0,0	25,6	66,7	0,0	0,0
SiO2	3,89	Cu	0,00	C tot	0,028	0,000	0,049	0,047	0,000	0,000
CaO	0,01	Cr	0,00	MD	28,2	0,0	0,5	0,3	0,0	0,0
MgO	0,01	S	0,00	RD (CA)	46,7	0,0	10,5	25,2	0,0	0,0
TiO2	0,09	P	0,08	RD (cal)	52,1	0,0	0,0	0,0	0,0	0,0
K2O	0,02	Zn	0,00	FeOx	0,8	0,0	0,0	0,0	0,0	0,0
V2O5	0,00	LOI (900°	5,82	Fe bal.	97,2	0,0	0,0	0,0	0,0	0,0

calculation of test parameter: 3-stage 480/750/760°C FINEX

		concentration, temp. plant				concentration test rig				gas flow test rig						
gas composition		R1 [%]	R2 [%]	R3 [%]	R4 [%]	R1 [%]	R2 [%]	R3 [%]	R4 [%]	R1 [Nl/min]	heating [Nl/min]	R2 [Nl/min]	heating [Nl/min]	R3 [Nl/min]	heating [Nl/min]	R4 [Nl/min]
species	H2	17,7%	16,5%	16,0%	0,00%	17,6%	17,3%	14,7%	0,0%	**68,1**		**67,7**		**77,9**		**0,0**
	H2O	5,6%	7,1%	8,7%	0,00%	5,6%	7,5%	8,0%	0,0%	**21,5**		**29,1**		**42,4**		**0,0**
	CO	46,7%	38,9%	36,5%	0,00%	46,4%	40,9%	33,5%	0,0%	**179,6**		**159,6**		**177,8**		**0,0**
	CO2	21,0%	28,5%	29,8%	0,00%	20,9%	29,9%	27,4%	0,0%	**80,8**		**116,9**		**145,2**		**0,0**
	CH4	1,5%	1,6%	1,6%	0,00%	0,0%	0,0%	0,0%	0,0%	**0,0**		**0,0**		**0,0**		**0,0**
	N2	7,5%	7,4%	7,4%	0,00%	9,5%	4,4%	16,4%	0,0%	**36,7**		**17,2**		**87,2**		**0,0**
	total dry	94,4%	92,9%	91,3%	0,0%	94,4%	92,5%	92,0%	0,0%	365,2		361,4		488,1		0,0
	total wet	100,0%	100,0%	100,0%	0,0%	100,0%	100,0%	100,0%	0,0%	386,7		390,5		530,5		0,0
	GOD	29,2%	39,1%	42,3%	0,0%	29,2%	39,1%	42,3%	0,0%	29,2%		39,1%		42,3%		0,0%
	H2/H2O	3,16	2,32	1,84	0,00	3,16	2,32	1,84	0,00							
	CO/CO2	2,22	1,36	1,22	0,00	2,22	1,36	1,22	0,00							
temperature [°C]		760	750	480	0					**760**	**760**	**750**	**750**	**480**	**480**	**0**
residence time [min]		40	30	30	0					**40**	**19**	**30**	**32**	**30**	**0**	**0**
spec. gas rate plant [Nm³/t]		810	810	810	0											
supposed gas rate red. [Nm³/t]		4000	3200	3800	0											
defined uL retort [m/s]		0,9	0,9	0,9	0											
flow rate red. comp. [Ndm³/h]		21000	22400	26600	0											

diameter retort [m]	0,158
cross section retort [m²]	0,020
absolute pressure [bar]	1,4
atmospherical pressure [bar]	1,013

Baur-Glaessner-Diagram for gas mixtures of H_2, H_2O, CO, CO_2 / process conditions

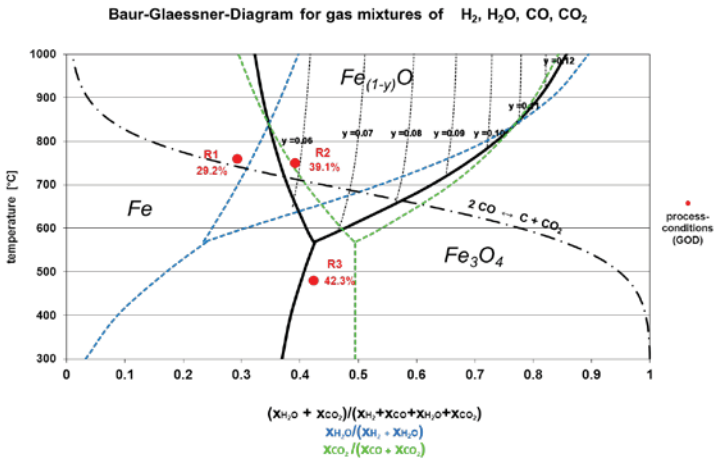

Copyright Chair of Metallurgy

CHAIR OF METALLURGY
MONTANUNIVERSITAET LEOBEN
PRIMARY METALLURGY
METALLURGICAL PROCESSES

Tel.: +43 3842 402-2201 Fax: DW 2202
Web: http://www.metallurgy.ac.at

160 mm Fluidized Bed Reactor test
Test information

Test number: Test L **Date:**
Customer: Siemens VAI

Kind of test: 3-stage 480/750/760°C FINEX
Target of the test: reduction behaviour of hematite (industria

Test carried out by: Michael Skorianz Dial: 2255
michael.skorianz@unileoben.ac.at

Test information and results

Gas supply (reduction phases)

species	gas flow [Ndm³]	content/unit [Ndm³]	unit [pcs]
H2	7092,3	8900,0	**0,80**
H2O	3006,9	0,0	**0,00**
CO	17306,9	5900,0	**2,93**
CO2	11093,8	20300,0	**0,55**
CH4	0,0	12600,0	**0,00**
N2	4597,6	10700,0	**0,43**
sum	**43097,6**		**4,7**

Pressure test at 300 °C

position	200 Nl/min [mbar]	400 Nl/min [mbar]
Δp internal cyclone	ok	ok
p retort outlet	ok	ok
Δp grid	ok	ok
p before grid	ok	ok

Cleaning of grid before test -
Temperature sample after test 19 °C

Re-weight of input

position	[g]
bed	**2381**
int. cycl.	**7**
ext. cycl. vor Start	0
ext. cycl. R3	2
ext. cycl. R2	6
ext. cycl. R1	96
sum ext. cycl.	**104**
Filter	19
Rest	98
sum re-weight	**2819**

Test progress: 3-stage 480/750/760°C FINEX

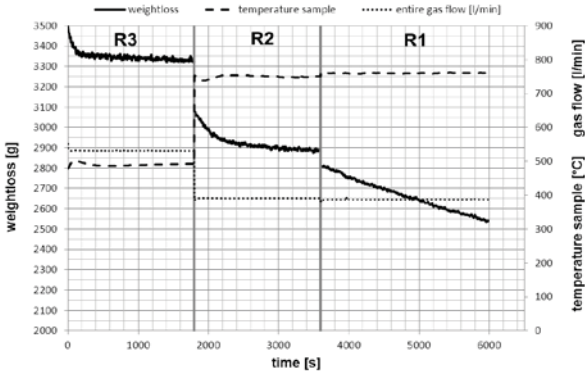

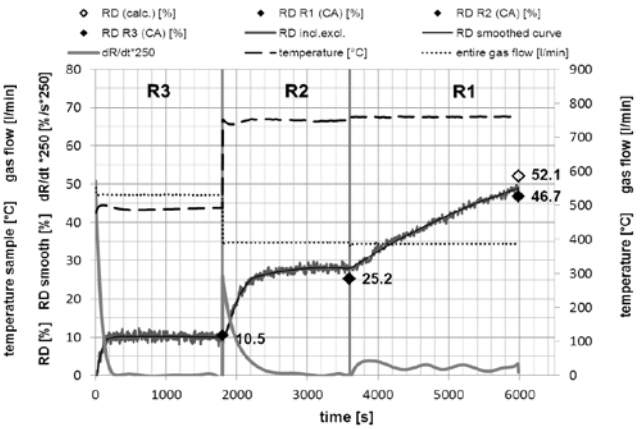

comments

Ore drying 5 h at 105 °C. Increase N2 after filling in steps.

Test progress ok

Copyright Chair of Metallurgy

CHAIR OF METALLURGY
MONTANUNIVERSITAET LEOBEN
PRIMARY METALLURGY
METALLURGICAL PROCESSES

Tel.: +43 3842 402-2201 Fax: DW 2202
Web: http://www.metallurgy.ac.at

160 mm Fluidized Bed Reactor test
Determination of grain size distribution

Test carried out by: Michael Skorianz Dial: 2255
michael.skorianz@unileoben.ac.at

Date:

Customer: Siemens VAI

Test number: **Test L**

Kind of test:
3-stage 480/750/760°C FINEX

Target of the test: reduction behaviour of hematite (industrial)
Ore type 1: MAC.F (marra mamba) MUL2010/0005
Ore type 2: -
MUL sample number: MUL2010/0005
VASL sample number: -

kind of sieving: wet dry x
sieving method: three dimensional
standard:
apparatus: RETSCH AS 200
sieves size: 200 x 50 mm
sieving time: 10 min.
interval time: 10 sec.
amplitude: 1,5 mm

sieve analysis - results

sieves	raw material		bed			internal cyclone			bed + internal cyclone			bed + internal cyclone + discharge			summary	
fraction	fraction	cum.	weight	fraction	cum.	weight	fraction	cum.	weight	fraction	cum.	weight	fraction	cum.	fraction change	
[mm]	p3 [%]	Q3 [%]	m [g]	p3 [%]	Q3 [%]	m [g]	p3 [%]	Q3 [%]	m [g]	p3 [%]	Q3 [%]	m [g]	p3 [%]	Q3 [%]	Δp3 [%]	comment
4-6,3	0,0		0,0	0,0		0,0	0,0		0,0	0,0		0,0	0,0		0,0	0
2,8-4	13,3	100,0	165,4	6,9	100,0	0,0	0,0	100,0	165,4	6,9	100,0	165,4	6,3	100,0	-7,0	0
1,0-2,8	13,3	86,7	428,5	18,0	93,1	0,0	0,0	100,0	428,5	17,9	93,1	428,5	16,4	93,7	3,1	0
0,5-1,0	16,0	73,4	315,5	13,3	75,1	0,0	0,0	100,0	315,5	13,2	75,1	315,5	12,1	77,2	-3,9	0
0,25-0,5	17,4	57,4	309,0	13,0	61,8	0,0	0,0	100,0	309,0	12,9	61,9	309,0	11,8	65,1	-5,6	0
0,125-0,25	14,7	40,0	326,5	13,7	48,8	0,0	0,0	100,0	326,5	13,7	49,0	326,5	12,5	53,3	-2,2	0
0,063-0,125	25,3	25,3	595,1	25,0	35,1	0,0	0,0	100,0	595,1	24,9	35,3	595,1	22,8	40,8	-2,5	0
0-0,063	0,0	0,0	241,0	10,1	10,1	7,0	100,0	100,0	248,0	10,4	10,4	469,0	18,0	18,0	18,0	0
sum	**100**		**2381**	**100**		**7**	**100**		**2388**	**100**		**2609**	**100**		**0**	

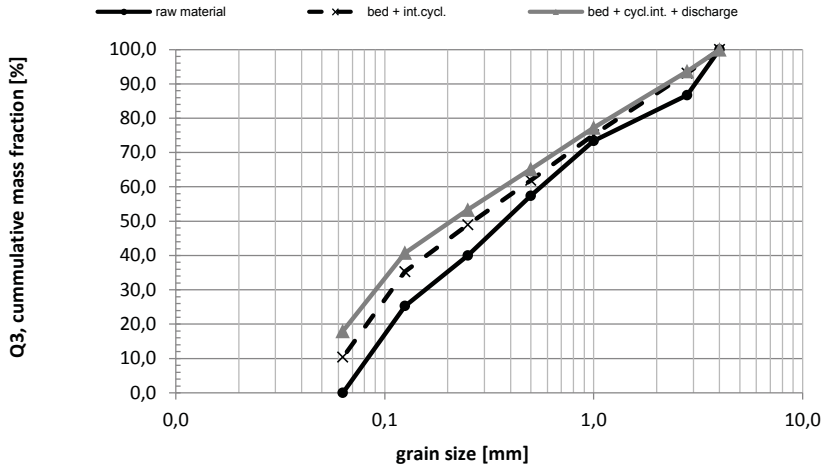

Copyright Chair of Metallurgy

CHAIR OF METALLURGY
MONTANUNIVERSITAET LEOBEN
PRIMARY METALLURGY
METALLURGICAL PROCESSES

Tel.: +43 3842 402-2201 Fax: DW 2202
Web: http://www.metallurgy.ac.at

160 mm Fluidized Bed Reactor test
Process conditions and test parameter

Test number: **Test M** **Date:**
Customer: Siemens VAI

Kind of test: 3-stage 480/750/760°C FINEX
Target of the test: reduction behaviour of hematite (industria

Test carried out by: Michael Skorianz Dial: 2255
michael.skorianz@unileoben.ac.at

Raw material input

sieves	sieve analyis		input	comments
mesh size [mm]	fraction [%]	cum. [%]	mass [g]	
4-6,3	0		0,0	
2,8-4	13,3	100	465,5	PBF.F (Pilbara) MUL2010/0004
1,0-2,8	13,3	86,7	465,5	
0,5-1,0	16	73,4	560,0	
0,25-0,5	17,4	57,4	609,0	
0,125-0,25	14,7	40	514,5	
0,063-0,125	25,3	25,3	885,5	
0-0,063	0	0	0,0	
sum	100,0		3500,0	

chemical analyses

raw material				reduced material						
PBF.F (Pilbara) MUL2010/0004				species	bed Ø	R4	R3	R2	int.cyc.	ex.cyc.
species	[%]	species	[%]		[%]	[%]	[%]	[%]	[%]	[%]
Fe(tot)	61,90	Na2O	0,00	Fe tot	75,5	0,0	66,9	69,4	0,0	0,0
FeO	0,54	Mn	0,07	Fe met	23,4	0,0	0,7	0,1	0,0	0,0
Al2O3	2,14	Ni	0,00	FeO	51,2	0,0	27,0	63,0	0,0	0,0
SiO2	2,99	Cu	0,00	C tot	0,046	0,000	0,660	0,054	0,000	0,000
CaO	0,01	Cr	0,00	MD	31,0	0,0	1,1	0,2	0,0	0,0
MgO	0,01	S	0,00	RD (CA)	48,6	0,0	11,6	23,7	0,0	0,0
TiO2	0,12	P	0,06	RD (cal)	53,3	0,0	0,0	0,0	0,0	0,0
K2O	0,02	Zn	0,00	FeOx	0,8	0,0	0,0	0,0	0,0	0,0
V2O5	0,00	LOI (900°	6,45	Fe bal.	96,9	0,0	0,0	0,0	0,0	0,0

calculation of test parameter: 3-stage 480/750/760°C FINEX

		concentration, temp. plant				concentration test rig				gas flow test rig						
gas composition		R1 [%]	R2 [%]	R3 [%]	R4 [%]	R1 [%]	R2 [%]	R3 [%]	R4 [%]	R1 [Nl/min]	heating [Nl/min]	R2 [Nl/min]	heating [Nl/min]	R3 [Nl/min]	heating [Nl/min]	R4 [Nl/min]
species	H2	17,7%	16,5%	16,0%	0,00%	17,6%	17,3%	14,7%	0,0%	**68,1**		**67,7**		**77,9**		**0,0**
	H2O	5,6%	7,1%	8,7%	0,00%	5,6%	7,5%	8,0%	0,0%	**21,5**		**29,1**		**42,4**		**0,0**
	CO	46,7%	38,9%	36,5%	0,00%	46,4%	40,9%	33,5%	0,0%	**179,6**		**159,6**		**177,8**		**0,0**
	CO2	21,0%	28,5%	29,8%	0,00%	20,9%	29,9%	27,4%	0,0%	**80,8**		**116,9**		**145,2**		**0,0**
	CH4	1,5%	1,6%	1,6%	0,00%	0,0%	0,0%	0,0%	0,0%	**0,0**		**0,0**		**0,0**		**0,0**
	N2	7,5%	7,4%	7,4%	0,00%	9,5%	4,4%	16,4%	0,0%	**36,7**		**17,2**		**87,2**		**0,0**
	total dry	94,4%	92,9%	91,3%	0,0%	94,4%	92,5%	92,0%	0,0%	365,2		361,4		488,1		0,0
	total wet	100,0%	100,0%	100,0%	0,0%	100,0%	100,0%	100,0%	0,0%	386,7		390,5		530,5		0,0
	GOD	29,2%	39,1%	42,3%	0,0%	29,2%	39,1%	42,3%	0,0%	29,2%		39,1%		42,3%		0,0%
	H2/H2O	3,16	2,32	1,84	0,00	3,16	2,32	1,84	0,00							
	CO/CO2	2,22	1,36	1,22	0,00	2,22	1,36	1,22	0,00							
temperature [°C]		760	750	480	0					**760**	**760**	**750**	**750**	**480**	**480**	**0**
residence time [min]		40	30	30	0					**40**	**15**	**30**	**30**	**30**	**0**	**0**
spec. gas rate plant [Nm³/t]		810	810	810	0											
supposed gas rate red. [Nm³/t]		4000	3200	3800	0											
defined uL retort [m/s]		0,9	0,9	0,9	0											
flow rate red. comp. [Ndm³/h]		21000	22400	26600	0											

diameter retort [m]			0,158
cross section retort [m²]			0,020
absolute pressure [bar]			1,4
atmospherical pressure [bar]			1,013

Baur-Glaessner-Diagram for gas mixtures of H_2, H_2O, CO, CO_2 / process conditions

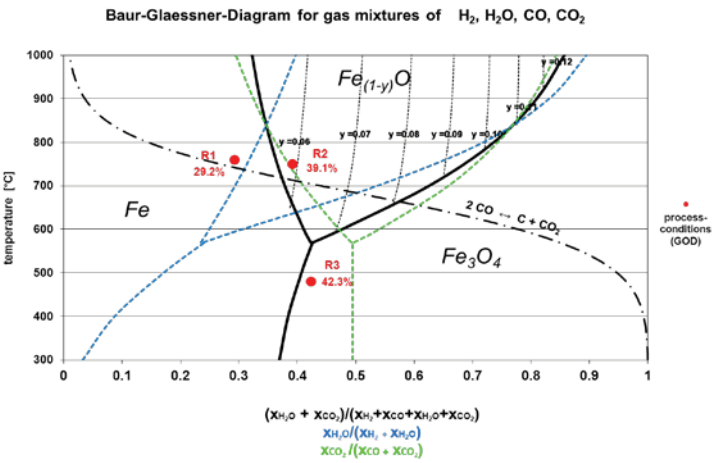

Copyright Chair of Metallurgy

CHAIR OF METALLURGY
MONTANUNIVERSITAET LEOBEN
PRIMARY METALLURGY
METALLURGICAL PROCESSES

Tel.: +43 3842 402-2201 Fax: DW 2202
Web: http://www.metallurgy.ac.at

160 mm Fluidized Bed Reactor test
Test information

Test number: **Test M** **Date:**
Customer: Siemens VAI

Kind of test: 3-stage 480/750/760°C FINEX
Target of the test: reduction behaviour of hematite (industria

Test carried out by: Michael Skorianz Dial: 2255
michael.skorianz@unileoben.ac.at

Test information and results

Gas supply (reduction phases)

species	gas flow [Ndm³]	content/unit [Ndm³]	unit [pcs]
H2	7092,3	8900,0	**0,80**
H2O	3006,9	0,0	**0,00**
CO	17306,9	5900,0	**2,93**
CO2	11093,8	20300,0	**0,55**
CH4	0,0	12600,0	**0,00**
N2	4597,6	10700,0	**0,43**
sum	**43097,6**		**4,7**

Pressure test at 300 °C

position	200 Nl/min [mbar]	400 Nl/min [mbar]
Δp internal cyclone	2,3	5,5
p retort outlet	1022	1153
Δp grid	8,7	29,8
p before grid	1030	1188

Cleaning of grid before test 0
Temperature sample after test 0 °C

Re-weight of input

position	[g]
bed	**2339**
int. cycl.	**8**
ext. cycl. vor Start	0
ext. cycl. R3	8
ext. cycl. R2	1
ext. cycl. R1	147
sum ext. cycl.	**156**
Filter	7
Rest	35
sum re-weight	**2782**

Test progress: 3-stage 480/750/760°C FINEX

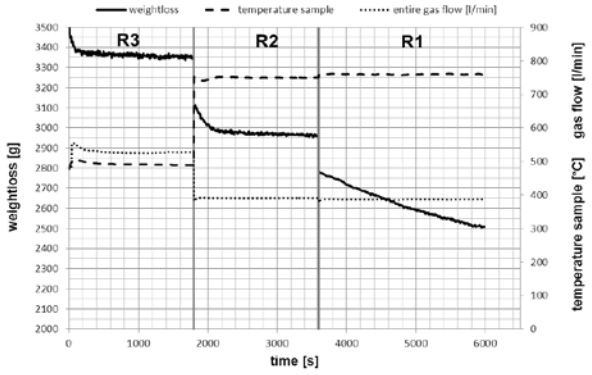

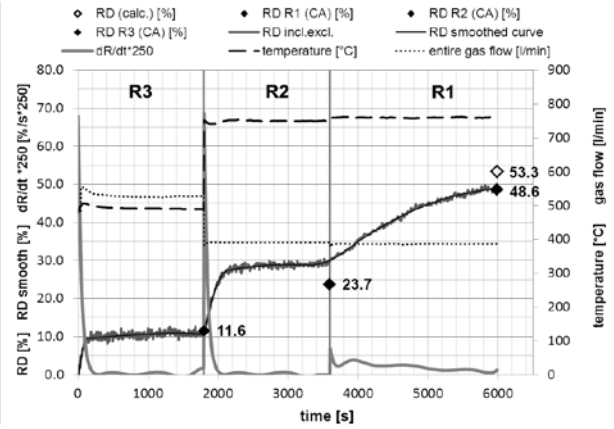

comments

Ore drying 5 h at 105 °C. Increase N2 after filling in steps.

Test progress ok

Copyright Chair of Metallurgy

CHAIR OF METALLURGY
MONTANUNIVERSITAET LEOBEN
PRIMARY METALLURGY
METALLURGICAL PROCESSES

Tel.: +43 3842 402-2201 Fax: DW 2202
Web: http://www.metallurgy.ac.at

160 mm Fluidized Bed Reactor test
Determination of grain size distribution

Test carried out by: Michael Skorianz Dial: 2255
michael.skorianz@unileoben.ac.at

Date:
Customer: Siemens VAI

Test number: **Test M**
Kind of test: 3-stage 480/750/760°C FINEX
Target of the test: reduction behaviour of hematite (industrial)
Ore type 1: PBF.F (Pilbara) MUL2010/0004
Ore type 2: -
MUL sample number: MUL2010/0005
VASL sample number: -

kind of sieving: wet dry x
sieving method: three dimensional
standard:
apparatus: RETSCH AS 200
sieves size: 200 x 50 mm
sieving time: 10 min.
interval time: 10 sec.
amplitude: 1,5 mm

sieve analysis - results

sieves	raw material		bed			internal cyclone			bed + internal cyclone			bed + internal cyclone + discharge			summary	
fraction	fraction	cum.	weight	fraction	cum.	weight	fraction	cum.	weight	fraction	cum.	weight	fraction	cum.	fraction change	
[mm]	p3 [%]	Q3 [%]	m [g]	p3 [%]	Q3 [%]	m [g]	p3 [%]	Q3 [%]	m [g]	p3 [%]	Q3 [%]	m [g]	p3 [%]	Q3 [%]	Δp3 [%]	comment
4-6,3	0,0		0,0	0,0		0,0	0,0		0,0	0,0		0,0	0,0		0,0	0
2,8-4	13,3	100,0	205,0	8,8	100,0	0,0	0,0	100,0	205,0	8,7	100,0	205,0	8,1	100,0	-5,2	0
1,0-2,8	13,3	86,7	412,1	17,6	91,2	0,0	0,0	100,0	412,1	17,6	91,3	412,1	16,2	91,9	2,9	0
0,5-1,0	16,0	73,4	353,9	15,1	73,6	0,0	0,0	100,0	353,9	15,1	73,7	353,9	13,9	75,8	-2,1	0
0,25-0,5	17,4	57,4	302,1	12,9	58,5	0,0	0,0	100,0	302,1	12,9	58,6	302,1	11,9	61,8	-5,5	0
0,125-0,25	14,7	40,0	278,3	11,9	45,6	0,0	0,0	100,0	278,3	11,9	45,8	278,3	10,9	50,0	-3,8	0
0,063-0,125	25,3	25,3	565,3	24,2	33,7	0,0	0,0	100,0	565,3	24,1	33,9	565,3	22,2	39,0	-3,1	0
0-0,063	0,0	0,0	222,2	9,5	9,5	8,0	100,0	100,0	230,2	9,8	9,8	428,2	16,8	16,8	16,8	0
sum	**100**		**2339**	**100**		**8**	**100**		**2347**	**100**		**2545**	**100**		**0**	

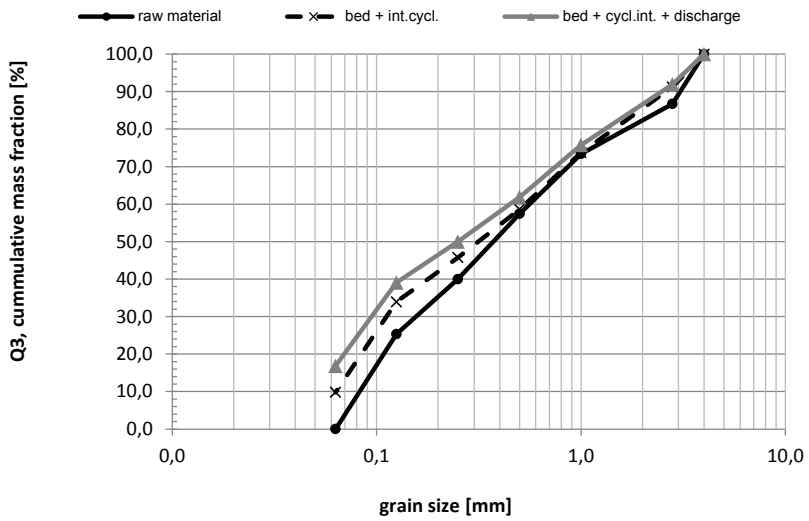

Copyright Chair of Metallurgy